Using sulfur isotope fractionation to understand the atmospheric oxidation of SO_2

Dissertation

zur Erlangung des akademischen Grades
'doctor rerum naturalium (Dr. rer. nat.)' der
Fachbereiche:
08 - Physik, Mathematik und Informatik
09 - Chemie, Pharmazie und Geowissenschaften
10 - Biologie
Universitätsmedizin

vorgelegt von
Eliza Harris
Max Planck Graduate Center
Johannes Gutenberg-Universität Mainz

verfasst am Max-Planck-Institut für Chemie

I hearby declare that I wrote the dissertation submitted without any unauthorised external assistance and used only sources acknowledged in the work. All textual passages which are appropriated verbatim or paraphrased from published and unpublished texts as well as all information obtained from oral sources are duly indicated and listed in accordance with bibliographical rules. In carrying out this research, I complied with the rules of standard scientific practice as formulated in the statutes of the Johannes Gutenberg University, Mainz, to ensure standard scientific practice.

May 23, 2012
Eliza Harris

Abstract

Sulfate aerosol plays an important but uncertain role in cloud formation and radiative forcing of the climate, and is also important for acid deposition and human health. The oxidation of SO_2 to sulfate is a key reaction in determining the impact of sulfate in the environment through its effect on aerosol size distribution and composition. This thesis presents a laboratory investigation of sulfur isotope fractionation during SO_2 oxidation by the most important gas-phase and heterogeneous pathways occurring in the atmosphere. The fractionation factors are then used to examine the role of sulfate formation in cloud processing of aerosol particles during the HCCT campaign in Thuringia, central Germany.

The fractionation factor for the oxidation of SO_2 by ·OH radicals was measured by reacting SO_2 gas, with a known initial isotopic composition, with ·OH radicals generated from the photolysis of water at -25, 0, 19 and 40°C (Chapter 2). The product sulfate and the residual SO_2 were collected as $BaSO_4$ and the sulfur isotopic compositions measured with the Cameca NanoSIMS 50. The measured fractionation factor for $^{34}S/^{32}S$ during gas phase oxidation is $\alpha_{OH} = (1.0089 \pm 0.0007) - ((4 \pm 5) \times 10^{-5})T$ (°C). Fractionation during oxidation by major aqueous pathways was measured by bubbling the SO_2 gas through a solution of H_2O_2, and by bubbling SO_2 and O_3 gas through water. The total fractionation factor for SO_2 (g) $\rightarrow\rightarrow$ sulfate (aq) with O_3 or H_2O_2 as the terminating oxidant is $\alpha_{aq} = (1.0167 \pm 0.0019) - ((8.7 \pm 3.5) \times 10^{-5})T$ (°C). Measurements at different pH values were used to constrain the fractionation factor for each individual step of this oxidation pathway (Chapter 3). Phase transfer made the smallest contribution to the total fractionation, while hydration accounted for the majority of fractionation ($\alpha_{phase} = 1.00256 \pm 0.00024$ and $\alpha_{hydration} = 1.0105 \pm 0.0037$ at 19°C). Fractionation factors were also measured in the droplet phase, and it was found that droplet microphysical processes do not alter the fractionation factors from their values in bulk aqueous phase.

Mineral dust and sea salt both represent a large proportion of total atmospheric aerosol loading, and play a very important role in heterogeneous SO_2 oxidation, which shifts the

size distribution of sulfate towards coarse particles, and limits H_2SO_4 (g) production and new particle nucleation. Thus, oxidation pathways associated with these two aerosol types were examined in more detail. The alkalinity of sea salt aerosols is critical for heterogeneous sulfate production: SO_2 oxidation by ·Cl catalysis and O_3 only occurs at high pH and is thus limited by the neutralisation capacity of the aerosol, while oxidation by transition metal catalysis and by hypohalous acids can continue once aerosols are acidified. Thus, the partitioning between these oxidation pathways is extremely important for the extent of sulfate production in the marine boundary layer. The isotopic fractionation factors for these pathways were measured by generating aerosol from pure water, NaOCl, and sulfate-free sea salt solutions (Chapter 3). Oxidation by the alkalinity-limited pathways, O_3 and ·Cl catalysis, was found to favour the heavy isotope ($\alpha_{34} = 1.0163 \pm 0.0018$ at low pH and $\alpha_{34} = 1.0199 \pm 0.0024$ at high pH at 19°C) while oxidation by the non-limited pathways, transition metal catalysis and hypohalous acids, favours the light isotope ($\alpha_{\mathrm{TM-cat}} = 0.9905 \pm 0.0031$ and $\alpha_{\mathrm{OCl}} = 0.9882 \pm 0.0036$ at 19°C). Fractionation during oxidation in the synthetic sea salt aerosol ($\alpha_{\mathrm{seasalt}} = 1.0124 \pm 0.0017$ at 19°C) showed that hypohalous acids contributed 29% of total sulfate production on the short timescale of the experiments, while O_3 and ·Cl catalysis accounted for the remaining 71%, highlighting the potential importance of the hypohalous acid pathway in the environment. The measured fractionation factors, particularly when used in combination with the $\Delta^{17}O$ isotope anomaly, will allow quantification of the different sulfate production pathways in the marine boundary layer.

Oxidation of SO_2 on mineral dust aerosol, which represents the dominant mass fraction of particulate matter in the atmosphere, can occur in the aqueous phase as leached transition metals catalyse a radical chain reaction oxidation pathway, or on the surface of dust following SO_2 chemisorption. Although the former is much faster and dominates globally, high humidities are usually first encountered only after dust has travelled for several days, thus surface oxidation can be regionally important in dust source regions. Sahara dust from the Cape Verde Islands was used to examine these two oxidation pathways (Chapter 4). Aqueous phase oxidation was investigated by bubbling SO_2 through leachate from the dust, and resulted in a fractionation factor of $\alpha_{\mathrm{leachate}} = 0.9917 \pm 0.0046$ at 19°C. Although this is equal to isotopic fractionation in a solution of Fe^{2+}/Fe^{3+} ($\alpha_{\mathrm{Fe}} = 0.9894 \pm 0.0043$), the reaction in the dust leachate was several orders of magnitude faster than in the pure Fe solution, showing that interactions between multiple metal ions are critical for oxidation rate. Oxidation on the dust surface was examined by passing SO_2 over dust mounted on a filter under various combinations of humidity, irradiation and O_3 exposure for 6-9 hours

at 19°C. A multivariate analysis model was used to investigate the isotopic composition of the sulfate produced in relation to the chemical composition of the dust and the reaction conditions. The overall fractionation factor for surface oxidation on Sahara dust is $\alpha_{\text{surface}} = 1.0096 \pm 0.0036$. The majority of oxidation was due to iron and titanium oxides in the dust, however the clay fraction of dust accounted for 12% of sulfate production and had a very distinct fractionation factor of $\alpha_{\text{clay}} = 1.085 \pm 0.013$. These fractionation factors will be very useful to understand sulfate production on mineral dust in field studies, particularly the importance of surface vs. aqueous oxidation and the role of clay minerals.

Sulfur isotopes were measured in SO_2 and H_2SO_4 gas and sulfate-containing particulate matter upwind, in-cloud and downwind of an orographic cloud during the Hill Cap Cloud Thuringia (HCCT) campaign in central Germany in Autumn, 2010 (Chapter 5). The sulfur isotopic composition of gas-phase sulfur was measured following precipitation to $BaSO_4$, while for particulate matter combined SEM and NanoSIMS analyses allowed $\delta^{34}S$ values to be resolved for particle size and type. The fractionation factors measured in the laboratory were used to investigate in-cloud sulfate production and particle processing, which modifies particle size and hygroscopicity and thus plays an important role in determining the magnitude of direct and indirect aerosol radiative forcing. In contrast to modelling studies, which predict that H_2O_2 is the dominant in-cloud oxidant for SO_2, the change in the isotopic composition of SO_2 gas following the cloud showed that transition metal-catalysed oxidation was the most important pathway for SO_2 removal in the cloud. The results show that this pathway is underestimated in models, which either approximate its rate with the much slower rate of Fe-catalysed oxidation or omit the pathway entirely. Although oxidation of SO_2 is responsible for the majority of sulfate production in clouds, the single particle $\delta^{34}S$ measurements showed that condensation of sulfuric acid gas and coagulation of ultrafine particulate dominate sulfate addition to fine particulate, and are therefore the most important in-cloud sulfate sources with respect to modification of the aerosol size distribution and the magnitude of direct and indirect radiative forcing.

Zusammenfassung

Sulfathaltiger atmosphärischer Feinstaub spielt eine große aber schwer zu quantifizierende Rolle im Klimasystem. Sulfathaltiger Feinstaub beeinflusst die Wolkenbildung, den Strahlungsantrieb und damit das Klimasystem, ist für die Entstehung von saurem Regen verantwortlich und kann die menschliche Gesundheit schädigen. Die Oxidation von Schwefeldioxid zu Sulfat ist eine wichtige Reaktion, die über die Auswirkungen des sulfathaltigen Feinstaubs in der Umwelt entscheidet, weil sie die Größenverteilung und chemische Zusammensetzung der Partikel beeinflusst. Diese Dissertation befasst sich mit der Bestimmung der stabilen Schwefelisotopenfraktionierung während der Oxidation von Schwefeldioxid zu Sulfat in der Gasphase und auf flüssigen oder festen Feinstaubpartikeln. Die neu bestimmten Isotopenfraktionierungskonstanten wurden verwendet um die Sulfat Neubildung in Feinstaubpartikeln während des Durchgangs durch eine orographische Wolke, als Teil des "Hill Cap Cloud Thuringia" HCCT Experiments, in Thüringen in Mitteldeutschland zu untersuchen.

Die stabile Schwefelisotopenfraktionierung für die Oxidation von SO_2 durch das ·OH Radikal wurde bestimmt, indem Schwefeldioxid mit einer bekannten Isotopenzusammensetzung in einem Durchflussreaktor ·OH Radikalen ausgesetzt wurde. Die ·OH Radikale wurden durch die Photolyse von Wasserdampf generiert und die Reaktion wurde bei Temperaturen von -25°C, 0°C, 19°C und 40°C durchgeführt (Kapitel 2). Am Ausgang des Reaktors wurden das Produkt, Sulfat, und das verbliebene Edukt, Schwefeldioxid, gesammelt und zu $BaSO_4$ umgefällt. Die stabile Schwefelisotopenzusammensetzung von beiden wurde mittels Cameca NanoSIMS 50 bestimmt. Die Schwefelisotopenfraktionierungskonstante für das $^{34}S/^{32}S$-Verhältnis während der Oxidation von Schwefeldioxid in der Gasphase ist $\alpha_{OH} = (1.0089 \pm 0.0007) - ((4 \pm 5) \times 10^{-5})T$ (°C). Die stabile Isotopenfraktionierungskonstante der wichtigsten Oxidationswege in der Flüssigphase wurde bestimmt, indem SO_2 (g) durch eine flüssige Lösung mit H_2O_2 geblubbert wurde, und indem SO_2 (g) und O_3 (g) gemeinsam durch Wasser geblubbert wurden. Die stabile Schwefelisotopenfraktionierung für die Reaktion SO_2 (g) $\rightarrow\rightarrow$ Sulfat (aq) ist unabhängig vom Oxidationsmittel (O_3 oder

H_2O_2) $\alpha_{aq} = (1.0167 \pm 0.0019) - ((8.7 \pm 3.5) \times 10^{-5})$T (°C) (Kapitel 2). Messungen in Lösungen mit unterschiedlichem pH Wert wurden genutzt, um die stabile Isotopenfraktionierung während der einzelnen Reaktionen dieser Umwandlung zu bestimmen (Kapitel 3). Der Beitrag des Phasenübergangs war am kleinsten, während die Hydratation für den größten Teil der Fraktionierung verantwortlich ist ($\alpha_{phase} = 1.00256 \pm 0.00024$ und $\alpha_{hydration} = 1.0105 \pm 0.0037$, bei 19°C). Außerdem wurde die stabile Schwefelisotopenfraktionierung auch für einzelne Tropfen anstatt für eine Bulklösung bestimmt. Die Ergebnisse zeigen, dass mikrophysikalische Prozesse in Tropfen die Isotopenfraktionierung nicht beeinflussen.

Mineralstaub und Seesalz stellen nicht nur den größten Masseanteil des Feinstaubs in der Atmosphäre, sie spielen auch eine wichtige Rolle für die heterogene Oxidation von SO_2 auf der Oberfläche von Feinstaubpartikeln, die die Größenverteilung des Sulfats in Richtung größerer Partikel verschiebt und die Neubildung von gasförmiger Schwefelsäure unterdrückt und damit sowohl die Partikelneubildung als auch die Entstehung von saurem Regen einschränkt. Aus diesem Grund wurde die Oxidation von Schwefeldioxid auf diesen beiden Feinstaubarten genauer untersucht. Die Alkalinität von Seesalzaerosol ist für die Sulfat Neubildung besonders wichtig: SO_2 Oxidation katalysiert durch das ·Cl Radikal und Oxidation durch O_3 kann nur bei hohen pH Werten effizient stattfinden und ist deshalb durch die Neutralisationsfähigkeit des Seesalzes begrenzt. Die Oxidation, welche durch Metalle der Übergangsgruppe katalysiert wird, und die Oxidation durch HOCl, sind unabhängig vom pH Wert und können daher weiter stattfinden, auch wenn der Feinstaub bereits säurehaltig ist. Die Aufteilung zwischen pH limitierten und nicht pH limitierten Reaktionswegen ist daher sehr wichtig, um abzuschätzen, wie viel Sulfat insgesamt in der marinen Grenzschicht produziert wird. Die stabilen Schwefelisotopenfraktionierungskonstanten für diese Reaktionen wurden bestimmt, indem Aerosol aus Wasser, NaOCl und sulfatfreier Seesalzlösung hergestellt wurde, und eine Reaktion mit SO_2 mit bekannter Isotopenzusammensetzung in einem Aerosolflussreaktor durchgeführt wurde (Kapitel 3). Oxidation durch die pH limitierten Reaktionswege (durch O_3 und die ·Cl Katalyse) reichern das schwerere Isotop im Produkt an ($\alpha_{34} = 1.0163 \pm 0.0018$ bei niedrigen pH Werten und $\alpha_{34} = 1.0199 \pm 0.0024$ bei hohen pH Werten, bei 19°C) während nicht pH limitierte Reaktionswege (Übergangsmetalle und HOCl) das leichtere Isotop im Produkt anreichern ($\alpha_{TM-Kat} = 0.9905 \pm 0.0031$ und $\alpha_{OCl} = 0.9882 \pm 0.0036$, bei 19°C). Die Fraktionierung auf synthetischem Seesalzaerosol ($\alpha_{Seesalz} = 1.0124 \pm 0.0017$ bei 19°C) zeigt, dass HOCl, trotz der kurzen Dauer des Experiments, ungefähr 19% zur gesamten Sulfatneubildung beiträgt. Dies unterstreicht die potentielle Bedeutung dieses Reaktionswegs

in der Umwelt, wenn die Reaktion über längere Zeit fortschreitet nachdem die Feinstaubpartikel bereits angesäuert sind. Wenn die Messung der stabilen Schwefelisotopen in den verschiedenen schwefelhaltigen Komponenten der Atmosphäre (SO_2 (g), H_2SO_4 (g) und Feinstaubpartikel) mit der Bestimmung der $\Delta^{17}O$ Werte der Feinstaubpartikel kombiniert wird, ist es möglich, den relativen Beitrag aller Reaktionswege, die in der Atmosphäre zur Sulfatbildung beitragen können, einzuschränken.

Mineralstaub stellt insgesamt den größten Masseanteil des Feinstaubs in der Atmosphäre. Oxidation von SO_2 auf Mineralstaub kann in einer Flüssigphase stattfinden, wenn Übergangsmetallionen, welche aus den Staubpartikeln ausgelaugt werden, eine Radikalkettenreaktion einleiten. Auch auf der Oberfläche von trockenen Staubpartikeln kann eine Oxidation als Folgereaktion von Chemisorption von SO_2 auf der Stauboberfläche stattfinden. Obwohl die erstgenannte Reaktion um vieles schneller ist und global dominiert, wirkt Mineralstaub in der Regel erst mehrere Tage nach seiner Emission als Wolkenkondensationskeim. Deshalb kann die Oxidation auf der Oberfläche des trockenen Staubes gerade in den Quellgebieten des Mineralstaubes sehr wichtig sein. Um die stabile Schwefelisotopenfraktionierung während der Oxidation auf trockenem Mineralstaub zu untersuchen, wurde Mineralstaub aus der Sahara auf den Cap Verde Inseln gesammelt und in einem modifizierten Knudsen Reaktor SO_2 mit bekannter Isotopenzusammensetzung ausgesetzt (Kapitel 4). Die Oxidation in der Flüssigphase wurde untersucht, indem der Staub mit MilliQ-Wasser ausgelaugt wurde und dann SO_2 mit bekannter Schwefelisotopenzusammensetzung durch diese Lösung geblubbert wurde. Die Schwefelisotopenfraktionierung betrug $\alpha_{\text{leachate}} = 0.9917 \pm 0.0046$ bei 19°C und war damit im Rahmen des Messfehlers identisch mit der Fraktionierung in Fe^{2+}/Fe^{3+}-Lösung ($\alpha_{\text{Fe}} = 0.9894 \pm 0.0043$). Die Reaktion in der Laugungslösung war mehrere Größenordnungen schneller als die in der reinen Eisenlösung, was zeigt, dass das Zusammenwirken mehrerer Metallionen die Reaktionsgeschwindigkeit entscheidend beeinflusst. Die Oxidation auf der Oberfläche von Mineralstaubpartikeln wurde untersucht, indem SO_2 bei 19°C unter verschiedenen experimentellen Bedingungen (z.B. mit und ohne Bestrahlung, O_3 und 40% relative Luftfeuchte) über einen Filter mit Mineralstaubpartikeln geführt wurde. Ein multivariates Modell wurde benutzt, um den Einfluss der chemischen Zusammensetzung des Mineralstaubs und der verschiedenen Reaktionsbedingungen auf die stabile Schwefelisotopenzusammensetzung des produzierten Sulfats zu untersuchen. Der Mittelwert für die Schwefelisotopenfraktionierung auf trockenem Saharastaub betrug $\alpha_{\text{surface}} = 1.0096 \pm 0.0036$. Der größte Teil der Oxidation erfolgte auf Eisen- und Titanoxiden. Nur die Tonmineralfraktion (12% der Oxidation) produzierte eine Schwefelisotopenfraktionierung, die es erlaubt, den

Beitrag dieser Fraktion unter atmosphärischen Bedingungen vom Beitrag anderer Reaktionen zu unterscheiden ($\alpha_{\text{clay}} = 1.085 \pm 0.013$). Die in dieser Arbeit bestimmten Schwefelisotopenfraktionierungskonstanten erlauben unter atmosphärischen Bedingungen insbesondere den Beitrag der Oxidation in Mineralstaublauge in der Flüssigphase und die Rolle der Reaktion auf Tonmineralen einzugrenzen.

Während des HCCT Experiments in Thüringen im Herbst 2010 wurden die stabilen Schwefelisotope in SO_2 (g), H_2SO_4 (g) und die schwefelhaltigen Feinstaubpartikel in ein und derselben Luftmasse untersucht, bevor, während und nachdem sich diese Luftmasse in einer orographischen Wolke aufhielt (Kapitel 5). Die Schwefelisotopenverhältnisse des gasförmigen Schwefels wurden gemessen, nachdem dieser als $BaSO_4$ ausgefällt wurde. Bei den Feinstaubpartikeln erlaubte eine Kombination von rasterelektronenmikroskopischen Untersuchungen und NanoSIMS Analysen die gemessenen Schwefelisotopenverhältnisse einzelner Partikelgruppen in Größen und Typen einzuordnen. Die gemessenen Werte wurden mit den im Labor bestimmten Isotopenfraktionierungskonstanten für die unterschiedlichen Oxidationswege verglichen. Dies erlaubt die Sulfatneubildung und Partikelumwandlungen innerhalb der Wolke und deren Einfluss auf die Partikelgrößenverteilung und Hygroskopizität zu untersuchen. Beide Faktoren sind sehr wichtig, um den direkten und indirekten Effekt von Aerosolen auf die Klimabilanz einzuschränken. Im Gegensatz zu den derzeit genutzten Atmosphären-Chemie-Modellen, die voraussagen, dass H_2O_2 die Oxidation von Schwefeldioxid in Wolken dominiert, zeigen die in diesem Kapitel präsentierten Ergebnisse, dass die Oxidation durch Metalle der Übergangsgruppe die Umwandlung von Schwefeldioxid zu Sulfat innerhalb der Wolke dominiert. Die Ergebnisse zeigen, dass die Bedeutung dieses Oxidationsweges global unterschätzt wird, weil Modelle die Geschwindigkeit dieser Reaktion entweder mit der Geschwindigkeit der Reaktion in reiner Eisenlösung annähern, oder diese Reaktion überhaupt nicht berücksichtigen. Obwohl die Oxidation von SO_2 für den Großteil der Sulfatneubildung innerhalb der Wolke verantwortlich ist, zeigen die Einzelpartikelmessungen, dass die Kondensation von gasförmiger Schwefelsäure und die Koagulation mit ultrafeinen Partikeln hauptverantwortlich für die Sulfatneubildung in Partikeln des Akkumulationsmodus sind. Diese beiden Sulfatquellen beeinflussen deshalb maßgeblich die Veränderungen der Größenverteilung und die chemische Zusammensetzung von Feinstaubpartikeln innerhalb von Wolken, und in weiterer Folge die Klimabilanz von Feinstaub.

Contents

Chapter 1

Introduction

Sulfate and sulfur dioxide play an important role in radiative forcing of the climate through their effect on aerosols, and are also important for acid deposition, human health, and heterogeneous chemical reactions. The majority of anthropogenic sulfur is released directly as SO_2, and a significant fraction of biogenic and natural sulfur (e.g. OCS, DMS) is also either directly released as SO_2 or oxidised to SO_2 in the atmosphere (Berresheim et al., 2002; Seinfeld and Pandis, 1998). Around 50% of global atmospheric sulfur dioxide is then oxidised to sulfate, while the rest is lost through dry and wet deposition (Chin et al., 1996, 2000). Sea salt is the only major source of primary sulfate to the atmosphere. The pathway by which SO_2 is oxidised to sulfate is critical in determining the radiative and environmental effects of sulfate. While results are able to show with a moderately high level of confidence that sulfate aerosols are responsible for cooling that has partially counteracted the effects of Greenhouse gas warming (Denman, 2007), the magnitude and expected future changes in indirect and direct sulfate aerosol forcing remain one of the largest uncertainties associated with assessments of climate change (Solomon, 2007). This thesis explores the use of sulfur isotopes to understand SO_2 oxidation in the atmosphere, in order to improve our understanding of the sulfur cycle and its effect on the environment and climate.

1.1 The sulfur cycle

Sulfur is released into the atmosphere from a wide variety of emission sources (Table 1.1). Although the uncertainty in estimates is high, non-sea salt sulfur emissions are clearly dominated by anthropogenic and volcanic SO_2 and oceanic DMS. After release, sulfur compounds tend to become oxidised (Seinfeld and Pandis, 1998). The yield of SO_2

Table 1.1: **Global sulfur emissions** in Tg(S) yr^{-1}, adapted from Seinfeld and Pandis (1998).

	H_2S	**DMS**	**CS_2**	**OCS**	**SO_2**	**Sulfate**	**Total**
Anthropogenic				0.08	72-8	2.3	73-80
Marine	<0.3	15-25	0.08	0.08		40-320	55-345
Volcanic	0.5-1.5			0.01	7-8	2-4	9-12
Other natural sources	0.2-1.6	0.05-0.8	0.02-0.05			2-4	0.3-3
Total							98-120

from DMS oxidation is 50-90% (Faloona, 2009; Faloona et al., 2009; Shon et al., 2001). Slightly more than 50% of atmospheric SO_2 is oxidised to form sulfate (Koch et al., 1999; Liao et al., 2003). The oxidation of SO_2 to sulfate follows several major pathways in the atmosphere. ∼20% of sulfate is produced in the gas phase from the reaction of SO_2 with ·OH radicals (Tanaka et al., 1994; Berglen et al., 2004):

$$SO_2 + \cdot OH + M \rightarrow \cdot HOSO_2 + M \tag{1.1}$$

$$\cdot HOSO_2 + O_2 \rightarrow SO_3 + HO_2 \tag{1.2}$$

$$SO_3 + H_2O \rightarrow H_2SO_4 \tag{1.3}$$

The majority of oxidation occurs in the aqueous phase following the dissolution of SO_2 (Eriksen, 1972a):

$$SO_2(g) \rightleftharpoons SO_2(aq) \tag{1.4}$$

$$SO_2(aq) + H_2O \rightleftharpoons HSO_3^- + H^+ \tag{1.5}$$

$$HSO_3^- + H^+ \rightleftharpoons H_2SO_3 \tag{1.6}$$

$$HSO_3^- \rightleftharpoons SO_3^{2-} + H^+ \tag{1.7}$$

$$2HSO_3^- \rightleftharpoons H_2O + S_2O_5^{2-} \tag{1.8}$$

Equation 1.6 has a pK_a of 1.77 and Equation 1.7 has a pK_a of 7.19 (Moore et al., 2005). Following dissolution, S(IV) is primarily oxidised by H_2O_2, O_3, and O_2 catalysed by transition metals such as Fe and Mn, while other oxidants such as hypohalous acids, HO_2NO_2, and catalysis by ·Cl radicals are important in certain environments (Hoppel and Caffrey, 2005; von Glasow, 2006; Tsai et al., 2010). Sulfur dioxide can also be directly oxidised on the surface of particles such as mineral dust (Dentener et al., 1996).

The environmental and climatic effect of sulfate depends strongly on the formation pathway. Gas-phase oxidation produces gaseous H_2SO_4 which can nucleate to form new

particles. Nucleation is not well understood, and field and laboratory studies suggest other products of the reaction between SO_2 and ·OH (Berndt et al., 2008; Laaksonen et al., 2008) or other chemical species such as NH_3 and ions (Maekelae et al., 1997; Eisele et al., 2006; Iida et al., 2006) may play a role in nucleation. Nucleation events can cover a local or a regional scale, and typically increase particle concentrations by a factor of between 2 and 10 (Kulmala et al., 2004). The nucleation rate $J_{3\mathrm{nm}}$ is usually 0.01 - 10 cm^{-3} s^{-1} but it can reach 100 cm^{-3} s^{-1} in urban areas and 10^4 - 10^5 cm^{-3} s^{-1} in coastal areas or industrial plumes (Kulmala et al., 2004). Newly formed particles grow throughout the day at rates of 1 - 20 nm hr^{-1} and may grow large enough to act as cloud condensation nuclei (CCN) before being lost through coagulation (Kulmala, 2003). Heterogeneous and aqueous oxidation of SO_2 does not lead to the production of new particles, as the sulfate produced is added to pre-existing particles. Sulfate addition increases the size, hygroscopicity and acidity of these particles, which has important effects on climate and the environment, in particular by increasing CCN activity and altering direct scattering efficiency. The following section focusses on the climatic effects of sulfate.

1.2 Aerosol radiative forcing

This section presents a discussion of aerosol radiative forcing, and how the magnitude and expected future changes in sulfate aerosol cooling are dependent on partitioning between sulfate formation pathways. The magnitude of past and current aerosol radiative forcing and the direction of future changes contributes the largest uncertainty in current estimates of climate change, as shown in Figure 1.1 (Solomon et al., 2007), although results are able to show with a moderately high level of confidence that sulfate aerosols are responsible for cooling that has partially counteracted the effects of Greenhouse gas warming (Denman, 2007).

The direct aerosol effect refers to the direct scattering of solar radiation back to space by aerosol particles, and results in a cooling of -0.3 to -1.0 W m^{-2} (Jones et al., 1994; Boucher and Lohmann, 1995). Scattering is most efficient for particles with sizes equal to the wavelength range of visible light, ie. the size range 0.3 - 0.8 μm. Ultrafine particulate produced from nucleation following homogeneous oxidation is too small for efficient scattering, therefore sulfate produced by heterogeneous oxidation pathways makes the greatest contribution to direct aerosol cooling (Yuskiewicz et al., 1999; Hegg et al., 2004).

The magnitude of the indirect effect is -1 W m^{-2} (Jones et al., 1994; Boucher and Lohmann, 1995), although the uncertainty in this estimate is much greater than uncer-

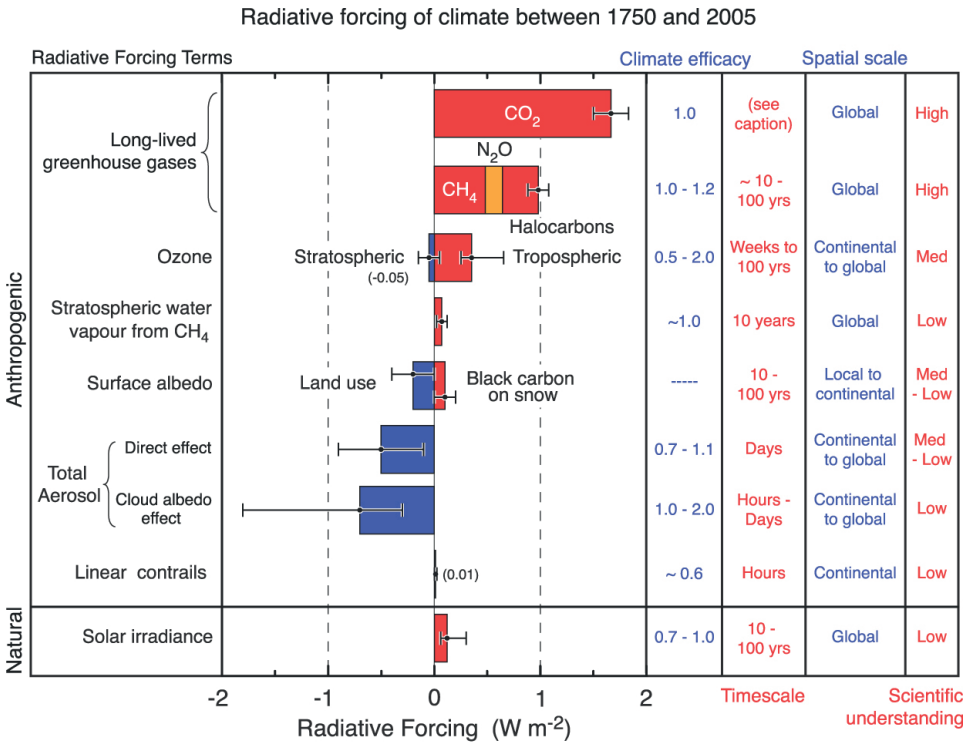

Figure 1.1: **Global mean radiative forcings from different agents and mechanisms**. The level of scientific understanding depends on both the evidence for the forcing and the level of consensus among forcing estimates. From Solomon et al. (2007).

tainty in the magnitude of direct radiative forcing. The first indirect effect, also known as the "Twomey effect", describes the increase in cloud albedo that results from having a larger number of CCN due to anthropogenic pollution emissions. If the liquid water content (LWC) is the same, the perturbed cloud has smaller, more numerous cloud droplets than the unperturbed cloud, and thus a higher albedo (Twomey, 1974, 1991). Sulfate produced by both gas-phase and heterogeneous pathways affects the CCN number concentration: New particles formed from H_2SO_4 (g) can grow by condensation of organics to a sufficient size to act as CCN, and sulfate produced on pre-existing particles increases both their hygroscopicity and size, making them more efficient CCN (Hegg, 1994). The increase in cloud droplet number concentration (CDNC) resulting from increased CCN concentration leads to the second indirect effect, whereby cooling is enhanced through reduced drizzle, increased cloud thickness, and longer cloud lifetimes (Albrecht, 1989; Pincus and Baker, 1994). The semi-direct effect can somewhat offset aerosol cooling, when dark, absorbing aerosols such as soot heat clouds, leading to evaporation and reduced cloud lifetime (Ackerman et al., 2000).

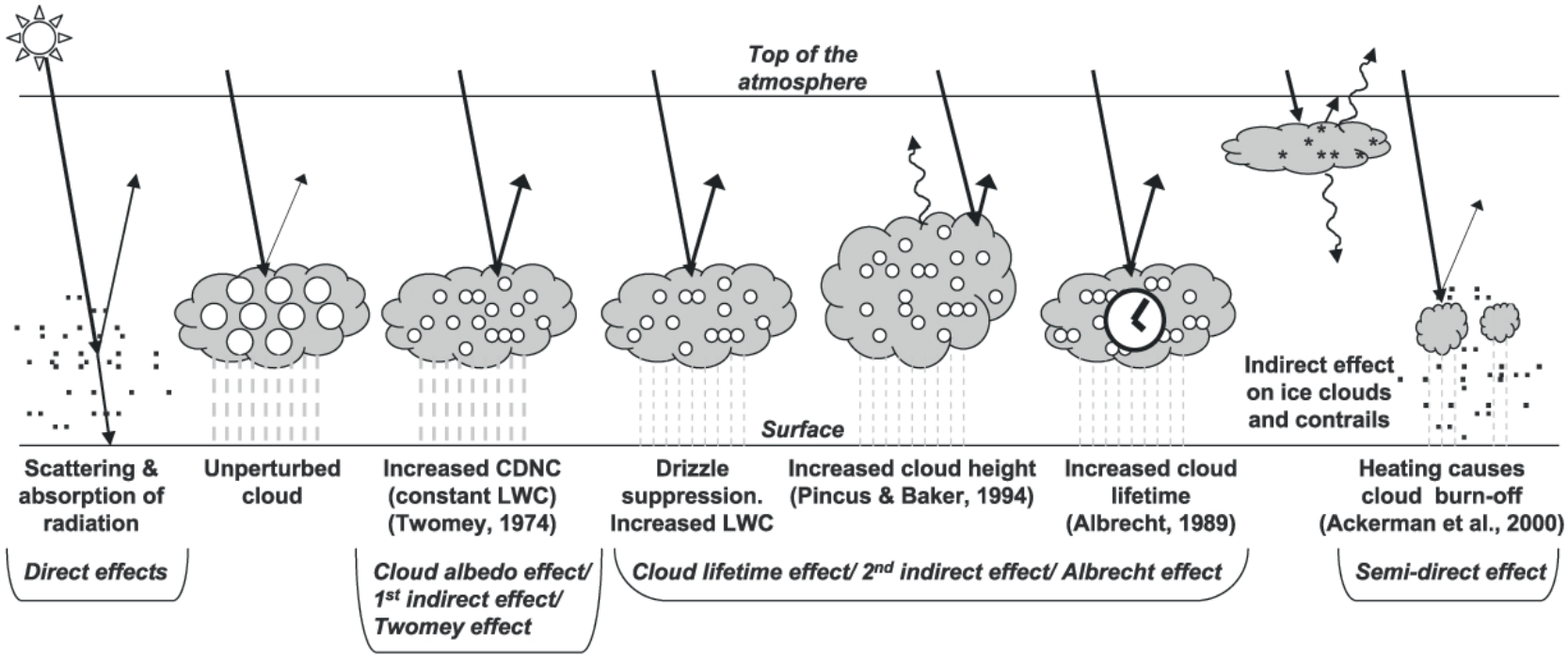

Figure 1.2: **Schematic diagram of significant aerosol radiative forcing effects** from Solomon et al. (2007). Small black dots are aerosol particles, larger open circles are cloud droplets and vertical grey dashes are rainfall. Straight lines represent incident and reflected solar radiation while wavy lines represent terrestrial solar radiation.

The various mechanisms of aerosol radiative forcing are summarised in Figure 1.2 (Solomon et al., 2007). The complexity of aerosol forcing mechanisms causes the relationship between SO_2 emissions and sulfate aerosol cooling to be highly non-linear and strongly dependent on the oxidation pathway by which sulfate is produced. The partitioning between oxidation pathways is not well understood, as it is dependent on the availability of oxidants, the SO_2 concentration, the relative humidity or cloud LWC, and the pH of the aqueous phase, which can vary with aerosol size and composition within a single aerosol population. In order to improve our understanding of aerosol radiative forcing and reduce uncertainty in climate change assessments, a greater understanding of partitioning between SO_2 oxidation pathways in different meteorological and chemical regimes is needed.

1.3 Sulfur isotopes in the environment

Sulfur has four naturally-occurring stable isotopes: ^{32}S, ^{33}S, ^{34}S and ^{36}S. The isotopic composition of a sample is described by the delta notation, which is the permil deviation of the ratio of a heavy isotope to the most abundant isotope (^{32}S) in the sample, compared to a standard ratio:

$$\delta^x S\ (‰) = [\frac{(\frac{n(^xS)}{n(^{32}S)})_{\text{sample}}}{(\frac{n(^xS)}{n(^{32}S)})_{\text{V-CDT}}} - 1] \times 1000 \tag{1.9}$$

where n is the number of atoms, ^xS is one of the heavy isotopes, ^{33}S, ^{34}S or ^{36}S, and V-CDT is the international sulfur isotope standard, Vienna Canyon Diablo Troilite, which has isotopic ratios of $^{34}S/^{32}S = 0.044163$ and $^{33}S/^{32}S = 0.007877$ (Ding et al., 2001).

The isotopic compositions of many major sulfur sources are well-constrained, and these are summarised in Figure 1.3. Sea salt sulfate and marine biogenic SO_2 (from DMS) are isotopically heavy, with $\delta^{34}S$ values of 21‰ and 14-22‰ respectively (Rees et al., 1978; Calhoun et al., 1991; Sanusi et al., 2006). Volcanic SO_2 emissions typically have an isotopic composition of $\delta^{34}S$ = 0-5‰. Geological sulfate, for example present in freshly-emitted mineral dust, has a sulfur isotopic composition of between 10 and 30‰ (Strauss, 1997). Anthropogenic SO_2 commonly has a $\delta^{34}S$ between -5 and 7‰ (Krouse et al., 1991; Nielsen et al., 1991), although values can vary widely on a global scale and are also affected by process technology such as flue gas desulfurization (Derda et al., 2007). SO_2 from biological sources is generally isotopically lighter than all other sources (Novak et al., 2001; Norman et al., 1999).

Isotopic composition changes during chemical reactions, depending on the relative

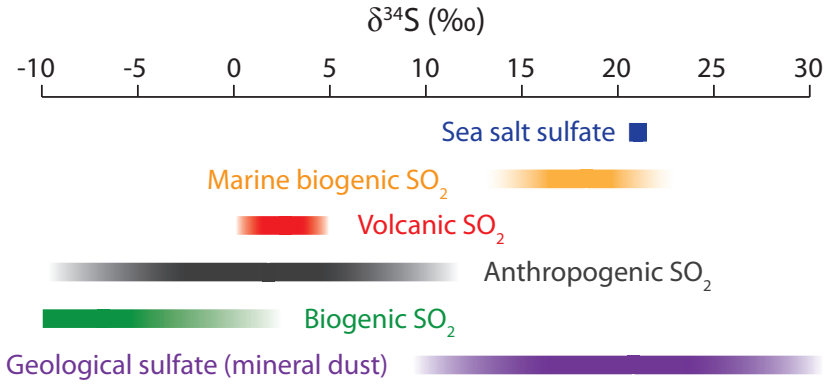

Figure 1.3: **Sulfur isotopic composition of major atmospheric sources**. Color gradients represent the normal range of variation. δ^{34}S values are from: sea salt, Rees et al. 1978; marine biogenic, Calhoun et al. 1991; Sanusi et al. 2006; volcanic, anthropogenic, Krouse et al. 1991; Nielsen et al. 1991; biogenic, Novak et al. 2001; Norman et al. 1999; geological, Strauss 1997.

reaction rates of the different isotopes. The relative reactions rates of the different isotopes are described by the kinetic fractionation factor α, which is represented by the ratio of the heavy to light isotope amounts in the instantaneously-formed product, divided by the ratio in the reactant:

$$\alpha_{34} = \frac{\left(\frac{n(^{34}\mathrm{S})}{n(^{32}\mathrm{S})}\right)_{\mathrm{products}}}{\left(\frac{n(^{34}\mathrm{S})}{n(^{32}\mathrm{S})}\right)_{\mathrm{reactants}}} \tag{1.10}$$

Values of α are characteristic for different reactions, such as the different SO_2 oxidation pathways. Seasonality and regional variations in isotopic composition are seen during field studies, reflecting both changing sources and the partitioning between SO_2 oxidation pathways. Measuring sulfur isotope ratios in ambient SO_2 and sulfate is therefore an ideal way to quantify partitioning between oxidation pathways, and to investigate how sulfate production varies across different regions and seasons. However, this relies on an accurate knowledge of the isotopic fractionation produced by the different pathways.

The fractionation factor for SO_2 oxidation in the aqueous phase has only been measured for SO_2 (g) $\rightleftharpoons$ S(IV) (aq), and measured values of the overall fractionation factor at 25°C range from $\alpha_{34} = 1.0103$ to 1.0173 with temperature dependencies from negligible to 0.14‰ $^{\circ}C^{-1}$ (Eriksen 1972a,d and Egiazarov et al. 1971 respectively). The effect of the terminating oxidant, ionic strength and pH on isotopic fractionation have not been investigated in previous laboratory studies. The fractionation factor for oxidation in the gas phase has not previously been measured, but it has been estimated to

be $\alpha_{34} = 0.991$ from *ab initio* calculations (Tanaka et al., 1994) and $\alpha_{34} = 1.14$ from RRKM theory (Leung et al., 2001). As the range between these estimates is larger than the range of sulfur isotope compositions observed in atmospheric samples (Figure 1.3), these values are not useful for interpreting ambient measurements. Seasonality in sulfur isotopic composition and measured differences between $\delta^{34}S_{SO_2}$ and $\delta^{34}S_{sulfate}$ in ambient samples have been proposed as a way to infer fractionation during the major oxidation pathways, however results are inconclusive due to factors such as seasonality in sources, temperature-dependence of fractionation factors, and the effect of transport and mixing on $\delta^{34}S$ (discussed futher in Section 2.4.3). The aim of this thesis is to measure the sulfur isotope fractionation for the major atmospheric oxidation pathways for SO_2, and to investigate the effect of different heterogeneous surfaces (sea salt and mineral dust) and pH on isotope fractionation. The measured fractionation factors are then used to understand the sulfur cycle occurring in orographic clouds during the HCCT campaign.

1.4 Thesis outline

The second chapter of this thesis (published as Harris et al. 2012b) presents measurements of sulfur isotopic fractionation during the major oxidation pathways: Oxidation in the aqueous phase by O_3, H_2O_2 and O_2 catalysed by a radical chain reaction pathway, and oxidation in the gas phase by ·OH radicals. The results presented in Chapter 2 provide characteristic fractionation factors for these oxidation pathways under laboratory conditions, however, atmospheric reactions occur in complex heterogeneous systems with varying pH and chemical composition. Chapters 3 and 4 therefore consider isotope fractionation during SO_2 oxidation on the two most important heterogeneous reaction surfaces, sea salt aerosol and mineral dust. Chapter 3, published as Harris et al. (2012c), presents experiments relating to oxidation on sea salt aerosol in the marine boundary layer. As sea salt aerosol is alkaline, experiments were carried out at different pHs allow the isotope fractionation factors for each step from SO_2 (g) $\rightarrow\rightarrow$ SO_3^{2-} (aq) to be isolated. The fractionation factors for oxidants specific to the marine boundary layer - HOCl and ·Cl catalysis - are presented, and isotope fractionation during oxidation in synthetic sea salt aerosol highlights the potential importance of the HOCl oxidation pathway. Chapter 4 considers oxidation in the aqueous phase in mineral dust leachate and on the surface of mineral dust at subsaturated relative humidity (published as Harris et al. 2012a). A multivariate analysis model is used to unravel the contribution of different minerals to the overall sulfate production and isotope fractionation on the dust surface.

The importance of the measured fractionation factors for interpreting field results is shown in Chapter 5, which presents measurements from the Hill Cap Cloud Thuringia Campaign (Harris et al., 2012d). The aim of the campaign was to investigate the chemical and physical processes occurring as an air parcel passed through an orographic cloud. Sulfur isotope measurements were used to determine the major SO_2 removal pathways in three cloud events, and to examine which sulfate sources and formation pathways were responsible for adding sulfate to the different particle classes observed in the cloud: fine and coarse secondary organic aerosol droplets containing inorganic salts, coated soot particles, and mineral dust. The results from the HCCT campaign demonstrate the use of the newly-measured fractionation factors in understanding atmospheric sulfate production, and illustrate the potential of sulfur isotope measurements for improving our understanding of the sulfur cycle and how it varies globally across different meteorological and chemical regimes.

Chapter 2

Sulfur isotope fractionation during oxidation of sulfur dioxide: Gas-phase oxidation by ·OH radicals and aqueous oxidation by H_2O_2, O_3 and iron catalysis

This chapter is published as Harris, E., Sinha, B., Hoppe, P., Crowley, J.N., Ono, S., and Foley, S. (2012) *Atmospheric Chemistry and Physics*, 12, 407-423, doi:10.5194/acp-12-407-2012

2.1 Introduction

Sulfate and sulfur dioxide play an important role in environmental chemistry and climate through their effect on aerosols. The majority of anthropogenic sulfur is released directly as SO_2, and a significant fraction of biogenic and natural sulfur (e.g. OCS, DMS) is also either directly released as SO_2 or oxidised to SO_2 in the atmosphere (Berresheim et al., 2002; Seinfeld and Pandis, 1998). Around 50% of global atmospheric sulfur dioxide is then oxidised to sulfate, while the rest is lost through dry and wet deposition (Chin et al., 1996). The oxidation pathway – heterogeneous or homogeneous – is an important factor, because it determines the effect that sulfate will have on the environment.

Homogeneous oxidation in the gas phase by ·OH radicals follows several steps (Tanaka

et al., 1994):

$$SO_2 + \cdot OH + M \rightarrow \cdot HOSO_2 + M \tag{2.1}$$

$$\cdot HOSO_2 + O_2 \rightarrow SO_3 + HO_2 \tag{2.2}$$

$$SO_3 + H_2O \rightarrow H_2SO_4 \tag{2.3}$$

The product is sulfuric acid, which can stick to the surface of existing particles or nucleate to form new particles in the atmosphere (Benson et al., 2008; Kulmala et al., 2004). These new particles have a direct radiative effect and may also grow to act as cloud condensation nuclei (CCN).

Heterogeneous oxidation acts upon S(IV) in solution or on particle surfaces. The major oxidants are H_2O_2, O_3 and O_2, the latter being catalysed by Fe^{3+} and other transition metal ions in a radical chain reaction pathway (Herrmann et al., 2000). The dissolution of SO_2 before oxidation follows several steps (Eriksen, 1972a):

$$SO_2(g) \rightleftharpoons SO_2(aq) \tag{2.4}$$

$$SO_2(aq) + H_2O \rightleftharpoons HSO_3^- + H^+ \tag{2.5}$$

$$HSO_3^- + H^+ \rightleftharpoons H_2SO_3 \tag{2.6}$$

$$HSO_3^- \rightleftharpoons SO_3^{2-} + H^+ \tag{2.7}$$

$$2HSO_3^- \rightleftharpoons H_2O + S_2O_5^{2-} \tag{2.8}$$

Equation 2.6 has a pK_a of 1.77 and Equation 2.7 has a pK_a of 7.19 (Moore et al., 2005). Oxidation by H_2O_2 is not significantly dependent on pH within normal atmospheric pH ranges (pH = 2–7), while oxidation by transition metal catalysis and O_3 becomes faster as pH increases (Seinfeld and Pandis, 1998). Heterogeneous oxidation produces sulfate on the surface of particles or in droplets, changing their CCN activity and lifetime through growth and increased hygroscopicity (Bower and Choularton, 1993; Mertes et al., 2005b). Thus, a comprehensive knowledge of the oxidation and removal of SO_2 and sulfate is key to understanding and modelling aerosol and cloud formation and processes and their effects on past and future climate.

Aerosol direct and indirect effects continue to contribute the largest uncertainty to estimates of anthropogenic global mean radiative forcing (Solomon et al., 2007). Global emissions of anthropogenic sulfur in Europe and North America have decreased significantly in the past few decades, however as Asian sulfur emissions are increasing due to energy demand and coal use, and are not expected to decrease until at least 2020 (Solomon

et al., 2007), anthropogenic emissions are likely to remain the major global source of non-sea salt sulfate (Chin et al., 1996; Seinfeld and Pandis, 1998). Understanding the sulfur cycle is therefore necessary to reduce the uncertainty in aerosol forcing estimates.

This study presents measurements of stable sulfur isotope fractionation during gas-phase oxidation by the ·OH radical and oxidation in the aqueous phase with H_2O_2, O_3 and iron catalysis as terminating reactions. These reactions are considered to be the most important sulfur dioxide oxidation pathways on a global scale. We demonstrate that stable sulfur isotope ratios can be used to investigate partitioning between atmospheric sulfur oxidation pathways and are particularly useful to estimate the importance of radical chain reactions for the atmospheric sulfur cycle. Differentiating between gas-phase oxidation by the ·OH radical and oxidation in the aqueous phase by H_2O_2 or O_3 will only be possible if stable sulfur isotope analysis is combined with measurements of the oxygen isotope anomaly $\Delta^{17}O$.

2.2 Sulfur isotopes in the environment

The isotopic composition of sulfur in the environment reflects its sources, transport and chemistry, so measurements of stable sulfur isotopes can be effectively used to constrain the sulfur cycle. Sulfur has four naturally-occurring stable isotopes: ^{32}S, ^{33}S, ^{34}S and ^{36}S. The isotopic composition of a sulfur sample is described with the delta notation, which is the permil deviation of the ratio of a heavy isotope to the most abundant isotope (^{32}S) in the sample compared to a standard ratio:

$$\delta^x S\ (‰) = [\frac{(\frac{n(^xS)}{n(^{32}S)})_{\text{sample}}}{(\frac{n(^xS)}{n(^{32}S)})_{\text{V-CDT}}} - 1] \times 1000 \tag{2.9}$$

where n is the number of atoms, ^xS is one of the heavy isotopes, ^{33}S, ^{34}S or ^{36}S, and V-CDT is the international sulfur isotope standard, Vienna Canyon Diablo Troilite, which has isotopic ratios of $^{34}S/^{32}S = 0.044163$ and $^{33}S/^{32}S = 0.007877$ (Ding et al., 2001).

Chemical reactions, for example the oxidation of SO_2 to sulfate, cause fractionation of isotope ratios between reactants and products as long as the reaction does not go to completion. The fractionation may be due to equilibrium or kinetic discrimination, and is represented by the fractionation factor α. For an irreversible reaction, fractionation is kinetic and α is the ratio of the rate constants: $\alpha = k_x/k_{32}$. When the reactant is present as an infinite reservoir and not affected by the reaction, α_{34} can be calculated from the isotopic compositions of products and reactants:

$$\alpha_{34} = \frac{R_{\text{products}}}{R_{\text{reactants}}} \tag{2.10}$$

where R = $\frac{^{34}S}{^{32}S}$. Thus, α>1 indicates that the heavy isotopes react faster than the light isotopes. The permil differences between reactants and products with regards to α and reaction extent in a closed system are described by the Rayleigh laws (Mariotti et al., 1981; Krouse and Grinenko, 1991), which are discussed in Sections 2.3.2 and 2.4.1. Thus, isotopic fractionation can not only distinguish between reactions: For known irreversible reactions in a closed system, the isotopic fractionation can provide quantitative information about how far the reaction has gone to completion.

The isotopic composition of many major sources of atmospheric sulfur have been measured (e.g., Rees et al., 1978; Krouse et al., 1991; Nielsen et al., 1991; Sanusi et al., 2006). The isotopic composition of anthropogenic sources is highly variable on a global scale, though individual sources are often well constrained. The isotopic composition of industrial emissions is also affected by process technology such as the flue gas desulfurization unit of an industrial plant (Derda et al., 2007). However, for field studies measuring the isotopic composition of both ambient SO_2 and sulfate, the major limitation to interpreting atmospheric isotope measurements is the lack of laboratory studies of the isotopic fractionation factors involved in the most common atmospheric reactions of sulfur (Tanaka et al., 1994; Novak et al., 2001; Tichomirowa et al., 2007). For heterogeneous oxidation, equilibrium fractionation of $^{34}S/^{32}S$ during the uptake of SO_2 into solution and the subsequent acid-base equilibria has been measured in several studies. The results range between $\alpha_{het} = 1.010$ and 1.017 at 25 °C (Egiazarov et al., 1971; Eriksen, 1972a). So far, the isotopic effect of the terminating oxidation of S(IV) to S(VI) has not been investigated.

The kinetic fractionation during homogeneous gas-phase oxidation of SO_2 by ·OH radicals has been estimated to be $\alpha_{hom} = 0.991$ by ab initio calculations (Tanaka et al., 1994) or to be $\alpha_{hom} = 1.14$ by RRKM theory (Leung et al., 2001). The discrepancy between these two estimates is larger than the measured variation in atmospheric sulfur samples (Norman et al., 2006). Several atmospheric studies have also tried to infer the fractionation during this reaction. Seasonality in data, with lower $\delta^{34}S$ values measured in summer, could show that the gas-phase fractionation factor is less than the heterogeneous fractionation factor and probably less than 1 (Saltzman et al., 1983; Sinha et al., 2008a). However, seasonality may also be explained by changing sources or the temperature-dependence of fractionation factors (Caron et al., 1986; Novak et al., 2001; Ohizumi et al., 1997). The study of $\Delta^{17}O$ of sulfate trapped in ice cores showed that the ratio of gas-phase to aqueous-phase oxidation was higher and the $\delta^{34}S$ was lower during the last glacial maximum than the preceeding and subsequent interglacials (Alexander et al., 2002, 2003). The authors suggest isotopic fractionation progressively affects the SO_2 reservoir during

transport as the sulfate is removed quickly, thus the data would show that $\alpha_{\mathrm{hom}}>\alpha_{\mathrm{het}}$. However, this progressive depletion in the reservoir signature has not been explicitly modelled and compared with measurements, so the isotopic composition in the ice-core could be directly representative of the oxidation and show that $\alpha_{\mathrm{hom}}<\alpha_{\mathrm{het}}$. Therefore, the goal of this study is to determine sulfur isotope fractionation factors for the main oxidation pathways of SO_2 to facilitate the use of sulfur isotopes in understanding the atmospheric sulfur cycle.

2.3 Experimental

2.3.1 Apparatus

The reaction system used to investigate the oxidation of SO_2 is shown in Figure 2.1. The reactors were made of glass and their internal surfaces were coated with FEP 121a (Dupont) to minimise wall loss of H_2SO_4. PFA tubing and connectors were used for gas transfer between experimental components. Pressure was monitored with a capacitance manometer. The reactor had a thermostatted jacket connected to a circulating cooler (Julabo Labortechnik GmbH, Model F81-HL) to regulate temperature. The actual gas-phase reaction temperature was calibrated to the set temperature of the Julabo instrument with a PT-100 Ω resistance sensor fitted into the glass reactor. The flows of all gases to the reactor were controlled using mass flow controllers referenced to standard conditions of temperature and pressure for N_2 ($T_s = 273.15$ K, $P_s = 1013.25$ mBar) (MKS Instruments Deutschland GmbH, uncertainty = 0.5% of reading plus 0.2% of full scale), and flows and leaks were checked regularly with a Gilibrator (Sensidyne, uncertainty < 1% of reading). SO_2 gas (Westfalen AG, Linde AG, both 102 ppm ± 2% in synthetic air) was diluted with synthetic air (Westfalen AG, 20.5% O_2 in N_2) to the desired concentration before it entered the reactor. The outflow from the reactor passed through the H_2SO_4 glass and SO_2 bubbler collectors, described in detail in Section 2.3.4. The length of tubing from the reactor to the H_2SO_4 collectors was <7 cm, which would lead to a maximum of ∼22% loss of H_2SO_4 according to the wall loss calculations from Zasypkin et al. (1997) (Equation 2.15). This will be higher than the actual wall loss as the estimate is for glass and not PFA. The sulfuric acid will at this stage be nucleated (see Section 2.3.4), thus the isotopic effect will be negligible as the relative mass difference due to an isotopic substitution in a particle will be <<1%. Most experiments were run for 7–8 hours to generate sufficient product for isotopic analysis. The exact conditions of each experiment are detailed in the relevant section.

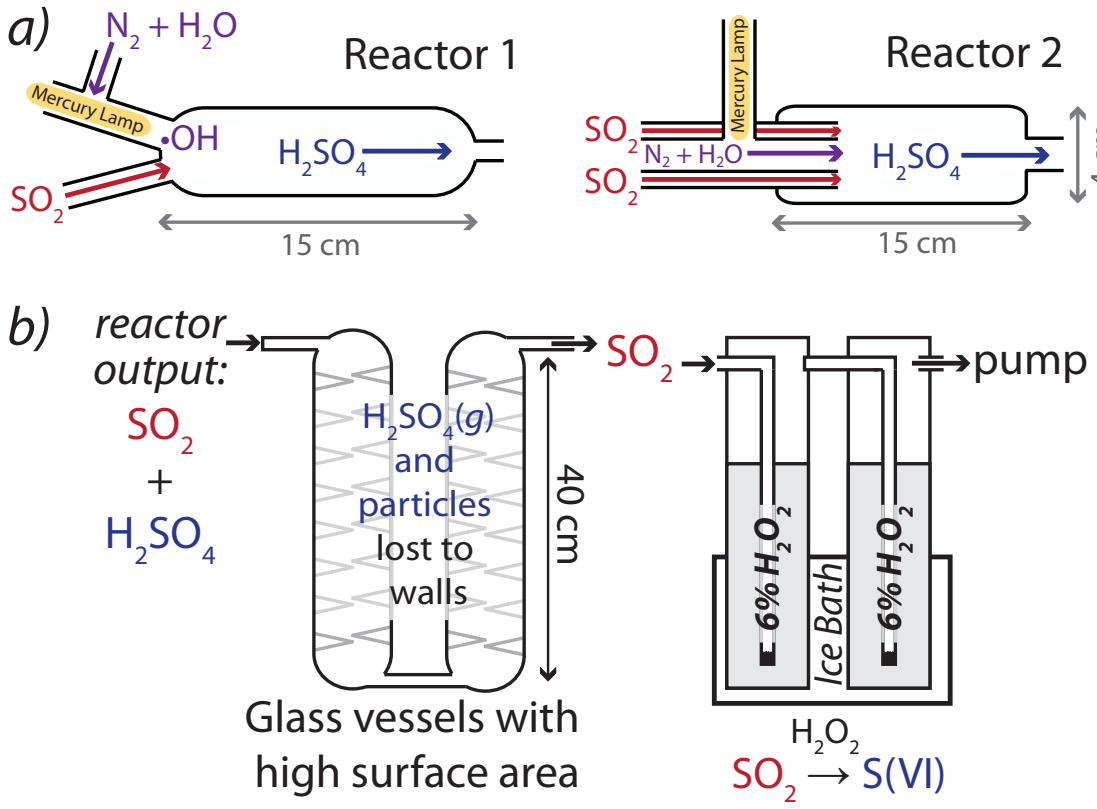

Figure 2.1: **Reaction system used to investigate oxidation of SO_2**: **(a)** reactors, **(b)** collection system.

Following each experiment, the collection systems were emptied immediately. The solution from the SO_2 bubblers, containing hydrogen peroxide and sulfate, was poured into a clean beaker and the bubblers were rinsed with MilliQ water several times into the beaker. The H_2SO_4 trap was rinsed at least five times with MilliQ water to remove all the adsorbed H_2SO_4, and the solution was collected in a beaker. An excess of $BaCl_2$ was added to each solution to precipitate S(VI) as $BaSO_4$, as well as sufficient HCl to lower the pH to approximately 3 for optimal precipitation (Rees and Holt, 1991). After at least 12 hours to ensure complete precipitation, the solutions were filtered through Nuclepore track-etch polycarbonate membrane filters (Whatman Ltd.) with 0.2 μm pores, which had been coated with a 10 nm thick gold layer using a sputter coater (Bal-tec GmbH, Model SCD-050) prior to sample collection. Several rinses with MilliQ water removed the majority of remaining $BaCl_2$ from the $BaSO_4$ precipitate and the filters were dried at room temperature. Samples with a large amount of material, where sulfate grains were clumped in groups, were gold-coated to prevent charging during SEM and NanoSIMS analysis.

2.3.2 Aqueous oxidation

Aqueous oxidation by the radical chain reaction mechanism

Aqueous oxidation by a radical chain reaction initiated by Fe^{3+} (Herrmann et al., 2000) was measured by bubbling SO_2 through a solution containing 0.1 M $Fe(Cl)_2$ and 0.1 M $Fe(Cl)_3$. The product sulfate was collected from two bubblers in series. The quantity and isotopic composition of the sulfate in the second bubbler was equal to that in the first bubbler, showing the SO_2 was not significantly depleted.

Aqueous oxidation by H_2O_2 in bulk aqueous phase

SO_2 gas was collected by bubbling through a solution of 6% H_2O_2 in an ice bath, thus the fractionation during collection of SO_2 is a direct measure of the fractionation during oxidation of SO_2 by H_2O_2 in solution at 0 °C under non-equilibrium conditions. This reaction was run eight times under a variety of conditions to fully characterise collection of SO_2 as described later in Section 2.3.4, and these experiments gave a robust value for the fractionation of sulfur isotopes during oxidation of SO_2 by H_2O_2.

Aqueous oxidation by H_2O_2 and O_3 in droplets

Oxidation by H_2O_2 and O_3 in the atmosphere occurs primarily in droplets and not in the bulk phase, thus it is necessary to investigate whether droplet-specific effects such as surface tension, the difference in saturation vapour pressure over a curved surface compared to a bulk solution, and changes in droplet pH as the reaction proceeds, affect the isotopic fractionation.

Reactor 2 (Figure 2.1) did not produce detectable ·OH (see Section 2.3.3 for details of ·OH quantification) at the reaction point where the humid, UV-irradiated air was mixed with the SO_2 flow. A small amount of ·OH was generated at the lamp tip in this reactor, however the residence time of humidifed air at the lamp was short and all ·OH generated was lost before reaching the reaction point. H_2O_2 was produced following H_2O photolysis to ·OH, and as the lifetime of H_2O_2 is longer than that of the ·OH radical, ∼5 ppbv (mol mol^{-1} gas at atmospheric pressure; ppbv will only be used to discuss gas phase concentrations) of H_2O_2 is present at the reaction point. O_3 resulting from photolysis of O_2 was present at concentrations of >10 ppmv at the reaction point.

The reaction was therefore run in Reactor 2 at close to 100% relative humidity to investigate aqueous oxidation by H_2O_2 and O_3 in droplets rather than a bulk solution in the absence of ·OH. The experiments were run at room temperature. Humid air

was generated by bubbling synthetic air through water and was added both through the photolysis tube and through a second entry into the reactor normally used to monitor pressure. Neither flow passed through a trap to break up or remove large droplets and the humidity was negligibly reduced by the addition of 10 cm^3 min^{-1} (at standard conditions of T = 273.15 K, P = 1013.25 mBar) dry SO_2 gas to make a total flow of 600 cm^3 min^{-1}, so the reactor was operated at 98% relative humidity in the presence of droplets. Although oxidation by ozone would initially dominate, the pH in the system would very quickly decrease as sulfate was generated so the bulk of the reaction would be due to H_2O_2 (Seinfeld and Pandis, 1998). A very large amount of product (>1 mg) was generated, which significantly altered the isotopic composition of the SO_2 gas. The fractionation factor α must therefore be found from the Rayleigh equations for residual reactants and products (Mariotti et al., 1981; Nriagu et al., 1991):

$$\alpha = \frac{\ln\left[\frac{R_R}{R_0}\right]}{\ln(f)} + 1 \tag{2.11}$$

and

$$\alpha = \frac{\ln\left[1 - (1-f)\frac{R_P}{R_0}\right]}{\ln(f)} \tag{2.12}$$

where f is the fraction of reactant (SO_2) remaining after the reaction time (residence time = 26 seconds) and R_0, R_R and R_P are the isotope ratios $^{34}S/^{32}S$ for the initial gas, the residual reactant and the product respectively. The reaction extent can be found from the isotopic mass balance:

$$\delta^{34}S_i = f \cdot \delta^{34}S_{SO_2} + (1-f) \cdot \delta^{34}S_{H_2SO_4} \tag{2.13}$$

where $\delta^{34}S_i$ is the initial composition of SO_2 and $\delta^{34}S_{SO_2}$and $\delta^{34}S_{H_2SO_4}$ are the isotopic compositions of residual SO_2 and product H_2SO_4 when a fraction f of the initial SO_2 remains. Around 65% of SO_2 was oxidised under high humidity conditions.

To isolate the effect of O_3 on the product isotopic composition, the reaction was run with a glass attachment that passed dry synthetic air over the Hg lamp to generate 1000 ppm ozone. As the photolysed air was dry the H_2O_2 concentration will be negligible. Humidified air at 40% relative humidity was added to the reactor and was not exposed to UV light. The product sulfate and the residual SO_2 were collected and there was no significant change in the SO_2 isotopic composition.

2.3.3 Gas-phase oxidation

·OH radicals were generated from the photolysis of water vapour, and allowed to react with SO_2 in the reactor shown in Figure 2.1. The SO_2 concentration was much higher than the ·OH concentration so the isotopic composition of SO_2 was not significantly affected by the reaction. The sulfuric acid gas product was collected, as described previously in Section 2.3.1, to determine the value of the fractionation factor for the reaction of SO_2 and ·OH.

·OH generation

·OH was generated from the photolysis of water vapour at around 30% relative humidity. 100 cm^3 min^{-1} of humidified nitrogen was passed over a low-pressure mercury vapour lamp (Jelight Company Inc., USA), which produces light at 184.9 nm resulting in the generation of ·OH radicals (Cantrell et al., 1997):

$$H_2O + h\nu \rightarrow \cdot OH + H \tag{2.14}$$

The ·OH concentration was determined from chemical titration of pyrrole (Sinha et al., 2008b, 2009), which entered the reactor through the SO_2 inlet and thus saw the same ·OH flux as SO_2. Two similar reactors were used to measure the ·OH + SO_2 reaction and the influence of potential interfering reactions (Figure 2.1, described further in Section 2.4.2). Reactor 1 produced 11 ppbv of ·OH. Reactor 2 did not produce detectable ·OH at the reaction point and was used to measure interferences. A small amount of ·OH would have been generated at the lamp tip, however the residence time of humidifed water at the lamp was short and all ·OH generated was lost before entering the reactor.

The ·OH concentration is dependent on the water vapour concentration (Young et al., 2008). In these experiments the relative humidity is kept constant by passing the humid air stream through glass wool held at the reaction temperature, in order to remove excess humidity and large droplets so that aqueous oxidation is minimised, thus the water vapour concentration will change exponentially with temperature according to the vapour pressure of water. The quantity of sulfate produced at the four different reaction temperatures was measured as described in Section 2.3.5 and found to follow the expected exponential relationship as shown in Figure 2.2b.

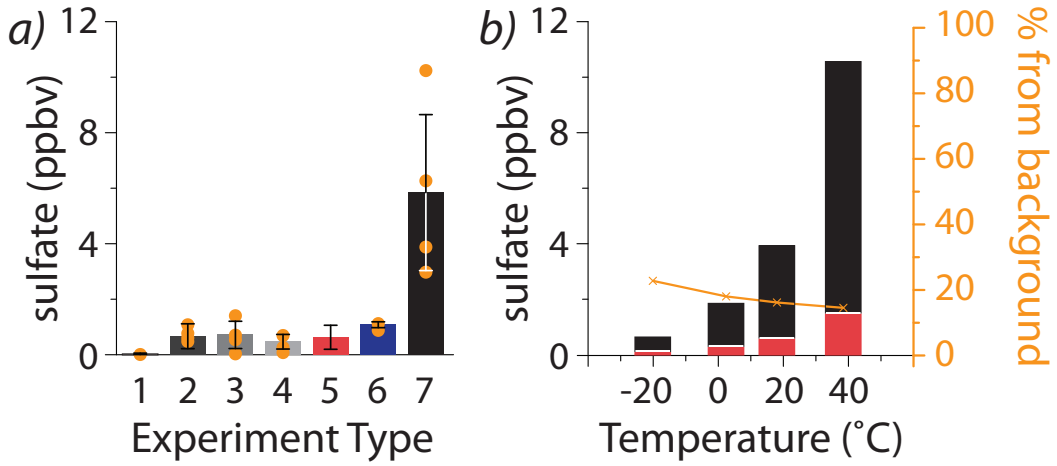

Figure 2.2: **Quantification of background in the reaction of SO_2 and ·OH**. **(a)** Total sulfate collected at room temperature under various conditions (individual samples are shown as orange dots, error bars are 1σ standard deviation of individual samples): (1) Background from impurities in MilliQ water and $BaCl_2$; (2) Direct photolysis of SO_2, 254 nm and 185 nm lines; (3) Direct photolysis, 254 nm line; (4) 254 nm and 185 nm lines, humidity passing over lamp; (5) 2–4 combined to show total production under UV light in the absence of ·OH; (6) no irradiation, no added oxidant; 7) 11 ppbv ·OH. **(b)** Temperature-dependence of sulfate production from ·OH reaction (black) and background from sulfate impurities in water (white) and background sulfate production (red), with the percentage contribution of the background to the total sulfate collected shown in orange.

2.3.4 Collection of SO_2 and H_2SO_4 products

H_2SO_4 collection

Sulfate is removed from the gas stream by passing through two 40-cm long glass vessels with a rough inside wall, which will increase turbulence and internal surface area (Figure 2.1). Two forms of sulfate product need to be collected in the experiments:

1. Aqueous droplet oxidation will results in water droplets containing sulfate. These will be lost to the glass walls by gravitational settling and by electrostatic attraction, which leads to collisions with the walls (Lai, 2006). This is a bulk process and is assumed not to introduce a significant isotopic effect, and will be very efficient given the length and roughness of the collectors.

2. Sulfuric acid gas will initially be produced in the gas-phase oxidation experiments but will nucleate to form particles of 1.5-2 nm diameter as the concentration of H_2SO_4 is >0.01-0.1 of the saturation vapour pressure (33 ppbv for 99% H_2SO_4)

(Kulmala et al., 2004, 2007). The loss of H_2SO_4(g) to the walls of glass vessels is described by:

$$[H_2SO_4]_t = [H_2SO_4]_0 \, e^{-kt} \tag{2.15}$$

where $[H_2SO_4]_0$ and $[H_2SO_4]_t$ are the gas phase concentrations of H_2SO_4 at time = 0 and time = t, k is the diffusion-limited first order reaction coefficient: $k = 3.65\frac{D}{r^2}$, D is the diffusion coefficient and r is the radius of the reactor (Zasypkin et al., 1997; Young et al., 2008). $D = 0.095\,\mathrm{cm^2\,s^{-1}}$ in dry air at atmospheric pressure and decreases to $0.075\,\mathrm{cm^2\ s^{-1}}$ at high humidity (Hanson and Eisele, 2000). These equations apply only to well-established laminar flow conditions in a cylindrical reactor and can provide a lower limit to wall loss in this system. Nanoparticles in the size range ∼2 nm will follow Brownian motion, like the sulfuric acid gas molecules, thus the wall loss calculation can be extended to estimate the loss of these ultrafine particles. The diffusion coefficient for 2 nm particles is ∼0.035 $\mathrm{cm^2\ s^{-1}}$ (extrapolated from Rudyak et al. (2009)), so the predicted wall loss will be >97% in the two condensers. The actual wall loss will be considerably higher than predicted as turbulence and electrostatic attraction in the system will increase the frequency of collisions with the walls. At this efficiency, there should be no significant difference between the initial and the product isotopic composition.

No isotopic standard of gaseous H_2SO_4 was available, so the fractionation during collection was measured by analysing the product from two collectors arranged in series. A flow of N_2 *6.0* (Westfalen AG) was passed through a 1 M solution of H_2SO_4 and the resulting mixture flowed through the two 40 cm-long glass collection vessels. This experiment will involve collection primarily of sulfuric acid droplets and not gas, however the results are relevant to the collection in the experiments since the gas-phase experiments will primarily result in freshly-nucleated particles while the aqueous droplet phase experiments will result in sulfate in droplets. Following the experiment, the collectors were rinsed and sulfate was precipitated by adding $BaCl_2$ and analysed as described in Section 2.3.5. The average measured differences between the $\delta^{34}S$ and $\delta^{33}S$ of the two collectors are -1.1 ± 2.6‰ and -0.3 ± 1.5‰ respectively, showing that there is no systematic fractionation introduced beyond the precision of the measurement (Table 2.1). A small or insignificant difference between the two collectors can only be achieved with a low collection efficiency or a fractionation factor close to 1, otherwise the $\delta^{34}S$ and $\delta^{33}S$ of the H_2SO_4 entering the second collector would be altered by the first collector. A high efficiency was theoretically predicted, and supported by the fact that very little product was seen on the second filter during analysis. Therefore, the fractionation introduced by

this collection method is insignificant and the δ^{33}S and δ^{34}S of H_2SO_4 in later experiments does not need to be corrected for an isotopic change during collection.

Table 2.1: **Fractionation of $^{34}S/^{32}S$ and $^{33}S/^{32}S$ between two collectors in series during collection of H_2SO_4.**

Run #	*1*	*2*	*3*	**Average**
Date	02.11.09	03.11.09	23.02.10	
N_2 flow rate (cm^3 min^{-1})	1500	1500	1720	
Length (hr)	6.3	8.3	6.1	
$\delta^{34}S_{C_1} - \delta^{34}S_{C_2}$	−3.3±2.1	2.4±2.5	−4.2±7.9	**−1.1±2.6**
$\delta^{33}S_{C_1} - \delta^{33}S_{C_2}$	0.7±2.2	−0.4±2.3	0.9±3.6	**0.3±1.5**

It is important to consider possible breakthrough of H_2SO_4 gas to the SO_2 gas collection system. Although H_2SO_4 is efficiently removed, when the H_2SO_4 concentration was more than three times as high as the SO_2 concentration, breakthrough of H_2SO_4 could be detected in the isotopic composition of SO_2. The sensitivity of the isotopic composition of the SO_2 to breakthrough also depends on the difference in δ^{34}S between SO_2 and H_2SO_4. To completely avoid effects from breakthrough of H_2SO_4 the reaction yield was kept below two thirds of the total SO_2.

SO_2 collection

Sulfur dioxide is traditionally collected on filters impregnated with alkaline solutions such as Na_2CO_3 (Novak et al., 2001; Huygen, 1963). A variety of solutions were tested with varying amounts of Na_2CO_3, $BaCl_2$, triethanolamine, glycerol and H_2O_2, and the average fractionation factor was measured as $\alpha = 1.007\pm0.003$ for all methods tested. The recovery of SO_2 was found to vary from less than 5% to more than 40% depending on the length of time that SO_2 was collected and the amount taken up relative to the alkalinity capacity of the filter, rather than on the solution composition. The fractionation in the final product could then vary from at least 4.5 to 10.6‰, with even larger variations introduced for longer experiments or very high filter loads. This method of collection is not suitable for our laboratory experiments due to the low relative humidity and high concentrations of SO_2 in our samples combined with the need for a constant, correctable isotopic fractionation.

Alternatively, SO_2 can be collected by passing the gas stream through bubblers containing hydrogen peroxide, which oxidises the S(IV) in the solution to sulfate (US-EPA,

2010). This method was tested by passing SO_2 of known isotopic composition ($\delta^{34}S$ = 1.25±0.3‰) through two bubblers in series containing a solution of 6% hydrogen peroxide, held at 0 °C in an ice bath to increase SO_2 solubility (Figure 2.1). Following the experiment a $BaSO_4$ precipitate was prepared by adding $BaCl_2$, and the precipitate was collected on a gold-coated Nuclepore filter. This experiment was repeated eight times, seven of which were analysed with the NanoSIMS as described in Section 2.3.5. One sample was analysed by traditional dual-inlet isotope ratio mass spectrometry at the Massachusetts Institute of Technology according to the methods described in Ono et al. (2006). The reaction conditions and measured fractionation factors are shown in Table 2.2.

Table 2.2: **Fractionation of $^{34}S/^{32}S$ during collection of SO_2** in a solution of 6% H_2O_2. [1]Measured by traditional duel-inlet isotope ratio mass spectrometry (Ono et al., 2006). [2]All values are corrected for the initial isotopic composition of +1.25 ‰. [3]Found from $\delta^{34}S_{tot} = (\delta^{34}S_{P_1} + f.\delta^{34}S_{P_2})\,/(1+f)$ for samples where the bubblers were measured separately.

Run #	*1*	*2*	*3*	*4*	*5*	*6*	*7*	*8*[1]	**Average**
Date	30.10.09	05.11.09	10.11.09	19.02.10	22.02.10	31.03.10	21.04.10	19.07.10	
Length (h)	6.0	6.6	5.6	3.0	2.9	4.1	5.6	3.2	
H_2O_2 volume (mL)	180	180	180	300	300	300	300	300	
$[H_2O_2]$ (%)	5	5	6	5	5	6	6	6	
$[SO_2]$ (ppm)	7.6	7.6	7.6	0.35	0.35	0.13	0.39	2.0	
SO_2 flow rate ($cm^3\ min^{-1}$)	1022	1022	1022	1700	1700	1700	600	510	
Gas Temperature	Room T	Room T	Room T	Room T	Room T	40 °C	Room T	Room T	
f	0.57	0.83		0.58	0.61	0.66			0.61±0.11
$\delta^{34}S$, 1st bubbler[2]	14.3±2.1	9.6±3.5	8.7±7.8	12.5±1.5	11.4±2.4	11.5±1.3			11.1±0.8
$\delta^{34}S$, 2nd bubbler[2]	3.2±1.8	8.9±3.5		3.2±0.9	4.3±5.5	5.4±2.2			3.7±0.7
$\delta^{34}S$, product[3]	10.1±2.8	9.3±4.9	6.6±7.9	9.1±1.7	8.7±6.0	9.2±2.5	11.1±3.2	9.1±1.0	9.2±0.7
α	1.017	1.016	1.011	1.015	1.015	1.015	1.019	1.016	**1.016±0.001**

2.3.5 SEM and NanoSIMS analysis

Scanning electron microscopy

A LEO 1530 field emission scanning electron microscope (SEM) with an Oxford Instruments ultra-thin-window energy-dispersive x-ray detector (EDX) was used to locate and characterise particles before NanoSIMS analysis. The samples were directly analysed in the SEM after collection on gold-coated filters without any further treatment. The SEM was operated with an accelerating voltage of between 10 and 20 keV, a 60 μm aperture and a working distance of 9.6 mm. "High current mode" was used to increase the EDX signal and improve elemental sensitivity. All samples were viewed with the SEM to investigate the coverage, size and shape of sulfate grains. A transfer of the coordinate system between the NanoSIMS and the SEM is possible using several well-defined origin points, which allows the same grain or area to be found and analysed in both instruments. An example of a barium sulfate grain with its EDX spectrum is shown in Figure 2.3.

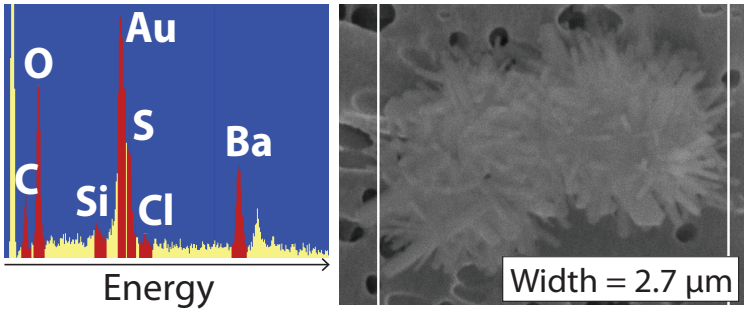

Figure 2.3: **EDX spectrum and SEM image of a typical $BaSO_4$ grain.**

Quantification with the SEM

The EDX spectrum can be used to roughly quantify compounds and particles on the filters, and thus estimate the extent of reactions. An automatic analysis of the filter is taken, with EDX analysis points distributed at regular intervals in each image. As long as the diameter of the largest particle is smaller than the distance between EDX points, the probability of the point falling on a particular particle is proportional to the area covered by that type of particle (Winterholler, 2007). Moreover, if an element is just in one form, for example sulfur is only present as $BaSO_4$, the number of points with a sulfur signal will be proportional to the area covered by $BaSO_4$. The volume and hence mass of $BaSO_4$ can be found by considering the average height of the $BaSO_4$ grains, as long as it is evenly distributed and not clumped in large heaps. The sample height was estimated to be 0.2

μm based on the movement in the Z-direction of the microscope needed to focus on the filter and on the top of a representative number of $BaSO_4$ grains. The largest source of uncertainty for quantification of the collected $BaSO_4$ is that grains can flake off the filter during handling of the samples.

The presence of a "signal" for an element in this quantification method requires differentiating between background noise and actual signal. Quantifying sulfur compounds on gold filters is challenging, because the gold peak overlaps strongly with the sulfur peak, as shown in Figure 2.3. The contribution of the gold peak to the sulfur peak approximately follows a Gaussian distribution, as gold is present in all sampled EDX points. An example is shown in Figure 2.4. The sulfur signal is superimposed on the Gaussian distribution of the gold signal, as the X-ray emission depth and spot size means the gold signal will always be present even when the sampling point falls on a barium sulfate grain (Goldstein et al., 1981). Thus, the presence of a significant sulfur signal was defined as falling above the 99.9% confidence limit for the gold Gaussian distribution ($x > \mu + 3.09\sigma$). The contribution of S in $BaSO_4$ to the signal in the sulfur channel shows a peak, however the number of sulfur points is too low to calculate the Gaussian distribution for these samples. To account for the tail of the Gaussian curve of Au that is above the 3.09σ limit, which could be a large part of the signal at low sulfate concentrations, the integrated background (bcg) above the 3.09σ limit was subtracted, and the number of points with a significant sulfur signal was defined as:

$$n(x > \text{bcg}) = n(x > \mu + 3.09\sigma) - 0.001[n(\text{total})] \tag{2.16}$$

The Gaussian curve does not always fit cleanly to the data. For samples where the area coverage is significantly less than 25%, a second estimate of the 3σ limit can be approximated by $Q_u + 1.726(Q_u - Q_l)$, where Q_u and Q_l are the upper and lower quartiles of the raw signal for the element of interest. This has previously been used to define the background of an SEM-EDX signal for a similar quantification method (Winterholler, 2007; Stoyan, 1998). EDX points with the signal for both barium and sulfur above the background are then used to quantify $BaSO_4$. The quantity of sulfate measured for a sample with the two methods has an average uncertainty of 40% and shows no systematic offset. The sulfate production in each experiment is an average of at least two duplicate samples both measured with the two methods. The limit of detection for quantification is the amount of sulfate when only one point shows a significant signal, and thus it depends on the total number of points taken. For most samples 10 000 EDX points were measured, giving a detection limit of 0.2 nmol of sulfate, or 0.18 ppbv at the typical flow rate of 600 cm^3 min^{-1}.

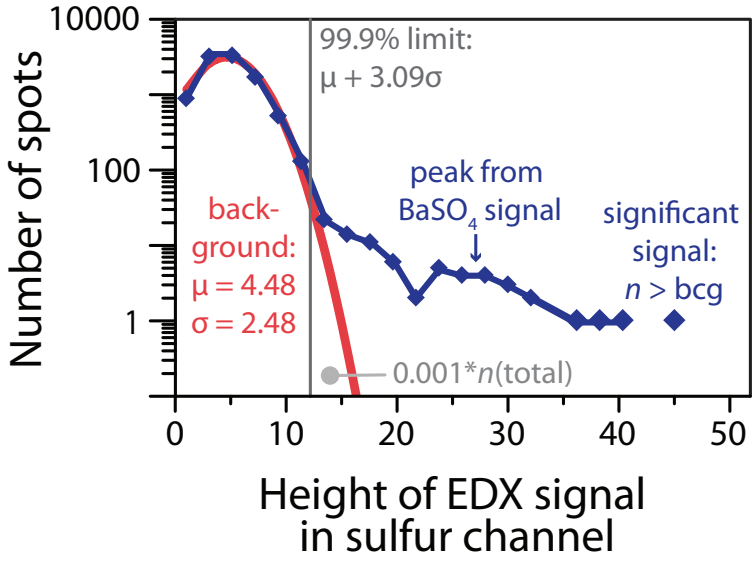

Figure 2.4: **Frequency of signal height in the sulfur channel of an automatic EDX analysis of $BaSO_4$ on a gold-coated filter**. The measured signal for the sulfur channel is shown in blue and the Gaussian fit to the contribution from the gold peak is shown in red.

NanoSIMS

The sulfur isotopic composition was determined with the Cameca NanoSIMS 50 ion probe at the Max Planck Institute for Chemistry in Mainz (Hoppe, 2006; Groener and Hoppe, 2006). The NanoSIMS 50 has a high lateral resolution (<100 nm) and high sensitivity and can simultaneously measure up to five different masses through a multicollection system, allowing high precision analysis of the small sample quantities (<<1 mg) required for this study. The use of this instrument to analyse sulfur isotope ratios is described in detail elsewhere (Winterholler et al., 2006, 2008), and only a brief description will be given here.

$BaSO_4$ is analysed directly without further processing after it is collected on gold-coated filters as described in Section 2.3.1. A ∼1 pA Cs^+ beam is focussed onto a ∼100 nm sized spot and rastered in a 2 μm × 2 μm grid over the grain of interest. The ejected secondary ions are carried into the mass spectrometer and multicollection system. Each measurement consists of 200–400 cycles of 4.096 s duration preceded by varying lengths of presputtering until the gold coating is removed and the count rate is stable. Presputtering is carried out on an area of at least 10 μm × 10 μm to avoid crater effects in the analysed area. Secondary ions of $^{16}O^-$, $^{32}S^-$, $^{33}S^-$, $^{34}S^-$ and $^{36}S^-$ were simultaneously detected in five electron multipliers at high mass resolution (M/ΔM >3900 for ^{33}S). The detector dead time is 44 ns and the count rates were corrected accordingly. The energy slit was set

at a bandpass of 20 eV and the transmission was set at 15–20% with the fifth entrance slit (10 × 100 μm) and the fourth aperture slit (80 × 80 μm) in order to reduce the effect of quasi-simultaneous arrival (QSA; Slodzian et al. (2001)).

Mass-dependent and mass-independent instrumental mass fractionation (IMF) can occur at several stages of the SIMS analysis, so the IMF correction factor in each measurement session is determined with the commercially available $BaSO_4$ isotope standards IAEA-SO5 and IAEA-SO6. Correction for the quasi-simultaneous arrival (QSA) effect was carried out as described by Slodzian et al. (2004), however a factor of 0.75 rather than 0.69 was used as this minimised the dependence on count rate best for these samples.

The number of counts is assumed to follow a Poisson distribution, so the counting statistical error is $\sqrt{n}$, i.e. the relative error is $1/\sqrt{n}$ (Bevington and Robinson, 1992). Some spot-to-spot variation is also seen between individual measurements on a filter, most likely due to topographic effects or nanoscale inhomogeneity. Thus, at least five grains on each sample filter were measured, and a weighted average was calculated using $1/\sigma^2$ for the weighting function, where σ is the counting statistical error of individual measurements. To calculate the overall measurement uncertainty the error of the weighted mean is multiplied by $\sqrt{\chi^2}$ for χ^2 >1 in order to account for the larger uncertainty introduced by the spot-to-spot variability. The counting statistical error was typically 1–2‰ and the overall error for each sample 2–5‰.

2.4 Results and discussion

2.4.1 Aqueous oxidation

The fractionation factors during aqueous oxidation by H_2O_2, O_3 and radical chain reaction initiated by Fe are shown in Figure 2.5 and Table 2.3. All oxidants other than O_3 produce mass-dependent fractionation, and the deviation from the mass-dependent fractionation line seen for O_3 is almost certainly a measurement artefact as only two samples were measured. ^{33}S measurements with the NanoSIMS are more uncertain than ^{34}S measurements, as they can be systematically inaccurate on a individual filter due to factors such as a change in the interference from ^{32}SH between the sample and the standard; thus they are only reliable if a larger number of samples are measured. The radical chain reaction, which has a fractionation factor of $\alpha_{34} = 0.9894 \pm 0.0043$ at 19°C, is the only measured aqueous reaction to favour the light isotope. This agrees relatively well with measurements by Saltzman et al. (1983), where a fractionation factor of 0.996 for oxidation of HSO_3^- by dissolved O_2 was indicated by laboratory experiments.

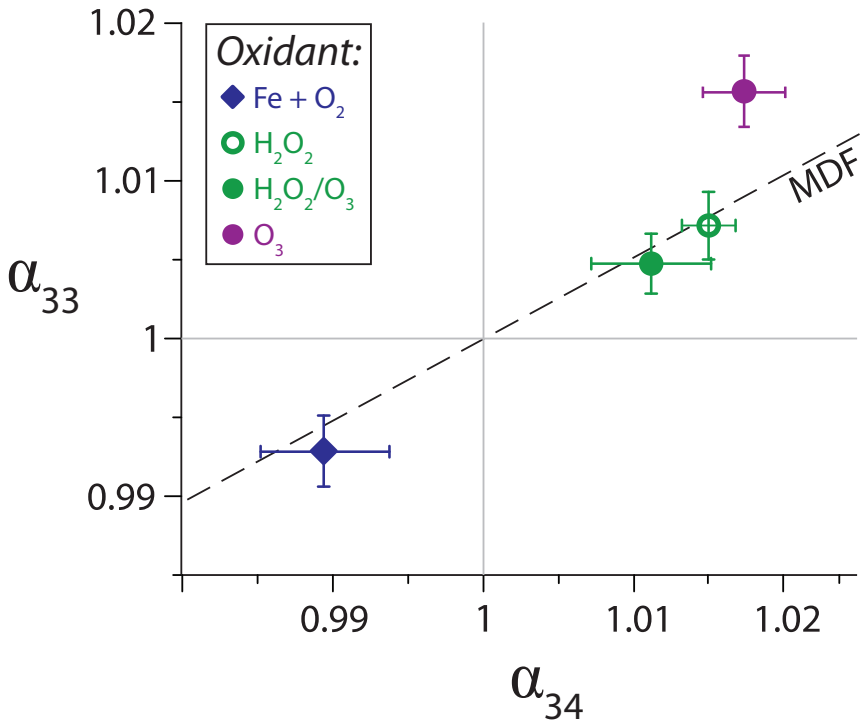

Figure 2.5: **Fractionation factors for the aqueous oxidation of SO_2 at 19 °C** by radical chain reaction initiated by Fe, H_2O_2 bulk solution (from temperature-dependent regression), and H_2O_2/O_3 and only O_3 in aerosol droplets. Error bars are the 1σ standard deviation and MDF is the mass-dependent fractionation line.

Table 2.3: **Fractionation factors at 19 °C for the aqueous oxidation of SO_2** by radical chain reaction initiated by Fe, H_2O_2 bulk solution (from temperature-dependent regression), and H_2O_2/O_3 and only O_3 in aerosol droplets.

Oxidant	α_{34}	1 σ	α_{33}	1 σ
H_2O_2	1.0151	0.0013	1.0071	0.0016
O_3	1.0174	0.0028	1.0157	0.0022
H_2O_2/O_3	1.0118	0.0040	1.0048	0.0019
radical chain	0.9894	0.0043	0.9928	0.0022

Isotopic fractionation during SO_2 collection

SO_2 was collected by bubbling through a solution of H_2O_2, which oxidises the S(IV) to sulfate. The collection is not complete, and as >1% of SO_2 is oxidised it can no longer be considered an unchanged reservoir. Thus the isotopic composition of the product depends on the value of the kinetic fractionation factor α ($= k_{34}/k_{32}$) and the fraction of reactant remaining, as described by the Rayleigh fractionation laws (Mariotti et al., 1981; Nriagu et al., 1991). Equation 2.12 from Section 2.3.2 can be used directly for the first bubbler, and adapted to represent the second bubblers in series:

$$\alpha_2 = \frac{\ln\left[1-(1-f)\frac{R_{P_2}}{R_0^*}\right]}{\ln(f)} \tag{2.17}$$

where f is the fraction of reactant (SO_2) remaining and R_0, and R_{P_2} are the isotope ratios $^{34}S/^{32}S$ for the initial gas and the product of the second bubbler respectively. R_0^* is the initial isotopic composition entering the second bubbler, that is, the residual SO_2 remaining after the first bubbler: $R_0^* = R_0 f^{\alpha_1 - 1}$.

The collection efficiency $(1-f)$ must be known to find α from these equations. Grains can flake off the filter during handling when a large amount of product is present (i.e. a layer rather than individual grains, >1 mg), leading to greater losses from the filter from the first bubbler as it has more product. Thus quantification by SEM-EDX as described in Section 2.3.5 does not give an accurate value for f. Gravimetric determination of f is not possible due to the interference from coprecipitated $BaCl_2$ and the very small quantities of sulfate on the second filter. The fraction of SO_2 remaining was therefore determined as the value that would give an equal α for the first and second collectors, found for each experiment by iteration with Equations 2.12 and 2.17. The weighted average of the individual values shows that 39% of SO_2 is collected per bubbler. The total collection efficiency of two bubblers in series is 63±11%. A higher concentration of H_2O_2 may be expected to improve collection efficiency, however this was not possible as it resulted in destruction of the gold coating on the filters during filtering to collect $BaSO_4$.

Equations 2.12 and 2.17 were then used to find α for each bubbler measurement. The reaction conditions and results are shown in Table 2.2 and Figure 2.6. The weighted average α_{34} is 1.0160±0.0013 at 0 °C, which results in a product $\delta^{34}S$ change of +9.2±0.7 ‰ following the two bubblers. This is consistent with expectations for aqueous oxidation by H_2O_2 (Eriksen, 1972a; Egiazarov et al., 1971) and is robust over a large range of flows and SO_2 concentrations. The gas temperature does not affect the measured fractionation since the collector is held at 0 °C and the quantity of gas passed through the sampling system is not sufficient to change the temperature within the collection system.

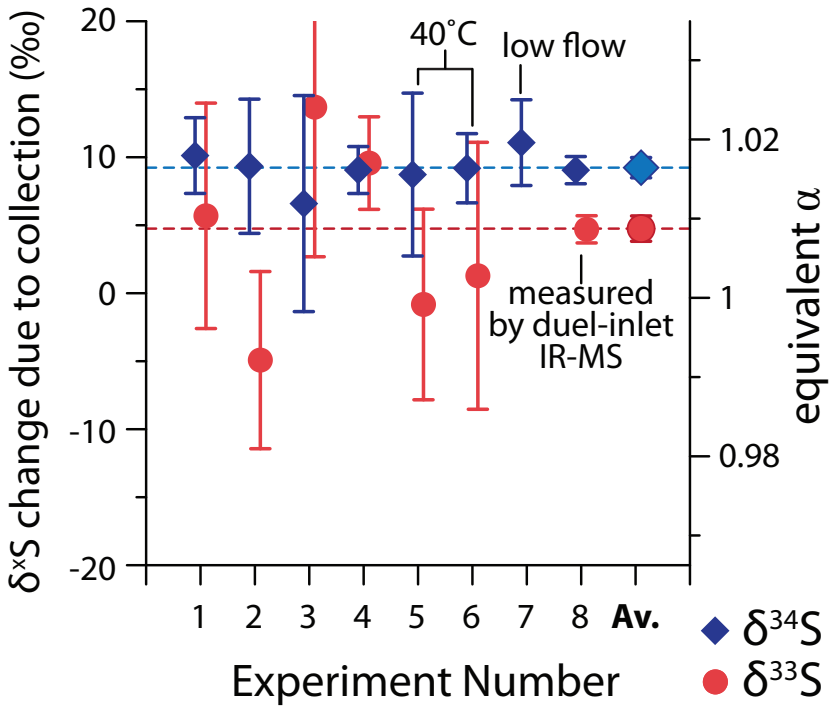

Figure 2.6: **Fractionation introduced during collection of SO_2 in H_2O_2 solution**. The duel-inlet IR-MS sample was measured as described in Ono et al. (2006). The shown data of experiments 1–7 are the weighted averages of individual NanoSIMS measurements, while the horizontal dashed lines and the two data points at the right side show the weighted averages of all experiments. Error bars are the 1σ standard deviation.

Measurements of $\delta^{33}S$ by NanoSIMS are more uncertain than $\delta^{34}S$ due to counting statistics. The measured α_{33} is 1.007±0.002, which is not significantly different from the value expected for mass-dependent fractionation (MDF: $\alpha_{33}/\alpha_{34} = 0.515$, t-test, $P = 0.05$). The mass-dependent nature of the fractionation is confirmed by the high precision measurement of Sample 8, which showed $\Delta^{33}S = 0.05‰$. The change in $\delta^{34}S_{SO_2}$ and $\delta^{33}S_{SO_2}$ due to reactions of interest in all other experiments can be isolated by considering the measured fractionation due to collection and the initial isotopic composition.

Oxidation by H_2O_2 and O_3

Several previous studies have considered the fractionation during aqueous SO_2 oxidation and the combined results are presented in Figure 2.7. The weighted linear fit to all points shown in Figure 2.7 (except those for $SO_2(g) \rightleftharpoons SO_2(aq)$) shows that:

$$\alpha_{aq} = (1.0167 \pm 0.0019) - ((8.7 \pm 3.5) \times 10^{-5})\, T \tag{2.18}$$

where T is the temperature in degrees celsius. There is no significant difference between the α_{34} at 19°C measured for H_2O_2/O_3 ($\alpha_{34} = 1.0118 \pm 0.0040$) and O_3 ($\alpha_{34} = 1.0174 \pm 0.0028$) in droplets and the bulk H_2O_2 measurements ($\alpha_{34} = 1.0151 \pm 0.0013$). This shows that droplet-specific effects do not affect isotopic fractionation, and thus the results of bulk phase experiments are relevant to atmospheric reactions, which will primarily occur in droplets. The droplet measurements have a larger uncertainty which is due to small variations in reaction conditions, particularly relative humidity.

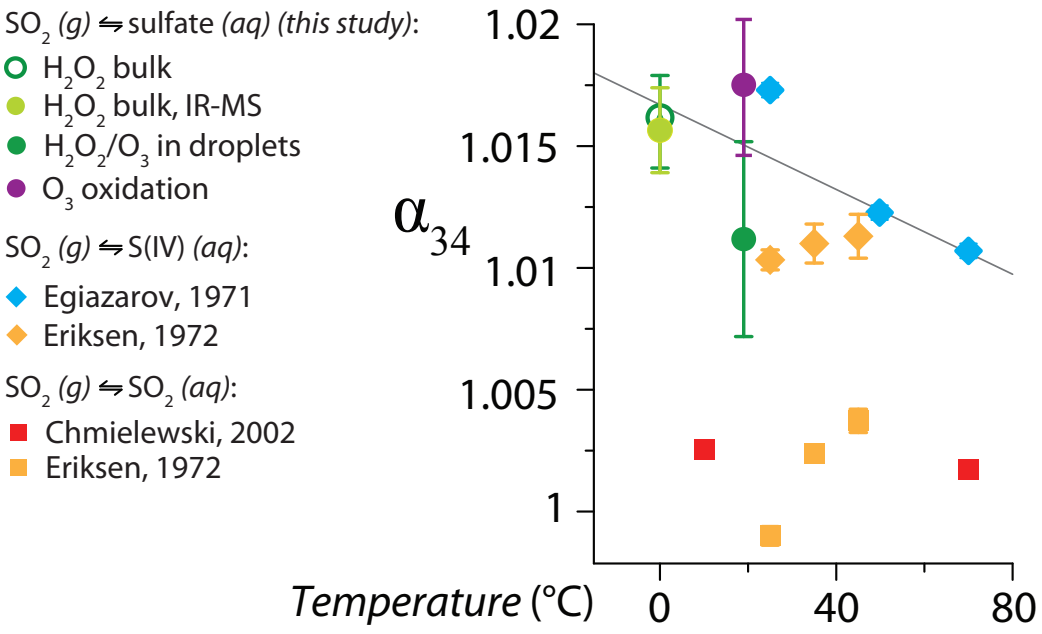

Figure 2.7: **Temperature dependence of fractionation during aqueous oxidation of SO_2 by H_2O_2 and O_3.** Error bars are the 1σ standard deviation.

The previous studies do not consider oxidation to S(VI) (see Equations 2.4-2.8), and comparison of the measured fractionation factors can show which stages of the reaction are most important for isotopic fractionation. Chmielewski et al. (2002) and Eriksen (1972b) consider only the equilibrium SO_2 (g) $\rightleftharpoons SO_2$ (aq) and measure a much lower fractionation factor ($\alpha = 1.00256$ at 10 °C). This shows that physical phase transfer is responsible for only a small part of isotopic fractionation, and protonation and acid-base equilibria in solution cause the majority of fractionation for the SO_2 (g) - S(IV) (aq) system.

The results of Egiazarov et al. (1971) and Eriksen (1972a,b,c,d) compare well with the results of this chapter, although these earlier studies both consider only the equilibrium to S(IV) in solution while this study includes oxidation to S(VI). This shows that the terminating oxidation reaction has a negligible effect on isotopic fractionation, explaining why H_2O_2 and O_3 produce the same fractionation factors despite very different mechanisms

(Savarino et al., 2000). Eriksen (1972a) considers the equilibriation of 1 M $NaHSO_3$ at low pH as acid is constantly added to the system, thus the concentration of SO_3^{2-} will be negligible. The experiments of Egiazarov et al. (1971) consider the equilibration of 3 M $NaHSO_3$ at pH ≈ 4, so unlike Eriksen (1972a) these results will include some equilibration to SO_3^{2-} as well as significant production of $S_2O_5^{2-}$. The fractionation factor measured by Egiazarov et al. (1971) ($\alpha = 1.0173 \pm 0.0003$ at 25 °C) is slightly higher than the fractionation factor measured by Eriksen (1972a) ($\alpha = 1.01033 \pm 0.00041$ at 25 °C), suggesting that equilibration towards higher-pH forms of S(IV) introduces a further enrichment of ^{34}S. The rate of S(IV) oxidation by O_3 increases by several orders of magnitude as the pH increases above 5.5 (Botha et al., 1994), and the fractionation factor measured for O_3 in this study ($\alpha = 1.0174 \pm 0.0028$) is slightly higher than that measured for H_2O_2 oxidation ($\alpha = 1.0151 \pm 0.0013$), supporting the hypothesis that equilibration to higher pH increases fractionation, while the terminating oxidation by O_3 may have little effect on isotopic fractionation. Results investigating the isotopic effect of flue gas desulfurization provide another value of the fractionation factor at high pH for comparison: Derda et al. (2007) measured α_{34} of 1.0026 for aqueous oxidation in a wet lime solution producing gypsum (the fractionation factor has been adjusted to have the same definition as the present study). This would provide a first estimate for the isotope fractionation during oxidation in an alkaline solution, but meaningful comparison with the results obtained in the present study is difficult, since an industrial scale process is not comparable to the carefully controlled environment of a laboratory reactor, and the process temperature has not been reported by Derda et al. (2007). The difference between measured fractionation during oxidation by O_3 and H_2O_2 in this study is not significant considering the experimental error and a more detailed study of the pH-dependence of this system would be needed to fully resolve isotopic effects for each step in the pathway from $SO_2(g) \rightarrow$ sulfate.

2.4.2 Gas-phase oxidation of SO_2 by ·OH radicals

Quantification of interferences

Before calculating fractionation factors for SO_2 oxidation by ·OH radicals, a consideration of interferences from background sulfate is necessary. Possible interferences are sulfate impurities in reagents, direct photolysis of SO_2, and reaction in the gaseous or aqueous phase with oxidants such as H_2O_2, $\cdot HO_2$ and O_3, which are also generated during the photolysis of water (Atkinson et al., 2004). SO_2 photolysis can follow a number of pathways under UV light (Farquhar et al., 2001). The wavelength-dependent quantum yield

of the different pathways is not well known and the fractionation occurring is not well-constrained (Farquhar et al., 2001; Lyons, 2009). The gas phase reactions of SO_2 with photochemical products other than ·OH are very slow (Atkinson et al., 2004), however oxidation on glass surfaces with adsorbed water could lead to sulfate production.

The trace sulfate content present in the MilliQ water used to rinse the product sulfate from the collectors was tested by adding $BaCl_2$ to 500 mL of MilliQ water. The $BaSO_4$ was then collected and quantified in the SEM. The effect of this blank (1.6 ± 1 μg L^{-1}) on the measured sulfate concentration was then converted to mol of blank per mole of sulfur produced during the experiment based on the volume of MilliQ used to wash the collectors and the quantity of sulfate produced in the individual experiment. The interference from sulfate impurities in MilliQ water contributed 6% by mass of the total sulfate at $-25\,^{\circ}C$ and less than 2.5% of sulfate for all other temperatures. The equivalent in ppbv based on the average volume of MilliQ used to wash the collectors and the quantity of sulfate produced for an 8 hour experiment considering flow rate, concentration temperature and pressure is shown in Figure 2.2.

Oxidation by photochemical products other than ·OH, such as H_2O_2, ·HO_2 and O_3, was tested with Reactor 2, which passed water vapour through UV light but did not produce detectable ·OH at the reaction point. A numerical simulation (Facsimile model, MCPA Software, Ltd.) of the chemical processes involved was run to investigate the species that would be present in the reactor following the photolysis of water and may oxidise SO_2. The species produced by Reactor 1 for the photolysis of water in synthetic air to generate 11 ppbv ·OH followed by immediate mixing with 1 ppm SO_2 are shown in Figure 2.8.

Direct photolysis of SO_2 was measured by adding humidity 10 cm after the lamp, to ensure the water was not photolysed while allowing the reaction $SO_3 + H_2O \rightarrow H_2SO_4$ to occur. This was done with both Reactors 1 and 2 so that direct photolysis of SO_2 and reaction with other lamp products, discussed in the previous paragraph, could be separated. The rate of pyrrole photolysis was measured to be the same for both reactors, so it can be assumed that the photolysis of SO_2 is also comparable between the two reactors. Direct photolysis was measured with both the standard Hg lamp, which produces 185 and 254 nm lines, and with an O_3-free Hg lamp, which emits only the 254 nm line. The whole reaction system was also run with no lamps switched on to measure the quantity of sulfate oxidised by trace compounds in the water or glass walls. The quantification of these interferences is shown in Figure 2.2. No sulfate was measured when SO_2 was run through the reaction system in the absence of humidity.

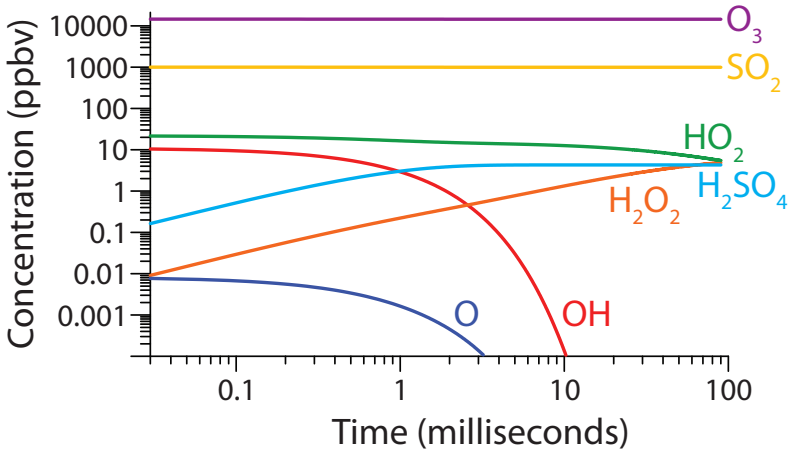

Figure 2.8: **Facsimile model of potential oxidants and H_2SO_4** produced as 11 ppbv ·OH is generated from the photolysis of water in 20 % oxygen and mixed with 1 ppm SO_2 at atmospheric pressure.

The quantity of sulfate produced under UV light does not significantly differ between Reactors 1 and 2, O_3-free or normal Hg lamps, and whether humidity is passed over the lamp or not. Thus, all experiments with UV light were combined to find a background of 0.60±0.40 ppbv sulfate in the absence of ·OH radicals at room temperature. The quantity of sulfate produced in the absence of UV light was 1.04±0.10 ppbv, i.e., compatible with the former value within errors, and the $\delta^{34}S$ values of the products in experiments with irradiation are not significantly different from the $\delta^{34}S$ of the products in the absence of UV light (Figure 2.9), thus the background sulfate is not due to irradiation. The quantity of sulfate collected in the absence of ·OH radicals was found to have an exponential relationship to temperature and thus was proportional to water vapour pressure. The measured temperature dependencies of sulfate quantity for no ·OH and ·OH experiments were adequately described by exponential curves and the fits were used to quantify the percentage contribution of the background to the total sulfate at each experimental temperature. The reaction of interest, SO_2 + ·OH, contributes between 77 and 85% of the total collected sulfate, depending on the reaction temperature. As the average isotopic composition of the background ($\delta^{34}S = 13.0\pm1.5‰$) is consistent with that expected from aqueous oxidation ($\delta^{34}S = 15.1\pm1.3‰$), and the quantity of background sulfate varies with the vapour pressure of water, it can be assumed the background sulfate reaction is aqueous oxidation due to an impurity in the water or an oxidation reaction in an H_2O surface layer on the glass walls of the collector. As the fractionation for aqueous oxidation has a much lower uncertainty due to the large number of measurements and its temperature

dependence is known, it can be used to correct for the background in the SO_2 + ·OH reaction.

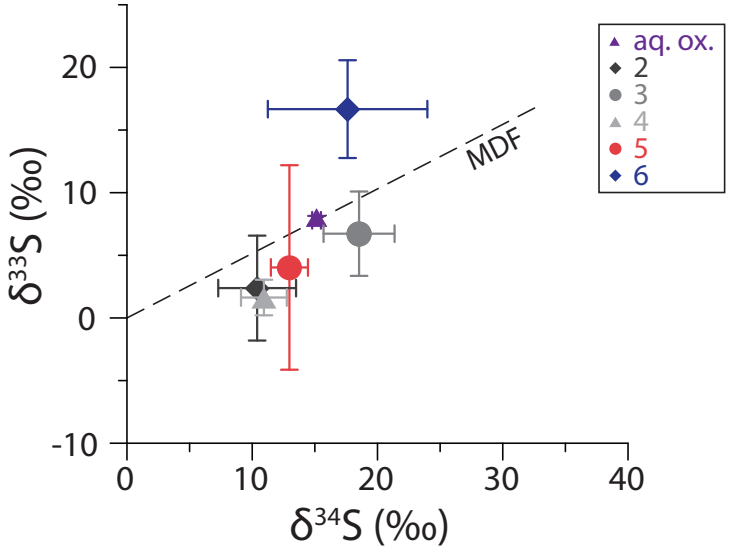

Figure 2.9: **Isotopic composition of interferences in the reaction of SO_2 and ·OH**. See Figure 2.2 for explanation of legend numbers. Aq. ox. shows the isotopic composition of the products of aqueous oxidation by H_2O_2 or O_3. Error bars are the 1σ standard deviation.

Isotopic fractionation during the gas-phase oxidation of SO_2 by ·OH radicals

The oxidation of SO_2 by ·OH radicals in the gas phase was measured at four different temperatures in twelve individual experiments. The results are presented in Figure 2.10 and Table 2.4. The correction for aqueous background oxidation as described in Section 2.4.2 has only a small effect on the results as it accounts for less than 25% of sulfate production. The weighted fit to all points gives a temperature-dependent fractionation factor for ^{34}S of:

$$\alpha_{OH} = (1.0089 \pm 0.0007) - ((4 \pm 5) \times 10^{-5})\, T. \tag{2.19}$$

The measured fractionation factor for ^{33}S is

$$\alpha_{OH} = (1.0043 \pm 0.0010) + ((1 \pm 4) \times 10^{-5})\, T. \tag{2.20}$$

This is not significantly different from the fractionation of ^{33}S predicted from a mass-dependent relationship to ^{34}S.

Ab initio calculations using transition state theory for the reaction SO_2 + ·OH → $HOSO_2$ by Tanaka et al. (1994) estimated a fractionation factor for $^{34}S/^{32}S$ of 0.991,

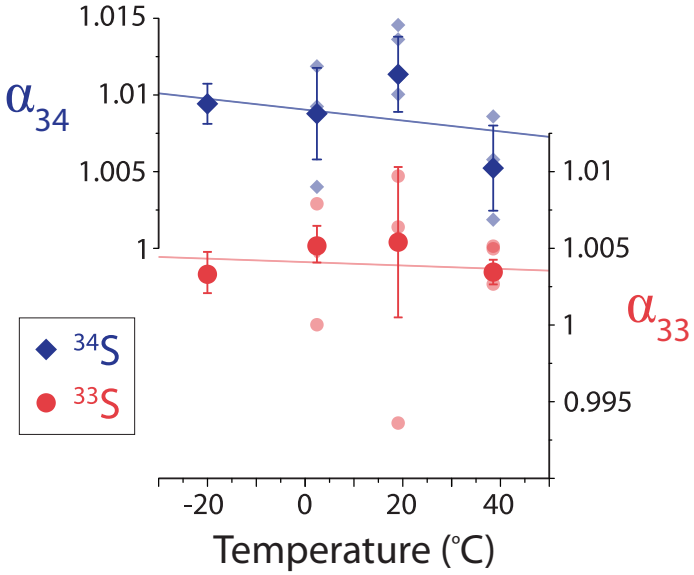

Figure 2.10: **Temperature dependent fractionation factors during the gas-phase oxidation of SO_2 by ·OH radicals**. Pale points represent individual experiments while dark points with error bars are the average and 1σ error of the mean at each temperature.

Table 2.4: **Temperature dependent fractionation factors during the gas-phase oxidation of SO_2 by ·OH radicals**.

T (°C)	n	α_{34}	$1\ \sigma$	α_{33}	$1\ \sigma$
−20	2	1.0095	0.0013	1.0034	0.0014
2	3	1.0088	0.0030	1.0053	0.0012
19	4	1.0113	0.0024	1.0053	0.0049
38	3	1.0052	0.0028	1.0034	0.0009

similar in magnitude but opposite in direction to the fractionation factor measured in this study. Leung et al. (2001) calculated the fractionation factor to be 1.14 based on RRKM theory. They found that although the positive difference in critical energies of the transition states would lead to a fractionation factor of < 1, this is overcome by the denser vibrational manifolds of the ^{34}S transition state. However, the authors state that even considering the uncertainties in all parameters used they predict a fractionation factor > 1.07, almost 10 times larger in magnitude than the factor measured in this study. Even a fractionation factor of 1.07 rather than 1.14 is significantly larger than the variation observed in atmospheric samples (e.g. Norman et al. (2006); Novak et al. (2001)), so it is likely that RRKM theory can accurately predict only the direction and

not the magnitude of this isotope effect. This is in agreement with recent results from Lin et al. (2011) and Hattori et al. (2011), which found a similar overprediction of the sulfur isotopic fractionation during the photolysis of OCS by RRKM theory (Leung et al., 2002).

2.4.3 Comparison to previous studies

A number of studies have used field measurements to estimate the value of the fractionation factors for SO_2 oxidation. Atmospheric measurements of $\delta^{34}S_{SO_4}$ and ($\delta^{34}S_{SO_4} - \delta^{34}S_{SO_2}$) are often lower in summer than in winter (Mukai et al., 2001; Mayer et al., 1995; Saltzman et al., 1983). Oxidation by ·OH is expected to be highest in summer and this may therefore show that the fractionation factor for gas-phase oxidation is lower than that for aqueous oxidation, in agreement with the results of this study. Observations that sometimes $\delta^{34}S_{SO_4} < \delta^{34}S_{SO_2}$ have previously been suggested to show that $\alpha_{OH}<1$, however the results of this study point to a dominance of transition-metal catalysed oxidation for these samples. Seasonality is not a direct measurement of oxidation and fractionation but reflects changing sources and oxidation pathways as well as lifetime and removal mechanisms such as dry and wet deposition. Hence, in order to estimate fractionation factors from seasonal data, seasonal changes in oxidant concentrations, local sources and climatic conditions would need to be considered very carefully.

The $\delta^{34}S$ of stratospheric sulfate aerosol has been observed to first increase and then strongly decrease in the months following the eruption of Mt. Agung (Castleman et al., 1974), consistent with stratospheric oxidation favouring ^{34}S and progressively depleting the SO_2 reservoir. This was suggested to show that oxidation by ·OH favours the heavy isotope, as ·OH is normally the dominant stratospheric oxidant for SO_2 (Leung et al., 2001). However, strong $\Delta^{33}S$ signals found in ice core records of volcanic sulfate from the same event suggest photochemical oxidation is the dominant process producing these aerosols: The huge amount of SO_2 released during the eruption depletes the stratosphere of ·OH which means oxidation pathways, such as photolysis, which are normally not important in stratospheric SO_2 oxidation can begin to have a significant effect (Savarino et al., 2003a,b; Baroni et al., 2007, 2008). The contribution of ·OH and other oxidation pathways to oxidation of SO_2 following a stratospheric volcanic eruption is not well constrained, thus measurements from these eruptions are not reliable indicators of the magnitude and direction of α_{OH}.

Interglacial-glacial changes in $\Delta^{17}O$ of ice core sulfate can provide information on the oxidation pathways of sulfur due to the large $\Delta^{17}O$ signal in O_3 and the smaller but

significant $\Delta^{17}O$ signal in H_2O_2 (Sofen et al., 2011; Alexander et al., 2002, 2003; Savarino et al., 2000). Transition metal-catalysed oxidation by O_2 and gas phase oxidation by ·OH both result in $\Delta^{17}O$ very close to 0‰ (Luz and Barkan, 2005; Sofen et al., 2011). The $\Delta^{17}O$ of ice core sulfate was larger in the surrounding interglacials than in the last glacial period, showing that oxidation by H_2O_2 and O_3 was proportionally more important in the interglacial periods. The $\delta^{34}S$ of sulfate was measured to be lower during glacial periods than surrounding interglacials (Alexander et al., 2003). It has been suggested that this shows a progressive depletion in ^{34}S during transport of SO_2 from lower latitude source regions, based on the α_{OH} of > 1.07 from Leung et al. (2001). However, the results of this study suggest that the fractionation signature is directly transferred to ice-core sulfate, and increased oxidation by transition metal catalysis due to higher abundance of windblow dust could account for the lower values of $\delta^{34}S$ measured in glacial periods. Considering the pre-industrial partitioning between the sulfate production pathways from Sofen et al. (2011) and the fractionation factors measured in this chapter, the overall preindustrial change in $\delta^{34}S$ between SO_2 and product sulfate would be +5.5‰. Alexander et al. (2003) saw a decrease in $\delta^{34}S_{nss}$ of ∼3‰ during glacial periods, which would mean a change in $\delta^{34}S$ between SO_2 and product sulfate of +2.5‰ if sources were unchanged. Oxidation by transitional metal catalysis would need to increase from 8% to 35% of the total sulfate production to account for this change if the proportions of sulfate produced from the other oxidation pathways and the overall sulfur budget remained the same. A 10% increase in transition-metal catalysed sulfate production was modelled for the pre-industrial to industrial periods by Sofen et al. (2011), thus a 27% increase due to much higher dust loads in glacial times is not unreasonable.

2.5 Conclusions

This study measured the fractionation factors for the most common SO_2 oxidation pathways: gas phase oxidation by ·OH radicals, and aqueous phase oxidation by H_2O_2, O_3 and a radical chain reaction initiated by Fe. The fractionation factors for these oxidation pathways are now well constrained compared to the previous estimates. A summary diagram of the main processes in the continental sulfur cycle and the fractionation factors involved is shown in Figure 2.11. Isotopic measurements can now be used to constrain the dominant oxidation pathway in environmental samples by excluding pathways that do not agree with observed fractionation. A Cameca NanoSIMS 50 was used to measure the iso-

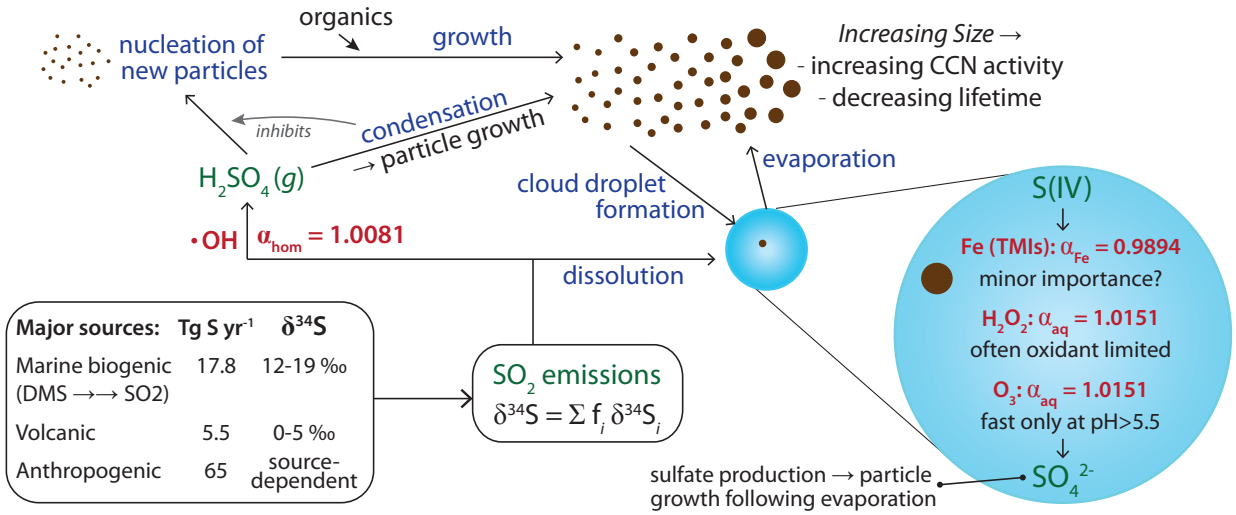

Figure 2.11: **A summary of sulfur isotopes and the continental sulfur cycle**. Fractionation factors are shown for 19°C. Emission quantities for the different sources are taken from Sofen et al. (2011) and δ^{34}S values from sources are from Rees et al. (1978), Krouse et al. (1991), Nielsen et al. (1991) and Sanusi et al. (2006).

topic composition of the sulfate produced from the different reactions, which allowed these previously unknown fractionation factors to be measured despite the difficulties of obtaining enough product for traditional isotope measurement instruments. However, factors such as sample topography and charging mean that NanoSIMS results have a far greater uncertainty than traditional measurement techniques, and NanoSIMS measurement error contributes the major uncertainty in the results. NanoSIMS analysis allowed the reactor and collection system to be developed and the reaction to be thoroughly investigated for interfering reactions; the next step in laboratory studies of these fractionation factors would be to increase the sulfate production capacity of the system to allow traditional measurements with high precision, such as isotope ratio mass spectrometry (Ono et al., 2006).

The fractionation factors presented in this paper will allow stable sulfur isotopes to be used to understand the partitioning between these pathways in atmospheric samples, particularly if Δ^{17}O of sulfate is also measured to allow differentiation between oxidation by H_2O_2, O_3 and all other oxidants. The combined effect of uncertainty and variation in the isotopic composition of sources, and fractionation during oxidation, means field studies need to simultaneously measure both SO_2 and sulfate isotopic composition to gain insight into the sulfur cycle. Combining modelling with field studies of sulfur isotopes in the

atmosphere can then use these fractionation factors to gain an increased understanding of the sulfur cycle and its effect on radiative forcing, aerosols and cloud condensation nuclei. Based on the unique fractionation factor of the reaction, sulfur isotope ratios will be particularly useful to constrain the importance of transition metal-catalysed sulfur oxidation in the atmosphere, which was the only reaction found to favour the light isotope in the current study.

Acknowledgements

We thank Elmar Gröner for his support with the NanoSIMS analyses, Joachim Huth for his help with the SEM/EDX analyses, Sergey Gromov for translation of Egiazarov et al. (1971) and Anke Nölscher and Vinayak Sinha for measurements of ·OH concentration. The Teflon FEP 121a suspension used to coat the reactor was kindly provided by DuPont. This research was funded by the Max Planck Society and the Max Planck Graduate Centre.

Chapter 3

Fractionation of sulfur isotopes during heterogeneous oxidation of SO_2 on sea salt aerosol: A new tool to investigate non-sea salt sulfate production in the marine boundary layer

This chapter is published for discussion as Harris, E., Sinha, B., Hoppe, P., Foley, S., and Borrmann, S. (2012) *Atmospheric Chemistry and Physics Discussions*, 12, 2707-2742, doi:10.5194/acpd-12-2707-2012.

3.1 Introduction

Sea-salt aerosol is the dominant form of aerosol in the marine environment. The potential for heterogeneous oxidation of SO_2 on sea salt aerosol was first appreciated when ambient measurements showed that excess non-sea salt sulfate (*nss*-sulfate), particularly in coarse particles, could not be explained by homogeneous oxidation and in-cloud processes alone (Sievering et al., 1991). Oxidation of SO_2 in sea salt aerosol can reduce marine boundary layer (MBL) SO_2 concentrations by up to 70%, limiting gas phase production of H_2SO_4 and thus reducing or preventing new particle nucleation and CCN production (Chameides and Stelson, 1992; Katoshevski et al., 1999; Alexander et al., 2005). Sulfate production

on sea salt aerosols shifts the sulfate size distribution towards coarse particles, leading to faster removal from the atmosphere, while having a relatively small effect on the CCN activity of the hygroscopic sea salt particles (Chameides and Stelson, 1992; Sievering et al., 1995; von Glasow, 2006). The effects of heterogeneous SO_2 oxidation on the sulfur cycle in the MBL are particularly important due to the low albedo of the ocean and the strong climatic effect of marine clouds (von Glasow and Crutzen, 2004).

There are a number of different pathways by which SO_2 can be oxidised on sea salt aerosol. Oxidation can occur directly on deliquescent aerosol, or in clouds when sea salt aerosol has acted as a CCN. Ozone is thought to be one of the most important oxidants in the MBL (Chameides and Stelson, 1992; Sievering et al., 1995). However, oxidation by ozone is strongly pH dependent and self-limiting as aerosol becomes acidified following sulfate production. The amount of sulfate generated by this pathway is therefore constrained by the alkalinity of the aerosol and the concentration of other gases, such as HNO_3, which also titrate alkalinity (Chameides and Stelson, 1992; Zhang and Millero, 1991; von Glasow and Sander, 2001; Hoppel and Caffrey, 2005). Thus, O_3 can only efficiently oxidise SO_2 in sea salt aerosol in the first 10-20 minutes following emission, and oxidation by O_3 occurs mainly in the lowest 50-100 m of the MBL, which leads to rapid deposition of the sulfate produced (Chameides and Stelson, 1992; von Glasow and Sander, 2001; von Glasow and Crutzen, 2004). Field measurements and laboratory studies commonly find that sulfate production is larger than would be expected from the neutralisation capacity of sea salt aerosol estimated from the alkalinity of bulk sea water (Sievering et al., 1999; Caffrey et al., 2001). Two explanations have been proposed: i) oxidants other than O_3 play a more important role than currently known, and ii) the alkalinity of sea salt aerosol is larger than the alkalinity of bulk sea water.

The alkalinity of sea salt aerosol is somewhat higher than the alkalinity of bulk sea water due to shifting of the carbonate equilibrium with evaporation, however this is insufficient to explain excess sulfate concentrations (Sievering et al., 1999). As sea salt aerosol form from bursting bubbles, they efficiently skim the surface microlayer which can have high alkalinity due to cations associated with organic molecules and biogenic skeletal fragments. This could provide up to 2.5 times additional alkalinity at typical marine sites, and >200 times more at especially favourable sites (Sievering et al., 1999, 2004). Laskin et al. (2003) proposed that interface reactions between ·OH (g) and surface chloride ions could also generate excess alkalinity in sea salt aerosol, however observations and models show that this pathway will account for <1% extra sulfate production in the ambient environment (Sander et al., 2004; Keene and Pszenny, 2004; Alexander et al., 2005; von

Glasow, 2006).

Several reactions have been identified that may be as or more important than oxidation by O_3 in the marine boundary layer. Oxidation by H_2O_2 is believed to be unimportant and contributes <4% of *nss*-sulfate (Gurciullo et al., 1999). Transition metal ions and radicals such as Fe^{3+}, ·Br, ·OH and ·Cl can initiate radical chain reactions in which SO_2 is oxidised by O_2 (Zhang and Millero, 1991). In a chamber study with sea salt and pure NaCl aerosols, Hoppel et al. (2001) saw production of sulfate but no uptake of ozone. They proposed that oxidation catalysed by ·Cl, which is second order in $[SO_2]$, is the dominant oxidation pathway in the MBL at high SO_2 concentrations (Hoppel and Caffrey, 2005). However, oxidation by ·Cl catalysis, like oxidation by O_3, is strongly pH dependent and limited by alkalinity. Oxidation by hypohalites and hypohalous acids (HOX) is not limited by alkalinity and may be the 'missing' oxidation pathway in MBL models (von Glasow, 2006), although at low pH HOCl and HOBr are converted to Cl_2, Br_2 or BrCl according to (IUPAC, 2009):

$$HOCl + H^+ + Cl^- \rightarrow Cl_2 + H_2O \tag{3.1}$$

Oxidation by HOBr is faster, however HOCl is likely to be the more important oxidant due to the relative abundances of Br and Cl (Troy and Margerum, 1991). von Glasow et al. (2002) modelled oxidation in the MBL and found that under almost all conditions, HOCl - not O_3 - was the dominant oxidant for SO_2.

3.2 Sulfur isotopes in the marine environment

The isotopic composition of sulfate in the environment reflects its sources, transport and chemistry, so stable isotopes of oxygen and sulfur in *nss*-sulfate can be especially useful to investigate the different oxidation pathways of SO_2 in the MBL. Sulfur has four naturally-occurring stable isotopes: ^{32}S, ^{33}S, ^{34}S and ^{36}S. The isotopic composition of a sulfur sample is described with the delta notation, which is the ratio of a heavy isotope to the most abundant isotope (^{32}S) in the sample compared to a standard ratio and expressed in permil:

$$\delta^x S = \frac{\left(\frac{n(^xS)}{n(^{32}S)}\right)_{\text{sample}}}{\left(\frac{n(^xS)}{n(^{32}S)}\right)_{\text{V-CDT}}} - 1 \tag{3.2}$$

where n is the number of atoms, ^xS is one of the heavy isotopes, ^{33}S, ^{34}S or ^{36}S, and V-CDT is the international sulfur isotope standard, Vienna Canyon Diablo Troilite, which has isotopic ratios of $^{34}S/^{32}S = 0.044163$ and $^{33}S/^{32}S = 0.007877$ (Ding et al., 2001). The kinetic isotope fractionation factor (α) is represented by the ratio of the heavy to the

light isotope amount in the instantaneously formed product divided by the ratio in the reactant:

$$\alpha_{34} = \frac{\left(\frac{n(^{34}\mathrm{S})}{n(^{32}\mathrm{S})}\right)_{\mathrm{products}}}{\left(\frac{n(^{34}\mathrm{S})}{n(^{32}\mathrm{S})}\right)_{\mathrm{reactants}}} \tag{3.3}$$

Values of α_{34} are characteristic for different reaction pathways and will therefore be useful to investigate the different oxidation pathways for SO_2 in the marine environment.

The major sources of sulfate in the marine environment are isotopically distinct: sea salt sulfate has a δ^{34}S of 21‰ (Rees et al., 1978), marine biogenic *nss*-sulfate has a δ^{34}S between 12 and 19‰ (Calhoun et al., 1991; Sanusi et al., 2006), and anthropogenic sulfur emissions are often lighter, although there is significant variation between sources (Krouse et al., 1991; Nielsen et al., 1991). Sulfur isotope fractionation during SO_2 oxidation has not usually been considered in analyses of MBL sulfate as the fractionation factors were not well known: α_{34} for gas phase oxidation of SO_2 by ·OH radicals and for aqueous oxidation by H_2O_2 and O_3 were presented in Chapter 2, but the effect of heterogeneous processes on complex environmental substrates such as sea salt aerosol have not been measured. The results in Chapter 2 suggested isotopic fractionation during aqueous oxidation may increase at higher pH, however the pH dependence was within the uncertainty of the measurements. Sea salt aerosols have much higher pH than typical cloud droplets, thus the pH dependence of isotopic fractionation will be particularly important in the MBL.

This study presents measurements of $^{34}S/^{32}S$ fractionation during SO_2 oxidation in sea salt aerosol and NaOCl aerosol, and examines the role of pH, ozone and irradiation in determining isotopic fractionation. We demonstrate that stable sulfur isotope ratios can be used to constrain the contributions of different oxidation pathways to sulfate formation in the MBL, and will be particularly useful in combination with Δ^{17}O measurements to determine the importance of alkalinity-limited pathways compared to alkalinity non-limited pathways.

3.3 Methods

3.3.1 Experimental set-up

Dependence of isotopic fractionation on pH

The pH dependence of isotopic fractionation during sulfate production was measured by oxidising SO_2 in buffer solutions at high and low pHs. Two bubblers in series were used: the first bubbler contained buffer solution, along with 1% H_2O_2 to oxidise SO_2, and the

second buffer contained 6% H_2O_2 to collect residual SO_2 as sulfate as described in Section 2.3.4. 600 cm^3 min^{-1} (at standard conditions of T = 273.15 K, P = 1013.25 mBar) of 7 ppm SO_2 gas (Linde AG) in synthetic air (Westfalen AG, 20.5 % O_2 in N_2) was passed through the bubblers for 8-9 hours. Two buffer solutions were used: The first buffer contained 0.1 M H_3PO_4 and 0.1 M KH_2PO_4 and had an initial pH of 2.1, and the second buffer contained 0.1 M KH_2PO_4 and 0.1 M K_2HPO_4 and had an initial pH of 7.2 (Moore et al., 2005). The buffer concentration is >150 times in excess of the maximum acidity generated if all the SO_2 was oxidised to sulfate, thus the buffer pH will not change significantly during the course of the experiment. The phosphate buffer system was chosen as it allows the pH to be held at two atmospherically-relevant values (pH ∼2 represents the lower boundary of typical cloud water pH and can be reached in sea salt aerosol in highly polluted areas, while the pH of sea water is 7.5-8.5; Sander and Crutzen 1996; van Loon and Duffy 2000) without the large change in the chemical environment that would be introduced by using different buffer systems for the two pHs.

Experiments at each of the two pHs were run in duplicate. Following the experiments, $BaCl_2$ was added to the solutions from the bubblers to precipitate sulfate as $BaSO_4$. The $BaSO_4$ was collected on Nuclepore track-etch polycarbonate membrane filters (Whatman Ltd.) with 0.2 μm pores, which had been coated with a 10 nm thick gold layer using a sputter coater (Bal-tec GmbH, Model SCD-050) prior to sample collection. The $BaSO_4$ was then analysed in the NanoSIMS as described in Section 3.3.3. The reacted fraction was found from isotope mass balance between the products and the reactants:

$$\delta^{34}S_i = f \cdot \delta^{34}S_{SO_2} + (1 - f) \cdot \delta^{34}S_{\text{sulfate}} \tag{3.4}$$

where f is the fraction of reactant (SO_2) remaining and $\delta^{34}S_i$, $\delta^{34}S_{SO_2}$ and $\delta^{34}S_{\text{sulfate}}$ are the isotopic compositions of the initial SO_2 gas, residual SO_2 gas and product sulfate respectively. The sulfate generated could not be determined gravimetrically due to interference from co-precipitated barium phosphates. More than 5% of the SO_2 was oxidised, thus the isotopic composition of the SO_2 reservoir was affected by the reaction and the fractionation factors must be calculated according to the Rayleigh equations, which describe the relationship between accumulated product and reactant isotopic composition and reaction extent (Mariotti et al., 1981; Krouse and Grinenko, 1991):

$$\alpha_{34} = \frac{\ln \frac{R_r}{R_0}}{\ln f} + 1 \tag{3.5}$$

$$\alpha_{34} = \frac{\ln(1 - \frac{R_p}{R_0}(1 - f))}{\ln f} \tag{3.6}$$

where R_0, R_r and R_p are the isotope ratios $^{34}S/^{32}S$ for the initial SO_2 gas, the residual SO_2 gas and the product sulfate respectively and f is the fraction of reactant remaining following the reaction as in Equation 3.4.

Aqueous oxidation in droplets

SO_2 oxidation in aqueous aerosol was measured with three different solutions using the apparatus shown in Figure 3.1: Pure water (LiChrosolv chromatography water, Merck GmbH), synthetic sea salt solution and NaOCl solution. The pure water solution was used to measure the background (when no oxidant was added) and to measure the fractionation factor from SO_2 oxidation by O_3. Commercial NaOCl (reagent grade, Sigma-Aldrich GmbH) was diluted 1:20 with MilliQ water to make the NaOCl solution with 0.5-0.75% active chlorine. The synthetic sea salt solution is described in the next subsection.

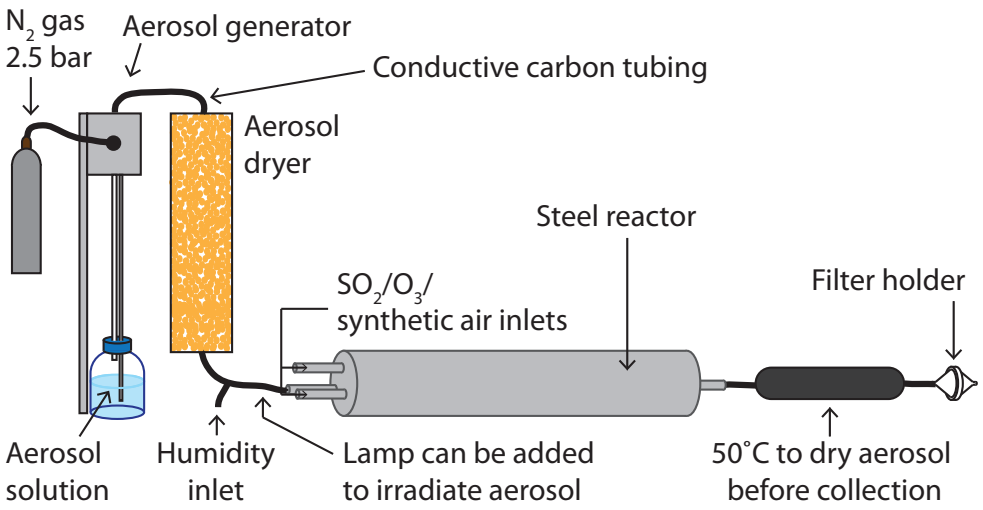

Figure 3.1: **Experimental set-up used to investigate isotopic fractionation during the oxidation of SO_2 by sea salt aerosol**.

Aerosol was generated from the solutions with an atomizer built in-house: 2.5 bar N_2 *6.0* (Westfalen AG) expanded through a small orifice to form a high velocity gas jet which atomized the liquid as it was sucked up from a reservoir. Only fine spray leaves the atomizer as large droplets are removed by impaction on the wall facing the jet. PFA fittings were used for all connections. The reactor was made of steel and carbon-coated tubing was used to minimise aerosol loss through electrostatic attraction. The size and volume distributions measured with an optical particle counter (OPC; Grimm Portable Aerosol Spectrometer, Model 1.108) and a scanning mobility particle sizer (SMPS; TSI

Electrostatic Classifier, Model 3080 coupled to TSI Ultrafine CPC, Model 3025A) are shown in Figure 3.2. The aerosol was passed through a drier containing silica gel, which reduced the volume of aerosol by 20% for the sea salt solution and ∼90% for pure water and NaOCl solution, and shifted the size distribution towards smaller particles.

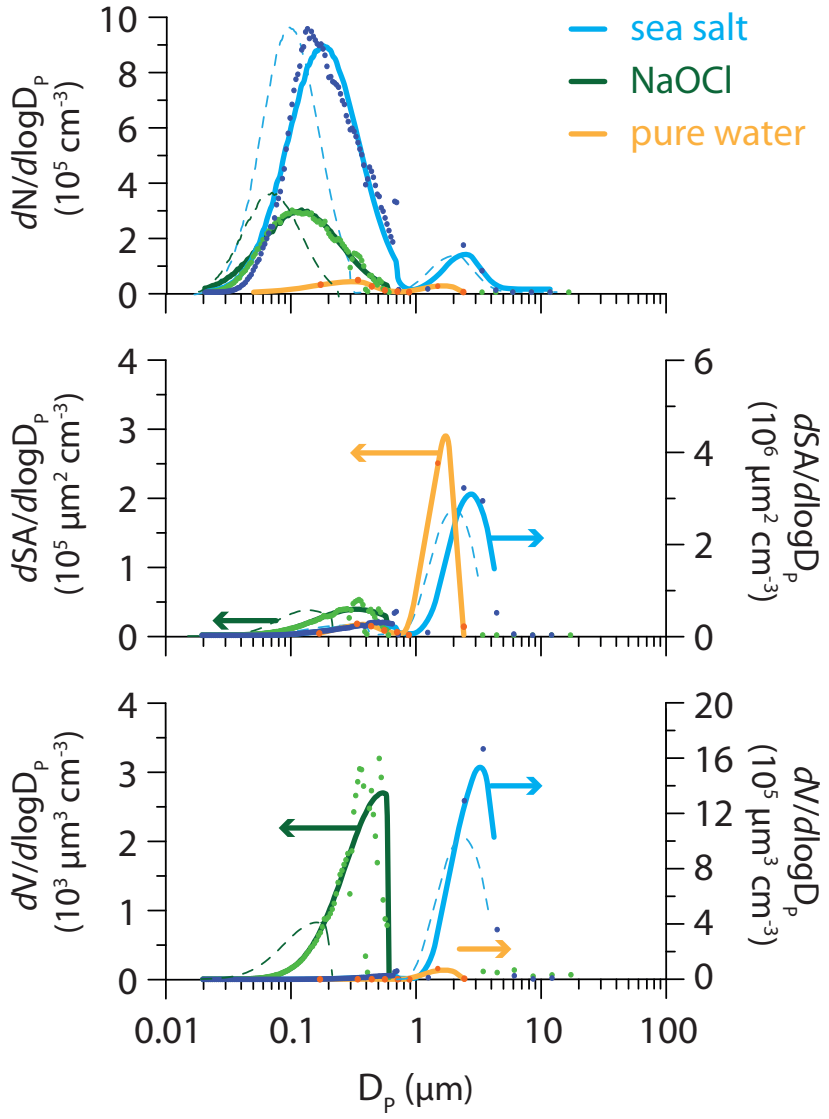

Figure 3.2: **Size, surface area and volume distributions of aerosol** produced from various solutions: synthetic sea salt solution is shown in blue, water is shown in orange and NaOCl solution is shown in green. Individual points represent measurements while solid lines show fits to a log-normal distribution before the aerosol was dried. The log-normal fit following the dryer is shown as a dashed line. The axis on which each aerosol type is plotted is indicated with arrows.

50 cm^3 min^{-1} of SO_2 gas (Linde AG, 102 ppm ± 2% in synthetic air) was added to the reactor along with 300 cm^3 min^{-1} of aerosol in N_2, 100 cm^3 min^{-1} of humidified synthetic air (Westfalen AG, 20.5% O_2 in N_2), and 100 cm^3 min^{-1} of extra synthetic air, giving a total flow of 550 cm^3 min^{-1}, a relative humidity of ∼35%, and an SO_2 concentration of 9 ppm. The reactor was 55 cm long and had a diameter of 8 cm, resulting in a residence time for the aerosol of 302 seconds. The reacted aerosol was collected on a Nuclepore track-etch polycarbonate membrane filter (Whatman Ltd.) with 0.2 μm pores. The filter was changed every 1.5 - 3.5 hours depending on the accumulation of aerosol. Following each experiment, the filters were extracted for 30 minutes in an ultrasonic bath, rinsed, and extracted for another 30 minutes. The rinses and extracts were collected and $BaCl_2$ was added to precipitate sulfate as $BaSO_4$, which was then collected by filtration on to gold-coated Nuclepore filters. One sample of sea salt aerosol + O_3 (ssaltO_3, see following paragraph) was collected directly on to a gold-coated Nuclepore filter and analysed as untreated sea salt + sulfate particles, as this more closely resembles sea salt sampling in field campaigns. This sample will be referred to as 'ssaltO3direct'. However, the concentration of sea salt in the droplets was so high that this sample could only be collected for <20 minutes before the filter was too heavily loaded for NanoSIMS analysis.

The aerosol was subjected to a number of different conditions, to investigate the effect of various parameters on SO_2 oxidation. 20 ppm ozone was added by passing the 100 cm^3 min^{-1} extra synthetic air flow over a low-pressure mercury vapour lamp (Jelight Company Inc., USA) in 6 experiments. The aerosol itself was passed over the high-energy UV light from the low-pressure mercury vapour lamp before entering the reactor in 8 experiments, to investigate the effect of ·OH radicals and other compounds resulting from irradiation. This was done before mixing with synthetic air and SO_2 to avoid O_3 production and SO_2 photolysis, and as close to the reactor inlet as possible to minimise loss of radicals. All experiments are summarised in Table 3.1 along with abbreviations that will be used throughout this paper.

Table 3.1: **Experiments to investigate isotopic fractionation during oxidation of SO_2 on sea salt aerosol**. [1]SO_2 flow was replaced with synthetic air to measure sulfate in sea salt samples that had not been exposed to SO_2. [2]Collected directly on a gold-coated filter and analysed in the NanoSIMS without extracting to $BaSO_4$.

Abb.	**Solution**	**O_3**	**Irradiated**	**Run**	**Length** (hours)
ssaltblank[1]	sea salt	✗	✗	1	7.0
				2	3.2
				3	8.6
ssalt	sea salt	✗	✗	1	7.8
				2	8
ssaltO3	sea salt	✓	✗	1	8
				2	7.9
ssaltO3direct[2]	sea salt	✓	✗	1	0.3
				2	0.3
ssaltirr	sea salt	✗	✓	1	10.2
				2	8.4
ssaltirrO3	sea salt	✓	✓	1	7.0
				2	7.8
OCl	NaOCl	✗	✗	1	7.6
				2	7.6
OClirr	NaOCl	✗	✓	1	7.7
				2	7.0
waterA	pure water	✗	✗	1	7.8
waterAO3	pure water	✓	✗	1	7.8
				2	8.5

Seawater preparation

Synthetic sea salt was prepared according to Kester et al. (1967) and Millero (1974). However, Na_2SO_4 was replaced with NaCl to avoid background sulfate in the solution, which would complicate measurements of the isotopic fractionation during sulfate production. The compounds used to prepare the sea salt solution along with their contributions to background sulfate are shown in Table 3.2. The sea salt stock solution, as shown in the table, was four times more concentrated than actual sea water. Its pH was measured to be 7.7 and the alkalinity (approximated as $0.005[Na^+]$; Sievering et al. 2004; Chameides and Stelson 1992) was 10 mmol L^{-1}. When used for aerosol generation, this was diluted to be twice as concentrated as normal sea water to represent the increased concentration of atmospheric sea salt aerosol compared to sea water due to evaporation and other processes occurring during and after emission (Sievering et al., 1999). Following drying the aerosol will be $\sim$3 times more concentrated than sea water. Sea salt aerosols are commonly up to ten times more concentrated than sea water (Sander and Crutzen, 1996), however this high concentration could not be achieved in the system as precipitating salts then caused small orifices to clog very quickly.

Table 3.2: **Compounds used to prepare a four-times concentrated sulfate-free synthetic sea salt solution**. [ ] = concentration. [1]Prepared solution was four times more concentrated than actual sea salt, so here it is divided by four to facilitate comparison with actual concentrations. [2]From Millero (1974).

	Amount	**Supplier**	**max. SO_4**	**[SO_4] contributed**	**Ion**	$[\ ]_{synthetic}$ [1]	$[\ ]_{actual}$ [2]
	g/kg		(mg/kg dry)	(mmol/kg soln)		g/kg	g/kg
NaCl	111.75	Applichem	10	2.91	Na^+	11.0	10.8
Na_2SO_4	0				Cl^-	21.8	19.4
KCl	2.79	VWR	10	0.07	K^+	0.399	0.399
KBr	0.40	Applichem	50	0.05	Br^-	0.0674	0.0674
NaF	0.012	Applichem	100	0.003	F^-	0.0013	0.0013
$NaHCO_3$	0.62	Sigma-Aldrich	30	0.05	HCO_3^-	0.113	0.112
H_3BO_3	0.11	Applichem	50	0.01	H_3BO_3	0.0269	0.0269
$MgCl_2.6H_2O$	43.29	Fisher	9.92	1.12	Mg^{2+}	1.29	1.29
$CaCl_2.2H_2O$	6.04	Sigma-Aldrich	100	1.57	Ca^{2+}	0.412	0.412
$SrCl_2.6H_2O$	0.10	Sigma-Aldrich	10	0.003	Sr^{2+}	0.0079	0.0079
			Total sulfate	5.79	SO_4^{2-}	0.0006	2.712

3.3.2 SEM Analysis

A LEO 1530 field emission scanning electron microscope (SEM) with an Oxford Instruments ultra-thin-window energy-dispersive x-ray detector (EDX) was used to quantify the sulfate produced in the droplet experiments. The SEM was operated with an accelerating voltage of 10 keV, a 60 μm aperture and a working distance of 9.6 mm. 'High current mode' was used to increase the EDX signal and improve elemental sensitivity. The SEM was run in automatic mode and took 400 evenly-spaced images of each filter at 19 500$\times$ magnification. The EDX spectrum was measured with a 1 second integration time at 25 points on a 5 $\times$ 5 grid for each image, leading to 10 000 EDX measurements across each filter. The quantity of sulfate on each filter was then determined by estimating the background from both the Gaussian distribution of the gold signal and the quartile method, as described in Section 2.3.5. This quantification method is ideal for NanoSIMS studies, as quantification is achieved without extra sample treatment and the limit of detection is very low. The precision is fairly low ($\sim$40%, decreasing with increasing $BaSO_4$ quantity due to Poisson statistics) and the method is not ideal for samples with a large amount of $BaSO_4$ due to the possibility of the sample flaking off the filter during mounting. The precision of quantification did not affect the calculated isotopic fractionation factors as the SEM quantification was only used to estimate reactive uptake coefficients in the different aerosol types.

3.3.3 NanoSIMS analysis

The sulfur isotopic composition was determined with the Cameca NanoSIMS 50 ion probe at the Max Planck Institute for Chemistry in Mainz (Hoppe, 2006; Groener and Hoppe, 2006). The NanoSIMS 50 has high lateral resolution (<100 nm) and high sensitivity and can simultaneously measure up to five different masses through a multicollection system, allowing high precision analysis of the small sample quantities required for this study. The use of this instrument to analyse sulfur isotope ratios is described in detail elsewhere (Winterholler et al., 2006, 2008) so only a brief description will be given here.

$BaSO_4$ is analysed directly without further processing after it is collected on gold-coated filters as described in Section 3.3.1. The ssaltO3direct sample and all other samples with a particularly high $BaSO_4$ loading were gold-coated on top of the sample before NanoSIMS analysis to prevent excessive charging. The analysis conditions were the same as those described in Section 2.3.5. To correct for instrumental mass fractionation (IMF) in ssdirectO_3, which consisted of $NaSO_4$ rather than $BaSO_4$, the IMF correction for $NaSO_4$

relative to $BaSO_4$ from Winterholler et al. (2008) was used, along with an Na_2SO_4 standard (VWR GmbH) for control. The reported results for each experiment are the average of at least 5 measurement spots weighted according to the counting statistical error, as described in Section 2.3.5.

3.4 Results and discussion

3.4.1 Background and interferences

The background sulfate production in the absence of an added oxidant was measured by running the reactor with MilliQ water and SO_2. The SEM measurements showed that 0.65±0.74 nmol hr^{-1} of sulfate was generated, with a $\delta^{34}S$ of 17.0±4.7‰. This is consistent with measurements of SO_2 aqueous oxidation ($\delta^{34}S$ = 15.1±1.3‰) and of sulfate production from SO_2 on glass walls in the absence of an added oxidant ($\delta^{34}S$ = 13.0±1.5‰) (Section 2.4.2), showing that the background sulfate is produced from aqueous oxidation by oxidising impurities in the MilliQ water and/or on the reactor walls. The background contributes <13% of sulfate to all samples and a correction was made to take this into account when calculating the fractionation factors.

Background sulfate will also be present in the sea salt aerosol experiments from the sea salt mixture itself. The predicted background of sulfate was $<9.7\times10^{-6}$ nmol hr^{-1}, calculated from the maximum impurity levels in the salts used for preparation and the total volume of aerosol measured by OPC and SMPS. This was tested by running the reactor with sea salt aerosol but no SO_2. 0.01±0.01 nmol hr^{-1} of sulfate was measured on the sea salt blank filters in the SEM. The SEM value may be higher than the actual quantity due to the extremely small amount of sulfate present and the difficulty of separating the gold and sulfur peaks in the EDX (see Section 2.3.5). The two blank filters were also examined in the NanoSIMS. Four (two per filter) 40 x 40 μm images integrating the signal over ∼15 minutes were taken to test if any sulfate particles could be seen. Only one sulfate particle was noticeable, on a total filter area of 9600 μm^2. This results in a blank of 1 particle in >900 analyte particles. Such a blank can be caused by deposition of laboratory dust or by dislodging particles from another filter during handling of the sample. 5 x 5 μm isotope analyses were taken to quantify the ^{32}S signal from the salt on the filter. The average count rate was 61±61 counts per second for 9 analyses taken at random points on the two blank filters. This is not significantly different from the background count rate of untreated Nuclepore filters (32 counts per second). Thus, the background sulfate contributed by the sea salt solution is insignificant and does not need

to be corrected for in the following analyses.

The ssaltO3direct sample was measured to test if extra fractionation was introduced by extracting the collected sulfate and precipitating it as $BaSO_4$. The IMF for Na_2SO_4 was measured to test that different instrumental conditions had not affected the correction for $NaSO_4$ relative to $BaSO_4$; the measured relative IMF agreed with the value quoted in Winterholler et al. (2008). The value in Winterholler et al. (2008) was used for the correction as it has a smaller uncertainty than the value measured in the present study. The fractionation measured for ssaltO3direct agreed with the sea salt samples that were extracted and analysed as $BaSO_4$, with measured fractionation factors of α_{34} = 1.014±0.011 and α_{34} = 1.0137±0.0035 respectively. This shows that no information is lost and no isotopic fractionation is introduced by extracting and precipitating the sulfate as $BaSO_4$ for analysis. The counting statistical error for ssaltO3direct was very high as the sample could only be collected for <20 minutes before the filter loading was too high for NanoSIMS analysis (>5 μm-thick cover over whole filter).

3.4.2 Dependence of isotopic fractionation on pH during aqueous oxidation by H_2O_2

The fractionation factors measured at high and low pH are shown in Table 3.3. These measurements can be used to assign the fractionation to each step of (Eriksen, 1972a):

$$SO_2(g) \rightleftharpoons SO_2(aq) \tag{3.7}$$

$$SO_2(aq) + H_2O \rightleftharpoons H_2SO_3 \tag{3.8}$$

$$H_2SO_3 \rightleftharpoons HSO_3^- + H^+ \tag{3.9}$$

$$HSO_3^- \rightleftharpoons SO_3^{2-} + H^+ \tag{3.10}$$

Equation 3.9 has a pK_a of 1.77 and Equation 3.10 has a pK_a of 7.19 (Moore et al., 2005). Chmielewski et al. (2002) measured the fractionation factor for phase change (Equation 3.7) to be α_{phase} = 1.00256±0.00024 at 18°C. The fractionation factors for hydration (Equation 3.8) and the first proton loss (Equation 3.9) can be found by plotting the fractionation factors at pH = 2.1 and pH = 4 against the fraction of HSO_3^-: The intercept at $f(HSO_3^-) = 0$ gives the fractionation factor for hydration as $\alpha_{\text{hydration}}$ = 1.0105±0.0037, and the increase in fractionation at $f(HSO_3^-) = 1$ gives the fractionation factor for the first proton loss as $\alpha_{K_{a_1}}$ = 1.0042±0.0037 (Figure 3.3). A plot of the fractionation factors at pH = 4 and pH = 7.2 against the fraction of SO_3^{2-} can be used to find the fractionation factor for the second proton loss (Equation 3.10) at the intercept where $f(SO_3^{2-}) = 1$: $\alpha_{K_{a_2}}$

= 1.0052±0.0044. Previous results have shown that the terminating oxidation reaction is unimportant for isotopic fractionation at this level of uncertainty (Section 2.4.1). The measurements and fractionations introduced at each step from SO_2 (g) to SO_3^{2-} (aq) are summarised in Figure 3.3.

Table 3.3: **Fractionation factors for SO_2 uptake and oxidation at different pH values**. Values at pH = 2.1 and 7.2 were measured at 19°C during the aqueous oxidation of SO_2 in 1% H_2O_2 at two different pHs. The fractionation factors are the average of duplicate experiments and the uncertainty is the 1σ error in the measurements. [1]pH = 4 was measured by Egiazarov et al. (1971) and does not include a terminating oxidation reaction.

pH	$f(H_2SO_3)$	$f(HSO_3^-)$	$f(SO_3^{2-})$	α_{34}	1σ
2.1	0.46	0.54	0	1.0154	0.0037
4[1]	0	1	0	1.0173	0.0003
7.2	0	0.5	0.5	1.0199	0.0024

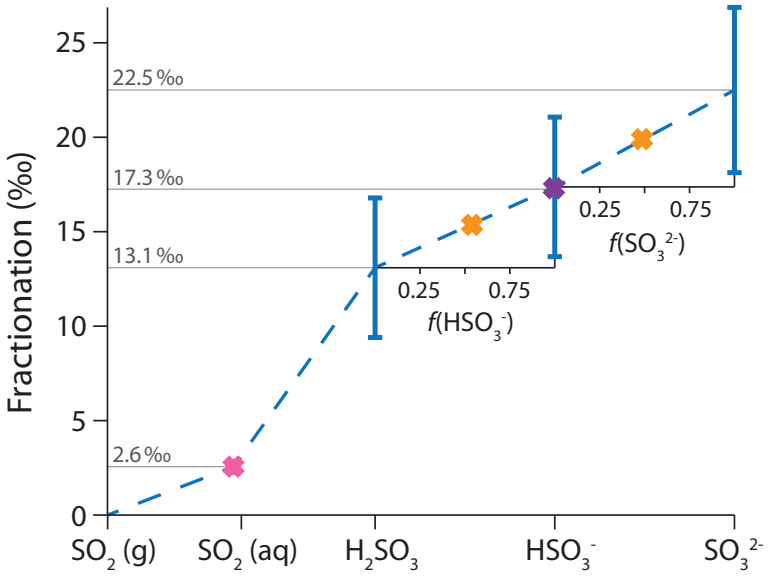

Figure 3.3: **Fractionation of $^{34}S/^{32}S$ at the different stages of SO_2 (g) $\rightarrow\rightarrow$ SO_3^{2-} (aq)**. The blue line and error bars show the cumulative change in $\delta^{34}S$ as the reactions proceed. The crosses show measurements: yellow crosses are results from this paper, the pink cross is from Chmielewski et al. (2002) and the purple cross is from Egiazarov et al. (1971). All values are shown for 18-19°C.

3.4.3 Sulfate production rate during aqueous oxidation in droplets

The quantity of sulfate produced from 9 ppm SO_2 (11.5 μmol hr^{-1}) in the different droplet experiments is shown in Figure 3.4. The amount of sulfate generated in sea salt aerosol in the presence and absence of O_3 is not significantly different. Sulfate generation from oxidation by O_3 is limited by alkalinity, so this suggests that either i) another pathway also limited by alkalinity is fast enough to titrate alkalinity completely in the absence of O_3, or ii) O_3 has no significant role in oxidation in sea salt aerosol, even when it is present in the reactor air. Hoppel et al. (2001) conducted chamber oxidation experiments for SO_2 in sea salt aerosol and found oxidation was dominated by ·Cl-catalysis: the 'ZM mechanism' (Zhang and Millero, 1991). This pathway is alkalinity-limited and favoured at high SO_2 concentrations (Hoppel and Caffrey, 2005), and it is the most likely oxidation pathway to be acting complementary to O_3 in the sea salt experiments.

Rough estimates of the uptake coefficients for the different experiments were made. The observed reactive uptake coefficient γ_{obs} for sulfate production represents a combination of mass transfer, accommodation and reaction limitations. It is approximated at low conversion to product according to (Jayne et al., 1990):

$$\gamma_{obs} = \frac{4F_g}{\bar{c}A}\frac{\Delta n}{n} \tag{3.11}$$

where F_g is the carrier gas flow rate (cm^3 s^{-1}), $\bar{c}$ is the mean thermal velocity (cm s^{-1}; $\sqrt{\frac{3k_B T}{m}}$), A is the total droplet surface area (cm^2) and $\frac{\Delta n}{n}$ is the reduction in gas concentration. The reduction in SO_2 was approximated as the sulfate production rate and therefore does not consider S(IV) (aq) that was taken up but not oxidised.

The uptake coefficients for NaOCl aerosol are very high, and significantly higher without irradiation ($\gamma_{obs} = 0.20 \pm 0.10$ and 0.49 ± 0.04 with and without irradiation respectively). Oxidation of sulfite by HOCl proceeds via nucleophilic attack of SO_2^{3-} on HOCl which results in Cl^+ transfer to form $ClSO_3^-$ (Yiin and Margerum, 1988). Hydrolysis of chlorosulfuric acid to form sulfate, H^+ and Cl^- is the rate-limiting step, thus the aerosol will not be acidified as rapidly as with other oxidation mechanisms (Yiin and Margerum, 1988; Fogelman et al., 1989; Troy and Margerum, 1991), which may partially explain the very high reactive uptake coefficient. Irradiation could speed up the hydrolysis of $ClSO_3^-$, decreasing the reactive uptake coefficient.

The values of γ_{obs} measured for the sea salt aerosols (average $\gamma_{obs} = 0.0009 \pm 0.0002$) are much lower than those for OCl droplets, and also lower than previously reported values: Jayne et al. (1990) measured $\gamma = 0.028 \pm 0.005$ at pH 6-8 and Gebel et al. (2000)

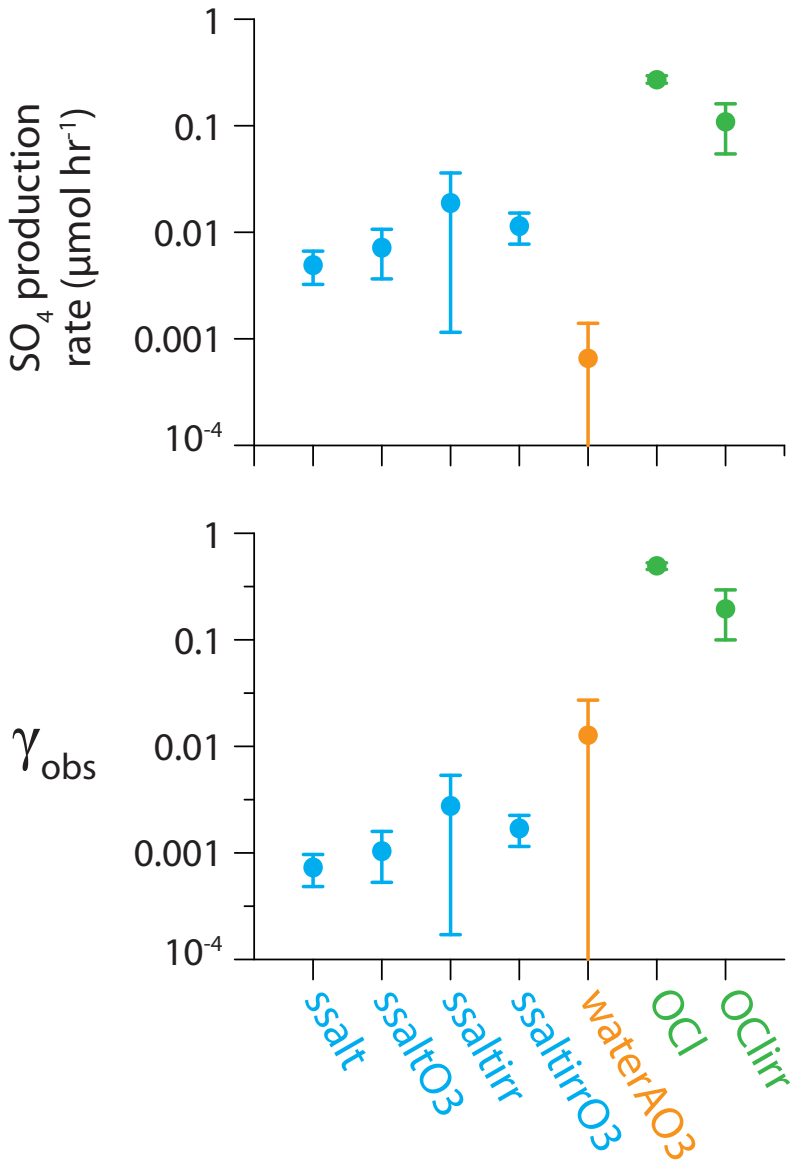

Figure 3.4: **Rates of sulfate production and reactive uptake coefficients for SO_2 (g) oxidation in different aerosol types subject to various experimental parameters**.

measured an initial uptake coefficient of $\gamma_i = 0.09$ which decreased rapidly with a $t^{-1/2}$ dependence. The low reactive uptake coefficients in this study are due to fast exhaustion of the alkalinity in the aerosols followed by much slower uptake in the acidified aerosols, resulting in low γ_{obs} for the overall experiment. Similar behaviour of the SO_2 uptake coefficient for sea salt aerosol was seen by Gebel et al. (2000). The values of γ_{obs} measured for the irradiated sea salt experiments are slightly higher than without irradiation, although the difference is within the experimental error. This suggests a small production of alkalinity from ·OH radicals due to reactions such as those described by Laskin et al. (2003); the effect of this pathway is expected to be more significant in the laboratory than in the ambient environment due to the absence of methane and acids such as HNO_3 (Keene and Pszenny, 2004; von Glasow, 2006). The uptake coefficient for waterAO_3 is 0.13±0.14, thus it is not significantly different to ssaltO_3, however the error in the estimate for waterAO3 is high as the absolute amount of sulfate and the aerosol number concentration are both low, leading to high measurement errors for both parameters.

3.4.4 Fractionation of sulfur isotopes during uptake and oxidation in droplets

In all droplet experiments, <3% of SO_2 reacted to form sulfate, therefore the isotopic composition of the product sulfate can be directly taken as the α_{34} without considering Rayleigh fractionation effects due to depletion of the reservoir (see Mariotti et al. 1981; Krouse and Grinenko 1991). The measured fractionation factors are shown in Figure 3.5 and Table 3.4. Irradiation and ozone did not cause significant changes in the measured fractionation factors: The fractionation factors under all experimental conditions for the two different droplet types (NaOCl and sea salt aerosols) agree within the measurement error, and the total average α_{34} values for the two droplet types are also shown in Table 3.4. Fractionation of $^{33}S/^{32}S$ was mass-dependent with respect to $^{34}S/^{32}S$ for all experiments.

The α_{34} for waterAO3 ($\alpha_{34} = 1.0157\pm0.0031$) agreed with the low pH value from Section 3.4.2 ($\alpha_{34} = 1.0154\pm0.0037$) and with previous measurements of oxidation by O_3 in water ($\alpha_{34} = 1.0174\pm0.0028$; Section 2.4.1), confirming that microphysical effects of droplet vs. bulk do not effect fractionation, and that the terminating oxidation for aqueous oxidation by O_3 and H_2O_2 oxidation is unimportant compared to the phase change and aqueous S(IV) equilibria. An overall α_{34} of 1.0163±0.0018 for oxidation by O_3 in water was calculated as a weighted average from this chapter and the previous value. This average represents oxidation at low pH even in non-buffered solutions, because although O_3 reacts several orders of magnitude faster with SO_3^{2-} than with HSO_3^-, sulfate production will

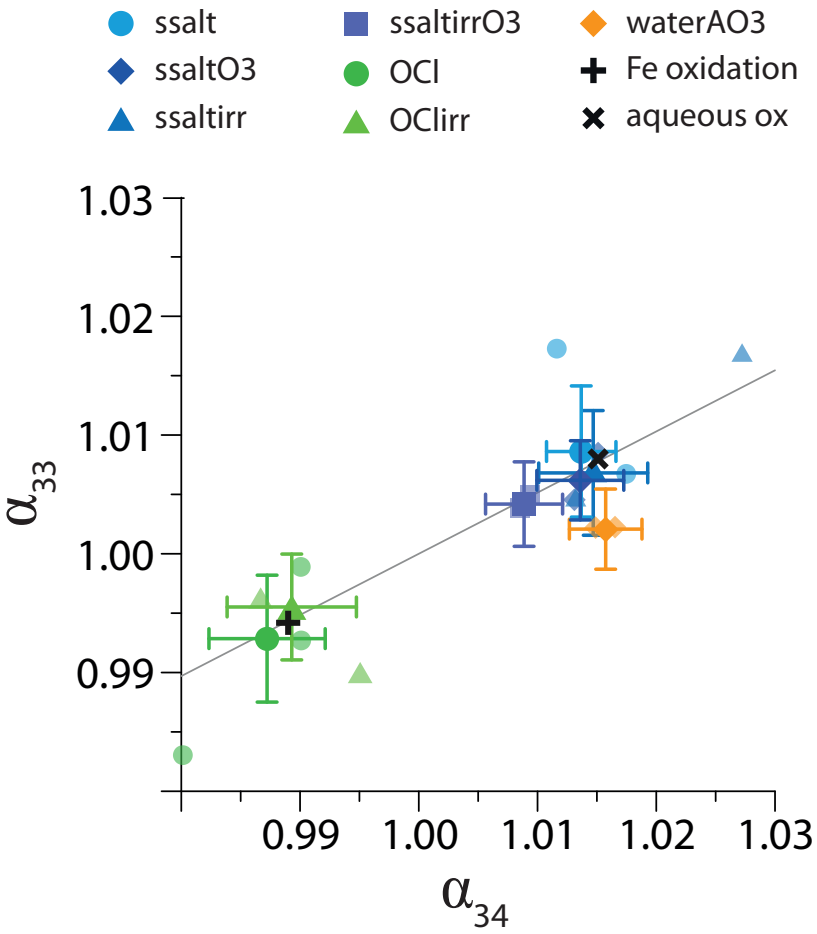

Figure 3.5: **Fractionation factors for the uptake and oxidation of SO_2 by droplets of pure water, sea salt aerosol and NaOCl aerosol**. Pale points are the individual experimental runs for each set of conditions, while dark points show the average with 1σ error bars. The grey line represents mass dependent fractionation and the black crosses show previously measured fractionation factors from Section 2.4.1.

Table 3.4: **Fractionation factors for the uptake and oxidation of SO_2 by droplets of pure water, sea salt aerosol and NaOCl aerosol**. Values in bold are the averages for a particular aerosol type; for the oxidation of SO_2 in pure water aerosol by O_3, the present value is averaged with previous measurements from Section 2.4.1. n is the number of measurements and 1σ is the error of the measurements.

	n	α_{34}	1σ	α_{33}	1σ
waterAO3	13	1.0157	0.0031	1.0022	0.0034
water + O_3		**1.0163**	0.0018	**1.0117**	0.0207
ssalt	16	1.0137	0.0029	1.0087	0.0055
ssaltO3	18	1.0136	0.0037	1.0063	0.0033
ssaltirr	14	1.0147	0.0046	1.0068	0.0052
ssaltirrO3	15	1.0089	0.0032	1.0043	0.0036
sea salt		**1.0124**	0.0017	**1.0061**	0.0020
OCl	18	0.9872	0.0049	0.9930	0.0053
OClirr	15	0.9893	0.0054	0.9956	0.0045
NaOCl		**0.9882**	0.0036	**0.9946**	0.0034

quickly acidify water until the pH is low enough for the $[SO_3^{2-}]$ to be negligible.

The fractionation factor for oxidation in NaOCl solution will represent oxidation by HOCl, as the pK_a of HOCl is 7.53 so the $[OCl^-]$ will be negligible in acidic solution, and the rate constant for oxidation of sulfite by HOCl is >4 orders of magnitude higher than for OCl^- (Yiin and Margerum, 1988; Shaka et al., 2007). The measured value of α_{34} (0.9882±0.0036) is not significantly different to oxidation by a radical chain reaction initiated by Fe(III) (α_{34} = 0.9905±0.0031; Section 4.4.2), although the mechanisms are not similar. This suggests that following the equilibrium fractionation of 17.3±3.7‰ for SO_2 (g) ↔ HSO_3^- at 19°C, kinetic effects related to fundamental differences in the energy and stability of sulfite and sulfate - which are common to both reactions - cause kinetic fractionation of -28‰.

The fractionation factor for oxidation in sea salt aerosol (α_{34} = 1.0124 ± 0.0017) is lower than the fractionation factor for aqueous oxidation of SO_3^{2-} (α_{34} = 1.0225 ± 0.0044), although the high pH and ionic strength of sea water mean SO_3^{2-} would be the dominant species oxidised by O_3 or ·Cl catalysis, thus showing the role of oxidation by HOCl in sea salt aerosol. Transition metal ions capable of catalysing oxidation (eg. Fe, Mn, V; Herrmann et al. (2000); Rani et al. (1992)) were not added to the synthetic sea salt mixture, so the contribution of HOCl oxidation to the total oxidation in sea

salt aerosol can be estimated by comparing the overall fractionation in sea salt aerosol to fractionation factors for SO_2 (g) $\rightarrow$ SO_3^{2-} (aq) and oxidation by HOCl. This shows that HOCl contributes 29±9% of oxidation in sea salt aerosol under the conditions of this study. The measured α_{34} in sea salt aerosol is lowest for ssaltirrO3, although the difference between the fractionation factors for ssaltirrO3 and ssaltO3 is within the experimental error. The ssaltirrO3 sample would be expected to have the highest concentration of hypochlorous acid from interface reactions where O_3 photolysis leads to formation of ·OH and subsequently HOCl (see Oum et al. (1998) and Knipping et al. (2000) for details). HOCl is calculated to contribute 40±16% of oxidation in this experiment.

The calculated contributions of the HOCl pathway are expected to be a minimum compared to the actual atmospheric proportion as HOCl oxidation is not pH limited, thus although it contributes only 29% of oxidation in the short timescale of this study it could become the major oxidation pathway over the lifetime of sea salt aerosol in the marine environment (von Glasow et al., 2002). Although the partitioning between oxidation mechanisms in this study will not be representative of the marine environment due to the complex relationship between oxidation pathways and alkalinity, light, droplet size, and reactant concentrations, the results show that sulfur isotopes are very useful to investigate relative contributions of these oxidation pathways.

3.4.5 Comparison to field observations

A number of studies have used oxygen and sulfur stable isotopes to investigate sources and oxidation pathways of sulfate in the marine boundary layer (MBL). Many of these studies have employed a three-source mixing scheme, explaining the isotopic observations with mixing between heavy sea salt sulfate and marine biogenic *nss*-sulfate, and a light source that is attributed to anthropogenic or continental sulfate (Patris et al., 2000; Wadleigh, 2004; Turekian et al., 2001). The general success of this mixing model suggests isotopic fractionation has overall only a small effect on measured δ^{34}S of *nss*-sulfate, thus it is likely the amount of sulfate produced by ^{34}S-enriching, alkalinity limited pathways (O_3 oxidation and ·Cl-catalysis) is roughly equal to that from ^{34}S-depleting pathways (Fe-catalysis and hypohalite oxidation).

Field measurements of δ^{34}S in marine environments are often lower than expected and many even fall below the three-source mixing region, while measurements for this regime are rarely enriched in ^{34}S compared to the three-source mixing region (Wadleigh, 2004). In some samples an isotopically-light 'continental' influence was seen although the back trajectories showed a pure marine origin of the air mass (Patris et al., 2000).

δ^{34}S of *nss*-sulfate is lower in smaller particles, which has been attributed to a larger continental influence in these particles (Turekian et al., 2001; Patris et al., 2000, 2007). These observations could all be explained by the influence of oxidation pathway on isotopic composition. It appears that under some atmospheric conditions the HOCl/Fe pathways are favoured over the O_3/Cl-catalysis pathways, leading to sulfate more depleted in ^{34}S. This may be when alkalinity is low due to low winds, or when aerosols have a longer lifetime to accumulate *nss*-sulfate after alkalinity has been depleted. Alkalinity is depleted in smaller aerosols faster than in larger aerosols, thus the partioning between the alkalinity-limited pathways and HOCl/Fe oxidation can account for the lower δ^{34}S values observed in smaller particles.

The triple oxygen isotope composition of sulfate, represented by Δ^{17}O, has also been used to investigate oxidation pathways of SO_2 in the marine environment (Alexander et al., 2005; Patris et al., 2007). ·OH radicals and O_2, which acts as the oxidant during transition metal catalysis, result in sulfate with $\Delta^{17}O = 0‰$, while oxidation by O_3 and H_2O_2 produces sulfate with $\Delta^{17}O = 8.8$ and $0.8‰$ respectively (Savarino et al., 2000; Lee and Thiemens, 2001). The Δ^{17}O of HOX has not been measured, however Patris et al. (2007) have estimated it based on the major formation pathways: HOX may have a Δ^{17}O similar to ozone due to formation from XNO_3, or it may have a Δ^{17}O of $0‰$ if the HOX oxygen atom comes from atmospheric water. If the Δ^{17}O of hypohalites was reliably known, it would be possible to distinguish between all the major MBL SO_2 oxidation pathways (gas-phase by ·OH, heterogeneous by O_3, ·Cl catalysis, Fe catalysis and hypohalites) based on the oxygen and sulfur isotopic composition of SO_2 and sulfate.

3.5 Conclusions

Sulfur isotope fractionation factors for the oxidation of SO_2 in water, synthetic sea water and concentrated NaOCl droplets were measured. Reactive uptake coefficients for NaOCl droplets were very high, in agreement with the rapid rate of the reaction, while γ_{obs} for sea water reflected alkalinity limitations for oxidation by O_3 and ·Cl catalysis. A summary of the measured isotopic fractionation factors in the marine boundary layer is shown in Figure 3.6.

The fractionation factors for each step from SO_2 (g) uptake to SO_3^{2-} (aq) formation were measured, showing an increase in isotopic fractionation at higher pH. α_{34} for oxidation by O_3 in water droplets agreed with previous results for aqueous oxidation by O_3 and with low pH measurements, while α_{34} for oxidation by O_3 in sea salt aerosol also

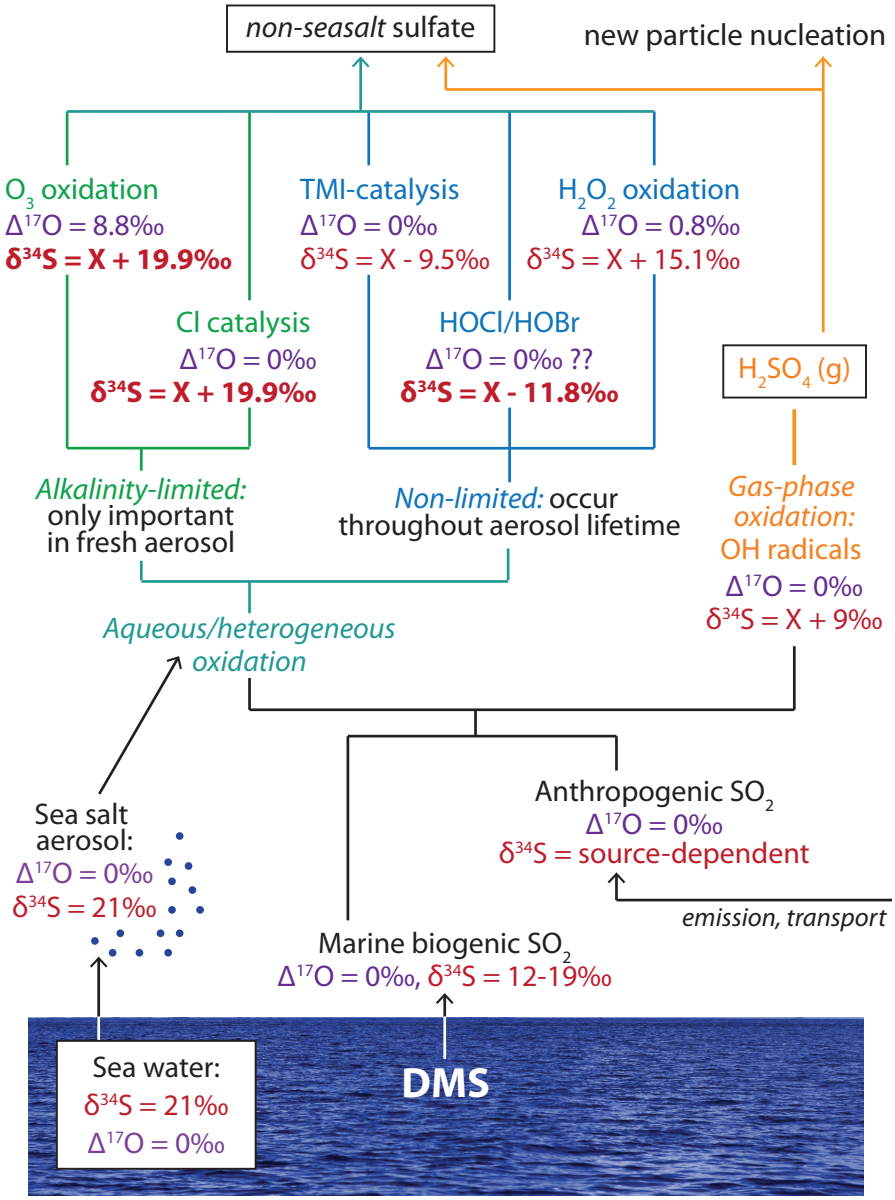

Figure 3.6: **Summary of the SO_2 oxidation reactions occurring in the marine boundary layer and their effect on the isotopic composition of product sulfate**. Initial isotopic compositions of sea water and marine biogenic sulfate are from Rees et al. (1978) and Calhoun et al. (1991) respectively. $\Delta^{17}O$ values refer to the sulfate resulting from oxidation, not the oxidant itself, and are from Savarino et al. (2000). $\delta^{34}S$ fractionations during oxidation reactions are shown as a change, where X is the $\delta^{34}S$ of the SO_2 reactant gas. Fractionation factors are for 19°C; those measured in this chapter are shown in bold and all other $^{34}S/^{32}S$ fractionations are from Chapters 2 and 4.

favoured the heavy isotope but with a lower magnitude. Oxidation in NaOCl droplets, on the other hand, favoured the light isotope and produced isotopic fractionation indistinguishable from previous measurements for oxidation by iron catalysis. Comparison of the fractionation factors showed that the HOCl pathway contributed 29% of oxidation on sea salt aerosol in the short experimental timescale, suggesting that it can play an important role in the marine sulfur cycle.

The opposite directions of isotopic fractionation mean that sulfur isotope measurements will be particularly useful to estimate the importance of SO_2 oxidation by alkalinity non-limited HOCl and iron catalysis pathways compared to alkalinity-limited pathways of oxidation, as they favour the light and the heavy sulfur isotopes respectively. In combination with measurements of $\Delta^{17}O$, $\delta^{34}S$ measurements have the potential to distinguish between all the SO_2 oxidation pathways occurring in the marine environment, which would allow direct measurements of oxidation in the marine sulfur cycle leading to a new understanding of its role in atmospheric chemistry and climate.

Acknowledgements

We thank Elmar Gröner for his support with the NanoSIMS analyses, John Crowley for valuable discussions on the material presented in this paper, Joachim Huth for his help with the SEM/EDX analyses, and Thomas Klimach for assistance with particle size distribution measurements. This research was funded by the Max Planck Society and the Max Planck Graduate Centre.

Chapter 4

Sulfur isotope fractionation during heterogeneous oxidation of SO_2 on mineral dust

This chapter is published for discussion as Harris, E., Sinha, B., Foley, S., Crowley, J.N., Borrmann, S. and Hoppe, P. (2012) *Atmospheric Chemistry and Physics Discussions*, 12, 2303-2353, doi:10.5194/acpd-12-2303-2012.

4.1 Introduction

Mineral dust represents the dominant mass fraction of atmospheric particulate matter, and it is responsible for a large amount of the uncertainty associated with aerosol climate forcing effects. Dust is important for heterogeneous chemistry, human health, visibility, ocean nutrification, and cloud formation. Emissions are estimated to be between 1000 and 2150 Tg yr^{-1}, resulting in a global dust load of 8 to 36 Tg (Zender et al., 2004; Tanaka and Chiba, 2006). Dust emissions are expected to increase due to erosion, mining and industrial activities, overgrazing and shifting precipitation patterns (Dentener et al., 1996). Mineral dust properties are altered during transport, as finer clays are transported far from source regions relative to coarse particles, and dust particles are chemically aged by uptake of gas-phase species and heterogeneous reactions (Morales, 1986; Kim and Park, 2001; Park et al., 2004; Zhu et al., 2010).

The uptake of sulfate on to mineral dust is important both for dust properties and for the sulfur cycle. Freshly-emitted Sahara dust is very hydrophobic (Kaaden et al., 2009), whereas sulfate-coated mineral dust has increased CCN activity and may even act

as 'giant CCN' (Levin et al., 1996), while sulfate coatings reduce the ice nuclei activity of mineral dust (Cziczo et al., 2009; Pruppacher and Klett, 1997). Mineral dust is a particularly important source of iron in nutrient-limited open ocean waters, and chemical ageing can reduce the pH of dust, increasing the solubility and bioavailability of iron (Jickells et al., 2005; Gasso et al., 2010; Rubasinghege et al., 2010; Kumar et al., 2010). Heterogeneous oxidation of SO_2 on dust can lead to reductions of >50% in SO_2 concentration, and may account for 50-70% of sulfate production in dust source regions (Dentener et al., 1996; Xiao et al., 1997; Zhu et al., 2010). Coagulation on to dust can also remove sulfuric acid aerosol and gas from the atmosphere. This means that dust reduces homogeneous nucleation of H_2SO_4 and changes the size distribution of sulfur towards coarse particles, reducing its lifetime compared to sulfate in finer particulate. It is estimated that heterogeneous reactions on mineral dust reduce sulfate and nitrate aerosol cooling near dust source regions by 0.5 - 1 W m^{-2} (Dentener et al., 1996; Liao and Seinfeld, 2005). Understanding the uptake and oxidation of SO_2 on mineral dust is a key part of investigating the interactions and feedbacks between dust, sulfur, climate and clouds.

Sulfur isotopes have previously been used to investigate homogeneous and aqueous oxidation of SO_2 by ·OH, H_2O_2 and O_3 in pure solutions and on sea salt aerosol (Chapter 2 and Chapter 3). Sulfur isotope abundances are described by the delta notation, which is the permil deviation of the ratio of a heavy isotope to the most abundant isotope (^{32}S) in the sample compared to a standard ratio:

$$\delta^{x}\mathrm{S}\ (‰) = [\frac{(\frac{n(^{x}\mathrm{S})}{n(^{32}\mathrm{S})})_{\mathrm{sample}}}{(\frac{n(^{x}\mathrm{S})}{n(^{32}\mathrm{S})})_{\mathrm{V-CDT}}} - 1] \times 1000 \tag{4.1}$$

where n is the number of atoms, ^{x}S is one of the heavy isotopes, ^{33}S, ^{34}S or ^{36}S, and V-CDT is the international sulfur isotope standard, Vienna Canyon Diablo Troilite, which has isotopic ratios of $^{34}S/^{32}S = 0.044163$ and $^{33}S/^{32}S = 0.007877$ (Ding et al., 2001). Isotopic fractionation is represented by the α value, which is the ratio of the heavy to the light isotope amount in the instantaneously-formed product divided by the ratio in the reactant:

$$\alpha_{34} = \frac{(\frac{^{34}\mathrm{S}}{^{32}\mathrm{S}})_{\mathrm{products}}}{(\frac{^{34}\mathrm{S}}{^{32}\mathrm{S}})_{\mathrm{reactants}}} \tag{4.2}$$

Values of α_{34} are characteristic for different reaction pathways and are therefore useful to investigate the different oxidation pathways for SO_2 on mineral dust in the laboratory and in the atmosphere.

This chapter presents measurements of the stable isotope fractionation of $^{34}S/^{32}S$ at room temperature (19°C) during heterogeneous oxidation on dust surfaces and aqueous

oxidation in dust leachate. The dust used is from the Sahara desert, which accounts for ∼60% of global dust emissions and loading (Tanaka and Chiba, 2006). The dust was collected on the Cape Verde islands (SDCV), and its mineralogy, composition and properties, as well as details on collection, are described in Coude-Gaussen et al. (1994) and Hanisch and Crowley (2001, 2003). We demonstrate that stable sulfur isotopes can be used to understand SO_2 oxidation on mineral dust both in the laboratory and in the field, and are particularly useful to investigate the roles of different minerals in surface oxidation and to quantify the importance of aqueous oxidation by transition metal ions in the atmosphere.

4.2 Background: Uptake and oxidation of SO_2 by mineral dust

Uptake of SO_2 to mineral dust can occur via the reversible, physisorption pathway, or the irreversible, chemisorption pathway, which can be followed by oxidation of the sorbed sulfite. This study will only consider irreversible uptake, which accounts for >98% of uptake at low SO_2 concentrations (Adams et al., 2005; Goodman et al., 2001). The initial uptake coefficient on Sahara dust, $\gamma = 4 \times 10^{-5}$, is not dependent on RH, $[SO_2]$ or O_3 (Crowley et al., 2010) which suggests SO_2 adsorption is the rate-limiting step, rather than subsequent reactions and oxidation (Ullerstam et al., 2002).

Oxidation of adsorbed S(IV) can follow a number of pathways: O_3 is a very efficient oxidant, and oxidation can also be catalysed by iron and manganese in dust (Usher et al., 2002; Ullerstam et al., 2002). NO_2 (g) and surface nitrate have been observed to oxidise surface sulfite (Ullerstam et al., 2003), and oxidation to $CaSO_4$ occurs when calcite is exposed to SO_2 and O_2 (Al-Hosney and Grassian, 2005). Sulfate production has even been observed on MgO in the absence of O_2 and O_3, and was attributed to the highly basic character of four-coordinated O anions on steps and corners (Pacchioni et al., 1994; Goodman et al., 2001). In this study, SO_2 will always be exposed to dust in synthetic air, and the reaction time will be very long, so the oxidation of adsorbed sulfite to sulfate should be close to completion (Ullerstam et al., 2002).

The SO_2 removal rate on dry dust decreases significantly with exposure to SO_2 as saturation is approached, suggesting uptake will only be important for ∼10 hours after dust emission (Judeikis et al., 1978). However, active sites can be regenerated by exposure to high humidity for a number of reasons, for example, carbonic acid dissociation and release as CO_2 (g), increased mobility of surface ions leading to microcrystallite formation,

and direct generation of new active sites (Ullerstam et al., 2002, 2003; Al-Hosney and Grassian, 2005; Li et al., 2006). IR absorption bands for adsorbed sulfate do not change upon exposure to humidity (Ullerstam et al., 2002, 2003). Saturation behaviour of SO_2 under exposure to UV light has not been measured, however irradiation prevents surface saturation for ozone uptake on TiO_2 (Nicolas et al., 2009). These results suggest that experimental conditions such as humidity, ozone and irradiation will change the quantity of SO_2 taken up and oxidised, while the initial uptake to form sorbed S(IV) is the rate-limiting step and is therefore expected to be the major factor controlling isotopic fractionation.

Aqueous oxidation by ions leached from dust may be a particularly important contributor to oxidation of SO_2 in the atmosphere, especially as sulfate production increases aerosol hygroscopicity and CCN activity, facilitating further aqueous SO_2 oxidation (Usher et al., 2002; Ullerstam et al., 2002, 2003; Li et al., 2006). The oxidative activity of leachates is due to catalysis by transition metal ions: Fe(III) is the most important of these ions, however comparison to experiments with pure Fe salts show trace ions such as Mn and Cr also make a significant contribution to catalytic activity (Tilly et al., 1991; Rani et al., 1992). Catalytic activity does not significantly change when the solid phase is filtered out of the leachate. This shows aqueous oxidation dominates over any surface effects of particles in the solution (Cohen et al., 1981; Rani et al., 1992), although, when aqueous iron and titanium oxide suspensions are irradiated, sulfate quantum yields $>>1$ have been observed due to desorption of $\cdot SO_3^-$ and initiation of a radical chain reaction (Hong et al., 1987; Faust et al., 1989).

Aqueous oxidation shows complex pH-dependence, as metal ions are more soluble but the more reactive SO_3^{2-} is less abundant at lower pH (Cohen et al., 1981; Rani et al., 1992). Dust is not the only contributor of transition metal ions for SO_2 oxidation: transition metals ions from anthropogenic sources are generally more soluble than ions in dust, and thus more available for reaction with S(IV) in solution (Kumar et al., 2010). The reaction pathways catalysed by anthropogenic and natural transition metal ions are the same once the ions are leached into solution, thus the fractionation factor measured for dust leachate in this study will also be applicable to leachate from combustion products such as fly ash (Cohen et al., 1981).

4.3 Methods

4.3.1 Apparatus and experiments

The dust used in this study was Sahara dust collected from the Cape Verde islands (SDVC). Its mineralogy, composition and properties are described in Coude-Gaussen et al. (1994) and Hanisch and Crowley (2001, 2003) and summarised in Table 4.1. The non-clay fraction of the dust contains primarily quartz, feldspars and calcite. Sahara sand obtained directly from the Sahara desert has a mean diameter of >150 μm (Morales, 1986), whereas transported dust contains dust particles as small as 200 nm and has a mean diameter of <10 μm that decreases with distance transported (Heinold et al., 2009; Kaaden et al., 2009; Wagner et al., 2009; Morales, 1986). Thus, Sahara dust from the Cape Verde Islands is much more relevant to atmospheric chemistry than a local sand sample which would include very coarse grain sizes.

Aqueous oxidation in mineral dust leachate

Leachate representing 0.5 g of dust per 100 mL was prepared by soaking the dust for two days in MilliQ water. The liquid phase was then poured off the solid dust, as aqueous oxidation has been shown not to be affected when the solid phase is removed (Cohen et al., 1981; Rani et al., 1992). The concentrations of Al, Ca, Fe, Mg, Ba, Mn, Ti, Cr and Sr in the leachate were measured by inductively-coupled plasma optical emission spectrometry with a Perkin-Elmer Optima 3300 XL. SO_2 gas (Linde AG, 102 ppm ± 2% in synthetic air) was diluted with synthetic air (Westfalen AG, 20.5% O_2 in N_2) to 6.7 ppm and 13.3 ppm in a total flow of 600 cm^3 min^{-1} (at standard conditions of T = 273.15 K, P = 1013.25 mBar) for experimental runs #1 and #2 respectively. This flow was passed through 300 mL of leachate in a bubbler, followed by a bubbler containing 6% H_2O_2 to collect residual SO_2 as described in Section 2.3.4. PFA fittings and tubings were used for all gas flows. The experiments were run for ∼8 hours. Following each experiment, both bubblers were rinsed and $BaCl_2$ was added to precipitate sulfate as $BaSO_4$. The $BaSO_4$ was collected by filtration through Nuclepore track-etch polycarbonate membrane filters (Whatman Ltd.) with 0.2 μm pores, which had been coated with a 10 nm-thick gold layer using a sputter coater (Bal-tec GmbH, Model SCD-050) prior to sample collection.

Table 4.1: **Composition and mineralogy of SDCV** adapted from Hanisch and Crowley (2003) and Coude-Gaussen et al. (1994) respectively.

Elemental composition	O	Si	Al	Mg	Ca	Fe	Ti	K	Na	Mn	P	S
Concentration (mg/g dust)	556.9	172.4	72.9	24.1	28.0	89.4	21.1	16.2	12.2	1.8	2.0	0.9
Mineralogy of clay fraction	Kaolinite		Smectite		Swelling chlorite		Chlorite		Illite			
Abundance (%)	34.3		10.5		14.2		7.9		30.3			

Heterogeneous oxidation on the Sahara dust surface at subsaturated humidity

Heterogeneous oxidation on mineral dust was investigated by passing 250 cm^3 min^{-1} of 4.2 ppm SO_2 gas in synthetic air through a dust-coated filter, as shown in Figure 4.1. Dust was pipetted on to gold-coated Nuclepore filters (0.2 μm pore) in a 1:2 ethanol:water mixture, which helped the dust to adhere to the filter better than mounting in pure water. A mixed cellulose ester filter (Whatman GmbH) was placed under the Nuclepore filter to prevent tearing when gas flows were switched on and off. The mounted dust had a modal diameter of 2 μm with maximum grain diameters of $\sim$8 μm, showing the dust was not significantly size-fractionated during mounting compared to the results of Coude-Gaussen et al. (1994). The reactor was made of glass with an FEP O-ring (Ralicks Industrie- und Umwelttechnik) connecting the two parts. PFA fittings and tubings were used for gas flows. SO_2 gas (Linde AG, 102 ppm $\pm$ 2% in synthetic air) was diluted with synthetic air (Westfalen AG, 20.5% O_2 in N_2) to the desired concentration before entering the reactor. A high concentration of SO_2 (4.2 ppm) was used to prevent significant isotopic changes to the residual SO_2. Less than 1% of the SO_2 gas reacted to form sulfate in all experiments. The residual SO_2 gas was collected in some experimental runs as described in Section 2.3.4 and the isotopic composition confirmed the SO_2 was not significantly altered during the experiments.

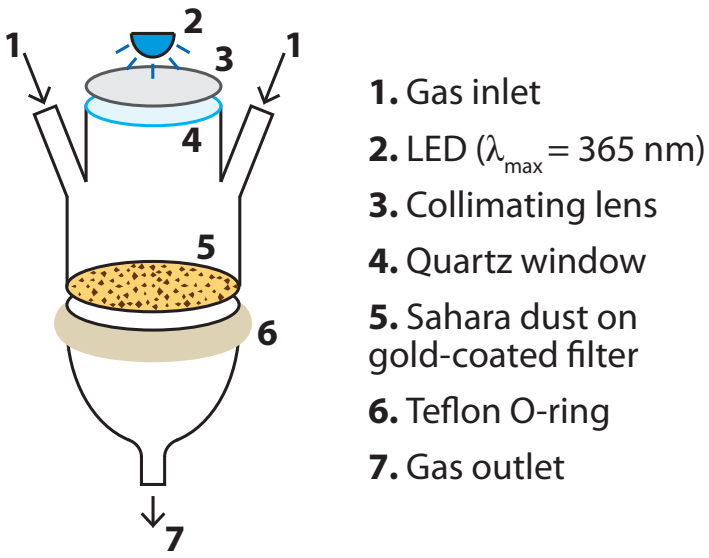

Figure 4.1: **Reactor used to investigate fractionation during oxidation of SO_2 on mineral dust**.

Table 4.2: **Experiments to investigate isotopic fractionation during oxidation of SO_2 on the surface of mineral dust**.

Abbreviation	**O_3**	**Light**	**Humidity**	**Run**	**Length (h)**
MDdark	✗	✗	✗	1	7.9
				2	7.2
MDO3	✓	✗	✗	1	7.9
				2	9.2
MDhv	✗	✓	✗	1	8.2
				2	8.2
MDO3hv	✓	✓	✗	1	7.8
				2	7.7
MDRHdark	✗	✗	✓	1	7.8
				2	8.3
MDRHO3	✓	✗	✓	1	7.5
				2	7.9
MDRHhv	✗	✓	✓	1	6.7
				2	7.3
MDRHO3hv	✓	✓	✓	1	6.3
				2	7.5

The reaction system was run under a variety of different conditions, which are summarised in Table 4.2 along with abbreviations that will be used throughout this paper. A high power LED (λ_{max} = 365 nm, 50 mW at 350 mA, Roithner Lasertechnik GmbH) was used to irradiate the dust in four experiments through a Suprasil quartz window (Heraeus Quarzglas GmbH), which has a transmittance of >90% between 200 and 1000 nm. The emission spectrum of the LED is shown in Figure 4.2, along with the absorption spectra of O_3 and SO_2. Neither O_3 or SO_2 absorb significantly in the wavelength range of the LED, so no gas-phase photolytic reactions will occur. Humidity was added to the reaction chamber in four experiments by passing the synthetic air flow through MilliQ water to achieve a relative humidity of around 40%, which would correspond to 2 monolayers of water on the dust (Gustafsson et al., 2005). The dust was not heated before use, so even samples with no added humidity will have surface-sorbed water molecules and interlamella water in the clay fraction. 20 ppm ozone was added to the gas mixture in four experiments by passing 100 cm^3 min^{-1} of the synthetic air flow over a low-pressure mercury vapour lamp (Jelight Company Inc., USA). The ozone concentration was measured

with a Thermo Electron Corporation UV Photometric O_3 Analyzer (Model 49C). Each experiment was done in duplicate with and without the addition of humidity, for a total of 16 experimental runs. The experiments were run for 6-9 hours to generate sufficient sulfate for NanoSIMS isotopic analysis. Following each experiment, filters were stored in airtight boxes before being mounted for NanoSIMS and SEM analysis.

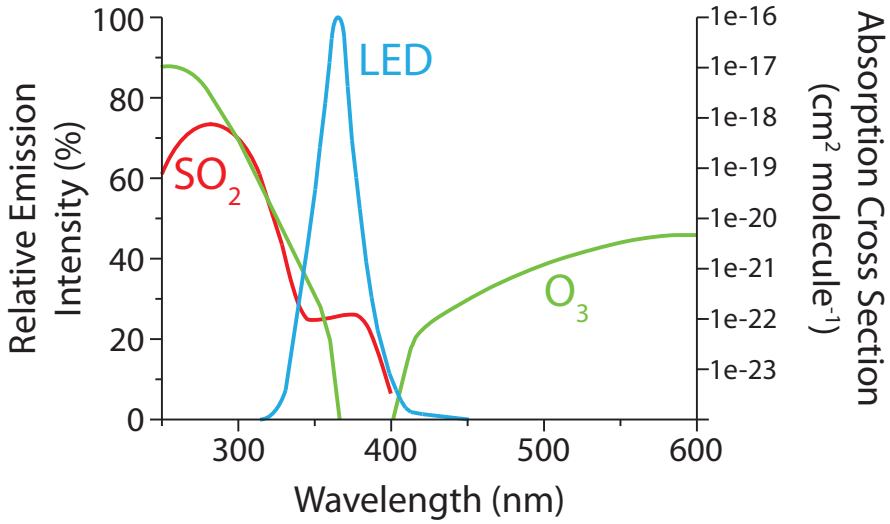

Figure 4.2: **Emission spectrum of LED used to irradiate mineral dust samples** (blue line, left axis, Roithner) and absorption spectra of SO_2 (red line, right axis, Rufus et al. 2003) and O_3 (green line, right axis, Bogumil et al. 2003)

4.3.2 SEM analysis

A scanning electron microscope (SEM) was used to investigate the quantity of sulfate produced during the leachate experiments and the composition of individual dust grains in the different samples for the surface reaction experiments. The $BaSO_4$ and dust samples on gold-coated filters were directly analysed in the SEM without any further treatment. A LEO 1530 field emission SEM with an Oxford Instruments ultra-thin-window energy-dispersive x-ray detector (EDX) was used for the analyses. The SEM was operated with an accelerating voltage of 10 keV, a 60 μm aperture, and a working distance of 9.6 mm. 'High current mode' was used to increase the EDX signal and improve elemental sensitivity.

Before NanoSIMS analysis of the samples, the SEM was run in automatic mode and took 400 evenly-spaced images of each filter at 19 500× magnification. The EDX spectrum was measured with a 1 second integration time at 25 points on a 5 × 5 grid for each image,

leading to 10 000 EDX measurements across each filter. For the leachate oxidation $BaSO_4$ samples, EDX signals were measured for O(K_α), Au(L_α), S(K_α) and Ba(L_α). The quantity of sulfate on each filter was then determined by estimating the background from both the Gaussian distribution of the gold signal and the quartile method, as described in Section 2.3.5 and Winterholler (2007). This quantification method is ideal for NanoSIMS studies, as quantification is achieved without extra sample treatment and the limit of detection is very low. The precision is fairly low (∼40%, decreasing with increasing $BaSO_4$ quantity due to Poisson statistics) and the method is not ideal for samples with a large amount of $BaSO_4$ due to the possibility of the sample flaking off the filter during mounting, thus isotope mass balance was also used to find the extent of reaction (see Section 4.4.1), as was used by Lin et al. (2011) and Derda et al. (2007), and in Chapter 2 of this thesis.

During the analyses of the dust grains from the surface oxidation experiments, seven EDX channels were measured in automatic mode: Fe(L_α), Mg(K_α), Al(K_α), Si(K_α), S(K_α), Ca(K_α) and Ti(K_α). The background was subtracted from the signals using the quartile method (see Section 2.3.5 and Winterholler 2007). The signals were used to investigate the composition of the mineral dust and association of sulfate with the different elements in the dust. The SEM images were also used to measure the size distribution of the dust, as described in Winterholler (2007). The density of the dust was estimated to be 3.1 g cm^{-3} from the densities of the three main components, SiO_2, Al_2O_3 and FeO, and this was used to calculate the mass of dust on each filter. The BET surface area of the dust was measured by Hanisch and Crowley (2001) to be 1.5 m^2 g^{-1} for grains with $d < 10$ μm.

Following NanoSIMS analysis, the dust grains from the surface oxidation experiments were again examined in the SEM, to determine the chemical composition of the dust grain for each NanoSIMS analysis point. Coordinate transfer was used to locate the grains in the SEM and an image and an EDX spectrum were then taken at each point. An example is shown in Figure 4.3. Peaks were counted if they were more than three times the noise at the peak position (Goldstein et al., 1981), and an approximate height was measured by overlaying a grid as shown in the figure. The known composition of the dust (Hanisch and Crowley, 2003) was used to determine relative sensitivity factors (RSF) for the different elements based on the EDX measurements on unreacted dust grains. RSF values were in the expected range of 0.1 to 2 (Goldstein et al., 1981). An approximate atomic percentage for all detectable elements could then be estimated for each experimental grain. The error in atomic percentage was defined as ±1 unit on the overlayed scale, multiplied by the RSF for the element. The resulting composition obtained for each dust grain is not surface-

sensitive as the X-rays are released from a depth of $< 1\mu$m (Goldstein et al., 1981), so the results will show the elements present at the analysis point but will not be especially sensitive to the newly-produced sulfate from the experimental treatment.

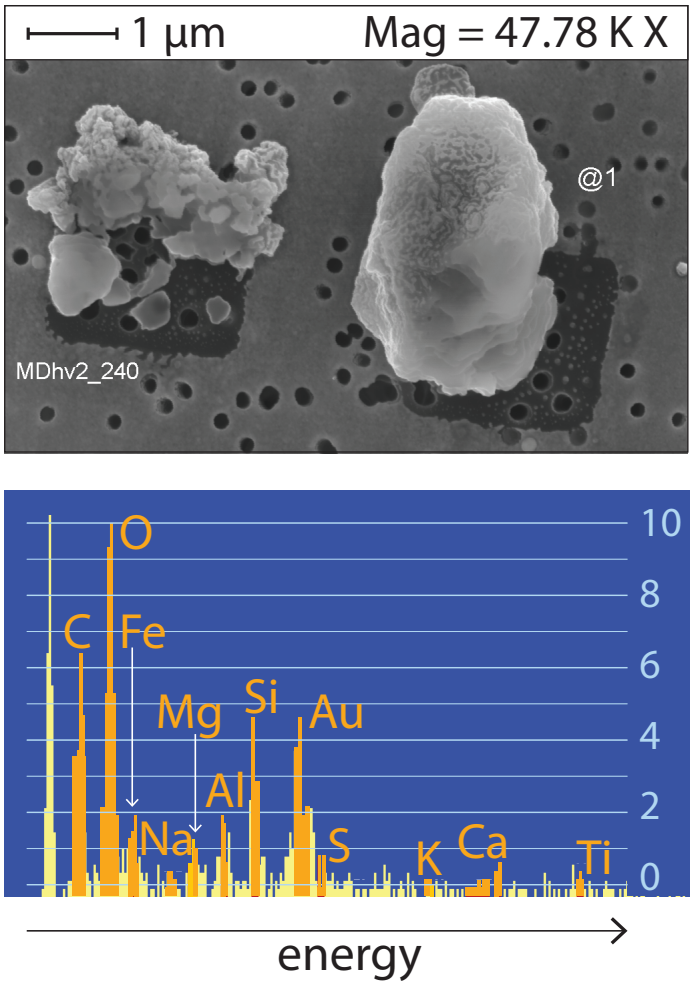

Figure 4.3: **SEM and EDX analysis of a mineral dust grain** (right-hand grain) following a NanoSIMS measurement. The dark squares on the filter in the SEM image show where the NanoSIMS analysis has sputtered away the gold-coating. In the SEM EDX spectrum, element windows are highlighted in orange while the background is shown in yellow.

4.3.3 NanoSIMS analysis

The sulfur isotopic composition was determined with the Cameca NanoSIMS 50 ion probe at the Max Planck Institute for Chemistry in Mainz (Hoppe, 2006; Groener and Hoppe,

2006). The NanoSIMS 50 has high lateral resolution (<100 nm) and high sensitivity and can simultaneously measure up to five different masses through a multicollection system, allowing high precision analysis of the small sample quantities required for this study. The use of this instrument to analyse sulfur isotope ratios is described in detail elsewhere (Winterholler et al., 2006, 2008) and the analysis conditions are described in Section 2.3.5, so only a brief description will be given here.

The samples are analysed directly on the gold-coated Nuclepore filters without further processing. Samples with a particularly high $BaSO_4$ loading and all dust samples are gold-coated on top of the sample before NanoSIMS analysis to prevent excessive charging. A $\sim$1 pA Cs^+ beam is focussed onto a $\sim$100 nm sized spot and rastered in a 2 μm $\times$ 2 μm grid over the grain of interest. The ejected secondary ions are carried into the mass spectrometer and multicollection system. For the $BaSO_4$ from leachate oxidation experiments, each measurement consists of 200 - 400 cycles of 4.096 seconds duration preceded by varying lengths of presputtering until the gold coating (if present) is removed and the count rate is stable. For the surface oxidation samples, the sulfate produced in the experiments will be on the surface of the particles, so analyses were fairly short and presputtering was kept to a minimum: Each measurement consisted of 120 cycles of 4.096 seconds duration, and presputtering and beam centering were carried out on an area of at least 10 μm $\times$ 10 μm so that the surface was conserved for analysis.

The session instrumental mass fractionation (IMF) was determined with IAEA $BaSO_4$ standards SO5 and SO6, however the IMF for sulfate on mineral dust grains will also be dependent on the matrix. The major cation was determined from SEM-EDX analysis taken on individual grains after the NanoSIMS analysis, as described in the previous section, and the IMF correction relative to $BaSO_4$ was then applied according to Winterholler et al. (2008). The untreated Sahara dust contained a measureable quantity of sulfate, so a background correction of the isotope ratio was needed for the surface oxidation samples. The effect of this was minimised by keeping analyses short so that primarily surface sulfate was analysed, however the background was still significant. 28 untreated grains were analysed to quantify the background sulfur isotope signal. The untreated grains had an average ^{32}S signal of 447$\pm$385 counts per second and a $\delta^{34}S$ of 18.6$\pm$5.9‰. This falls within the range of values previously reported for sediments in the Sahara desert (Drake et al., 2004) and Sahara dust collected in the North Atlantic (Winterholler et al., 2006). Thus, experimentally-treated grains were only considered in the data analysis if their ^{32}S signal was $>$ 900 counts per second, and values of $\delta^{34}S$ for these grains were corrected for the isotopic composition of the background. 102 experimental grains had high enough ^{32}S

counts for useful isotopic information, and these were distributed fairly evenly across the different experiments, so that at least eight grains per sample gave useful information for each set of experimental conditions.

For each sample of the leachate experiments, at least five spots were measured and the weighted average and error was calculated, as described in Section 2.3.5. The counting statistical error was typically 1-2‰ for each analysis spot and the overall error for each sample 2-5‰. For the surface oxidation experiments, the spot-to-spot error was added to the counting statistical error so that the measurements on each grain could be treated individually, rather than calculating an average for all grains on a particular sample filter. The spot-to-spot error of the SO5 and SO6 standards was used as an estimate of the spot-to-spot error for the measurement session, and this was then combined with the counting statistical error to determine the measurement uncertainty for each individual grain. For each individual grain, the counting statistical error was typically 4-5‰ and the overall error 5-6‰.

4.3.4 Positive Matrix Factorization

The composition of each grain from post-NanoSIMS SEM analysis was used as input for a Positive Matrix Factorization (PMF) model which was run with the software EPA PMF v3.0.2.2. This is a multivariate analysis tool which identifies factor profiles and factor contributions for data sets which have a large number of variables measured across many samples (Norris et al., 2008). Although the model is designed to identify source profiles and contributions to environmental data sets, it is ideal for this study as it allows data points to be individually weighted and it constrains results so that no factor can have a negative contribution to a sample.

Atomic percentages of O, Fe, Na, Mg, Al, Si, S, K, Ca and Ti were used as input for the model, as well as S isotope measurements from NanoSIMS analysis. When a peak was below the limit of detection, an atomic percentage of one third of the lowest measured concentration for the element was used, and the uncertainty was set to twice the normal uncertainty for the element to reduce the weighting of the point. All elements were classed as 'strong' as the uncertainties did not need to be increased, however $\delta^{33}S$ was classified as a 'weak' variable as its analysis in the NanoSIMS can be problematic due to counting statistics combined with topography and matrix effects. $\delta^{34}S$ was set as the 'total variable', leading to an automatic 'weak' classification. The 'Extra Modeling Uncertainty' was set to the recommended 5% (Norris et al., 2008). No two elements showed any significant correlation.

A random seed was used to initiate the model and 20 base runs were performed. The model was run with three, four and five factors and it was found that four factors gave the most consistent results with the lowest Q (object function) value and the best resolution of elements and isotopic compositions. Only the four factor analysis will be discussed further. The model described the data adequately: The residuals were approximately normally distributed and only one scaled residual for one Al value was outside the $\pm 3\sigma$ limit. The overall profiles of the four identified factors varied only a small amount between the 20 model runs, and the dominant species in each factor remained the same in all 20 runs.

4.4 Aqueous oxidation in Sahara dust leachate

4.4.1 Catalytic activity of the solution and rate of reaction

The concentrations of various elements present in the leachate, measured with ICP-OES, are shown in Table 4.3. The leachate was extremely efficient at oxidising SO_2, thus the fractionation factor must be found by considering the Rayleigh equations, which describe the isotopic composition of products and residual reactants as a function of the fractionation factor and the fraction of reactant remaining unreacted (Mariotti et al., 1981; Krouse and Grinenko, 1991). The fraction of SO_2 remaining was measured for each of the two experimental runs both with SEM quantification as described in Section 4.3.2 and by considering mass balance between the measured isotopic composition of the residual SO_2 and the product sulfate:

$$\delta^{34}S_i = f \cdot \delta^{34}S_{SO_2} + (1 - f) \cdot \delta^{34}S_{\text{sulfate}} \tag{4.3}$$

where f is the fraction of reactant (SO_2) remaining and $\delta^{34}S_i$, $\delta^{34}S_{SO_2}$ and $\delta^{34}S_{\text{sulfate}}$ are the isotopic compositions of the initial SO_2 gas, residual SO_2 gas and product sulfate respectively. For each experimental run both estimates differed by <1%, and the two estimates were averaged to find the fraction remaining for each of the experimental runs.

The oxidation of SO_2 by mineral dust leachate was very efficient. >99% of SO_2 was oxidised after passing through one bubbler, compared to the 39% of SO_2 that is collected in one bubbler containing 6% H_2O_2 and <1% that is oxidised in a bubbler with 0.1 M Fe^{2+}/Fe^{3+} (Section 2.4.1). The fraction oxidised at $[SO_2] = 6.7$ ppm (99.8%) was only slightly higher than the fraction oxidised at $[SO_2] = 13.3$ ppm (99%), showing the leachate was not close to exhausting its oxidation capacity. Thus, it is clear iron is not the most important transition metal for the catalysis of SO_2 oxidation in mineral dust leachate

Table 4.3: **The concentrations of various elements present in Sahara dust leachate measured with ICP-OES**. 'Concentration' refers to the solution used to oxidise SO_2 in this study, which was made with 0.5 g of dust per 100 mL of water, while 'μg/g dust' is the amount of the element that is soluble in 1 g of dust following 2 days in MilliQ water. 'RSD' is the relative standard deviation of 3 measurements from the ICP-OES.

Element	**Concentration**	**μg/g dust**	**RSD**
	mol L^{-1}		%
Al	3.19×10^{-5}	170	3.7
Mg	1.61×10^{-5}	77.1	3.1
Ca	1.53×10^{-5}	121	2.8
Fe	7.74×10^{-6}	85.2	8.4
Ba	2.64×10^{-6}	71.5	1.9
Ti	2.22×10^{-6}	20.9	1.3
Mn	7.48×10^{-7}	8.09	4.1
Sr	1.43×10^{-7}	2.47	0.95
Cr	6.2×10^{-8}	0.64	160
Ni	3.4×10^{-9}	0.04	840

solutions; other ions measured in the solution, such as manganese and chromium, are also highly active in oxidation. This is in agreement with the results of Tilly et al. (1991) and Rani et al. (1992), which showed that these ions do not just contribute independently to oxidation, but that mixtures of ions interact synergistically, resulting in greatly-enhanced oxidation rates. Thus, soluble iron alone is not a good indicator of SO_2 oxidising ability, which may explain why correlation between soluble Fe and sulfate is often poor (Kumar and Sarin, 2010; Baker et al., 2006).

4.4.2 Fractionation of $^{34}S/^{32}S$ during aqueous oxidation in Sahara dust leachate

The fractionation factor can be found from the Rayleigh equation describing the $\delta^{34}S$ of the sulfate product with respect to the fraction of SO_2 oxidised (Mariotti et al., 1981; Krouse and Grinenko, 1991):

$$\alpha_{34} = \frac{\ln(1 - (\frac{R_P}{R_i})(1 - f))}{\ln f} \tag{4.4}$$

where R_P and R_i are the ratios of $^{34}S/^{32}S$ for the product sulfate and the initial SO_2 gas respectively and f is the fraction of SO_2 remaining. The $\delta^{34}S$ of the sulfate formed in the leachate needs to be corrected for the contribution from sulfate that was leached from the dust itself. The effect of this correction on $\delta^{34}S_P$ was negligible as the leachate contained <1 μM of sulfate while the reaction added >200 μM of sulfate to the solution.

The fractionation factor can also be found from the Rayleigh equation describing the $\delta^{34}S$ of the residual SO_2 gas and the fraction of SO_2 oxidised (Mariotti et al., 1981; Krouse and Grinenko, 1991):

$$\alpha_{34} = \frac{\ln(\frac{R_R}{R_i})}{\ln f} - 1 \tag{4.5}$$

where R_R and R_i are the ratios of $^{34}S/^{32}S$ for the residual SO_2 gas and the initial SO_2 gas respectively and f is the fraction of SO_2 remaining. The measured $\delta^{34}S$ of the residual SO_2 was corrected for fractionation during collection in H_2O_2 as described in Section 2.4.1.

Four estimates of α_{34} were thus obtained; from the residual SO_2 and the product sulfate for each of the two experimental runs. The four measurements were averaged and the 1σ standard deviation taken as the error:

$$\alpha_{\text{leachate}} = 0.9917 \pm 0.0046 \tag{4.6}$$

at 19°C. The majority of the uncertainty in the fractionation factor is due to the uncertainty in the NanoSIMS measurements of the $\delta^{34}S$ values. The fractionation factor is not significantly different to the fractionation factor for the oxidation of SO_2 by a solution of Fe^{2+} and Fe^{3+} ($\alpha_{\text{Fe}} = 0.9894 \pm 0.0043$) presented in Section 2.4.1. However, in agreement with previous studies (Cohen et al., 1981; Tilly et al., 1991; Rani et al., 1992), the quantity of sulfate produced (see Section 4.4.1) shows that iron is not the only transition metal present in leachate that is active in catalysing SO_2 oxidation. Concentrations of other transition metals in the leachate that are also available for reaction, such as Cr and Mn, are presented in Table 4.3. Thus, the identity of the metal catalysing SO_2 oxidation does not affect the sulfur isotope fractionation, which suggests fractionation is not due to the initiation reaction but the subsequent reactions in the chain (Herrmann et al., 2000). The average fractionation factor for transition metal-catalysed oxidation of SO_2 from the current and previous measurements is:

$$\alpha_{\text{TMI}} = 0.9905 \pm 0.0031 \tag{4.7}$$

4.5 Fractionation of $^{34}S/^{32}S$ during heterogeneous oxidation on Sahara dust surfaces

4.5.1 Quantification of sulfate production

Sulfate production on the dust surface and subsaturated humidity was quantified with automatic SEM analysis, as described in Section 4.3.2, and the results are shown in Figure 4.4. Experiment lengths ranged from 6.3 to 9.2 hours, so the results shown were corrected and represent the estimated concentration after exactly 8 hours of experimental time, to facilitate comparison between experiments. The surface sulfate increase will be significantly more than the reported total atomic percentage increase, as EDX measurements are not surface-sensitive (Goldstein et al., 1981). As an estimate, for a grain 2 μm in diameter with experimentally-produced sulfate added only to the top 20 nm of the grain surface, the sulfate concentration in the surface layer would increase by more than 1000% for MDRHO3hv, rather than the 30% increase when the whole grain volume is considered. The total amount of sulfate was seen to increase in all experiments except for MDRHhv, although all changes are within the statistical error of the SEM measurement except for MDRHO3hv. The count rates observed during NanoSIMS analysis show an increase for all treated samples compared to the control, and are also much higher for MDRHO3hv, in agreement with the SEM samples. Thus, sulfate production is fairly slow and similar for all experiments except MDRHO3hv: This combination of conditions saw much more sulfate produced than the other experiments combined, showing ozone, light and water vapour interacted synergistically to oxidise SO_2 much more efficiently than any of these parameters alone.

4.5.2 Bulk elemental analysis of reactive particles

Correlations between the sulfur EDX signal and the EDX signal of other elements may provide information about the elements which are most important for sulfate production. Automatic EDX points with sulfur and at least one other element above the background were therefore examined for correlations, in both the untreated and treated dust samples. Each sample had >100 EDX points with significant signals for sulfate and at least one other element, so correlations could be examined individually within each sample type. In untreated dust, correlations can indicate whether the sulfate present is primary and present in the Sahara source region, or whether it is secondary and results from uptake and reactions during transport to the Cape Verde Islands. S and Ti signals show a slight

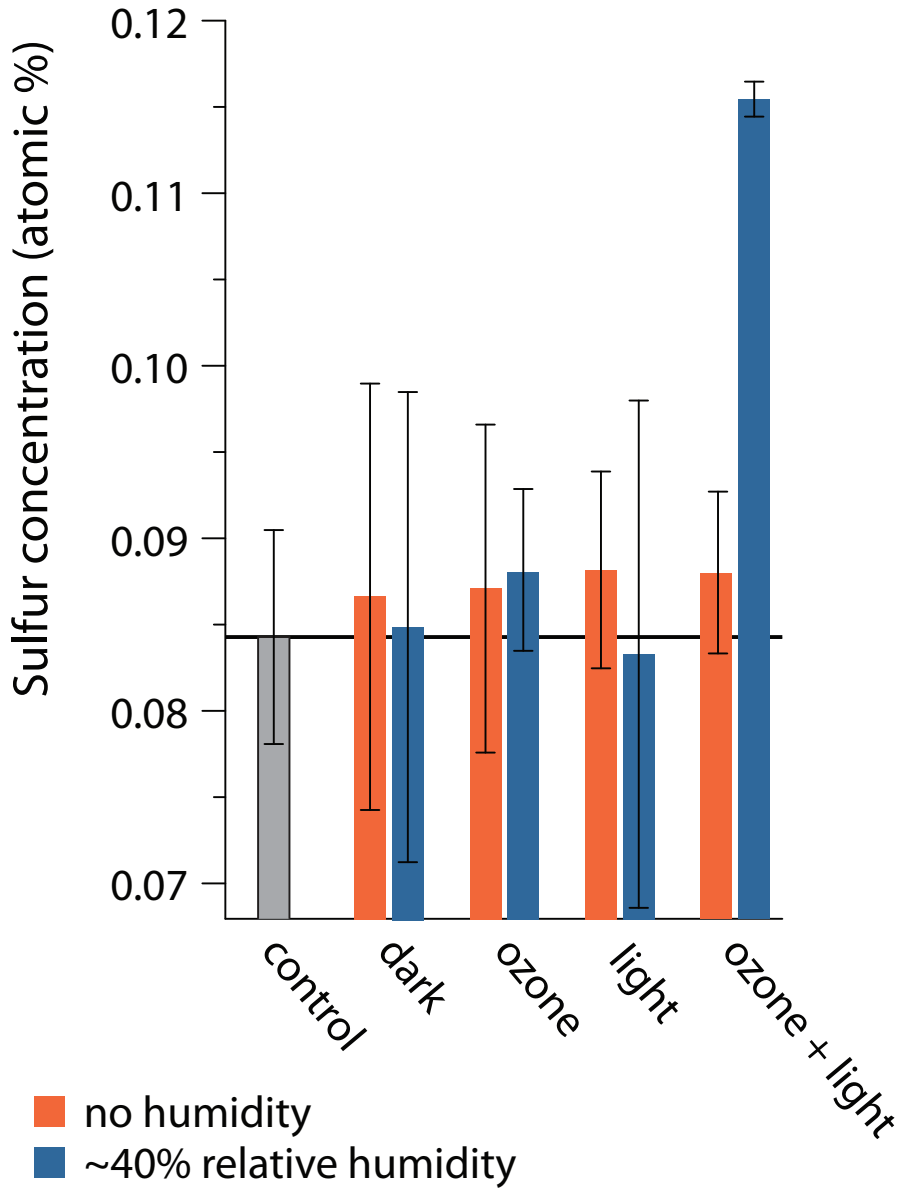

Figure 4.4: **Quantification of sulfate addition to mineral dust from surface SO_2 oxidation**. 'Control' shows the amount of sulfate present in untreated dust, and the labels on the x-axis refer to the different experimental conditions under which SO_2 was exposed to the dust. Error bars are the 1σ standard deviation from the Poisson distribution depending on the number of points with a significant signal.

positive correlation ($R^2 = 0.35$) in the untreated samples, which suggests the sulfate is secondary: primary sulfate would be more likely to be associated with Ca and Mg due to clays and minerals such as gypsum (Caquineau et al., 2002).

Correlations on experimental samples were only seen for those runs with no ozone or irradiation: S on MDdark dust was weakly correlated with Ti and Fe ($R^2 = 0.19$ and 0.13 respectively), while S on MDRHdark dust was strongly correlated with Ti and Ca ($R^2 = 0.66$ and 0.53 respectively). No mineralogical information is provided in automatic EDX analysis, and it is likely that the lack of correlation in other samples is because element concentrations are a poor representation of element availability for reaction, rather than an indicator that sulfate is produced evenly across dust grains. The SEM-EDX analysis also has a resolution of only $\sim$1 μm, and grain heterogeneity with regards to mineralogy on this scale (Falkovich et al., 2001) will obscure correlations in the SEM-EDX signal.

Elements which are associated with higher SO_2 oxidation rates can also be examined by looking at the elemental profile of dust grains (from post-NanoSIMS single-particle SEM-EDX analysis) with high enough ^{32}S count rates for isotopic analysis, compared to the overall dust profile. This comparison is shown in Figure 4.5. It can be seen that Ti is strongly enriched in oxidising dust, and K, Fe and Ca are slightly enriched, while Na, Mg, Al, Si and O show no relationship to oxidising ability of dust and only fall slightly below the 1:1 line because of mass balance. This is consistent with the correlations from automatic SEM analysis: Ti, Fe and Ca are the most important elements for oxidising ability, particularly in dark experiments where ozone and light are not available to facilitate further reaction pathways, while mineralogy is clearly the dominant factor controlling uptake.

4.5.3 $^{34}S/^{32}S$ fractionation on different dust components

The isotopic composition of sulfate on experimentally-treated samples was much more variable than on control grains, even within one set of experimental conditions. Variability within one set of experimental conditions was as large as the overall variability of the data set. As atmospheric dust is strongly internally mixed with regards to mineralogy (Falkovich et al., 2001) most analysed grains will represent a mix of minerals, so a multivariate analysis model (described in Section 4.3.4) was used to examine the relationship between grain composition and isotopic fractionation. Four factors were identified from the PMF analysis. Each factor is not representative of a single mineral, but rather of a group of minerals that, acting together or separately, cause the same isotopic fractionation during sulfate formation. The elemental profiles of these factors are shown in Figure 4.6.

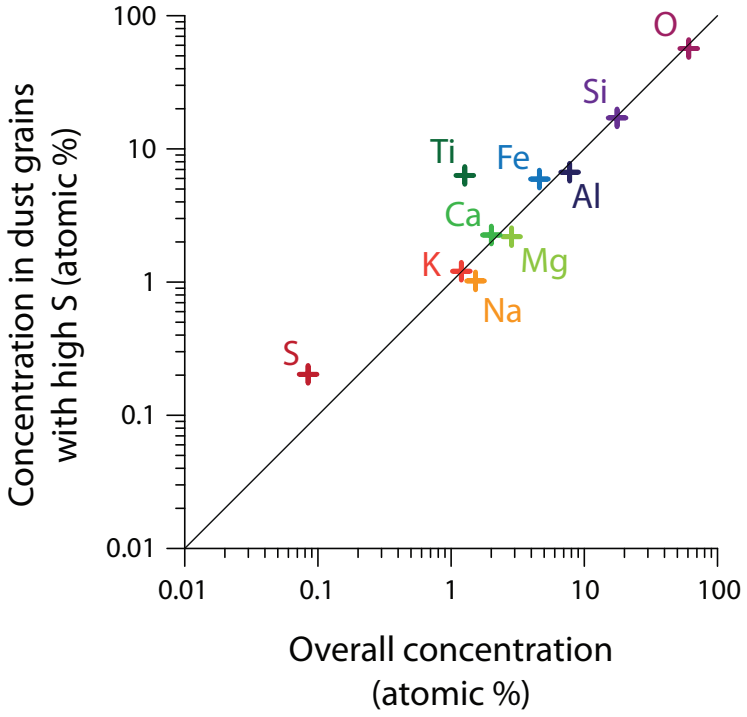

Figure 4.5: **Comparison of elemental composition of all dust and composition of dust with ^{32}S count rates high enough for reliable isotopic analysis**.

To determine the isotopic fractionation factor of the factor, factor contributions for each grain were plotted against δ^{34}S. The intercept where the factor contribution was one gave the fractionation factor α_{34} of the factor.

The factor α_{34} values were used to predict the δ^{34}S of the measured dust grains based on their composition, to test the fit between modelled and actual fractionation. The discrepancy between predicted and measured δ^{34}S was no greater than what would be expected from a normal distribution given the measurement error (Figure 4.7), and the regression line weighted by the error in the measurements was ($R^2 = 0.62$):

$$\delta^{34}\mathrm{S}_{\mathrm{observed}} = (0.90 \pm 0.11)\delta^{34}\mathrm{S}_{\mathrm{predicted}} - (5.81 \pm 2.54) \tag{4.8}$$

which shows that the model fits the data well. Although this is not a rigorous test of the model as the same 102 measurements were used to generate the factor α_{34} values and to test them, it indicates the factors are well-resolved with respect to isotopic fractionation.

Plots to determine fractionation factors were made for all samples together, as well as for sub-groups of samples, to determine the role of experimental conditions in isotopic fractionation. The results are shown in Figure 4.8. The error in the estimates of α_{34} for

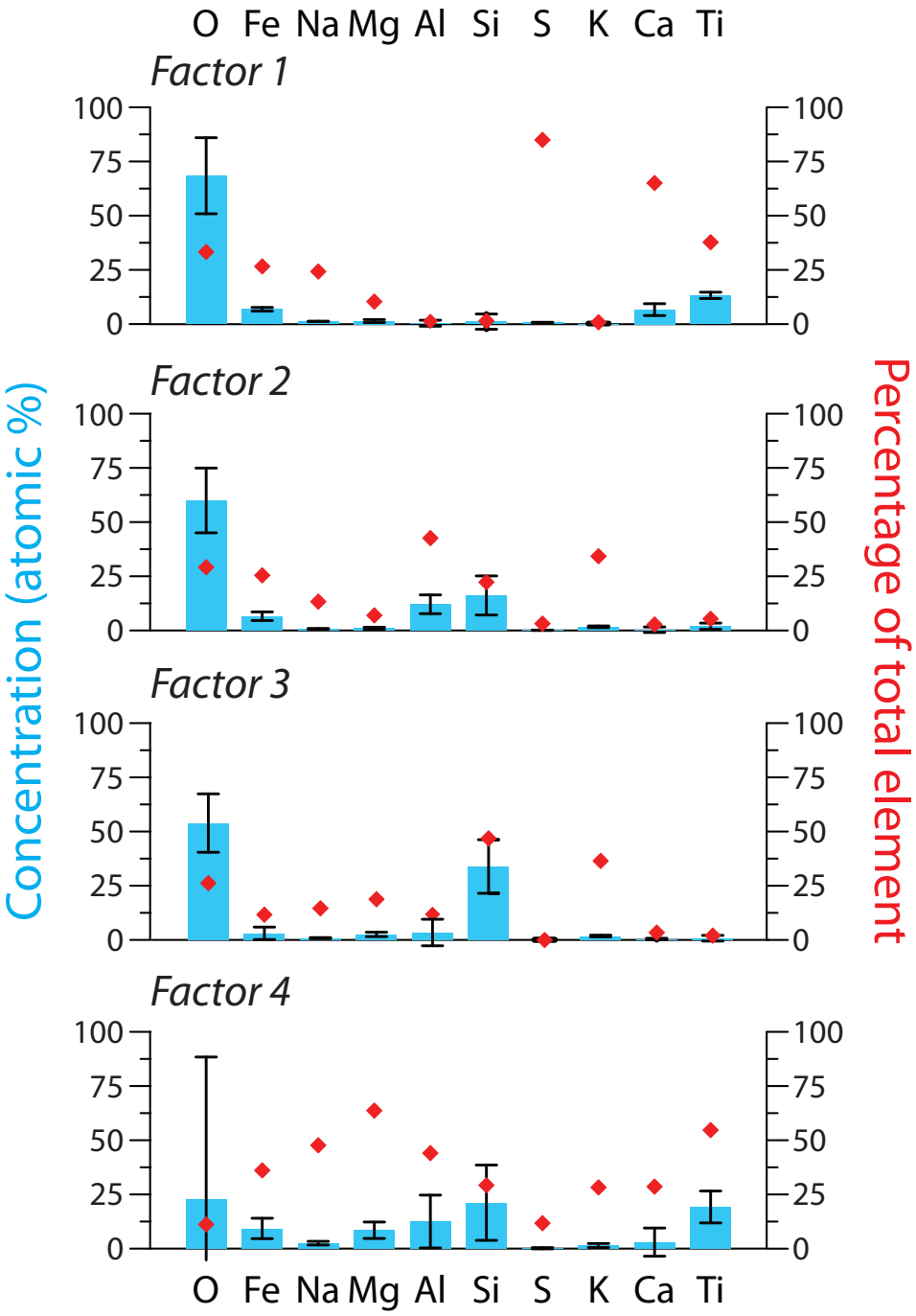

Figure 4.6: **Elemental profiles of the four 'factors' contributing to isotopic composition of sulfate produced from SO_2 oxidation, identified by PMF analysis**. Columns with 1σ error bars (standard deviation of the results of 20 model runs) correspond to the left-hand axis and show the concentration of the element in atomic percent, while diamonds correspond to the right-hand axis and show the percentage of the element's total concentration that is present in a particular factor.

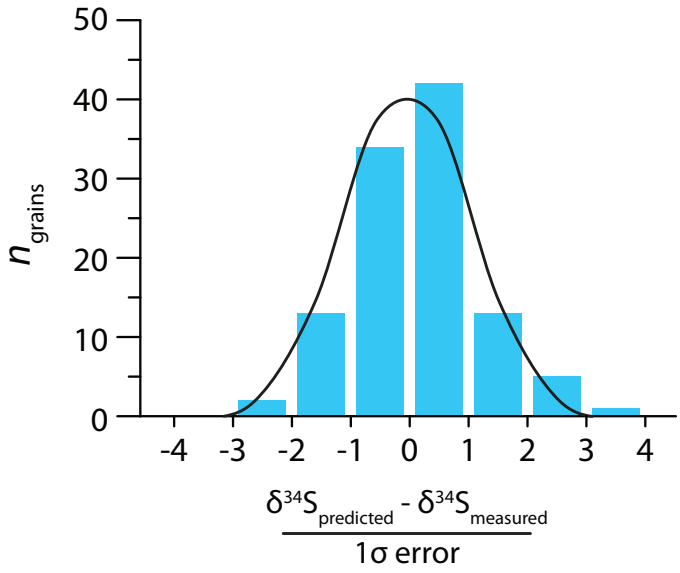

Figure 4.7: **Comparison of model accuracy (blue bars) with expected error from a normal distribution (black line)**.

the sub-groups are much higher due to the much smaller number of measurements (47 and 55 grains for 'all humid' and 'all dry' respectively; 20-31 grains for the effects of O_3 and light). The α_{34} could not be determined for individual experimental conditions (eg. MDO3 or MDRHhv) as the number of grains (8-14) was too small, thus the uncertainty in the result too large to be useful. It can be seen that presence or absence of humidity, light and ozone has much less effect on the isotopic fractionation than the dust composition: fractionation factors for different subsets generally agree with overall fractionation within the error for each factor. This shows that isotopic fractionation is primarily due to uptake of SO_2 (g) and not subsequent oxidation.

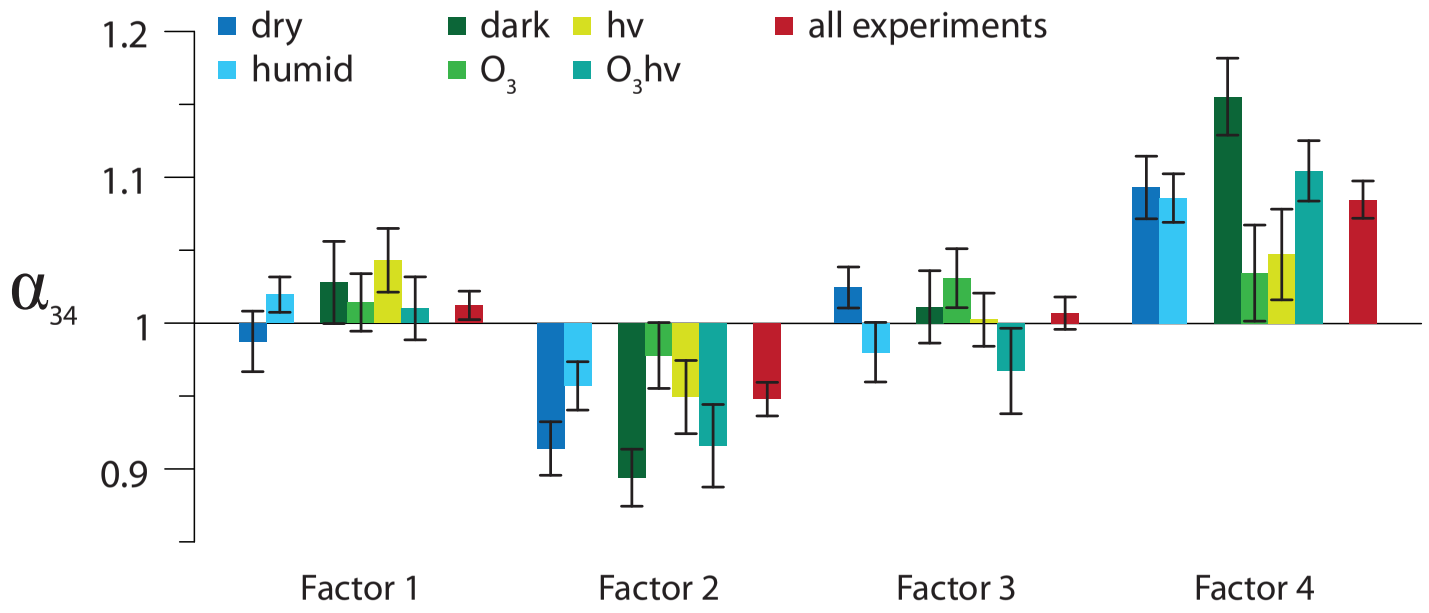

Figure 4.8: **Fractionation factors for $^{34}S/^{32}S$ for different mineral assemblages ('Factors') within Sahara dust**: 'dry' includes MDdark, MDO3, MDhv and MDO3hv, 'humid' includes MDRHdark, MDRHO3, MDRHhv and MDRHO3hv; 'dark' includes MDdark and MDRHdark, 'hv' includes MDhv and MDRHhv, 'O_3' includes MDO3 and MDRHO3, and 'O_3hv' includes MDO3hv and MDRHO3hv. Error bars show the 1σ error.

Based on the elemental profile of each factor, its interaction with experimental conditions, and its reactivity, the mineralogical identity and reaction mechanism associated with each factor was inferred. They are discussed in the following sections and summarised in Table 4.4. Several estimates of the oxidation rate for each factor were obtained: The sulfate production percentage refers to the percentage of the total sulfate that was generated by that factor during the experiment. The reactivity (μg sulfate /g mineral /hour) is the amount of sulfate produced per gram of the minerals represented by the factor, divided by length of the experiment; the calculation does not consider decreases in rate due to saturation of the dust surface, and it is assumed that the surface fractions of the minerals are the same as the bulk fractions. This rate is relevant for the length of the experiments (6-9 hours), but will eventually decrease as the dust is saturated. The reactivity could be used to estimate the rate of SO_2 oxidation and sulfate production on different dust types based on their mineral assemblages, however further investigation would be necessary given the strong role of mineral mixing in oxidation rate. The rate represented by the reactivity refers to the MDRHO3hv experiments, where the largest amount of sulfate was produced; oxidation under all other conditions is on average 16× slower and the uncertainty is much greater.

The reactivity and the BET surface area were used to estimate the reactive uptake coefficient γ for the dust according to Jayne et al. (1990):

$$\gamma_{obs} = \frac{4F_g}{\bar{c}A}\frac{\Delta n}{n} \tag{4.9}$$

where F_g is the carrier gas flow rate (cm^3 s^{-1}), $\bar{c}$ is the mean thermal velocity (cm s^{-1}; $\sqrt{\frac{3k_B\mathrm{T}}{m}}$), A is the total droplet surface area (cm^2) and $\frac{\Delta n}{n}$ is the reduction in gas concentration. The γ_{obs} value found from this expression represents a combination of mass transfer, accommodation and reaction limitations, and provides only an estimate of the reactive uptake rate as it does not account for diffusion rate within the solid. The overall γ_{obs} for the dust, considering both reactive and non-reactive components, is 2.7×10^{-6}, which is ∼1 order of magnitude lower than previously reported values (Crowley et al., 2010). This is well within the expected range considering the surface area of the dust is likely to be overestimated in this study as the dust is lying on a filter, rather than suspended in a flow reactor, and the previously reported values are for initial uptake coefficients before uptake slows due to ageing and saturation. The dust in this study is a good representation of atmospheric dust that has already been aged, as it was transported from the Sahara desert to the Cape Verde Islands before being collected for use in experiments.

Table 4.4: **Fractionation of $^{34}S/^{32}S$ during heterogeneous oxidation of SO_2 (g) on mineral dust surfaces**. 'Sulfate production' shows the percentage of the total sulfate production contributed by the factor while 'Reactivity' shows the amount of sulfate produced per gram of the minerals represented by the factor per hour of reaction time at an SO_2 concentration of 4.2 ppm for MDRHO3hv experiments. γ is the reactive uptake coefficient considering the BET surface area of the dust for MDRHO3hv experiments.

Factor	**Sulfate Production**	**Reactivity**	γ_{obs}	**Mineralogy**	α_{34}
	%	μg sulfate /g minerals /hr			
1	85.0	12.6	3×10^{-5}	ilmenite + rutile	1.012 ± 0.010
2	3.2	0.40	9×10^{-7}	feldspar + Fe minerals	0.948 ± 0.012
3	0.1	0.05	4×10^{-8}	silicates + basic components (eg. MgO)	1.007 ± 0.011
4	11.7	2.91	9×10^{-6}	clay (chlorite, illite, smectite)	1.085 ± 0.013

Factor 1

Factor 1 has a fractionation factor of $\alpha_{34} = 1.012 \pm 0.010$ which shows no significant variation depending on experimental conditions. It has high concentrations of Fe and Ti (6.8 and 13.2 atomic percent respectively) and the highest reactivity of any factor, which is in agreement with observations of relatively high uptake coefficients for SO_2 on TiO_2 and on iron oxides and oxyhydroxides (Zhang et al., 2006; Crowley et al., 2010). The co-occurence of Fe and Ti suggests that the factor is representative of ilmenite, with some degree of weathering towards pseudorutile and rutile accounting for the excess Ti (Janssen et al., 2007; Putnis, 2002). Ilmenite is a chemically stable mineral that would be likely to have survived transport from the Sahara to the Cape Verde Islands and ageing while on the Cape Verde Islands prior to collection (Janssen et al., 2007). The importance of Ti in the most reactive factor agrees with the EDX sulfur correlation results from Section 4.5.2, which found Ti to be enriched in areas where sulfate production was highest.

As the uptake of SO_2, rather than the oxidation, controls isotopic fractionation, the coordination mechanism for SO_2 should relate to the isotopic fractionation. Given that the α is robust to experimental conditions and well-resolved for Factor 1, the fractionation factor on the rutile (TiO_2) and on the parent ilmenite are the same. Hematite, goethite, magnetite and TiO_2 have all been shown to chemisorb SO_2 to a bidentate complex, with similar IR spectral bands observed for the adsorbed compounds where available. This suggests these three iron oxides will also have the same value for α as TiO_2 and by extension the same α as ilmenite (Fu et al., 2007; Zhang et al., 2006; Usher et al., 2002). Factor 1 also has a significant amount of Ca. This may be due to formation of $CaSO_4$ from colocated Ca^{2+}, possibly as the sample dries when it is put under vacuum for analysis. It is unlikely that CaO or $CaCO_3$ are directly taking up sulfate as the mechanisms of uptake (monodentate and direct reaction respectively) are very different to iron and titanium oxides, and would not be expected to show the same fractionation factor (Usher et al., 2002).

In summary, ilmenite and its weathering product rutile are the most active components in SO_2 uptake in Sahara dust, and chemisorb SO_2 to a bidentate complex with a fractionation factor of $\alpha_{34} = 1.012 \pm 0.010$, which is expected to also represent fractionation on hematite, goethite and magnetite. Sulfate production was calculated to be 12.64 μg per mg of iron and titanium oxides and their weathering products per hour.

Factor 2

Factor 2 contributes 3.2% of total sulfate production, and produces sulfate that is strongly enriched in ^{32}S. The elemental composition shows that the factor represents a mixture of feldspar and a component containing Fe such as mica or hematite, both of which are known to be common constituents of Sahara dust (Coude-Gaussen et al., 1994; Glaccum and Prospero, 1980). Al_2O_3 alone can have a relatively high uptake coefficient if it is basic in character (Judeikis et al., 1978; Crowley et al., 2010), while SiO_2 and acidic Al_2O_3 have low uptake coefficients (Zhang et al., 2006). Uptake to this factor is relatively slow, and the isotopic fractionation is opposite in direction the other factors, which have more basic character, thus uptake to Factor 2 appears to be dominated by less basic sites associated with Al. This is consistent with the expected effects of ageing during transport, which will remove alkali components, leaving aluminium oxides exposed. The Fe ions in the minerals associated with feldspar will increase the acidic character. Although Fe^{3+} can catalyse S(IV) oxidation (Herrmann et al., 2000), this reaction pathway will be insignificant without an aqueous phase. The adsorption of SO_2 to Al_2O_3 results in sulfite with significantly different IR absorption bands to, for example, MgO (Goodman et al., 2001), which explains the strongly negative isotope fractionation that is very distinct from the other factors.

In summary, aluminium oxide sites associated with feldspars, a common constituent of Sahara dust, take up SO_2 with a fractionation factor of $\alpha_{34} = 0.948 \pm 0.012$, which is also expected to be the fractionation factor for adsorption on to pure aluminium oxides. The sulfate production due to this factor is 0.40 μg of sulfate per mg of feldspar and aluminium oxide per hour.

Factor 3

The isotope fractionation produced by Factor 3 was slightly positive and very similar to Factor 1. The contribution of Factor 3 to total sulfate formation was minor (0.1%). The elemental composition of Factor 3 shows that it is primarily composed of quartz, as well as olivine, pyroxene, and derivatives serpentine and leucoxene, which are expected to be major components in Sahara dust (Coude-Gaussen et al., 1994; Glaccum and Prospero, 1980). However, pure SiO_2 has been measured to have very low or no reactivity with SO_2 (g) in the laboratory (Zhang et al. (2006) and Usher et al. (2002) respectively). Li et al. (2007) found that the addition of MgO to NaCl resulted in an increase in reactivity towards SO_2 larger than that expected from the individual uptake coefficients, and Zhang et al. (2006) also found excess reactivity in a mixture of continental crust components such

as SiO_2 and MgO. Factor 3 contains a significant amount of Mg as well as other cations so it is likely mixing of SiO_2 and components with basic character, such as magnesium oxides or olivine, has increased the reactivity of the quartz fraction of the dust to a significant level. Spectra and adsorption mechanisms for SO_2 on silicates are not available, but the similarity of the fractionation factor for Factor 3 to that of Factor 1 suggests a similar, but much slower, adsorption mechanism.

In summary, adsorption of SO_2 to mixtures of quartz and components with basic character results in a fractionation factor of $\alpha_{34} = 1.007 \pm 0.011$. The total sulfate production is 0.05 μg of sulfate per mg of quartz per hour.

Factor 4

Factor 4 contributes 11.7% of the total sulfate production and produces sulfate strongly enriched in ^{34}S. The elemental profile shows that the factor represents clays, particularly smectite, illite and chlorite, which have been shown to be major components of the clay fraction of Sahara dust from the Cape Verde Islands (Coude-Gaussen et al., 1994). Interlayer cations such as Mg^{2+}, Ca^{2+} and Na^{+} are likely to be the components most available for reaction with SO_2, which is consistent with the correlation between Ca and sulfate presented in Section 4.5.2. Uptake of SO_2 by MgO and CaO has a relatively high rate (Crowley et al., 2010; Usher et al., 2002; Zhang et al., 2006), however DRIFTS IR absorption bands for sorbed S(IV) suggest sulfite is adsorbed quite differently on CaO and MgO (Low et al., 1971; Goodsel et al., 1972), so it is unlikely the adsorption to interlayer cations in clays can be represented by adsorption to oxides. SO_2 will react directly with $CaCO_3$ to produce $CaSO_3$ which is readily oxidised to $CaSO_4$ (Al-Hosney and Grassian, 2005; Li et al., 2006), and an analogous reaction with interlayer Ca and Mg is most likely the cause of SO_2 uptake in Factor 4. Factor 4 also has a large amount of Ti, however the fractionation factor is not in agreement with Ti uptake from Factor 1. The calculated α_{34} for Factor 4 is lower, i.e. closer to the α_{34} of Factor 1, when the dust is exposed to O_3 or light, thus it appears that Ti associated with clay can only significantly contribute to SO_2 oxidation when the reaction is facilitated by light or O_3.

In summary, adsorption of SO_2 to interlayer cations, particularly Ca^{2+} and Mg^{2+}, in clays such as smectite results in a strongly positive fractionation of $\alpha_{34} = 1.085 \pm 0.013$. Sulfate production is 2.91 μg per mg of clay minerals per hour of reaction time.

4.5.4 Overall $^{34}S/^{32}S$ fractionation on Sahara dust

The total average fractionation factor for heterogeneous SO_2 oxidation on the surface of Sahara dust can be estimated by two methods. The weighted average of all 102 individual NanoSIMS measurements results in a $\delta^{34}S$ of 9.5 ± 3.9 ‰. The average composition from the PMF, found by weighting the α_{34} values from the different factors by their uptake efficiency and contribution to the total dust mass, is $\delta^{34}S$ = 10.1 ± 9.9 ‰. The two values agree very well and can be combined to estimate the average fractionation for the heterogeneous oxidation of SO_2 on the surface of Sahara dust:

$$\alpha_{\text{het}} = 1.0096 \pm 0.0036 \tag{4.10}$$

This average fractionation factor is only relevant for the particular dust sample measured in this study. The sulfur isotope fractionation factor for different dust sources should be calculated based on the factor-specific fractionation factors and the mineralogy and ageing of the dust of interest.

4.5.5 Sensitivity of sulfate production and isotopic fractionation to O_3, light and humidity

As discussed in the preceeding sections, isotopic fractionation shows little sensitivity to the parameters that were varied between experiments. The relative contributions of the four factors to sulfate production were also not significantly affected by the experimental conditions. This shows chemical composition and mineralogy of a dust grain are the most important parameters causing differences in isotopic fractionation, with the experimental conditions playing a secondary role. Isotopic fractionation will be controlled by the rate-limiting step, as the fraction reacted for other reaction steps will be ∼1, meaning that isotopic selectivity in these steps will not have an effect on the final product. The various experimental parameters would be likely to affect oxidation of adsorbed S(IV) but have less effect on initial uptake (Judeikis et al., 1978; Adams et al., 2005), thus the results of this chapter are consistent with previous laboratory studies, which have determined that SO_2 adsorption is the rate-limiting step for SO_2 uptake and oxidation on mineral dust (Ullerstam et al., 2002; Li et al., 2006).

The experimental parameters will affect the saturation behaviour of the dust, however in most experiments the oxidation rate was low and the dust was not exposed to SO_2 long enough to reach saturation (Mamane and Gottlieb, 1989). However, when the dust is exposed to humidity, light and ozone simultaneously (MDRHO3hv), the quantity of

sulfate produced is > 7 times higher than in any other experiment. Humidity regenerates the reactive capacity of dust for SO_2 uptake (Judeikis et al., 1978; Ullerstam et al., 2002), possibly due to the increased mobility of surface ions which leads to the re-exposure of active sites (Al-Hosney and Grassian, 2005). Uptake and decomposition of ozone, which increases the basicity and oxidising capacity of the surface, is highest when irradiated and at around ∼35% RH (Hanisch and Crowley, 2003; Nicolas et al., 2009). Many components of dust, particularly iron and titanium oxides, are photosensitive and show increased uptake and oxidation due to the formation of election-hole pairs (Nicolas et al., 2009; Ndour et al., 2009; Rubasinghege et al., 2010). The photoreactivity of Ti is supported by the lower fractionation factor for Factor 4 when exposed to O_3 or light as discussed in Section 4.5.3. There is no significant change in isotopic fractionation within any factor for the MDRHO3hv experiments, thus the increased sulfate production is not related to a change in mechanism. The combination of humidity, ozone and irradiation increases the rate of SO_2 oxidation, causing it to approach saturation. The experimental parameters can then have a significant impact on counteracting saturation of SO_2 uptake on dust, thus increasing the amount of SO_2 taken up and oxidised on the dust during the experiments. The rate is of uptake and oxidation is then approximately an order of magnitude higher than with any parameter alone.

4.6 Comparison to field studies

A number of studies have looked at isotopic ratios of sulfate in order to understand sulfur sources and oxidation pathways. As sulfur isotope fractionation factors were not previously available for data interpretation, $\Delta^{17}O$ values are generally used to examine oxidation pathways. Oxidation by ·OH radicals and O_2 (which acts as the oxidant during transition metal catalysis) result in sulfate with $\Delta^{17}O = 0‰$, while oxidation by O_3 and H_2O_2 produces sulfate with $\Delta^{17}O = 8.8$ and $0.8‰$ respectively (Savarino et al., 2000; Lee and Thiemens, 2001). Alexander et al. (2003) used $\Delta^{17}O$ measurements of sulfate in East Antarctic ice cores to show that oxidation by O_3 and H_2O_2 was less important in glacial periods than in the surrounding interglacials. $\delta^{34}S$ of sulfate is also lower during glacial periods, thus in Section 2.4.3, an increase in transition-metal catalysed SO_2 oxidation due to increased dust loads in glacial periods was proposed based on laboratory measurements of oxidation of SO_2 by Fe^{2+}/Fe^{3+} solutions. The results in this chapter show that sulfur isotope fractionation during oxidation by real mineral dust leachate is equal to fractionation during oxidation by iron catalysis, although oxidation is much faster in

the leachate, thus supporting the hypothesis that oxidation by transition metal catalysis is ∼27% more important in glacial periods than in interglacial periods due to increased dust loads. Similarly, McCabe et al. (2006) measured $\Delta^{17}O$ of sulfate aerosol in Alert, Canada, and proposed that the importance of transition metal-catalysed oxidation was underestimated in winter, when concentrations of Fe and Mn are approximately doubled due to transport of polluted air masses. Norman et al. (1999) found that $\delta^{34}S$ of non-sea salt sulfate aerosol at Alert was lower in winter than in summer, which is consistent with the results of McCabe et al. (2006) when the fractionation factor for transition metal catalysis measured in this chapter is considered. Although the suite of transition metals from a polluted source will be different to those from a dust source, this chapter has shown that the identity of the transition metals involved in catalysis does not affect the isotopic fractionation.

In the majority of field studies, measured $\delta^{34}S$ of SO_2 is lower than $\delta^{34}S$ of sulfate (eg. Saltzman et al. 1983; Mukai et al. 2001; Novak et al. 2001). Thus, considering the fractionation factors from this chapter and from the previous chapters, isotopic measurements are in agreement with modelling studies which show that transition metal catalysed oxidation of SO_2 is not the major global sulfate production pathway. For example, Sofen et al. (2011) suggest the pathway contributes 18% of sulfate production globally. Using the present-day partitioning between oxidation pathways from Sofen et al. (2011) and the sulfur isotope fractionation factors from this chapter and from Chapter 2, we would predict a global average difference of +4.7‰ between $\delta^{34}S$ of SO_2 and $\delta^{34}S$ of sulfate. Considering a number of studies that simultaneously measured $\delta^{34}S$ of SO_2 and sulfate (Saltzman et al., 1983; Mayer et al., 1995; Krouse et al., 1991; Tanaka et al., 1994; Torfs et al., 1997; Mukai et al., 2001; Novak et al., 2001), the best estimate of the globally-averaged difference between $\delta^{34}S$ of SO_2 and $\delta^{34}S$ of sulfate is +2.8±3.1‰. This would require 36% of oxidation to come from transition metal ion catalysis, if the relative proportions of the other pathways remained the same - an increase of 18% compared to the current model results. However, the area covered by these studies is mainly in Europe and North America, and there are no measurements from the polar regions and the Southern hemisphere, so the result may not be representative of the true global picture.

There are currently no regional studies focussing on the isotopic composition of sulfate formed on dust, although there are a number of field studies that have confirmed the important role dust can play in regional sulfur cycles (Falkovich et al., 2001; Umann et al., 2005; Sullivan et al., 2007). The importance of uptake at lower relative humidities is not well known, and although it is slow compared to aqueous oxidation, its climatic

role may be underestimated as dust does not generally encounter high humidity until some days after emission (Dentener et al., 1996). The fractionation factors presented in this chapter provide a new tool through which sulfur isotope measurements can be used to examine global and regional sulfur cycles, particularly the role of oxidation on clay minerals and in the aqueous phase.

4.7 Conclusions

The aim of this chapter was to measure fractionation of $^{34}S/^{32}S$ during oxidation of SO_2 by mineral dust leachate and on mineral dust surfaces, in order to better understand the role of SO_2 oxidation by mineral dust in the sulfur cycle. The fractionation factor α_{34} for oxidation in the leachate was $\alpha_{\text{leachate}} = 0.9917 \pm 0.0046$. Sulfate production was due to oxidation of SO_2 via the radical chain reaction pathway initiated by transition metal ions leached from the dust, and the oxidation rate was found to be more than 100× faster than oxidation by iron alone.

Heterogeneous oxidation on dry and humidified dust surfaces lead to isotopic fractionation that was controlled primarily by the dust composition and not by the reaction parameters: $[O_3]$, irradiation, and humidity. However, almost an order of magnitude more sulfate was produced when the dust was simultaneously exposed to SO_2, O_3, humidity and light. Isotopic fractionation from different reactions occurring within the same 2 μm^2 area was additive, thus a multivariate analysis model could predict $\delta^{34}S$ of the sulfate produced on the grains within expected experimental error. Not all particles reacted with SO_2, and the model identified the four major components of dust responsible for uptake and oxidation of SO_2. The most reactive components of dust were ilmenite, rutile and iron oxide, which produced sulfate with a fractionation factor of $\alpha_{34} = 1.012 \pm 0.010$. The overall fractionation factor on SDCV is $\alpha_{\text{het}} = 1.0096 \pm 0.0036$. Since the isotopic fractionation is controlled by the mineralogy of the dust, it will vary for dust from different dust source regions and between natural mineral dust and industrial dust sources.

The distinct fractionation factors for SO_2 oxidation by dust leachate - for example, in cloud droplets seeded on dust particles - and for uptake and oxidation on dust at subsaturated relative humidity will be particularly useful to investigate the relative importance of these two pathways as dust is transported. Although the aqueous reaction is much faster, the surface reaction may be fast enough to be important when the dust encounters O_3 and 30-40% relative humidity in the daytime, whereas high enough humidities for aqueous oxidation are unlikely to be reached for several days following emission (Dentener et al.,

1996). However, the isotopic fractionation during uptake and oxidation on Sahara dust surface, in particular on Ti and Fe oxides and silicates, does not significantly differ from the isotopic fractionation during gas phase oxidation of SO_2 by ·OH and oxidation by O_3 and H_2O_2 in the aqueous phase (Section 2.4.1. Therefore, further from dust sources when high enough humidity for all of the possible oxidation pathways has been encountered, ambient observations for Sahara dust may only be capable of quantifying the contribution of leached transition metal ions and surface reactions on clay minerals to sulfate formation. The fractionation factor for SO_2 oxidation by transition metal catalysis is distinct from oxidation on the dust surface, other than feldspar minerals, and by H_2O_2 and O_3 in the aqueous phase and ·OH in the gas phase. It will provide a means to assess the global and regional importance of transition metal-catalysed SO_2 oxidation, by both dust TMIs and anthropogenic TMIs, which cannot be easily predicted from measurable parameters such as soluble iron concentration. Oxidation on feldspar minerals was found to be slow and would only present a minor interference for these calculations.

Acknowledgements

We thank Elmar Gröner for his support with the NanoSIMS analyses, Joachim Huth for his help with the SEM/EDX analyses, Robert Oswald for assistance in measuring O_3 concentrations and Christa Sudek for help with the ICP-OES analysis. This research was funded by the Max Planck Society and the Max Planck Graduate Centre.

Chapter 5

Investigating cloud processing with sulfur isotope analysis of particles and gases during HCCT 2010

This chapter is in preparation for publication as Harris, E., Sinha, B., Hoppe, P., Schneider, J., van Pinxteren, D., Fomba, W., Mertes, S., Gnauk, T., Fahlbusch, B., Lee, T., Foley, S., Borrmann, S. and Herrmann, H. (2012) *Atmospheric Chemistry and Physics Discussions*, 12, HCCT Special Issue.

5.1 Introduction

Sulfate-containing atmospheric particles have a significant but uncertain climatic effect through their role in radiative forcing (Solomon et al., 2007), and are also important as heterogeneous reaction surfaces and for acid deposition, human health and visibility (Seinfeld and Pandis, 1998). In-cloud SO_2 oxidation and production of sulfate aerosol mass results in significant changes in aerosol size distribution and hygroscopicity, which is particularly important in controlling the climatic effect of aerosol. Understanding the effect of these changes on the magnitude of radiative forcing is essential to model the impact of anthropogenic SO_2 emissions and sulfate aerosol on the past and future climate.

In-cloud mass addition occurs as particles enter a cloud and are activated to form cloud droplets. Upon leaving the cloud, the droplets evaporate to form single particles containing both the initial mass and the aqueous phase products formed in the cloud, as droplets rarely break up during evaporation (Mitra et al., 1992). Mass is added to aerosols as they pass through clouds by a variety of processes. The uptake of gas-phase species such

as H_2SO_4, HCl, HNO_3 and ammonia can contribute the majority of in-cloud mass gain in some conditions (Flynn et al., 2000), but the oxidation of SO_2 to sulfate is generally considered to be the most important in-cloud mass production pathway (Bradbury et al., 1999; Laj et al., 1997a,b; Mertes et al., 2005a). SO_2 is oxidised to sulfate in the aqueous phase by O_3, H_2O_2 and transition metal-catalysed oxidation by O_2 (Sander et al., 1995; Bower et al., 1997). H_2O_2 is commonly modelled to be the most important in-cloud oxidant, due to the strong pH dependence of oxidation by O_3, and the low concentrations of transition metals combined with the slower modelled rate of transition metal-catalysed oxidation (Bower and Choularton, 1993; Sander et al., 1995; Suhre et al., 2000; Hegg et al., 2004).

In-cloud sulfate mass addition is not evenly distributed across the upwind aerosol population. CCN activity and activation depends on the size and hygroscopicity of particles, as well as the strength of the updraught, the wind speed and supersaturation, and other processes such as entrainment mixing of drier air (Mertes et al., 2005b; Kasper-Giebl et al., 2000; Bower and Choularton, 1993). Mass is only added to those particles which are able to activate in the cloud, resulting in a bimodal size distribution with the Hoppel gap at 50-100 nm following cloud processing (Hoppel et al., 1986, 1994; Bradbury et al., 1999; Yuskiewicz et al., 1999). Once activated, uptake of gas-phase sulfuric acid is most important for smaller droplets, which have a higher surface area to volume ratio and can take up gas-phase species much more efficiently than large droplets (Flynn et al., 2000). H_2O_2 is often a limiting oxidant, thus it adds the majority of sulfate to those particles activated early in the cloud - the most efficient CCN - and has little effect on the downwind CCN number concentration. Entrainment often adds H_2O_2 later in the cloud, but as the entrained air is dry it can cause the smallest droplets to evaporate (Bower et al., 1997). Oxidation by O_3 is strongly self-limiting as the oxidation rate decreases by several orders of magnitude below a pH of $\sim$5.5 (Seinfeld and Pandis, 1998), thus it is most important for particles with the highest pH (Kreidenweis et al., 2003). Even in these particles, the pH limitation means that oxidation by O_3 is a minor pathway unless a strong source of alkalinity or ammonia is present (Redington et al., 2009). Oxidation by transition metal catalysis is not pH-dependent and the oxidant (O_2) is not limiting, however the concentration of transition metals present in cloud water depends on the composition of the nucleating particle, which varies with size and particle type (Bruegge-mann et al., 2005). Thus, the total amount of sulfate added in the cloud is not evenly distributed across the aerosol population, and bulk analyses cannot adequately resolve size-dependent alterations in size and hygroscopicity.

The climatic effect of cloud processing is also size-dependent. The direct aerosol effect involves climatic cooling of -0.3 to -1 W m^{-2} due to scattering of solar radiation by particles (Jones et al., 1994; Boucher and Lohmann, 1995). Scattering is most efficient for particles in the size range of 0.3-0.8 μm, the wavelength of visible light, thus sulfate produced in-cloud on pre-existing particles has a greater direct aerosol effect than the ultrafine particles formed from gas-phase SO_2 oxidation (Hegg, 1994). Sulfate addition in clouds increases the magnitude of direct radiative forcing both by increasing particle size and by increasing particle hygroscopicity (Yuskiewicz et al., 1999), and can increase the scattering efficiency of the particle population by >10-100% (Lelieveld and Heintzenberg, 1992; Yuskiewicz et al., 1999; Hegg et al., 2004).

The indirect aerosol effect refers to the increase in cloud condensation nuclei (CCN) number concentration due to anthropogenic activities, which results in smaller, more numerous cloud droplets for the same liquid water content (LWC), and thus increased cloud albedo and lifetime (Twomey, 1991; Boucher and Lohmann, 1995). The magnitude of forcing from the indirect effect is highly uncertain due to the complex and non-linear relationships between sulfate concentration, CCN number, and cloud droplet number concentration (Twomey, 1991; Jones et al., 1994; Boucher and Lohmann, 1995). The effect of sulfate addition on CCN concentration is most significant for the smallest, least hygroscopic particles, which need only a small sulfate addition to be significantly more active as CCN (Bower and Choularton, 1993). The most prominent process adding sulfate to small or hydrophobic particulate during the daytime is condensation of H_2SO_4 (g), while cloud processing may play an important role at night. Eventually all processed particles can already act as efficient CCN, thus the effect of cloud processing on indirect radiative forcing is most important for freshly released particles; processing of aged aerosol primarily affects direct radiative forcing.

The environmental and climatic effects of sulfate addition are therefore not adequately described by bulk measurements: the processes contributing mass need to be resolved for particle type and size to determine how in-cloud mass production alters aerosol size distributions and radiative forcing. Measurement of stable sulfur isotope abundances is the only technique available that can distinguish between sulfate produced by different reaction pathways. Sulfur isotope abundances are described with the delta notation, which is the permil deviation of the ratio of a heavy isotope to the most abundant isotope (^{32}S) in the sample compared to a standard ratio:

$$\delta^x S\ (‰) = [\frac{(\frac{n(^xS)}{n(^{32}S)})_{\text{sample}}}{(\frac{n(^xS)}{n(^{32}S)})_{\text{V-CDT}}} - 1] \times 1000 \tag{5.1}$$

where n is the number of atoms, ^{x}S is one of the heavy isotopes, ^{33}S, ^{34}S or ^{36}S, and V-CDT is the international sulfur isotope standard, Vienna Canyon Diablo Troilite, which has isotopic ratios of $^{34}S/^{32}S = 0.044163$ and $^{33}S/^{32}S = 0.007877$ (Ding et al., 2001). Isotope fractionation is characteristic for reactions, thus isotopic measurements can be used to distiguish between different reaction pathways, such as the different oxidation pathways for SO_2. Kinetic isotopic fractionation is represented by the fractionation factor (α), which is the ratio of the heavy to the light isotope amount in the instantaneously-formed product divided by the ratio in the reactant:

$$\alpha_{34} = \frac{\left(\frac{n(^{34}S)}{n(^{32}S)}\right)_{\text{products}}}{\left(\frac{n(^{34}S)}{n(^{32}S)}\right)_{\text{reactants}}} \tag{5.2}$$

Values of α_{34} for the major oxidation pathways - oxidation by $\cdot$OH, H_2O_2, O_3 and transition metals - have been measured (Chapters 2 and 4), and will be particularly useful to quantify the importance of transition-metal catalysed oxidation of SO_2 compared to oxidation by H_2O_2 in clouds.

This study presents measurements of sulfur isotope abundances in SO_2 and H_2SO_4 gas and in particulate matter upwind, in-cloud, and downwind of an orographic cloud during the Hill Cap Cloud Thuringia (HCCT) campaign. Isotope ratios were measured with the NanoSIMS, which allowed different particle sizes and types to be resolved. The gas-phase results unexpectedly showed that transition metal-catalysed oxidation of SO_2, which is isotopically distinct as it is the only oxidation pathway favouring the light isotope, was the most important in-cloud SO_2 oxidation pathway. The measurements were able to determine the dominant process contributing sulfate mass to different particle classes in the cloud, and show that there is significant variation in the dominate sulfate source with particle size and type. Although it may not dominate the total quantity of sulfate addition, condensation and coagulation of H_2SO_4 and ultrafine particluate was the most important mass addition pathway for altering the CCN number concentration.

5.2 Experimental

5.2.1 Site description

The field measurements were carried out in the Thüringer Wald in central Germany in Autumn, 2010. The site is located on a low mountain ridge which extends for around 60 km in a south-east to north-west direction. South-westerly winds are forced to cross the ridge which often results in orographic cloud formation as air parcels are lifted and

supersaturations are reached. Measurements were taken at three stations. The in-cloud measurement station is located at the Umweltbundesamt (Federal Environment Agency) mountain station 'Schmücke' at a height of 937 m asl. The upwind station 'Goldlauter' (605 m asl) is located around 3 km southwest of Schmücke and the downwind station 'Gehlberg' (732 m asl) is around 3 km to the northeast of Schmücke, thus south-westerly winds cause air parcels to pass through the three stations in series.

5.2.2 Measurement periods and meteorology

Cloud events

Hill-cap cloud measurements were taken when the following conditions were met: The liquid water content at Schmücke was > 0.1 g m^{-3}, the wind direction was between 200° and 250° (to ensure connected flow between the sites), the wind speed was between 2 and 12 m s^{-1}, the valley stations were free of fog and all sites were free of precipitation, the temperature was > 0°C, and the meteorological conditions were stable. All measurement periods were rated according to ozone concentration cross-correlation and hydrodynamic flow analysis (Tilgner et al., 2005). Connected flow between the sites was also periodically measured with tracer experiments following the release of an inert gas (SF_6) at Goldlauter, with measurements at 5-minute intervals at nine sites including the in-cloud and downwind stations.

Samples for sulfur isotope analysis were collected during three cloud events. The sampling times and meteorological conditions are shown in Table 5.1. The HYSPLIT (NOAA Air Resources Laboratory) back trajectories for the three cloud events are shown in Figure 5.1 compared to the SO_2 emission strength (CEIP, 2010). The first event, FCE 7.1, was relatively short and had a lower LWC than the other two events, thus it was a less optimal event. FCE 11.2 showed some evidence of overflow in the connected flow analysis and FCE 11.3 had very good connected flow conditions. The concentration of SO_2 was higher in the events FCE 11.2 and 11.3 than in FCE 7.1. This can be attributed to the back trajectories, which passed over the high-emission region to the south east of the measurement area. Temperature and other meteorological parameters were similar across the three events.

Table 5.1: **Measurement periods for sulfur isotope analysis during the HCCT campaign**. Liquid water content, temperature and $[SO_2]$ represent average values for the measurement period. Ratings are based on how well the desired meteorological conditions were met and on connected flow validation from hydrodynamic flow analysis and ozone concentration cross-correlations between sites. Ratings are only available for cloud events.

Name	**Type**	**Sampling Times**	**LWC**	**T**	**$[SO_2]$ upwind**	**Rating**
			g m^{-3}	°C	ppb	
NC 1	non-cloud, day	08:30 29.09.10 - 16:00 29.09.10	<0.1		0.41	
FCE 7.1	cloud, night	23:00 24.09.10 - 02:00 25.09.10	0.14	8.5	0.24	medium: low LWC, overflow possible
FCE 11.2	cloud, night	23:00 01.10.10 - 07:00 02.10.10	0.37	6.2	0.50	good: overflow possible
FCE 11.3	cloud, day	14:30 02.10.10 - 20:00 02.10.10	0.32	7.7	0.47	very good

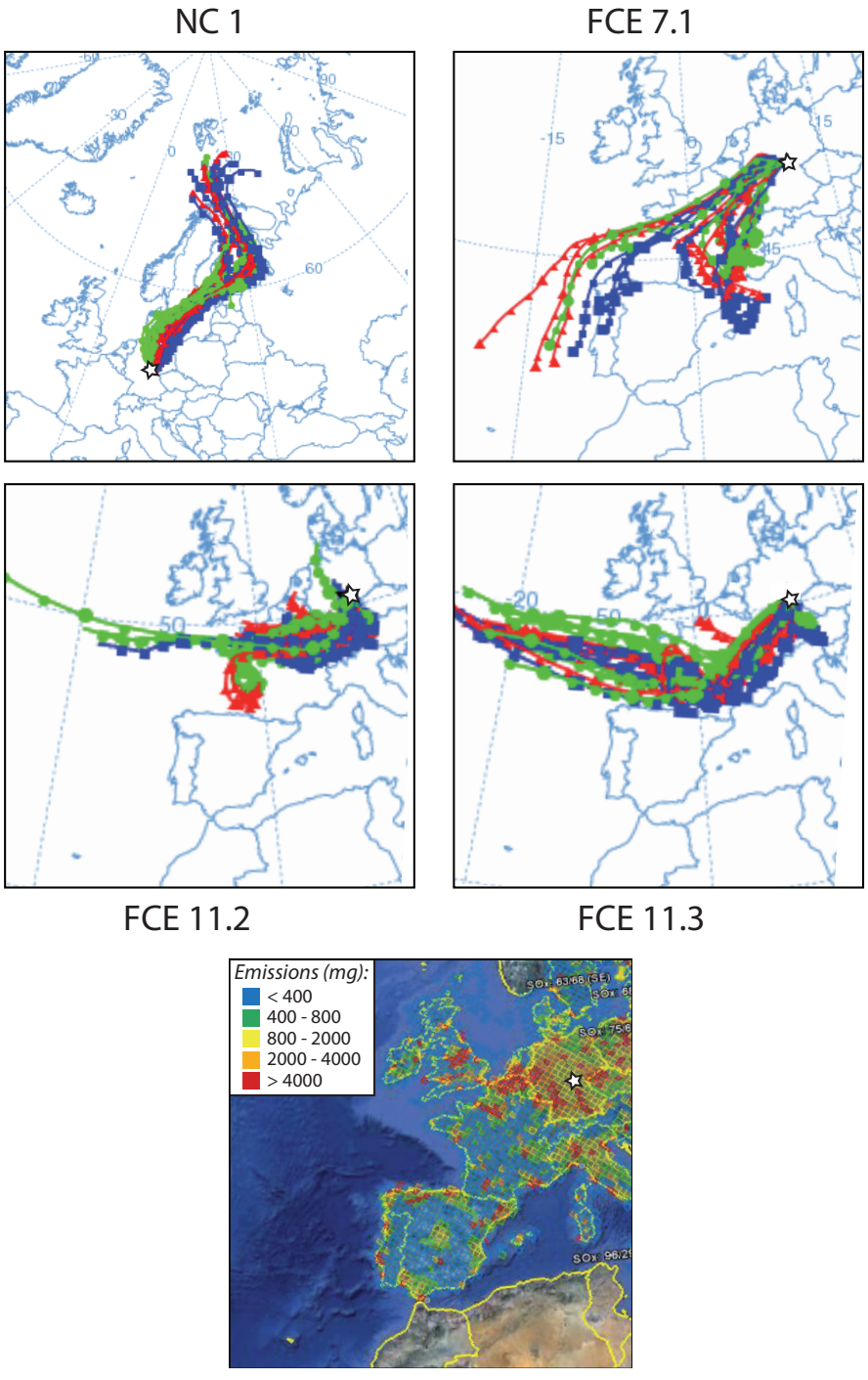

Figure 5.1: **Air mass back trajectories for cloud events at the HCCT campaign**. Emissions are in Mg (10^6 g) and are from the Centre on Emission Inventories and Projections (CEIP, 2010)

Non-cloud event

One sample was collected when no hill cap cloud was present at Schmücke, for comparison with the cloud events. LWC was <0.1 g m^{-3} at Schmücke although there were high clouds present. The details of the event are shown in Table 5.1 and the back trajectory in Figure 5.1. The non-cloud event does not present a perfect comparison to the cloud events as the wind was north-easterly rather than south-westerly; thus flow will proceed from Gehlberg over Schmücke to Goldlauter. No suitable non-cloud period with south-west winds occurred during the measurement time and this event represents the best possible comparison. For the rest of the chapter, stations will simply be referred to as upwind, in-cloud/mountain and downwind to avoid confusion.

5.2.3 Particulate sampling

Particulate samples were collected on filter packs at all three measurement stations, however they were unfortunately not collected during FCE 7.1 due to equipment problems. Nuclepore track-etch polycarbonate membrane filters (Whatman Ltd.), which had been coated with a 10 nm-thick gold layer using a sputter coater (Bal-tec GmbH, Model SCD-050) prior to sample collection, were used to collect particulate samples. Coarse particles were collected on a filter with 5 μm pores and fine particles were collected on a filter with 0.2 μm pores. The calculated 50% cut-off diameters at 1 L min^{-1} flow rate are 1.9 μm and 60 nm for coarse and fine filters respectively (John et al., 1983). The latter is in good agreement with the SEM-measured lower cut-off diameter of 50 nm for the fine particles (Sinha et al., 2012a). The effective cut-off between the coarse and fine filters found from SEM measurements is around 600 nm, with tails in both directions caused by the random distribution of pores across the filter and variations in particle density and shape (Sinha et al., 2012a). Whenever only particles <1 μm were encountered for a particular particle type in a particular sample, particles on both filters were combined and classified as fine. For particle classes where both "coarse" (>1 μm) and "fine" (<1 μm) particles were encountered in a given sample, the fine and coarse filters will be used as a guide to the size-dependency of different processes in the discussion in Section 5.3.5. The cut-off does not conform exactly to the traditional definitions of coarse particles > 1 μm > fine particles.

At the in-cloud measurement site, interstitial particles and cloud droplets were collected separately with a counterflow virtual impactor (CVI) and a complementary droplet-segregating interstitial inlet (INT) (Schwarzenboeck et al., 2000; Mertes et al., 2005b).

The system had an operationally-defined discrimination diameter of 5 μm for separation of the two aerosol populations. The two sample types, which represent droplet residuals - particles that were activated to form cloud droplets - and unactivated interstitial particles, will hereafter be referred to as 'cloud droplet residuals' and 'interstitial particles'. Particles with a dry diameter >5 μm (mineral dust) would be included in the cloud droplet residual fraction whether they were activated or not. The largest mineral dust particles were, however, not analysed to prevent artefacts due to the inlet cut-off and due to electrostatic charging, which affects the correction of the instrumental mass fractionation during NanoSIMS analysis (Winterholler et al., 2008).

5.2.4 Gas phase sulfur sampling

After particulate was removed from the sampling air flow, SO_2 and sulfuric acid gases were collected for isotopic analysis at the upwind and downwind sites. A detailed description and validation of the collection methods is presented in Section 2.3.4 and only a brief description will be given here. SO_2 was collected in a bubbler containing 6% H_2O_2. The H_2O_2 solutions were prepared freshly immediately before beginning collection. The collection efficiency is 39% and a fractionation of +11.5±1.3‰ is introduced, which will be corrected in all results presented in this chapter. Sulfuric acid gas was collected in glass vessels with a high internal surface area. This does not represent pure gas but will primarily contain ultrafine and freshly nucleated particles; as the 50% cut-off diameter of the fine filters is ∼50 nm, sulfate in particles below this size will contribute to the 'sulfuric acid' measurement. The collection efficiency for the sulfuric acid collectors is close to 100% so no correction is needed for isotopic fractionation during collection. Following an event (2-8 hours) the flow to the collectors was turned off. Within three hours after the end of sampling the two collectors were rinsed with MilliQ water into clean sample jars and $BaCl_2$ was added to precipitate sulfate as $BaSO_4$. The $BaSO_4$ was later collected for NanoSIMS and SEM analysis by filtering the samples through gold-coated Nuclepore filters with 0.2 μm pores.

5.2.5 Other measurements

In addition to sulfur samples for isotopic analysis, a wide variety of other measurements were taken during the campaign (see van Pinxteren et al. 2011). A brief description of the measurement techniques for all measurements used in this study will be given here; more details can be found in the accompanying papers in the HCCT special issue of

Atmospheric Chemistry and Physics.

SO_2 concentration was measured with a time resolution of one minute using a Thermo Environmental trace level pulsed fluoresence SO_2 analyser (model TE43C-TL) at Gehlberg and Goldlauter and an MLU enhanced trace level SO_2 analyzer (model 43i-) at Schmücke. H_2O_2 was measured in cloud water collected on a 3-stage impactor. The H_2O_2 is preserved on site with *p*-hydroxyphenylacetic acid (POPHA) to form a stable dimer; potassium hydrogen phthalate and EDTA are also added to buffer the solution and prevent interferences from metal ions. The POPHA-H_2O_2 dimer is later measured quantitatively with a fluorescence spectrophotometer (Moore et al., 2004a,b). Water-soluble gases and particles were measured with MARGA (Monitor for AeRosols and Gases in Air). Gases are collected in a wet rotating denuder, while particles are grown to droplets containing the water soluble inorganic ions at high supersaturation in the steam jet aerosol collector. The liquid samples are then analysed online via an ion chromatography system (Trebs et al., 2004). Particulate composition was measured with Aerosol Mass Spectrometry (AMS): a C-ToF-AMS was used for the cloud droplet residual fraction and an HR-ToF-AMS for the interstitial fractionation at Schmücke (Aerodyne Research, Inc.). Cloud droplet size distributions were measured with an FSSP-100 (Forward Scattering Spectrometer Probe, PMS Inc.) at all sites.

Transition metal ion (TMIs) were measured in bulk cloud water. Bulk cloud water was collected using a homemade bulk cloud water collector with an hourly sampling routine. 1 ml of cloud water was used for transition metal ion measurements. The sample was filtered using a 0.45 μm filter, and 0.5 ml of the filtrate was then used for TMI determination using an ion chromatograph (IC, Dionex ICS 900). The following TMI complexes were detected simultaneously at 530 nm using a variable wavelength UV/VIS detector: Fe (III), Cu (II), Ni (II), Zn (II), Cd (II), Co (II), Mn (II), and Fe (II). The ions were identified from their respective retention times on the chromatogram and quantification was done via external calibration. The detection limit of the iron species was about 0.1 M. Most other metals had similar detection limits to the iron species, except Ni and Cd, which had a detection limit 70-80% higher.

5.2.6 SEM and NanoSIMS analysis

Scanning electron microscope (SEM) measurements were used to classify different particle types and investigate their chemical composition. The samples could be directly analysed in the SEM after collection on gold-coated filters without any further treatment. A LEO 1530 field emission SEM with an Oxford Instruments ultra-thin-window energy-

dispersive x-ray detector (EDX) was run in automatic mode, taking regularly-spaced images of the coarse and fine filters at 6500× and 19500× magnification respectively. The SEM was operated with an accelerating voltage of 15 keV, a 60 μm aperture and a working distance of 9.6 mm. "High current mode" was used to increase the EDX signal and improve elemental sensitivity. The SEM automatic analysis leaves a grid pattern on the gold-coated filters that is visible in the CCD camera of the NanoSIMS, which allows NanoSIMS and SEM images of the filters to be matched. The SEM images of the filters were also used to calculate size distributions for the different particle types to investigate properties important for CCN activity (Sinha et al., 2012a).

Following automatic analysis in the SEM, the sulfur isotopic composition of the particles was determined with the Cameca NanoSIMS 50 ion probe at the Max Planck Institute for Chemistry in Mainz (Hoppe, 2006; Groener and Hoppe, 2006). The NanoSIMS 50 has a high lateral resolution (<100 nm) and high sensitivity and can simultaneously measure up to five different masses through a multicollection system, allowing high precision isotope analysis of single particles. Two types of NanoSIMS analysis were used in this study: an *image analysis*, where the counts of the various ions are recorded at each point of the raster to create an image of the ion intensity, such as that shown in Figure 5.2, and an *isotope analysis*, where the counts are integrated across the raster area to obtain an accurate value for the isotope ratios. Image analyses will be referred to only in Section 5.2.7 and will not be used to calculate values of δ^{34}S in the samples. The use of this instrument to analyse sulfur isotope ratios in the isotope ratio analysis mode is described in detail in Winterholler et al. (2006, 2008) and analysis conditions similar to those used for the current study are given in Section 2.3.5, so only a brief description will be included here.

The particulate samples and the $BaSO_4$ from the gas samples can be analysed directly on the gold-coated filters without further processing. A ∼1 pA Cs^+ beam is focussed onto a ∼100 nm sized spot and rastered in a 2 μm × 2 μm grid over the grain of interest. The ejected secondary ions are carried into the mass spectrometer and multicollection system. Each measurement consists of <400 cycles of 4.096 s duration preceded by varying lengths of presputtering until the count rate is stable. Very small particles are quickly completed sputtered away, so some analyses can be as short as 50 cycles. Presputtering is carried out on an area of at least 10 μm × 10 μm to conserve sulfate for analysis. For the particulate samples secondary ions of $^{16}O^-$, $^{12}C_2^-$, $^{26}CN^-$, $^{32}S^-$ and $^{34}S^-$ were measured. For the $BaSO_4$ samples of gas-phase sulfur, some samples were measured for secondary ions of $^{16}O^-$, $^{12}C_2^-$, $^{26}CN^-$, $^{32}S^-$ and $^{34}S^-$ and some for $^{16}O^-$, $^{32}S^-$, $^{33}S^-$, $^{34}S^-$ and $^{36}S^-$. In both

cases the $^{34}S/^{32}S$ ratio was measured with equal precision. The five secondary ion types were simultaneously detected in five electron multipliers at high mass resolution ($M/\Delta M > 3900$ for ^{33}S).

Mass-dependent and mass-independent instrumental mass fractionation (IMF) can occur at several stages of the SIMS analysis, so the IMF correction factor in each measurement session is determined with the commercially available $BaSO_4$ isotope standards IAEA-SO5 and IAEA-SO6. The IMF of the particles is also dependent on their matrix. The IMF correction factors for different matrices relative to $BaSO_4$ from Winterholler et al. (2008) were used to correct for matrix-dependent IMF on the different particle types. The method for determining particle type is presented in Section 5.2.7. Secondary organic aerosol (SOA) droplets containing inorganic salts, hereafter referred to as 'mixed droplets', with an O/S ratio (measured in the NanoSIMS) of < 2 were considered to be 'organic' and were corrected with the IMF for cysteine (-13.5 ± 1.7‰ relative to $BaSO_4$). The most abundant cations in 'inorganic' mixed droplets (O/S > 3 in NanoSIMS) were found from the SEM-EDX analysis to be Na and K, so these particles were corrected by weighting the individual IMFs for Na and K by their abundances (-8.4 ± 2.7‰ relative to $BaSO_4$). Mixed droplets with an O/S ratio between 2 and 3 were corrected by assuming they consisted of a mixture of organic and inorganic sulfates, thus the average IMF for organic and inorganic mixed droplets of -11.0 ± 3.2‰ relative to $BaSO_4$ was used. Coated soot particles were corrected for matrix-dependent IMF in the same manner as the mixed droplets. Chlorine was enriched on the mineral dust particle surfaces, suggesting the presence of condensed salts, which could supply cations to form sulfate salts. The cations within the dust are likely to be tightly-bound and not available to interact with sulfate. As with the inorganic mixed droplets, Na and K were found to be the most important cations and the abundance-weighted IMF was used (-8.4 ± 3.7‰ relative to $BaSO_4$; the error is higher than for the mixed droplet IMF as less mineral dust particles were measured).

The number of counts is assumed to follow a Poisson distribution, so the counting statistical error is $\sqrt{n}$, i.e. the relative error is $1/\sqrt{n}$ (Bevington and Robinson, 1992). The uncertainty in the isotopic composition of $BaSO_4$ from gas-phase sulfate was calculated as described in Section 2.3.5. Some spot-to-spot variation is also seen between individual measurements on a filter, most likely due to topographic effects or nanoscale inhomogeneity, and this must be accounted for in the particulate measurements. The spot-to-spot error of the SO5 and SO6 standards was used as an estimate of the spot-to-spot error for the measurement session, and this was then combined with the counting statistical

error to determine the measurement uncertainty for each individual grain. The error in the matrix-specific IMF was also included in the error for each grain. For each individual grain, the counting statistical error was typically 5-7‰ and the overall error 7-8‰. The weighted average of individual grain values was used as the average δ^{34}S for each particle class, with the uncertainty in the mean multiplied by $\sqrt{\chi^2}$ for $\chi^2 > 1$.

5.2.7 Classification of particle types

The different particle types present in the HCCT samples were investigated in both the SEM and the NanoSIMS to develop a classification method that would allow particle types to be identified with only the major element count rate ratios from NanoSIMS isotope analyses. This means that the particles with the highest sulfur count can be selected in the NanoSIMS real time image, resulting in isotopic analysis with the smallest uncertainty, without the constraint of only measuring the isotope ratios of particles for which there is an SEM image. Taking the SEM image after the NanoSIMS analysis is only possible for the largest and most robust particles; most particles are completely sputtered away during the NanoSIMS analysis.

Major elements ratios (^{16}O, $^{12}C_2$, ^{26}CN and ^{32}S) measured in the NanoSIMS were characterised for the different particle types by matching SEM and NanoSIMS images from 10 coarse and 5 fine particulate filters. Two examples of matched SEM and NanoSIMS images are shown in Figure 5.2. Five particle types were identified from the SEM images based on morphological characteristics and EDX signal: SOA, mixed droplets, mineral dust, soot, and soot with a coating. The major element ratios were converted to molar fractions according to Sinha et al. (2012b):

$$X_A = \frac{n_A}{n_O + n_C + n_N + n_S} \tag{5.3}$$

where A = O, C, N or S. The characteristic ranges of X_A for the five different particle types are shown in Figure 5.3.

Using these characteristic ranges as well as the ratio of oxygen to sulfur, it was possible to distinguish the different particle types from a NanoSIMS isotopic analysis without a corresponding SEM image. Although there is significant overlap in many ratios, all particle types could be distinguished. Soot and coated soot particles have high X_C, low X_S and high O/S, while SOA droplets and mixed droplets have the lowest O/S ratios and higher X_S, and mineral dust has high O/S and low X_C and X_S. The most overlap is between pure SOA and mixed droplets, indicating that the SEM is not a suitable tool to detect small amounts of inorganic material in organic particles. Many salts present in fine

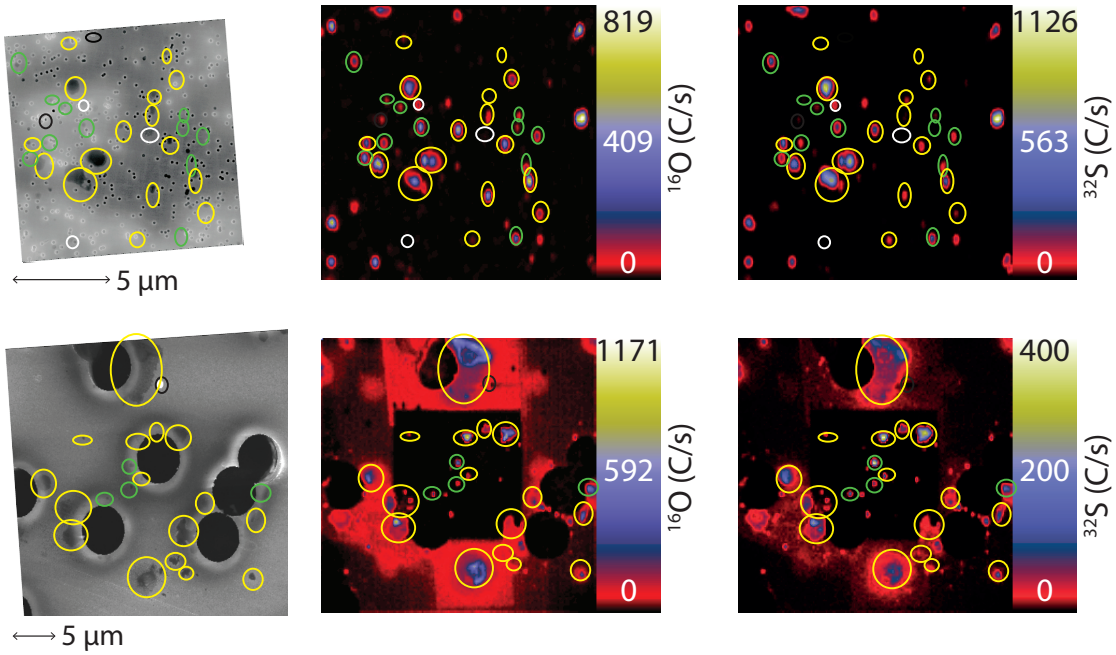

Figure 5.2: **SEM and NanoSIMS images of the same area on a fine (top) and coarse (bottom) particulate filter**. Particles are circled with different colours according to particle type: yellow = mixed droplet, green = secondary organic aerosol, black = soot, white = soot + coating.

mode aerosol are highly volatile under the electron beam (e.g. most salts of ammonium) but more stable under Cs^+ bombardment (Winterholler et al., 2008). Therefore, we will treat all droplets as mixed and consisting of secondary organic (SO) and secondary inorganic (SI) material in variable proportions, even if no SI fraction is visible in the SEM.

The accuracy of the classification method was tested on 21 particles which were all found in the SEM and the NanoSIMS and had sufficient sulfur counts for an isotopic analysis. These 21 particles were not used when defining the characteristic ranges of the ratios, thus they present a robust and independent test of the classification method. 19 of the 21 particles were correctly identified using the ratios, thus the classification is >90% successful.

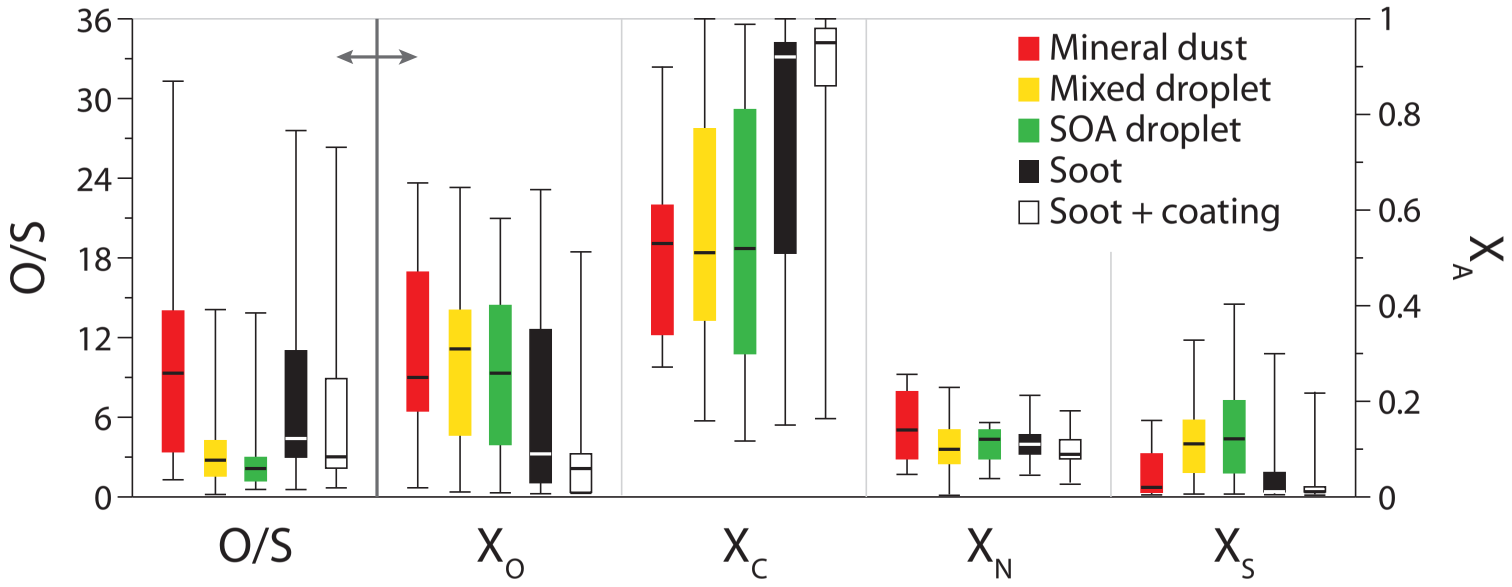

Figure 5.3: **Characteristic ratios of major elements in different particle types measured with NanoSIMS** and corrected according to Sinha et al. (2012b). Boxes represent the range from the 25th to the 75th percentile; the median is shown as a centre line in the boxes. Whiskers show the full range of the measurements. The O/S ratio is shown on the left-hand axis, while the molar ratios of O, C, N and S (X_A) are shown on the right-hand axis.

5.3 Results

5.3.1 SO_2 concentration

The SO_2 concentrations at the different stations show the amount of SO_2 removed in each cloud event and the effects of entrainment. Time series of SO_2 concentration during the measurement periods are shown in Figure 5.4. The concentration of SO_2 increases between the measurement stations in the non-cloud event ($[SO_2]_{upwind}$ = 0.15±0.23 ppb and $[SO_2]_{downwind}$ = 0.41±0.11 ppb); the average concentration at the in-cloud station is 0.17±0.04 ppb, which is very similar to the concentration upwind. As the setting is rural and there are no local pollution sources located between the stations, the SO_2 addition is due to mixing of free tropospheric SO_2. Free tropospheric SO_2 is long-lived and well-mixed compared to boundary layer SO_2, so it can be assumed that the free tropospheric SO_2 concentration is similar across the four measured events (Thornton and Bandy, 1993; Thornton et al., 1996). Thus, the increase in SO_2 concentration (0.26±0.25 ppb) during the non-cloud event will be used as the best estimate for the level of SO_2 added by entrainment during the cloud events. During all the cloud events, the SO_2 concentration decreases as the air parcel passes through the cloud. The fraction of SO_2 remaining at the downwind site f was calculated from $f = [SO_2]_{downwind}/[SO_2]_{upwind}$ with a 25 minute lag time to account for transport, based on the average transport time seen in the tracer experiments. The time series of the fraction of SO_2 lost (1 - f) is shown in Figure 5.4. The average values of f for each event calculated with and without the addition of 0.26±0.25 ppb from entrainment are shown in Table 5.2.

SO_2 can be lost during passage through the cloud by dry deposition and by uptake and oxidation in cloud droplets. The estimated dry deposition flux of SO_2 is ∼0.5 day^{-1} (Chin et al., 2000), which would account for <1% SO_2 loss during the 25 minute transport time between the upwind and downwind stations, thus the majority of SO_2 loss is due to uptake and oxidation in cloud droplets. The total fraction of SO_2 removed by uptake and oxidation is the same in all three events (83, 84 and 82% of upwind SO_2 for FCE 7.1, 11.2 and 11.3 respectively, considering entrainment), and in all three clouds a similar fraction of SO_2 is lost between the upwind and in-cloud stations and between the in-cloud and downwind stations. This shows the dominant oxidation pathway is not dependent on UV light, the oxidant is not quickly exhausted after the air parcel enters the cloud, and the rate of removal is proportional to the concentration of SO_2.

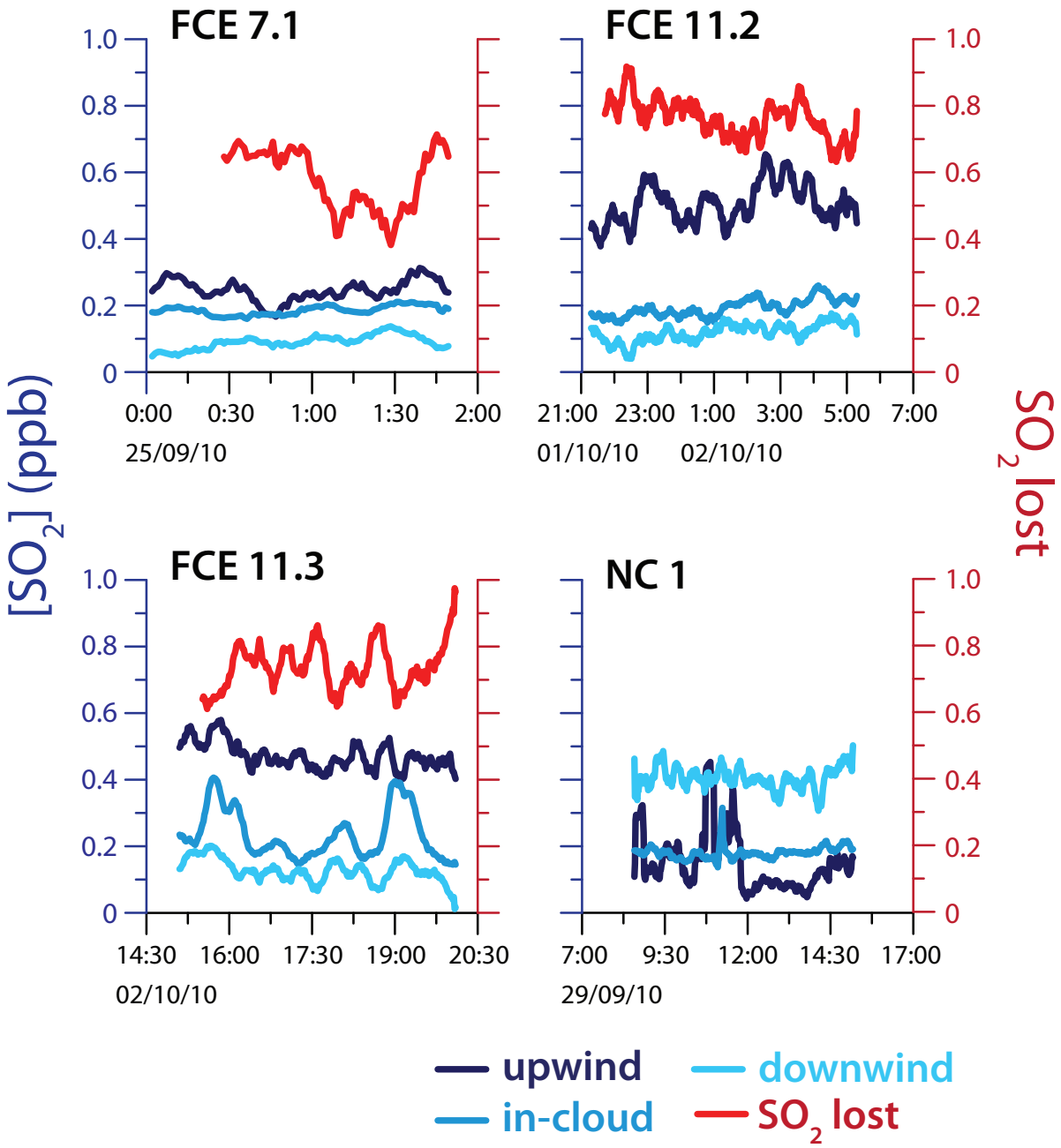

Figure 5.4: **SO_2 (g) concentrations upwind, within and downwind of an orographic cloud during the HCCT campaign**. SO_2 concentrations are shown in blue while the fraction of SO_2 lost (fraction lost $= 1 - f = 1 - [SO_2]_{\text{downwind}}/[SO_2]_{\text{upwind}}$) between the upwind and downwind stations is shown in red. During the non-cloud event NC 1 the SO_2 concentration was higher downwind than upwind thus the fraction lost is shown.

5.3.2 Isotopic composition of SO_2 gas

The $\delta^{34}S$ of sulfur dioxide at the different measurement stations reflects isotope discrimination during uptake and oxidation in cloud droplets. The different oxidants that could react in the cloud, such as H_2O_2 or transition metals, produce distinct sulfur isotope fractionation, thus the dominant oxidation pathway can be determined (see previous chapters for measurements). The $\delta^{34}S$ values for SO_2 measured at the upwind and downwind stations are shown in Table 5.2 and Figure 5.5. During FCE 11.2 and 11.3, SO_2 removal favours the light isotope, resulting in an increase in $\delta^{34}S$ of SO_2 between the upwind and downwind stations; during FCE 7.1 the opposite occurs, and the downwind SO_2 is isotopically lighter than the upwind SO_2. These isotopic changes can be compared to known isotopic fractionation factors for different oxidation pathways. The fractionation factor for the passage of the air parcel through the cloud is calculated from the Rayleigh equations (Mariotti et al., 1981; Krouse and Grinenko, 1991), which describe the relationship between the fractionation factor, fraction reacted, and initial and residual reactant isotopic composition:

$$\alpha_{\text{cloud}} = \frac{\ln(\frac{R_{\text{downwind}}}{R_{\text{upwind}}})}{\ln(f)} + 1 \tag{5.4}$$

where R_{upwind} and R_{downwind} are the isotope ratios $^{34}S/^{32}S$ of SO_2 at the upwind and downwind sites, which represent the initial and residual SO_2 isotopic composition respectively, and f is the fraction of the upwind SO_2 remaining at the downwind site as defined previously. α_{cloud} will not be representative of a single process but will be the sum of all the SO_2 removal processes occurring in the cloud:

$$\alpha_{\text{cloud}} = \frac{f_1.\alpha_1 + f_2.\alpha_2 ... f_n.\alpha_n}{f_1 + f_2 ... f_n} \tag{5.5}$$

when n different SO_2 removal processes are acting in the cloud, assuming processes are occurring simultaneously and at constant relative rates. This is a valid assumption as the pseudo-first order rate relative to SO_2 concentration is approximately constant throughout the cloud.

Table 5.2: **Isotopic composition of SO_2 (g) upwind and downwind of an orographic cloud**, with and without a correction for SO_2 entrainment ('Entrainment' and 'No entrainment' respectively). f is the fraction of SO_2 remaining at the downwind station and α_{cloud} is the fractionation factor for SO_2 loss in the cloud; these two values are not considered for the non-cloud event NC1.

				Entrainment		**No entrainment**	
	Time	$\delta^{34}S_{SO_2}$ upwind (‰)	$\delta^{34}S_{SO_2}$ downwind (‰)	f	α_{cloud}	f	α_{cloud}
NC 1	day	24.5±0.9	13.5±1.0				
FCE 7.1	night	29.6±1.9	-7.8±1.3	0.17±0.27	1.015±0.019	0.42±0.09	1.043±0.011
FCE 11.2	night	-9.4±3.2	32.1±1.2	0.16±0.26	0.981±0.020	0.24±0.06	0.971±0.005
FCE 11.3	day	13.1±1.4	34.1 ± 1.5	0.18±0.26	0.987±0.010	0.26±0.07	0.985±0.003

Entrainment and dry deposition are the two major interferences that could affect the comparison between α_{cloud} and potential oxidation pathways. Dry deposition of SO_2 will be expected to introduce isotopic fractionation as it is limited by the diffusion rate, which is mass-dependent according to (Tucker and Nelken, 1982):

$$D_{\text{air}} = \frac{0.001T^{1.75}M_r^{1/2}}{P(V_A^{1/3} + V_B^{1/3})^2} \tag{5.6}$$

where D_{air} is the diffusion coefficient of the molecule of interest in air ($cm^2\ s^{-1}$), T is the temperature (K), M_r is the reduced molecular weight $\frac{M_A+M_B}{M_A.M_B}$ where M_A is the molecular weight of air ($\sim$28.97 g mol^{-1}) and M_B is the molecular weight of the molecule of interest (SO_2), P is the pressure (atm) and V_A and V_B are the molar volumes of air and the compound of interest respectively ($cm^3\ mol^{-1}$). The value of α_{drydep} is then estimated as the ratio of $D_{\text{air}}(^{34}SO_2)$ to $D_{\text{air}}(^{32}SO_2)$: $\alpha_{\text{drydep}} = 0.991$. There is no temperature or pressure dependence as the terms cancel when the ratio of the two diffusion coefficients is calculated. However, as stated in Section 5.3.1, dry diffusion is expected to remove $< 1\%$ of SO_2 in the short time period between upwind and downwind measurements. Equation 5.4 can be used to estimate the change in $\delta^{34}S$ of SO_2 that can be accounted for by dry deposition: With $f = 0.99$ (1% removed) and $\alpha = 0.991$, the downwind (residual) SO_2 is just 0.09‰ heavier than the upwind SO_2. To account for the observed increase of >20‰ in $\delta^{34}S$ of SO_2 between the upwind and downwind stations during FCE 11.2 and 11.3, dry deposition would need to remove >88% of SO_2. This is not feasible, because i) dry deposition does not occur at this rate and ii) there is no SO_2 source between the stations that could account for downwind SO_2 concentrations if dry deposition was occurring at this rate. Thus, dry deposition has a negligible effect on the isotopic composition of SO_2 gas.

Entrainment affects the calculation of α_{cloud} as it adds SO_2 between the upwind and downwind stations, which affects both the calculated value of f and the $\delta^{34}S$ of downwind SO_2. As discussed in the previous section, the addition of SO_2 during the non-cloud event provides the best estimate for the level of entrainment during cloud events. The isotopic composition of the SO_2 added between upwind and downwind stations in NC 1 can be calculated from:

$$R_D = \frac{R_A \cdot [SO_2]_A + R_U \cdot [SO_2]_U}{[SO_2]_A + [SO_2]_U} \tag{5.7}$$

where R_U, R_D and R_A are the isotopic ratios $^{34}S/^{32}S$ for upwind, downwind and added SO_2 respectively, and $[SO_2]_U$, $[SO_2]_D$ and $[SO_2]_A$ are the SO_2 concentrations upwind, downwind, and contributed by the addition respectively ($[SO_2]_D = [SO_2]_U + [SO_2]_A$). The added SO_2 in NC 1 has a $\delta^{34}S$ of 7.4±3.4‰, which provides a good estimate for the

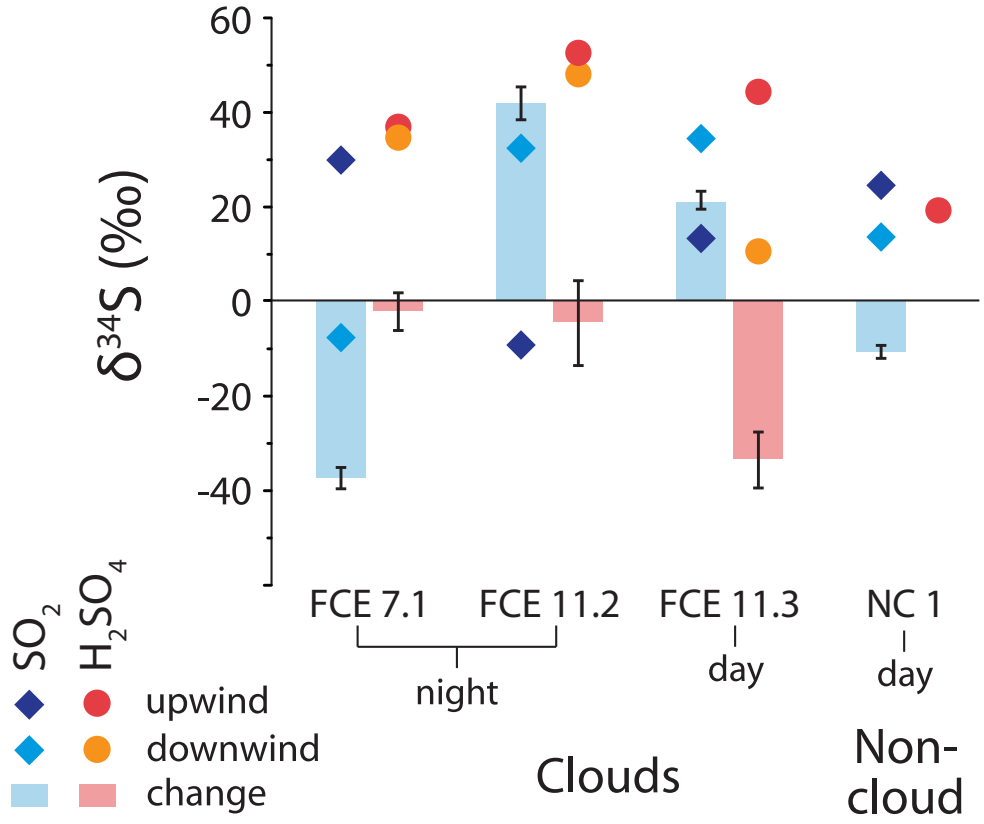

Figure 5.5: **Isotopic composition of SO_2 (gas) and H_2SO_4 (gas + ultrafine particulate) upwind and downwind of orographic clouds during the HCCT campaign**. Points show the upwind and downwind values of $\delta^{34}S$ while columns show the change (downwind minus upwind) and the 1σ error of the measurement.

isotopic composition of entrained SO_2 during cloud events, as free tropospheric SO_2 is relatively long-lived and well-mixed (Thornton and Bandy, 1993; Thornton et al., 1996). The effect of entrainment on α_{cloud} is calculated by assuming 0.26±0.25 ppb of SO_2 is simply added at the upwind station and then oxidised as the air parcel passes through the cloud. Although this is not a realistic picture, as SO_2 will be entrained in parcels throughout the cloud as updraughts and downdraughts change, the extra error introduced by the assumption is negligible. Accounting for the effect of entrainment on f reduces the magnitude of the calculated α_{cloud} by an average of 10.5‰ for the three events, while accounting for the effect of entrainment on $\delta^{34}S$ increases the calculated α_{cloud} by only 3.6‰ for the three events. The values of α_{cloud} accounting for the effect of entrainment on both f and $\delta^{34}S$ are shown in Table 5.2.

There are a number of potential oxidants that could contribute to SO_2 oxidation

in the cloud. The calculated values of α_{cloud} which have been corrected for the effects of entrainment can be used to identify the dominant oxidation pathway in each cloud event. Aqueous oxidation of SO_2 by O_3 and H_2O_2 results in a fractionation of α_{34} = 1.0167±0.0019 at 0°C (Section 2.4.1). Oxidation by H_2O_2 is generally thought to be the dominant oxidation process in continental clouds (Bower et al., 1997; Laj et al., 1997b). O_3 is unlikely to be a significant contributer to in-cloud oxidation as oxidation is observed to continue throughout the passage of the air parcel through the cloud; O_3 oxidation is strongly pH dependent and will very quickly be self-limiting (Sievering et al., 1991; Chameides and Stelson, 1992). Based on α_{cloud}, H_2O_2 oxidation is the major oxidation pathway in FCE 7.1, however during FCE 11.2 and 11.3 it cannot be a major oxidation pathway as it causes isotopic fractionation in the opposite direction to α_{cloud}. Oxidation of SO_2 by transition metal ion catalysis (Herrmann et al., 2000), from anthropogenic pollution or leached from mineral dust (Kumar et al., 2010; Kumar and Sarin, 2010), has an α_{34} of 0.9905±0.0031 (Section 4.4.2) which agrees with α_{cloud} for FCE 11.2 and 11.3 but not FCE 7.1. Thus, it can be inferred from the values of α_{cloud} that:

- During FCE 7.1 oxidation by H_2O_2 in cloud droplets was the major SO_2 removal process,
- During FCE 11.2 and 11.3 oxidation by transition metal catalysis, involving transition metal ions from anthropogenic and dust sources, was the major SO_2 removal process,
- The major SO_2 removal process does not depend on whether the cloud is present in the daytime or at nighttime, but is related to the liquid water content and the transition metal ion source and loading.

5.3.3 Isotopic composition of H_2SO_4 gas and ultrafine particles

The isotopic composition of sulfuric acid gas and ultrafine particulate reflects fractionation during removal and constrains the $\delta^{34}S$ value of the sulfate that can be added to particulate in the cloud by condensation and coagulation. The upwind and downwind measurements of the isotopic composition of ultrafine sulfate particulate and sulfuric acid gas are shown in Figure 5.5. A faulty sample meant no downwind isotopic composition could be measured for NC 1. The concentration of sulfuric acid gas was not measured during the campaign. Typical daytime sulfuric acid gas concentrations are 10^6 - 10^7 molec cm^{-3} (Weber et al., 1997). Ultrafine particles with a diameter of <60 nm are continuously present in the atmosphere (Kulmala et al., 2007). As the only known atmospheric source

of sulfuric acid gas is SO_2 oxidation by ·OH radicals, the sulfuric acid gas concentration will be very low during the nighttime events, so the sulfate measured during FCE 7.1 and 11.2 will primarily be due to ultrafine particles; the sulfate measured during FCE 11.3 will have a much greater contribution from H_2SO_4 gas.

The downwind $\delta^{34}S$ was lower than at the upwind station in all three cloud events, although the difference is not significant during the two nighttime events. No ·OH was measured in the cloud or at night (Whalley et al., 2012), and only very low concentrations at the valley sites in the daytime, so the change in isotopic composition is due to removal, rather than production, of gas-phase sulfuric acid. Isotopic fractionation during removal in the cloud could be influenced both by diffusion and by condensation and vapour pressure. Using Equation 5.6, the diffusion-dependent fractionation factor for gas-phase sulfuric acid is $\alpha_{\text{diff}} = 0.995$. This is the opposite direction to the observed fractionation, showing diffusion is not the limiting factor for loss. The vapour pressure for many analogous compounds is increased with a heavy isotope substitution, for example, deuterated methanol vapour pressure effects produce fractionation of 1.007 (Hopfner, 1969; Borowitz and Klein, 1971), however the effect has not been measured for sulfuric acid. The magnitude of the isotope effect is expected to be lower for ultrafine sulfate particles, as the relative mass difference from an isotopic substitution is less important.

It is not possible to quantitatively examine the isotopic composition as there is no relevant value of f. Calculating α_{cloud} would require separate values of f for sulfuric acid gas and for different size bins of ultrafine particulate, to account for the predicted dependence of isotopic fractionation on molecule/cluster size. Removal from one size bin could also result in addition to a larger size bin through condensation or coagulation, which would complicate the calculation further. The results can therefore only be examined qualitatively. The ratio of sulfuric acid gas to ultrafine particulate is much lower in the nighttime events than in the daytime, which explains why there is no significant change in the isotopic composition between the upwind and downwind stations in the two nighttime events and a large change in the daytime event. The observed isotope fractionation in sulfuric acid and ultrafine particles is consistent with condensation and coagulation removal to cloud droplets, controlled by vapour pressure and not by diffusion.

5.3.4 Isotopic fractionation during oxidation of SO_2 gas to sulfate

The upwind $\delta^{34}S$ of H_2SO_4 is higher than the $\delta^{34}S$ of SO_2 in all cloud events, whereas during NC 1 H_2SO_4 is isotopically lighter than SO_2 by 5.2±1.3‰. Evidence of air parcel

mixing was seen in the SO_2 isotopic composition for NC 1 (Section 5.3.2), thus the lighter H_2SO_4 compared to SO_2 in NC 1 can be attributed to recent mixing. The differences in the cloud events are 7.2±2.2‰, 61.7±4.2‰ and 31.0±4.7‰ for FCE 7.1, 11.2 and 11.3 respectively. The fractionation factor for gas-phase production of sulfuric acid from oxidation of SO_2 by ·OH radicals is 1.0089±0.0007 at 0°C (Section 2.4.2), which agrees with the SO_2-H_2SO_4 fractionation for FCE 7.1 but has a much smaller magnitude than for FCE 11.2 and 11.3. There is no known gas-phase production pathway for H_2SO_4 other than SO_2 oxidation by ·OH radicals.

The difference between the observed $\delta^{34}S$ of H_2SO_4-SO_2 and the expected difference from fractionation during gas-phase SO_2 oxidation in FCE 11.2 and 11.3 could be due to a number of processes, such as passage through clouds before the measurement site affecting the gas-phase sulfur isotopic composition, Rayleigh fractionation during oxidation of SO_2, or addition of fresh SO_2 to the air mass shortly prior to reaching the sample site. Passage through clouds prior to the sampling site will haved removed almost all sulfate and the majority of SO_2, resulting in strong isotopic fractionation of the residual fractions. The effect of previous clouds and of recent addition of SO_2 depends on the dominant sources and reactions and cannot be easily predicted. The most likely explanation, considering that gas-phase oxidation fits the isotopic composition in FCE 7.1 but not FCE 11.2 and 11.3, is that the air parcels in FCE 11.2 and 11.3 had recently passed through SO_2 source regions (the 'black triangle', see Figure 5.1), unlike the FCE 7.1 air parcel. Isotopic composition of anthropogenic SO_2 in these areas ranges from -5 to 10‰ (Krouse et al., 1991; Jedrysek et al., 2002; Jezierski et al., 2006; Derda et al., 2007), thus it would reduce the $\delta^{34}S$ of SO_2 from the expected values relative to sulfuric acid gas, resulting in the larger-than-expected observed differences between the two gases. Thus, although gas-phase sulfuric acid will have been produced by ·OH oxidation of SO_2 in all cases, the expected isotope fractionation between SO_2 and H_2SO_4 is only seen in FCE 7.1 due to recent addition of light sulfur in all other cases.

5.3.5 Isotopic composition of particulate sulfate

Sulfate is added to particles as they pass through the cloud: SO_2 is oxidised to sulfate in cloud droplets and added to the nucleating residual particles following evaporation, SO_2 may also be oxidised on the surface of interstitial particles, and sulfuric acid gas and ultrafine particulate may collide and coagulate with interstitial particles and cloud droplets. The change in the sulfur isotopic composition of particulate after passage through the cloud shows which sulfate sources dominate sulfate addition in the different

particle classes. This is very important to determine the effect of cloud processing on aerosol radiative forcing, as the sulfate sources and the sensitivity of radiative effects are not evenly distributed across all particles (see Section 5.1). The δ^{34}S of the sulfate that would be added from each source was calculated from the upwind isotopic composition of SO_2 or H_2SO_4. For SO_2 removal, the fractionation factors for SO_2 oxidation from Chapters 2 and 4 were used with the Rayleigh fractionation laws to account for depletion of the SO_2 reservoir (Mariotti et al., 1981; Krouse and Grinenko, 1991). The δ^{34}S values of the sulfate that would be added by each source are shown in Table 5.3, and will be compared to the isotopic changes observed in the particulate sulfate in the following sections, to determine the dominant process adding sulfate to each particle class and the amount of sulfate that must have been added to the particles to achieve isotope mass balance. The average composition of particulate matter from AMS measurements, shown in Figure 5.6, will be compared to the results obtained from the isotopic measurements.

Table 5.3: **δ^{34}S values (‰) of the potential sources of sulfate that could be contributed to particles during their passage through an orographic cloud**: SO_2 oxidation in the aqueous phase observed during the cloud (α_{cloud}), by H_2O_2 ($\alpha_{H_2O_2}$) and by transition metal catalysis (α_{TMcat}), SO_2 oxidation on the surface of Sahara dust with no aqueous phase (ie. on interstitial particles; α_{surf}), and condensation/coagulation of sulfuric acid gas and freshly nucleated particles (α_{cond}).

Source	**FCE 7.1**	**FCE 11.2**	**FCE 11.3**
SO_2 ox, α_{cloud}	56.8±7.2	-22.4±4.0	5.6±2.1
SO_2 ox, $\alpha_{H_2O_2}$	40.9±1.9	1.5±3.2	24.2±1.4
SO_2 ox, α_{TMcat}	22.4±1.9	-16.3±3.2	6.0±1.4
SO_2 ox, α_{surf}	39.0±1.3	-0.4±1.1	22.3±1.1
H_2SO_4, α_{cond}	37.3±5.0	54.8±5.6	44.8±4.5

δ^{34}S of particulate sulfate in the non-cloud event

Only fine particulate was measured for the non-cloud event, and only mixed droplets were found to have high enough S counts in the NanoSIMS for δ^{34}S measurements. The change in isotopic composition compared to possible sources of sulfate is shown in Figure 5.7b. Oxidation of SO_2 by H_2O_2 and condensation of H_2SO_4 are most likely both adding sulfate to the particles between the upwind and downwind stations; both of these sources would cause the observed enrichment in isotopic composition. The strong enrichment in

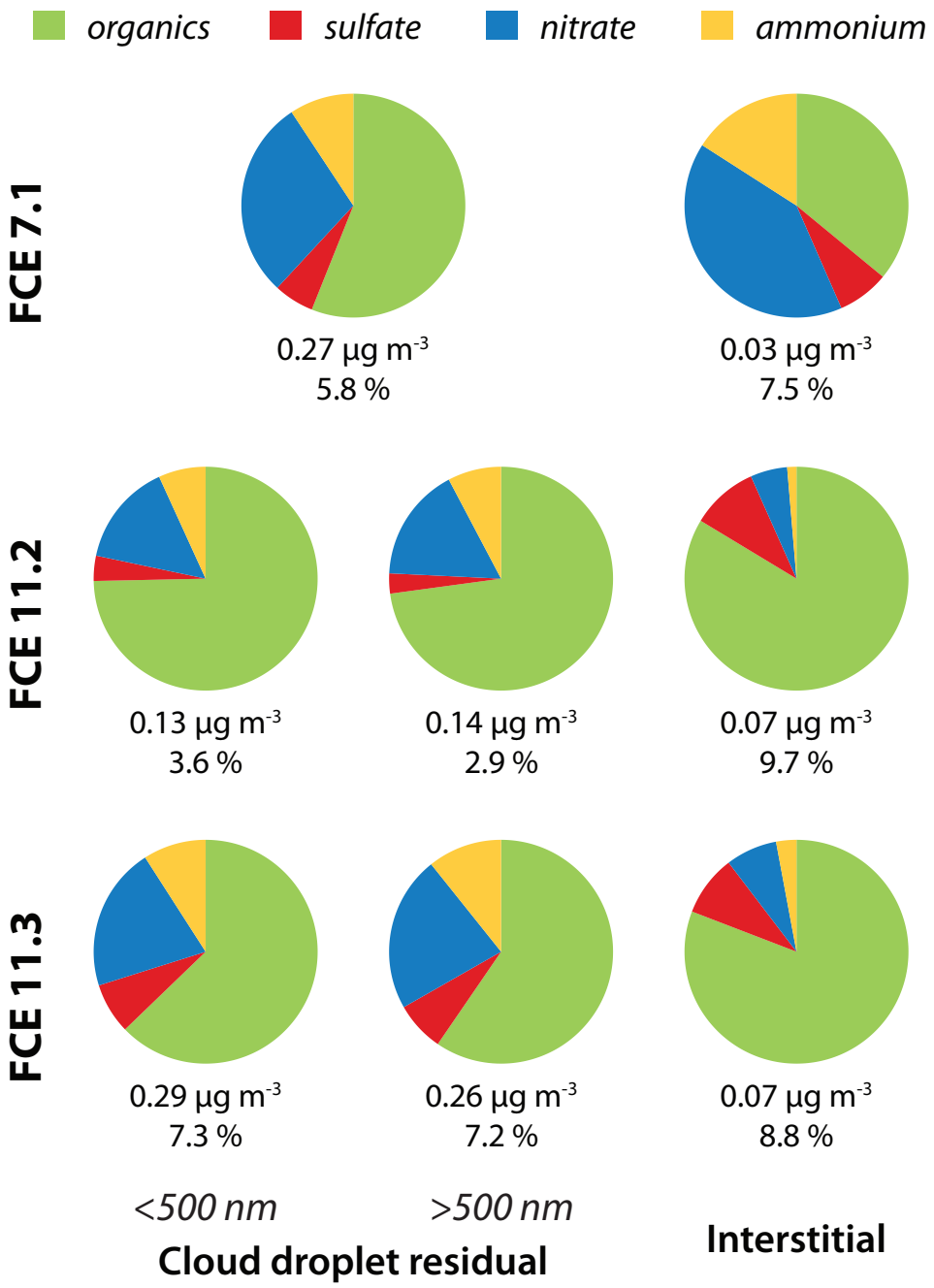

Figure 5.6: **Composition of particulate matter at Schmücke from AMS measurements**. Cloud droplet residual compositions are shown for fine (<500 nm) and coarse (>500 nm) fractions for FCE 11.2 and 11.3. The full measurement range is ∼60 nm to 1000 nm. The particulate sulfate concentration in μg m^{-3} and the percentage of particulate accounted for by sulfate is shown under each chart.

^{34}S shows that, despite the absence of a hill cap cloud, the surface sulfate concentration increased by >90% during the short time span of 25 minutes in the daytime.

Mixing of free tropospheric air contributes SO_2 during this event, however as ·OH concentrations are low in the free troposphere, sulfuric acid and ultrafine particulate are unlikely to be directly added and would instead only be produced in significant quantities once the air reached the boundary layer (Thornton et al., 1996). H_2O_2 and O_3 are often enriched in free tropospheric air (Bower et al., 1997; Liu and Seidl, 1998; Suhre et al., 2000) and could both be contributing to oxidation. SEM analysis of this filter showed that the mixed droplets contained high levels of inorganic compounds, and combined with the back trajectory which has fairly recently passed over the ocean this suggests the particles may also have relatively high alkalinity, facilitating oxidation by O_3. Sulfate produced from SO_2 oxidation by H_2O_2 or O_3 cannot be distinguished with sulfur isotope fractionation (Section 2.4.1), and measurements of $\Delta^{17}O$ would be need to confirm a role of O_3 in sulfate production (Savarino et al., 2000). The particulate isotopic composition from the non-cloud event shows that even in the absence of cloud, mixing of SO_2 and oxidant-rich free tropospheric air results in significant processing of particles by sulfate addition, from both condensing sulfuric acid and ultrafine particulate and in-situ oxidation of SO_2.

Mixed droplets and coated soot particles

Mixed droplets consist of secondary organic aerosol mixed with salt, and are the most numerous particles which take up significant sulfate in the cloud. Mixed droplets and coated soot particles >1 μm in diameter were only present on the cloud droplet residue filters; in the interstitial and at the valley sites these two types of particles were always <1 μm in size. Thus, size-resolved results are only presented for cloud droplet residual particles. The $\delta^{34}S$ of mixed droplets increased as the particles passed through the cloud in both FCE 11.2 and 11.3 (Figure 5.7c). The increase in $\delta^{34}S$ was significantly greater for fine than coarse mixed droplets during FCE 11.2, and slightly greater for fine mixed droplets during FCE 11.3. The sulfate fraction and the absolute amount of sulfate in the particulate was not significantly different depending on size (Figure 5.6), so relatively more sulfate was added to fine mixed droplets than to coarse mixed droplets.

The only sulfate source that could enrich fine mixed droplets in ^{34}S during FCE 11.2 is condensing sulfuric acid and coagulation of ultrafine particles; the latter will dominate as the event is at nighttime so the gas phase sulfuric acid concentration will be very low (Weber et al., 1997). If this is the only source of sulfate to the particles, the surface sulfate must increase by 40% to account for the change in isotopic composition. This

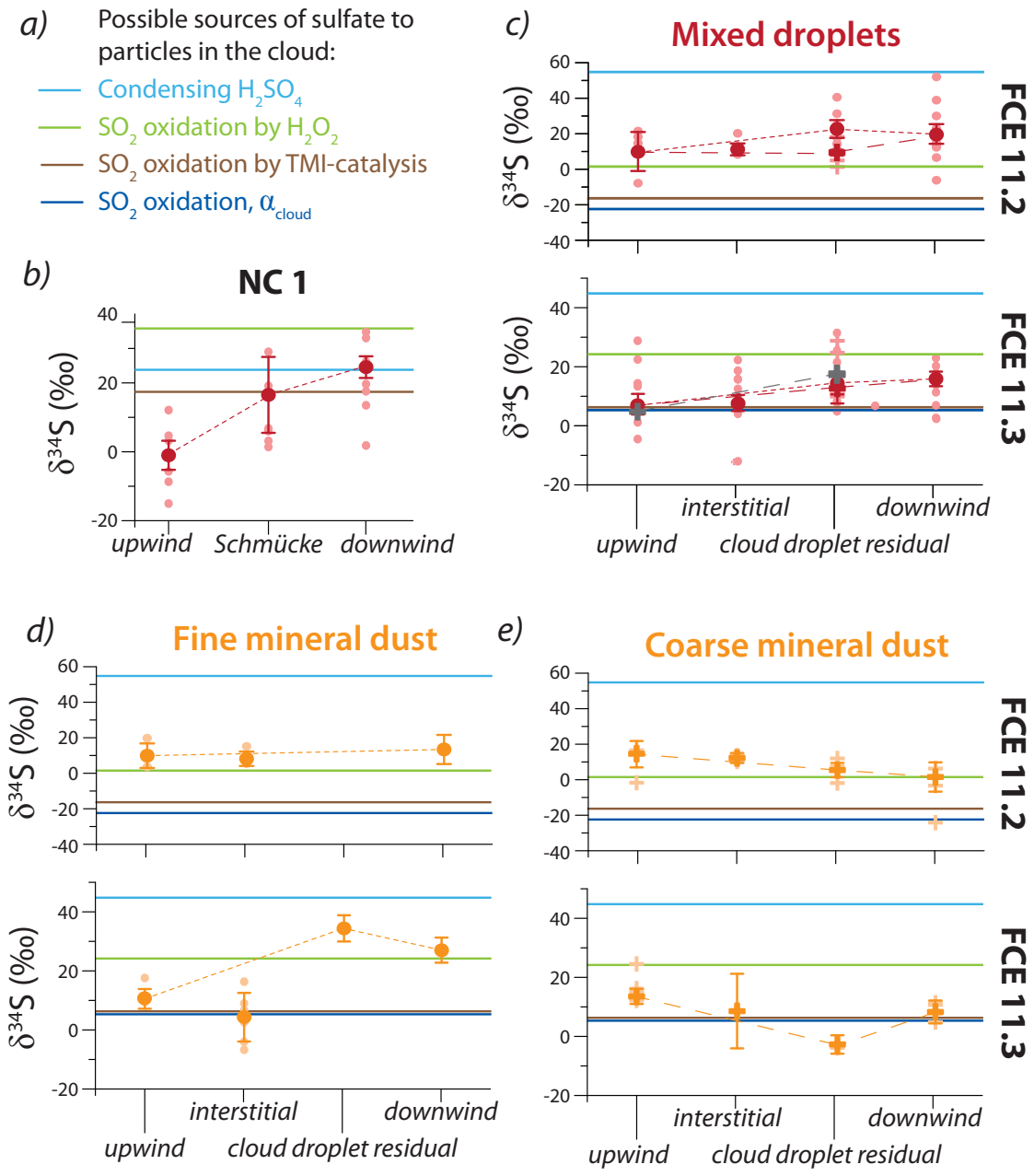

Figure 5.7: **Isotopic composition of particles measured during HCCT 2010**: *a)* legend, *b)* non-cloud event NC 1. From cloud events 11.2 and 11.3: *c)* mixed droplets (= SOA + salt), *d)* fine mineral dust, *e)* coarse mineral dust. Mixed droplets are shown in red and mineral dust in orange. In '*c)* Mixed droplets' for FCE 11.3 sulfur was also measured in coated soot particles, and these are shown in grey. Solid lines show the isotopic composition of sulfate that could added to particles in the cloud from different sources according to the legend in *a)*. Pale points show measurements for individual grains and dark points with error bars show the mean and the 1σ error. Dashed lines follow from upwind to in-cloud to downwind particles and show the change in δ^{34}S due to cloud processing; fine dashes with circle symbols show fine particulate and long dashes with cross symbols show coarse particulate.

represents a minimum sulfate addition as any other sulfate sources would change the isotopic composition in the opposite direction, requiring a larger addition from condensing H_2SO_4. During FCE 11.3 the increase in $\delta^{34}S$ could be due to either condensation of H_2SO_4 or in-situ oxidation of SO_2 by H_2O_2. Surface sulfate on mixed droplets increased by between 23 and 72% in this event. The concentration of H_2O_2 measured during FCE 11.3 was much higher than during FCE 11.2 (7.4 and 2.9 μM in cloud water respectively), explaining why sulfate addition from H_2O_2 oxidation of SO_2 (g) is more important during FCE 11.3 than FCE 11.2.

Mixed droplets on the coarse filter become slightly isotopically lighter as they pass through the cloud in FCE 11.2 (by -0.9±11.5‰) and heavier in FCE 11.3 (by +7.5±4.3‰) (Figure 5.7c). In both cases, this shows sulfate is being added to the particles from oxidation of SO_2 by H_2O_2 in the cloud droplets. This in-cloud reaction increases the surface sulfate by 10% and 100% in FCE 11.2 and 11.3 respectively, although for FCE 11.2 this value is quite uncertain, and for FCE 11.3 the addition could be lower if some sulfate was also added from H_2SO_4 (as low as 25% if all sulfate is from H_2SO_4). There was no significant change in H_2O_2 concentration with cloud droplet size seen in the different impactor stages of the cloud water collector.

Overall, H_2O_2 oxidation is more important in mixed droplets in the daytime due to higher H_2O_2 concentrations, but there is also variation due to particle size: H_2SO_4 and ultrafine particle condensation are more important for adding sulfate to smaller mixed droplets due to their higher surface area to volume ratio, while for larger mixed droplets the greater volume of aqueous phase means aqueous oxidation of SO_2 by H_2O_2 is comparatively more important. Comparison to AMS results showed that condensation and coagulation add more sulfate to fine particulate, relative to the initial amount of sulfate, than in-situ oxidation is able to add to coarse particulate. Thus, condensation and coagulation play a more important role than SO_2 oxidation in modifying the composition and size distribution of aerosol during passage through a cloud.

Soot particles with a coating only had a significant amount of sulfate on the coarse filter of FCE 11.3, the daytime event. The change in $\delta^{34}S$ shows the surface sulfate was increased by between 47 and 190% due to in-cloud sulfate production by condensing H_2SO_4 and ultrafine particulate and by H_2O_2 oxidation of SO_2, respectively. The change is not significantly different to what was seen in mixed droplets, thus the soot core does not influence the reaction, which proceeds in the coating as it would in a droplet. In FCE 11.2, the majority of coated soot remained in the interstitial phase. Activation to cloud droplets depended on the amount of soluble material (coating) associated with the soot

(Sinha et al., 2012a). In FCE 11.3 is appears that condensation of H_2SO_4 (g) during the daytime increases the hygroscopicity of the coated soot particles, facilitating activation and further sulfate addition through oxidation of SO_2 by H_2O_2. Similar behaviour was seen for fine mineral dust, discussed in the following section. Despite the significant effect H_2O_2 oxidation of SO_2 has had on the coarse mixed droplet and coated soot particles, the direction of isotopic change shows it is not the most important reaction for SO_2 removal in the cloud.

Comparing the cloud droplet residual and interstitial values with the downwind $\delta^{34}S$ can provide an estimate of i) sulfate addition to the interstitial particles during passage through the cloud, and ii) the proportion of sulfur in the interstitial phase compared to CCN-active particles. Sulfate can be added to interstitial particles from surface oxidation reactions, and from condensing and coagulating sulfuric acid and ultrafine particulate. Sulfate addition from these pathways would significantly alter the isotopic composition of the interstitial particles. This is not observed, hence sulfate mass addition to interstitial particles during passage through the cloud appears to be minor. The isotopic compositions in-cloud and downwind are not significantly different for the daytime or the nighttime event, whereas the interstitial $\delta^{34}S$ is lower, thus very little mixed-droplet sulfur was present in the interstitial phase. This shows efficient activation of sulfate-containing mixed droplets, consistent with the results from SEM analysis (Sinha et al., 2012a) and with AMS results.

Mineral dust

During FCE 11.2, no mineral dust was found on the cloud droplet residual fine filter, so it is likely that fine mineral dust was unable to act as a cloud condensation nucleus due to its hydrophobic nature (Kaaden et al., 2009). During FCE 11.3, single particle scanning electron microscopy showed that 70%-80% of mineral dust particles in the 400-1000 nm size range acted as a cloud condensation nucleus (Sinha et al., 2012a). Based on the decrease in $\delta^{34}S$ downwind as interstitial and cloud droplet residual particles are re-mixed, we estimate ∼30% of the sulfur in fine mineral dust remains in the interstitial phase as it passes through the cloud in the daytime, in contrast to all fine mineral dust sulfur being in the interstitial phase at night, which agrees well with the SEM observations. Two pathways could add sulfate to interstitial aerosol: condensation of sulfuric acid gas and coagulation of ultrafine particulate, and surface oxidation of SO_2. In FCE 11.2 oxidation directly on the dust surface would produce sulfate with an isotopic composition of $\delta^{34}S$ = -0.4±1.1‰, which is significantly lower than the $\delta^{34}S$ of the sulfate in the

dust (8.9±4.0‰), while condensation of sulfuric acid would produce very heavy sulfate ($\delta^{34}S = 54.8\pm5.6$‰). In FCE 11.3 surface oxidation and condensation would both produce sulfate that is significantly heavier ($\delta^{34}S = 22.3\pm1.1$ and 44.8 ± 4.5‰ respectively) than the interstitial aerosol ($\delta^{34}S = 4.4\pm8.3$‰). In both FCE 11.2 and 11.3, there is no significant difference in $\delta^{34}S$ between the upwind and interstitial particles (Figure 5.7d), thus no significant sulfate is added to fine-filter mineral dust as it passes through the cloud as interstitial aerosol.

In contrast, there is a large change in the $\delta^{34}S$ of sulfate in cloud droplet residual and downwind fine mineral dust in the daytime event FCE 11.3 (Figure 5.7d). The fine dust was able to act as CCN in this event, and the change to such high $\delta^{34}S$ values shows the importance of condensing sulfuric acid gas on to the cloud droplet for sulfate addition to fine mineral dust. The surface sulfate in these particles increased by >200%. [H_2SO_4] (g) is much higher in the daytime than at night because it is produced by ·OH radicals, which explains why condensation is unimportant in FCE 11.2. Thus, higher sulfuric acid concentrations in the daytime leads to sulfate addition on to fine mineral dust, increasing its hygroscopicity. This in turn increases its CCN activity, facilitating further uptake of H_2SO_4 (g) due to the higher surface area of a cloud droplet compared to the surface area of the particle serving as CCN.

During both FCE 11.2 and 11.3 the $\delta^{34}S$ of mineral dust on the coarse filter decreases as it passes through the cloud, by -8.9±8.5‰ and -16.3±4.0‰ respectively (Figure 5.7e). This can only be accounted for by sulfate addition from oxidation of SO_2 by transition metal catalysis; oxidation by H_2O_2 in FCE 11.2 would require an increase in sulfate of >400% and in FCE 11.3 no other source could add such isotopically light sulfate. SO_2 oxidation by transition metal catalysis increases the surface sulfate on the coarse mineral dust particles by >40-60% in both events. Considering both the number of particles found as droplet residue and on the interstitial filters, and the downwind isotopic composition, in both events the majority of sulfate addition to coarse mode mineral dust takes place inside cloud droplets and not in the interstitial phase. Coarse mineral dust is the only particle type where sulfate addition introduces an isotopic fractionation consistent with the major SO_2 removal process, i.e., causing the residual SO_2 to be enriched in ^{34}S. Thus, oxidation by the transition metal ion catalysis pathway in cloud droplets formed on coarse mineral dust particles dominates SO_2 uptake and oxidation in the measured events.

5.4 Discussion

5.4.1 The sulfur cycle in orographic clouds at Schmücke

The sulfur cycle observed during the HCCT campaign was complex, with different reactions responsible for adding sulfate to the different classes of particulate as they passed through the cloud. The sulfur cycles during the three cloud events are summarised in Figure 5.8. SO_2 gas became significantly enriched in ^{34}S following passage through the cloud in one nighttime event (FCE 11.2) and one daytime event (11.3), whereas during the other nighttime event (FCE 7.1), SO_2 gas became depleted in ^{34}S. Transition metal catalysis is the only known in-cloud oxidation pathway to favour the light isotope, thus the observations show that during FCE 11.2 and 11.3 the dominant SO_2 removal process was oxidation by transition metal ions, while during FCE 7.1 it was oxidation by H_2O_2.

Examining the isotopic changes in the particulate sulfur during FCE 11.2 and 11.3 provided further insight into in-cloud SO_2 oxidation and cloud processing of the particle spectrum. Fine and coarse mixed droplets showed a shift in the dominant sulfate source added in the cloud from condensing H_2SO_4 to H_2O_2 oxidation with increasing size, which was related to surface area to volume ratio rather than size-dependent changes in H_2O_2 concentration; in the daytime H_2O_2 oxidation was overall more important than at night due to higher daytime H_2O_2 concentrations. The same behaviour was seen in coarse coated soot particles in FCE 11.3. Fine mineral dust particles were able to act as CCN in the daytime as they had taken up H_2SO_4 (g) before the cloud, and as they passed through the cloud the increased surface area following activation lead to further H_2SO_4 (g) uptake, increasing hygroscopicity and thus facilitating CCN activity in subsequent clouds. At night they were unable to act as CCN and did not gain sulfur between the upwind and downwind stations. Although the surface sulfur in activated mixed droplets, coated soot and fine mineral dust increased by 40 to >200% as they passed through the cloud, the direction of the observed isotopic changes meant that none of these particle classes could account for the dominant loss of SO_2 (g).

In contrast, coarse mineral dust became enriched in ^{32}S as it passed through the cloud, consistent with isotope fractionation during SO_2 removal. Transition metal ions from mineral dust leachate cause very fast oxidation of SO_2 (Tilly et al. 1991; Rani et al. 1992, Chapter 4), so the observation that the major SO_2 removal pathway occurs on mineral dust rather than on the other particle types supports the hypothesis that transition metal catalysis is the major SO_2 oxidation pathway in the cloud. The efficiency of oxidation by this pathway means that, despite the relatively low number concentration of these

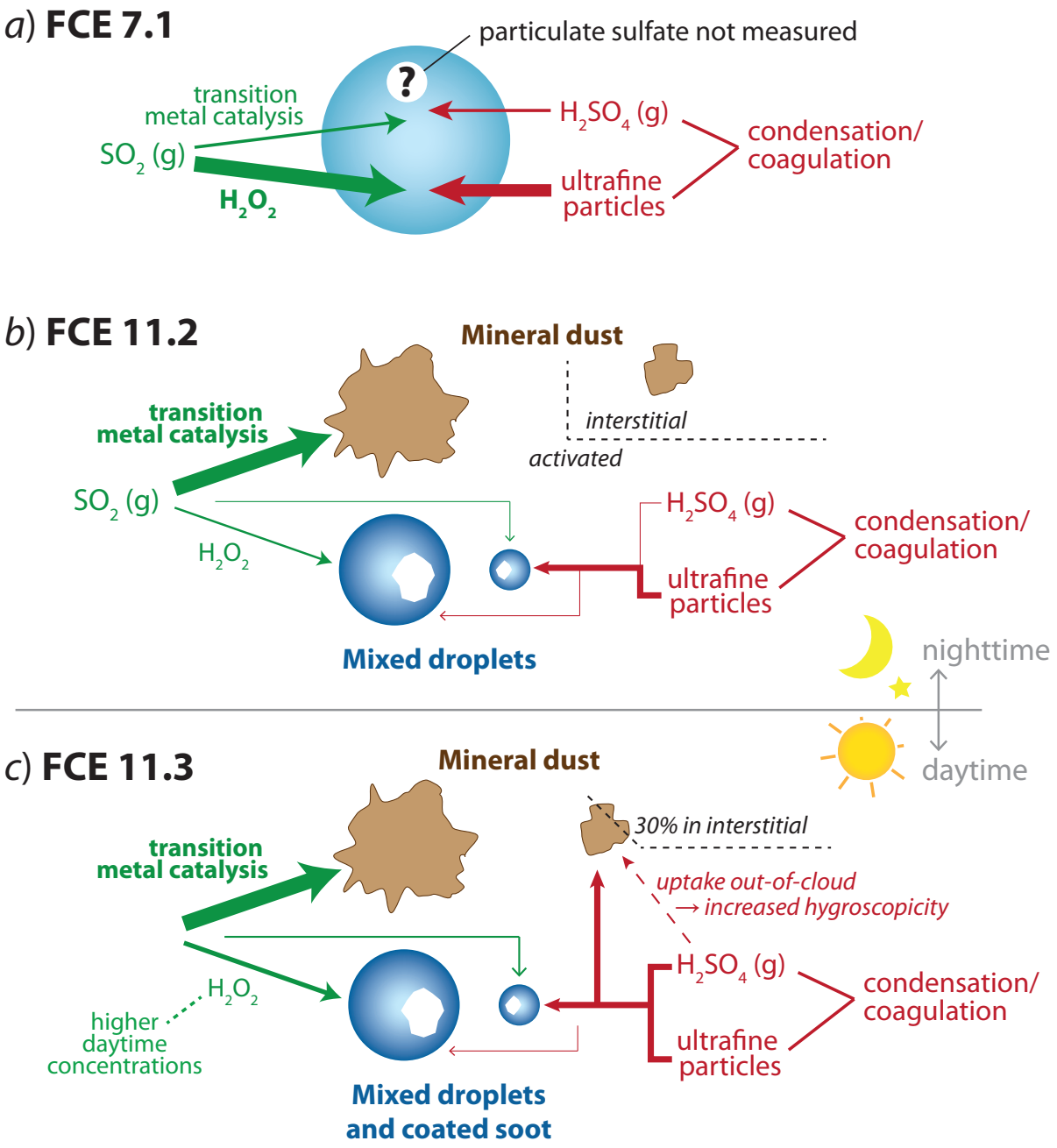

Figure 5.8: **Summary of the sulfur cycle occurring in clouds during three measurements periods** at Schmücke during the HCCT campaign. The thickness of the arrows shows the relative strength of the flux. The particulate sulfur isotopic composition was not measured for FCE 7.1 due to equipment problems.

particles compared to, for example, mixed droplets, they are able to account for the majority of in-cloud SO_2 oxidation at Schmücke.

Physical and chemical parameters measured during the cloud events were investigated to explain the different oxidation regimes in FCE 11.2 and 11.3 compared to FCE 7.1. FCE 11.2 and 11.3 had a higher liquid water content than FCE 7.1 (0.14 g m^{-3} for FCE 7.1 compared to 0.37 and 0.32 g m^{-3} for FCE 11.2 and 11.3 respectively), while temperature, wind direction, and other meteorological parameters were similar. The SO_2 concentration was higher in FCE 11.2 and 11.3 than FCE 7.1, and the back trajectories in the former two events showed more recent contact with pollution sources. Physical parameters describing the particles such as number concentration, volume and surface area density, and mean size were measured with FSSP and did not differ greatly between the three events. Chemical parameters which show some significant variation between the three events are shown in Figure 5.9. The nitrate content of particulate was much higher in FCE 7.1 than FCE 11.2 and 11.3 (Figure 5.6), however cloud water pH did not vary significantly, thus pH is not shown in Figure 5.9 although several sulfate production pathways are strongly pH dependent (Section 3.1). Organic compounds such as oxalate can complex with transition metals, reducing their efficiency as catalysts for SO_2 oxidation (Zuo and Zhan, 2005). The bulk organic concentration was similar in all three events, and the air parcels passed over the same area of forest directly preceeding the events, so there is no evidence that this affected the sulfur cycle at HCCT. The only chemical parameter which is significantly different for FCE 7.1 compared to FCE 11.2 and 11.3 is the particulate NH_3. An increase in particulate NH_3 could buffer cloud droplets, allowing more oxidation by O_3. However, as discussed in Section 5.3.2, the observed steady removal rate of SO_2 means it is very unlikely that O_3 is significantly contributing to SO_2 oxidation. Thus, the only physical and chemical parameters that may be able to explain the differing oxidation regimes are the liquid water content and the back trajectory.

The transition metal ion concentrations measured during the three events, shown in Figure 5.10, can provide further insight into the different oxidation regimes. There are some noticeable differences in the transition metal ion concentrations between the three events. Ni, Mn and Cu decrease in concentration in the order FCE 7.1 > FCE 11.2 > FCE 11.3. The relative concentration of Fe compared to Ni, Cu and Mn is quite different in FCE 7.1 compared to FCE 11.2 and 11.3, suggesting that the transition metal ions have a different source in FCE 7.1. This is most likely related to the lower liquid water content in FCE 7.1, which will have caused certain particle classes not to activate in this event. In FCE 11.2, the concentration of Fe^{2+} decreases strongly in the first hour. This

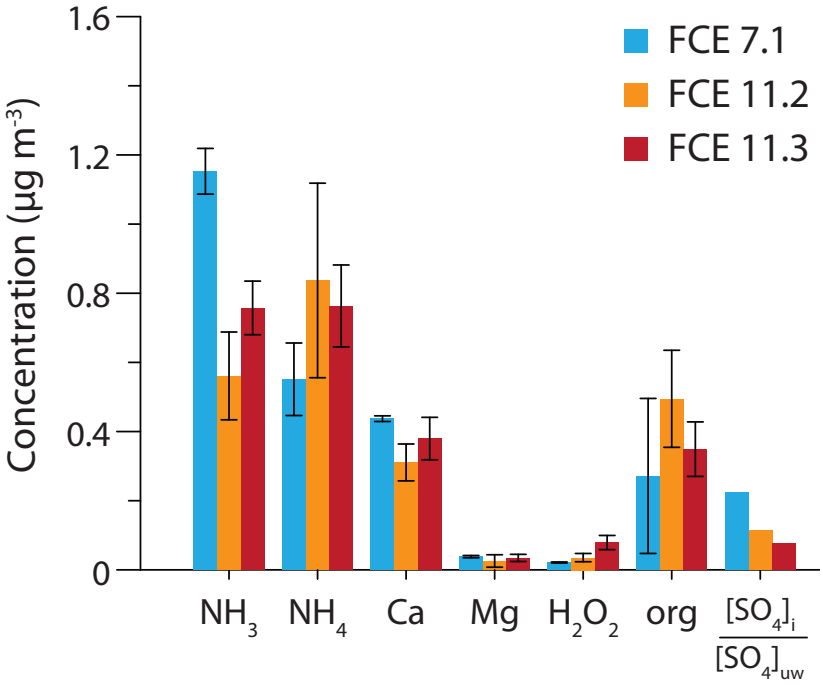

Figure 5.9: **Concentrations of various compounds measured during HCCT 2010**. NH_3, NH_4, Ca and Mg were measured in the particulate phase at the upwind station with MARGA, H_2O_2 was measured in cloud water by fluorospectrophotometry, 'org' is the organic particulate phase measured by AMS and $[SO_4]_i/[SO_4]_{uw}$ is the ratio of the sulfate concentration in the interstitial phase at Schmücke to the total upwind particulate sulfate, measured with MARGA.

is consistent with SO_2 oxidation: Tilly et al. (1991) observed that during SO_2 oxidation, Fe^{2+} is completely oxidised in the initial stages of the reaction, following which the SO_2 oxidation rate greatly increases. $[Fe^{2+}]$ is low in FCE 7.1 and below the detection limit during FCE 11.3. During FCE 11.2 and 11.3, $[Fe^{3+}]$ is initially high and decreases through the event, but this behaviour is not seen in FCE 7.1. This is consistent with Fe^{3+} being strongly involved in the SO_2 oxidation reaction in FCE 11.2 and 11.3 but not in FCE 7.1. Unfortunately, the concentrations of other transition metals such as Cr and V, which can participate in SO_2 oxidation and even at very low concentrations increase the rate of oxidation in mixtures so that it is much greater than the sum of the individual rates (Tilly et al. 1991; Rani et al. 1992, Chapter 4), were not measured during HCCT.

Strong interactions between different transition metals greatly increase the SO_2 oxidation rate (Tilly et al. 1991; Rani et al. 1992, Chapter 4), which means that the suite of transition metals present, rather than the concentrations of individual major species, de-

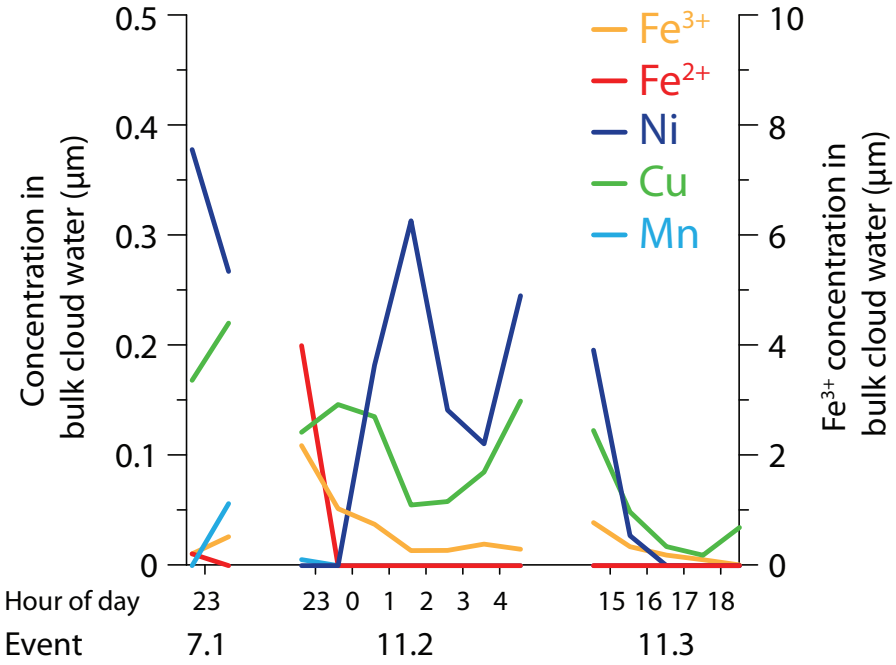

Figure 5.10: **Concentrations of transition metal ions measured in cloud water during HCCT 2010**. All concentrations except for Fe^{3+} are shown on the left-hand axis; the concentration of Fe^{3+} is shown on the right-hand axis.

termines the SO_2 oxidation rate in cloud droplets. In FCE 11.2 and 11.3 transition metals derived from mineral dust provided a TMI mixture that could strongly oxidise SO_2, which is evident from both the $\delta^{34}S$ observations and the measurements of $[Fe^{2+}]$ and $[Fe^{3+}]$. During FCE 7.1 coarse mineral dust was not the major TMI source. Unprocessed mineral dust is very hydrophobic (Kaaden et al., 2009), and fine mineral dust was not able to be activated in FCE 11.2, so the low liquid water content in FCE 7.1 is the most likely cause for the differing oxidation regimes. This is consistent with results of Kasper-Giebl et al. (2000), which showed that the scavenging efficiency of aerosol sulfate increases with liquid water content until $\sim$0.3 g m^{-3}, thus in FCE 11.2 and 11.3 the large majority of aerosol sulfate would be activated while in FCE 7.1 activation would be selective.

In summary, high liquid water content in FCE 11.2 and 11.3 meant mineral dust particles were activated to cloud droplets, and they released transition metal ions to form a solution that efficiently oxidised SO_2. In FCE 7.1 these particles were not activated due to low liquid water content, and the suite of transition metal ions present from other sources was not able to oxidise SO_2 with the same high efficiency, meaning that oxidation by H_2O_2 was the major SO_2 removal pathway.

5.4.2 Comparison to previous studies

The isotopic measurements made during the HCCT campaign showed that in two of three measured cloud events, transition metal-catalysed oxidation was the most important pathway for in-cloud SO_2 removal. This result is unexpected, as previous measurements and models have predicted H_2O_2 to be the most important in-cloud oxidant for SO_2 during orographic cloud experiments (eg. Bower et al. 1997; Bradbury et al. 1999; Suhre et al. 2000). Although Bradbury et al. (1999) found good agreement between observations and model results which predicted a dominance of H_2O_2 oxidation, SO_2 was completely oxidised thus the model results were not sensitive to the identity and rate of the dominant oxidation pathway. A number of similar studies have not been able to recreate the observed sulfur cycle in cloud experiments: Hegg et al. (2004) consistently underpredicted sulfate production compared to observations during the CARMA-1 study with a model that only considered oxidation by H_2O_2 and O_3, and Redington et al. (2009) required a fixed cloud water pH of 5.8 to match model results and observations, which is much higher than typical pH measurements (Laj et al., 1997a; Kreidenweis et al., 2003). These results suggest a pH-independent oxidation pathway - such as transition metal-catalysed oxidation (Seinfeld and Pandis, 1998) - is missing from or underestimated in models.

The rate of the transition metal-catalysed oxidation pathway is not well-characterised as it depends strongly on the combination of transition metals present and interactions between the different species (Tilly et al., 1991; Rani et al., 1992). The concentrations of transition metal ions measured in the cloud water during HCCT were not particularly high (see Herrmann et al. (2000) and references therein), and the presence of mineral dust in air masses is common, so the dominance of transition metal-catalysed oxidation observed in this study could be widespread among clouds with sufficiently high liquid water content to activate mineral dust. The reactive uptake coefficient γ_{obs} for SO_2 uptake and oxidation by different pathways in the cloud can be estimated according to (Jayne et al., 1990):

$$\gamma_{\mathrm{obs}} = \frac{4F_g}{\bar{c}A}\frac{\Delta n}{n} \tag{5.8}$$

F_g is the carrier gas flow rate ($cm^2\ s^{-1}$), $\bar{c}$ is the mean thermal velocity ($cm\ s^{-1}$; $\sqrt{\frac{3k_B T}{m}}$), A is the total droplet surface area (cm^2) and $\frac{\Delta n}{n}$ is the reduction in gas concentration. To adapt this equation to the observations during HCCT, the cloud was conceptualised as a flow reactor: the wind speed was the flow rate, the droplet surface area for different droplets types was estimated from the number concentration and the mean droplet radius for the event, and the maximum value of γ_{obs} was calculated as if SO_2 oxidation was only occurring on the particle type of interest. The values of γ_{obs} are shown in Table 5.4.

Table 5.4: **Reactive uptake coefficients for $SO_2 \rightarrow\rightarrow SO_4^{2-}$ in cloud droplets during HCCT 2010**. '% oxidised' refers to the proportion of SO_2 (g) taken up by the particle that goes on to be oxidised with an accommodation coefficient of $\alpha = 0.11$ (Sander et al., 1995). It was not possible to calculate γ_{obs} for FCE 7.1 as equipment problems meant particulate was not collected.

		FCE 11.2		**FCE 11.3**	
	Oxidant	γ_{obs}	% oxidised	γ_{obs}	% oxidised
Mineral dust	TMI catalysis	0.11±0.05	100	0.02±0.01	16
Mixed droplets	H_2O_2	$1.0\pm0.4\times10^{-5}$	0.009	$0.4\pm0.2\times10^{-5}$	0.004
Ratio (TMI/H_2O_2)		12000		4300	

The gas phase diffusion rates and accommodation coefficients for SO_2 in both oxidation reactions will be the same, thus the values show that at HCCT the rate of SO_2 oxidation by transition metal ion catalysis in cloud droplets formed on coarse mineral dust was >4000 times faster than oxidation by H_2O_2 on mixed droplets. During FCE 11.2, transition metal catalysed oxidation was so efficient that the reactive uptake coefficient was equal to the accommodation coefficient, i.e. all SO_2 being taken up by the particle was oxidised before it could repartition into the gas phase. In the commonly-used cloud chemistry regime of Sander et al. (1995), the transition metal-catalysed oxidation pathway is approximated by iron-catalysed oxidation. The rate of reaction of Fe^{3+} with HSO_3^- is >1000 times slower than the reaction of H_2O_2 with HSO_3^- in the model, with the exact ratio depending on pH. Thus, compared to our results, approximating the transition metal-catalysed oxidation pathway with the iron-catalysed pathway results in an underestimation of the rate of transition metal iron-catalysed oxidation by >>1000 times. This is consistent with laboratory studies considering the relative rates: Tilly et al. (1991) and Rani et al. (1992) observed strong synergistic effects on the rate of SO_2 oxidation in mixtures of transition metal ions, and in Section 4.4.1, the rate of SO_2 oxidation in mineral dust leachate was observed to be >100 times faster than in pure Fe salt solution.

Measurements of $\delta^{34}S$ from previous studies can provide an estimate of the importance of transition metal catalysed oxidation to compare with the rate of the reaction estimated in this study (Table 5.5). A number of studies have measured the $\delta^{34}S$ of SO_2 and sulfate simultaneously in the environment, and the average measured difference in $\delta^{34}S$ between SO_2 and product sulfate is -0.3±2.2‰ in rural environments (Mayer et al., 1995; Saltzman et al., 1983) and 4.6±2.5‰ in urban environments (Krouse et al., 1991; Torfs et al., 1997; Novak et al., 2001). No studies at coastal sites were considered in this analysis. Sofen et al. (2011) modelled the partitioning between SO_2 oxidation pathways for the pre-industrial period, and these values were used to calculate a baseline difference between $\delta^{34}S$ of SO_2 and sulfate to compare with measurements, as shown in Table 5.5. This comparison shows that the model underestimates transition metal catalysed oxidation by 1% in urban and 58% in rural environments, and suggests the pathway is significantly more important in rural than in urban environments. This is consistent with the large underestimation in modelled rates of transition metal-catalysed oxidation compared to the rate seen during the rural measurements at HCCT. The underestimation may be less important in the urban environment where mineral dust contributes a smaller proportion of the total transition metal ions (Kumar et al., 2010) and concentrations of O_3 and H_2O_2 are much higher. The comparison can only provide as estimate of the importance of the

Table 5.5: **Increase in transition metal catalysed oxidation of SO_2 from global baseline industrial-period model (Sofen et al., 2011) required to account for measured differences in $\delta^{34}S$ of SO_2 gas and product sulfate in urban and rural environments**.

	Sofen et al. (2011)	**Urban**	**Rural**
$f(OH)$	0.27	0.27	0.08
$f(H_2O_2)$	0.5	0.5	0.15
$f(O_3)$	0.05	0.05	0.015
$f(O_2$, TMI-catalysed)	0.18	0.18	0.76
$\delta^{34}S_{SO_4} - \delta^{34}S_{SO_2}$, model (‰)	4.7	4.6	-0.3
$\delta^{34}S_{SO_4} - \delta^{34}S_{SO_2}$, measurements (‰)		4.6±2.5	-0.3±2.2
Increase in TMI pathway	-	1%	58%

various pathways as the measurements are not seasonally and globally representative; the results are most relevant to the USA and Europe where the majority of the measurements were made.

Alexander et al. (2009) and Sofen et al. (2011) have recently shown from $\Delta^{17}O$ measurements and model results that transition metal-catalysed oxidation of SO_2 is of global importance, in agreement with the results of the present study. However, although these studies found that an increased rate of transition metal-catalysed oxidation was able to improve modelling of SO_2 concentrations, particularly in continental Europe, it resulted in a strong overprediction of atmospheric sulfate concentrations (Alexander et al., 2009; Barrie et al., 2001). The results of this study show that sulfate formed by transition metal-catalysed oxidation is concentrated on coarse aerosols, which would result in relatively fast removal of the sulfate from the atmosphere, meaning that transition metal-catalysed oxidation of SO_2 could indeed explain discrepancies between modelled and observed concentrations of SO_2 and sulfate.

The results of this study have important implications for the role of in-cloud sulfate production in the modification of the aerosol size distribution. When H_2O_2 is the dominant oxidant for SO_2, sulfate mass from SO_2 oxidation is modelled to be added early in the cloud, as H_2O_2 is quickly exhausted (Bower and Choularton, 1993; Bower et al., 1997). This means the sulfate mass is added primarily to the most CCN-active particles which are activated earliest in the cloud, and a high degree of supersaturation is needed early in the cloud to have a significant effect on the smallest, least efficient CCN (Bower et al., 1997). In contrast, transition metal-catalysed oxidation will proceed throughout the cloud,

consistent with the observed SO_2 concentrations (see Section 5.3.1). Thus, SO_2 oxidation is able to add sulfate mass to particles throughout the cloud: it is not only important for those particles activated earliest in the cloud. The particulate isotope measurements show, however, that condensation of H_2SO_4 gas and coagulation of ultrafine particulate is the dominant process adding sulfate mass to the smallest and least hygroscopic CCN - the fine mineral dust particles and fine mixed droplets. Therefore, condensation and coagulation of H_2SO_4 gas and ultrafine particulate in the cloud, rather than SO_2 oxidation, is the most important in-cloud sulfate addition process for modifying CCN activity and thus determining the strength of the indirect aerosol effect, while both pathways can be important, depending on the upwind aerosol population, in affecting the magnitude of direct aerosol cooling.

5.5 Conclusions

This study measured the isotopic composition of SO_2 and H_2SO_4 gas and sulfate in particulate as an air parcel passed through an orographic cloud. Unexpectedly, the most important in-cloud oxidation pathway for SO_2 was transition metal catalysis, which is isotopically distinctive as it favours the light isotope in the product sulfate (Section 4.4.2). SO_2 oxidation by transition metal catalysis was most important for in-cloud sulfate addition to coarse mineral dust particles, meaning that the sulfate produced from in-cloud SO_2 oxidation will be removed relatively quickly from the atmosphere. Uptake of gas-phase sulfate and ultrafine particulate were the dominant processes affecting fine mixed droplets and fine mineral dust particles, which were the least efficient CCN present. Thus, gas-phase sulfate is the most important in-cloud sulfate source for determining the downwind CCN number concentration and consequently the magnitude of indirect aerosol radiative forcing. The results demonstrate the potential of sulfur isotope measurements for investigating SO_2 oxidation, particularly when single-particle isotope ratios are measured in the NanoSIMS. Incorporating the findings of this study into models will result in a much more accurate depiction of both the continental sulfur cycle and the effect of cloud processing on direct and indirect radiative forcing.

Acknowledgements

We thank Elmar Gröner for his support with the NanoSIMS analyses, Joachim Huth for his help with the SEM/EDX analyses, Damien Amédro and Coralie Schoemaecker for

FAGE data from Goldlauter, and all the participants of HCCT for an interesting and successful campaign. This research was funded by the Max Planck Society and the Max Planck Graduate Centre.

Chapter 6

Conclusion: Main findings and outlook

The aim of this thesis was to measure isotopic fractionation during the major oxidation pathways of SO_2, in order to improve understanding of sulfate formation and the atmospheric sulfur cycle. In Chapter 2, the fractionation factors for the major atmospheric oxidation pathways were presented. Fractionation in the aqueous phase by H_2O_2 and O_3 agreed well with previous results for the uptake of SO_2 in solution. These were the first results to consider the role of the terminating oxidant, and show that the terminating oxidation step does not significantly affect the isotopic fractionation. The fractionation factors for oxidation in the gas phase by ·OH radicals and in the aqueous phase by a radical chain reaction initiated by Fe^{3+}, which have not previously been measured, are now well-constrained. The radical chain reaction is the only pathway to produce sulfate depleted in ^{34}S compared to the reactant SO_2, thus sulfur isotopes will be particularly useful to constrain the importance of this pathway.

In the third chapter, SO_2 oxidation in the marine boundary layer was examined. No study has previously considered sulfur isotope fractionation factors for marine boundary layer reactions. The pH dependence of isotopic fractionation was measured, which allowed the fractionation factors for each individual step of the reaction SO_2 (g) $\rightarrow\rightarrow$ SO_3^{2-} (aq) to be determined. Measurements of isotopic fractionation factors for the major marine boundary layer oxidation pathways showed that sulfur isotopes are especially suited to distinguish between oxidation by O_3 and ·Cl catalysis, which only occur at high pH and are therefore limited by sea salt aerosol alkalinity, and oxidation by transition metal catalysis or hypohalous acids, which occur relatively independently of pH, as the former two pathways favour the heavy and the latter two the light isotope. Sulfur isotopes are

therefore ideal to quantify partitioning between alkalinity-limited and non-limited SO_2 oxidation pathways, which is critical to accurately model the extent and climatic effects of sulfate production in the marine boundary layer.

The oxidation of SO_2 on mineral dust was investigated in Chapter 4. Experiments considering oxidation in mineral dust leachate showed that isotopic fractionation during the transition metal catalysis pathway was the same for a complex mixture of transition metals as for the pure Fe solution tested in Chapter 2. However, oxidation in the leachate solution was several orders of magnitude faster than in the pure Fe solution. Oxidation on the mineral dust surface was examined with a multivariate analysis model and the results showed isotopic fractionation depended primarily on the mineral assemblage and not significantly on the experimental conditions. Overall, oxidation on the dust surface favours the heavy isotope, while oxidation in leachate favours the light isotope, thus sulfur isotope measurements will be very useful to distinguish between these oxidation mechanisms in the ambient environment. Although the aqueous pathway dominates overall, the surface oxidation pathway could have a significant regional impact on both climate and iron bioavailability, as high humidity is rarely encountered close to dust source regions.

The final chapter of this thesis describes the results of the Hill Cap Cloud Thuringia Campaign. The fractionation factors measured in the laboratory were used to understand the sulfur cycle as an air parcel passed through an orographic cloud. The results, which are the first field measurements using sulfur isotope fractionation to understand oxidation pathways, showed an unexpected dominance of the transition metal-catalysed oxidation pathway. This suggests the global importance of this pathway is far greater than currently accepted. The sulfate produced by this pathway was seen to be concentrated on coarse mineral dust particles, thus it will have a relatively small climate impact and be removed quickly from the atmosphere. An increased importance of this pathway would thus explain the tendency of models to strongly overpredict SO_2 while only weakly underpredicting sulfate concentrations.

Although SO_2 oxidation is thought to account for the mass majority of sulfate addition in clouds, the results from HCCT showed that oxidation adds sulfate primarily to large particles, which have a greater volume for reaction. Condensation and coagulation of gas-phase sulfate and ultrafine particulate are the primary sulfate sources to small particles, which have a greater surface area to volume ratio. Condensation and coagulation, and not in-situ SO_2 oxidation, will therefore dominate the climatic effect of cloud processing.

The fractionation factors presented in this thesis allow sulfur isotope measurements to be used to investigate SO_2 oxidation and sulfate production in the ambient environment.

The results from the HCCT campaign illustrate the level of information that can be gained from isotopic measurements. However, sulfur isotopes cannot be used to distinguish between, for example, oxidation by H_2O_2 and by O_3. Simultaneous measurements of both sulfur ($\delta^{34}S$) and oxygen ($\Delta^{17}O$) in future studies, in combination with isotopic modelling, may be able to provide a quantitative view of the whole sulfur cycle. A number of laboratory questions also remain. The influence of ionic strength, and of other chemical species such as nitrate, on isotopic fractionation is unknown. The mechanism of isotopic fractionation during oxidation on the mineral dust surface also remains open: studies considering oxidation on pure single minerals, and on other major dust types such as China Loess, would help to answer this question. The results of this thesis show the potential of sulfur isotope fractionation to improve our understanding of atmospheric SO_2 oxidation, and illustrate the importance of further field, laboratory, and modelling studies in this area.

List of Figures

List of Tables

Bibliography

Ackerman, A., Toon, O., Stevens, D., Heymsfield, A., Ramanathan, V., and Welton, E.: Reduction of tropical cloudiness by soot, Science, 288, 1042–1047, doi: 10.1126/science.288.5468.1042, 2000.

Adams, J. W., Rodriguez, D., and Cox, R. A.: The uptake of SO2 on Saharan dust: a flow tube study, Atmospheric Chemistry and Physics, 5, 2679–2689, 2005.

Al-Hosney, H. A. and Grassian, V. H.: Water, sulfur dioxide and nitric acid adsorption on calcium carbonate: A transmission and ATR-FTIR study, Physical Chemistry Chemical Physics, 7, 1266–1276, 2005.

Albrecht, B.: Aerosols, cloud microphysics, and fractional cloudiness, Science, 245, 1227–1230, 1989.

Alexander, B., Savarino, J., Barkov, N. I., Delmas, R. J., and Thiemens, M. H.: Climate driven changes in the oxidation pathways of atmospheric sulfur, Geophysical Research Letters, 29, 1685, doi:10.1029/2002GL014879, 2002.

Alexander, B., Thiemens, M. H., Farquhar, J., Kaufman, A. J., Savarino, J., and Delmas, R. J.: East Antarctic ice core sulfur isotope measurements over a complete glacial-interglacial cycle, Journal of Geophysical Research-Atmospheres, 108, D24, 4786, doi: 10.1029/2003JD003513, 2003.

Alexander, B., Park, R. J., Jacob, D. J., Li, Q. B., Yantosca, R. M., Savarino, J., Lee, C. C. W., and Thiemens, M. H.: Sulfate formation in sea-salt aerosols: Constraints from oxygen isotopes, Journal of Geophysical Research-Atmospheres, 110, D10 307, doi:10.1029/2004JD005659, 2005.

Alexander, B., Park, R. J., Jacob, D. J., and Gong, S. L.: Transition metal-catalyzed oxidation of atmospheric sulfur: Global implications for the sulfur budget, Journal of Geophysical Research-Atmospheres, 114, D02 309, doi:10.1029/2008JD010486, 2009.

Atkinson, R., Baulch, D. L., Cox, R. A., Crowley, J. N., Hampson, R. F., Hynes, R. G., Jenkin, M. E., Rossi, M. J., and Troe, J.: Evaluated kinetic and photochemical data for atmospheric chemistry: volume I - gas phase reactions of Ox, HOx, NOx, and SOx species., Atmospheric Chemistry and Physics, 4, 1461–1738, URL http://www.iupac-kinetic.ch.cam.ac.uk/, 2004.

Baker, A. R., Jickells, T. D., Witt, M., and Linge, K. L.: Trends in the solubility of iron, aluminium, manganese and phosphorus in aerosol collected over the Atlantic Ocean RID D-1233-2011 RID B-2210-2010 RID B-8095-2008, Marine Chemistry, 98, 43–58, doi:10.1016/j.marchem.2005.06.004, 2006.

Baroni, M., Thiemens, M. H., Delmas, R. J., and Savarino, J.: Mass-independent sulfur isotopic compositions in stratospheric volcanic eruptions, Science, 315, 84–87, doi: 10.1126/science.1131754, 2007.

Baroni, M., Savarino, J., Cole-Dai, J. H., Rai, V. K., and Thiemens, M. H.: Anomalous sulfur isotope compositions of volcanic sulfate over the last millennium in Antarctic ice cores, Journal of Geophysical Research-atmospheres, 113, D20 112, doi: 10.1029/2008JD010185, 2008.

Barrie, L. A., Yi, Y., Leaitch, W. R., Lohmann, U., Kasibhatla, P., Roelofs, G. J., Wilson, J., McGovern, F., Benkovitz, C., Melieres, M. A., Law, K., Prospero, J., Kritz, M., Bergmann, D., Bridgeman, C., Chin, M., Christensen, J., Easter, R., Feichter, J., Land, C., Jeuken, A., Kjellstrom, E., Koch, D., and Rasch, P.: A comparison of large-scale atmospheric sulphate aerosol models (COSAM): overview and highlights, Tellus Series B-Chemical and Physical Meteorology, 53, 615–645, 2001.

Benson, D. R., Young, L. H., Kameel, F. R., and Lee, S. H.: Laboratory-measured nucleation rates of sulfuric acid and water binary homogeneous nucleation from the SO2 + OH reaction, Geophysical Research Letters, 35, L11 801, doi:10.1029/2008GL033387, 2008.

Berglen, T., Berntsen, T., Isaksen, I., and Sundet, J.: A global model of the coupled sulfur/oxidant chemistry in the troposphere: The sulfur cycle, Journal of Geophysical Research, 109, D19 310, doi:10.1029/2003JD003948, 2004.

Berndt, T., Stratmann, F., Brasel, S., Heintzenberg, J., Laaksonen, A., and Kulmala, M.: SO2 oxidation products other than H2SO4 as a trigger of new particle formation. Part 1: Laboratory investigations, Atmospheric Chemistry and Physics, 8, 6365–6374, 2008.

Berresheim, H., Elste, T., Tremmel, H. G., Allen, A. G., Hansson, H. C., Rosman, K., Dal Maso, M., Makela, J. M., Kulmala, M., and O'Dowd, C. D.: Gas-aerosol relationships of H_2SO_4, MSA, and OH: Observations in the coastal marine boundary layer at Mace Head, Ireland, Journal of Geophysical Research-atmospheres, 107, D19, doi: 10.1029/2000JD000229, 2002.

Bevington, P. and Robinson, D.: Data Reduction and Error Analysis for the Physical Sciences, Mc-Graw Hill, 1992.

Bogumil, K., Orphal, J., Homann, T., Voigt, S., Spietz, P., Fleischmann, O. C., Vogel, A., Hartmann, M., Kromminga, H., Bovensmann, H., Frerick, J., and Burrows, J. P.: Measurements of molecular absorption spectra with the SCIAMACHY pre-flight model: Instrument characterization and reference data for atmospheric remote-sensing in the 230-2380 nm region, Journal of Photochemistry and Photobiology A: Chemistry, 157, 167–184, 2003.

Borowitz, J. and Klein, F.: Vapor Pressure Isotope Effects in Methanol, The Journal of Physical Chemistry, 75, 1815–1820, 1971.

Botha, C. F., Hahn, J., Pienaar, J. J., and Vaneldik, R.: Kinetics and mechanism of the oxidation of sulfur(IV) by ozone in aqueous solutions, Atmospheric Environment, 28, 3207–3212, 1994.

Boucher, O. and Lohmann, U.: The sulfate-CCN-cloud albedo effect: A sensitivity study with two general circulation models, Tellus, 47B, 281–300, 1995.

Bower, K. N. and Choularton, T. W.: Cloud processing of the Cloud Condensation Nucleus spectrum and its climatological consequences, Quarterly Journal of the Royal Meteorological Society, 119, 655–679, 1993.

Bower, K. N., Choularton, T. W., Gallagher, M. W., Colvile, R. N., Wells, M., Beswick, K. M., Wiedensohler, A., Hansson, H. C., Svenningsson, B., Swietlicki, E., Wendisch, M., Berner, A., Kruisz, C., Laj, P., Facchini, M. C., Fuzzi, S., Bizjak, M., Dollard, G., Jones, B., Acker, K., Wieprecht, W., Preiss, M., Sutton, M. A., Hargreaves, K. J., StoretonWest, R. L., Cape, J. N., and Arends, B. G.: Observations and modelling of the processing of aerosol by a hill cap cloud, Atmospheric Environment, 31, 2527–2543, 1997.

Bradbury, C., Bower, K. N., Choularton, T. W., Swietlicki, E., Birmili, W., Wiedensohler, A., Yuskiewicz, B. A., Berner, A., Dusek, U., Dore, C., and Mcfadyen, G.: Modelling

of aerosol modification resulting from passage through a hill cap cloud, Atmospheric Research, 50, 185–204, 1999.

Brueggemann, E., Gnauk, T., Mertes, S., Acker, K., Auel, R., Wieprecht, W., Moeller, D., Collett, J., Chang, H., Galgon, D., Chemnitzer, R., Rued, C., Junek, R., Wiedensohler, A., and Herrmann, H.: Schmuecke hill cap cloud and valley stations aerosol charaterisation during FEBUKO (I): Particle size distribution, mass, and main components, Atmospheric Environment, 39, 4291–4303, 2005.

Caffrey, P., Hoppel, W., Frick, G., Fitzgerald, J., Shantz, N., Leaitch, W. R., Pasternack, L., Albrechcinski, T., and Ambrusko, J.: Chamber measurements of CI depletion in cloud-processed sea-salt aerosol, Journal of Geophysical Research-atmospheres, 106, 27 635–27 645, doi:10.1029/2000JD000105, 2001.

Calhoun, J. A., Bates, T. S., and Charlson, R. J.: Sulfur Isotope Measurements of Submicrometer Sulfate Aerosol-Particles over the Pacific-Ocean, Geophysical Research Letters, 18, 1877–1880, 1991.

Cantrell, C. A., Zimmer, A., and Tyndall, G. S.: Absorption cross sections for water vapor from 183 to 193 nm, Geophysical Research Letters, 24, 2195–2198, 1997.

Caquineau, S., Gaudichet, A., Gomes, L., and Legrand, M.: Mineralogy of Saharan dust transported over northwestern tropical Atlantic Ocean in relation to source regions, Journal of Geophysical Research-atmospheres, 107, 4251, doi:10.1029/2000JD000247, 2002.

Caron, F., Tessier, A., Kramer, J. R., Schwarcz, H. P., and Rees, C. E.: Sulfur and oxygen isotopes of sulfate in precipitation and lakewater, Quebec, Canada, Applied Geochemistry, 1, 601–606, 1986.

Castleman, A. W., Munkelwitz, H. R., and Manowitz, B.: Isotopic Studies of Sulfur Component of Stratospheric Aerosol Layer, Tellus, 26, 222–234, 1974.

CEIP: Sulfur dioxide emission data, URL `http://www.ceip.at/ceip`, 2010.

Chameides, W. L. and Stelson, A. W.: Aqueous-Phase Chemical Processes in Deliquescent Sea-Salt Aerosols: A Mechanism That Couples the Atmospheric Cycles of S and Sea Salt, J. Geophys. Res., 97, 20 565–20 580, 1992.

Chin, M., Jacob, D. J., Gardner, G. M., ForemanFowler, M. S., Spiro, P. A., and Savoie, D. L.: A global three-dimensional model of tropospheric sulfate, Journal of Geophysical Research-Atmospheres, 101, 18 667–18 690, 1996.

Chin, M., Savoie, D. L., Huebert, B. J., Bandy, A. R., Thornton, D. C., Bates, T. S., Quinn, P. K., Saltzman, E. S., and De Bruyn, W. J.: Atmospheric sulfur cycle simulated in the global model GOCART: Comparison with field observations and regional budgets, Journal of Geophysical Research-atmospheres, 105, 24 689–24 712, doi: 10.1029/2000JD900385, 2000.

Chmielewski, A. G., Derda, M., Wierzchnicki, R., and Mikolajczuk, A.: Sulfur isotope effects for the SO2(g)-SO2(aq) system, Nukleonika, 47, S69–S70, 2002.

Cohen, S., Chang, S. G., Markowitz, S. S., and Novakov, T.: Role of fly ash in catalytic oxidation of sulfur(IV) slurries, Environmental Science & Technology, 15, 1498–1502, doi:10.1021/es00094a013, 1981.

Coude-Gaussen, G., Rognon, P., and Le Coustumer, M.: Incorporation progressive de poussieres sahariennes aux limons des Iles orientales du Cap Vert, Comptes Rendus de l'Academie des Sciences, 319, 1343–1349, 1994.

Crowley, J. N., Ammann, M., Cox, R., Hynes, R., Jenkin, M., Mellouki, A., Rossi, M., Troe, J., and Wallington, T.: Evaluated kinetic and photochemical data for atmospheric chemistry: Volume V - heterogeneous reactions on solid substrates, Atmos. Chem. Phys., 10, 9059–9223, 2010.

Cziczo, D. J., Froyd, K. D., Gallavardin, S. J., Moehler, O., Benz, S., Saathoff, H., and Murphy, D. M.: Deactivation of ice nuclei due to atmospherically relevant surface coatings, Environmental Research Letters, 4, 044 013, doi:10.1088/1748-9326/4/4/044013, 2009.

Denman, K.: Couplings between changes in the climate system and biogeochemistry in Climate Change 2007: The physical science basis. Contribution of the working group I to the Fourth Assessment Report of the Intergovernmental Panel on Climate Change., Cambridge University Press, New York, 2007.

Dentener, F. J., Carmichael, G. R., Zhang, Y., Lelieveld, J., and Crutzen, P. J.: Role of mineral aerosol as a reactive surface in the global troposphere, Journal of Geophysical Research-Atmospheres, 101, 22 869–22 889, 1996.

Derda, M., Chmielewski, A. G., and Licki, J.: Sulphur isotope compositions of components of coal and S-isotope fractionation during its combustion and flue gas desulphurization, Isotopes in Environmental and Health Studies, 43, 57–63, 2007.

Ding, T., Valkiers, S., Kipphardt, H., De Bievre, P., Taylor, P. D. P., Gonfiantini, R., and Krouse, R.: Calibrated sulfur isotope abundance ratios of three IAEA sulfur isotope reference materials and V-CDT with a reassessment of the atomic weight of sulfur, Geochimica Et Cosmochimica Acta, 65, 2433–2437, 2001.

Drake, N. A., Eckardt, F. D., and White, Kevin, H.: Sources of sulphur in gypsiferous sediments and crusts and pathways of gypsum redistribution in southern Tunisia, Earth Surface Processes and Landforms, 29, 1459–1471, doi:10.1002/esp.1133, 2004.

Egiazarov, A. C., Kaviladze, M., Kerner, M. N., Oziashvili, E. L., Ebralidze, A., and Esakiya, A. D.: Separation of Sulfur Isotopes by Chemical Exchange, Isotopenpraxis: Isotopes in Environmental and Health Studies, 7, 379–383, 1971.

Eisele, F. L., Lovejoy, E. R., Kosciuch, E., Moore, K. F., Mauldin, R. L., I., Smith, J. N., McMurry, P. H., and Iida, K.: Negative atmospheric ions and their potential role in ion-induced nucleation, J. Geophys. Res., 111, D04 305, doi:10.1029/2005JD006568, 2006.

Eriksen, T. E.: Sulfur Isotope Effects 1. Isotopic Exchange Coefficient for Sulfur Isotopes 34S-32S in System SO2(g)-HSO3(aq) at 25, 35, and 45 Degrees C, Acta Chemica Scandinavica, 26, 573–580, 1972a.

Eriksen, T. E.: Sulfur Isotope Effects 2. Isotopic Exchange Coefficients for Sulfur Isotopes 34S-32S in System SO2(g)-Aqueous Solutions of SO2, Acta Chemica Scandinavica, 26, 581, 1972b.

Eriksen, T. E.: Sulfur Isotope Effects 3. Enrichment of 34S by Chemical Exchange between SO2(g) and Aqueous Solutions of SO2, Acta Chemica Scandinavica, 26, 975, 1972c.

Eriksen, T. E.: Sulfur Isotope Effects 4. Sulfur Isotope Effects in Anion-Exchange Systems, Acta Chemica Scandinavica, 26, 980, 1972d.

Falkovich, A. H., Ganor, E., Levin, Z., Formenti, P., and Rudich, Y.: Chemical and mineralogical analysis of individual mineral dust particles, Journal of Geophysical Research-atmospheres, 106, 18 029–18 036, 2001.

Faloona, I.: Sulfur processing in the marine atmospheric boundary layer: A review and critical assessment of modelling uncertainties, Atmospheric Environment, 43, 2841–2854, 2009.

Faloona, I., Conley, S. A., Blomquist, B., Clarke, A. D., Kapustin, V., Howell, S., Lenschow, D. H., and Bandy, A. R.: Sulfur dioxide in the tropical marine boundary layer: dry deposition and heterogeneous oxidation observed during the Pacific Atmospheric Sulfur Experiment, Journal of Atmospheric Chemistry, 63, 13–32, 2009.

Farquhar, J., Savarino, J., Airieau, S., and Thiemens, M. H.: Observation of wavelength-sensitive mass-independent sulfur isotope effects during SO2 photolysis: Implications for the early atmosphere, Journal of Geophysical Research-Planets, 106, 32 829–32 839, 2001.

Faust, B. C., Hoffmann, M. R., and Bahnemann, D. W.: Photocatalytic Oxidation of Sulfur-dioxide In Aqueous Suspensions of Alpha-fe2o3, Journal of Physical Chemistry, 93, 6371–6381, 1989.

Flynn, M., Bower, K. N., Choularton, T. W., Wobrock, W., J.M., M., Martinsson, B., Frank, G., Hannsson, H.-C., Karlsson, H., and Laj, P.: Modelling cloud processing of aerosol during the ACE-2 HILLCLOUD experiment, Tellus, 52B, 779–800, 2000.

Fogelman, K. D., Walker, D. M., and Magerum, D. W.: Non-metal Redox Kinetics - Hypochlorite and Hypochlorous Acid Reactions With Sulfite, Inorganic Chemistry, 28, 986–993, doi:10.1021/ic00305a002, 1989.

Fu, H. B., Wang, X., Wu, H. B., Yin, Y., and Chen, J. M.: Heterogeneous uptake and oxidation of SO2 on iron oxides, Journal of Physical Chemistry C, 111, 6077–6085, doi:10.1021/jp070087b, 2007.

Gasso, S., Grassian, V. H., and Miller, R. L.: Interactions between Mineral Dust, Climate, and Ocean Ecosystems, Elements, 6, 247–252, doi:10.2113/gselements.6.4.247, 2010.

Gebel, M. E., Finlayson, Pitts, B. J., and Ganske, J. A.: The uptake of SO2 on synthetic sea salt and some of its components, Geophys. Res. Lett., 27, 887–890, 2000.

Glaccum, R. A. and Prospero, J. M.: Saharan aerosols over the tropical North Atlantic – Mineralogy, Marine Geology, 37, 295 – 321, doi:10.1016/0025-3227(80)90107-3, 1980.

Goldstein, J., D.E., N., Echlin, P., Joy, D., Fiori, C., and Lifshin, E.: Scanning Electron Microscopy and X-ray Microanalysis, Plenum Press, New York, 1981.

Goodman, A. L., Li, P., Usher, C. R., and Grassian, V. H.: Heterogeneous uptake of sulfur dioxide on aluminum and magnesium oxide particles, Journal of Physical Chemistry A, 105, 6109–6120, 2001.

Goodsel, A. J., Low, M. J. D., and Takezawa, N.: Reactions of gaseous pollutants with solids. II. Infrared study of sorption of sulfur dioxide on magnesium oxide, Environmental Science & Technology, 6, 268–273, doi:10.1021/es60062a001, 1972.

Groener, E. and Hoppe, P.: Automated ion imaging with the NanoSIMS ion microprobe, Applied Surface Science, 252, 7148–7151, doi:10.1016/j.apsusc.2006.02.280, 2006.

Gurciullo, C., Lerner, B., Sievering, H., and Pandis, S. N.: Heterogeneous sulfate production in the remote marine environment: Cloud processing and sea-salt particle contributions, J. Geophys. Res., 104, 21 719–21 731, 1999.

Gustafsson, R. J., Orlov, A., Badger, C. L., Griffiths, P. T., Cox, R. A., and Lambert, R. M.: A comprehensive evaluation of water uptake on atmospherically relevant mineral surfaces: DRIFT spectroscopy, thermogravimetric analysis and aerosol growth measurements, Atmospheric Chemistry and Physics, 5, 3415–3421, 2005.

Hanisch, F. and Crowley, J. N.: Heterogeneous Reactivity of Gaseous Nitric Acid on Al2O3, CaCO3, and Atmospheric Dust Samples: A Knudsen Cell Study, The Journal of Physical Chemistry A, 105, 3096–3106, 2001.

Hanisch, F. and Crowley, J. N.: Ozone decomposition on Saharan dust: an experimental investigation, Atmospheric Chemistry and Physics, 3, 119–130, 2003.

Hanson, D. R. and Eisele, F.: Diffusion of H2SO4 in humidified nitrogen: Hydrated H2SO4, Journal of Physical Chemistry A, 104, 1715–1719, 2000.

Harris, E., Sinha, B., Foley, S., Crowley, J. N., Borrmann, S., and Hoppe, P.: Sulfur isotope fractionation during heterogeneous oxidation of SO2 on mineral dust, Atmos. Chem. Phys. Discuss., 12, 2303–2353, doi:10.5194/acpd-12-2303-2012, 2012a.

Harris, E., Sinha, B., Hoppe, P., Crowley, J. N., Ono, S., and Foley, S.: Sulfur isotope fractionation during oxidation of sulfur dioxide: Gas-phase oxidation by OH radicals and aqueous oxidation by H2O2, O3 and iron catalysis, Atmos. Chem. Phys., 12, 407–423, doi:doi:10.5194/acp-12-407-2012, 2012b.

Harris, E., Sinha, B., Hoppe, P., Foley, S., and Borrmann, S.: Fractionation of sulfur isotopes during heterogeneous oxidation of SO2 on sea salt aerosol: A new tool to

investigate non-sea salt sulfate production in the marine boundary layers, Atmos. Chem. Phys. Discuss., 12, 2707–2742, doi:10.5194/acpd-12-2707-2012, 2012c.

Harris, E., Sinha, B., Hoppe, P., van Pinxteren, D., Fomba, W., Lee, T., Gnauk, T., Fahlbusch, B., Crowley, J. N., Foley, S., Borrmann, S., and Herrmann, H.: Investigating cloud processing with sulfur isotope analysis of particles and gases during HCCT 2010, in preparation for Atmos. Chem. Phys., 12, 2012d.

Hattori, S., Danielache, S., Johnson, M., Schmidt, J., Kjaergaard, H., Toyoda, S., Ueno, Y., and Yoshida, N.: Ultraviolet absorption cross sections of carbonyl sulfide isotopologues OC32S, OC33S, OC34S and O13CS: isotopic fractionation in photolysis and atmospheric implications, Atmos. Chem. Phys., 11, 10 293–10 303, doi:doi:10.5194/acp-11-10293-2011, 2011.

Hegg, D.: Cloud condensation nucleus-sulfate mass relationship and cloud albedo, Journal of Geophysical Research, 99, 25 903–25 907, 1994.

Hegg, D. A., Covert, D. S., Jonsson, H., Khelif, D., and Friehe, C. A.: Observations of the impact of cloud processing on aerosol light-scattering efficiency, Tellus Series B-Chemical and Physical Meteorology, 56, 285–293, 2004.

Heinold, B., Tegen, I., Esselborn, M., Kandler, K., Knippertz, P., Mueller, D., Schadlitz, A., Tesche, M., Weinzerl, B., Ansmann, A., Althausen, D., Laurent, B., Massling, A., Mueller, T., Petzold, A., Schepanski, K., and Wiedensohler, A.: Regional Saharan dust modelling during the SAMUM 2006 campaign, Tellus B, 61, 307–324, doi: 10.1111/j.1600-0889.2008.00387.x, 2009.

Herrmann, H., Ervens, B., Jacobi, H. W., Wolke, R., Nowacki, P., and Zellner, R.: CAPRAM2.3: A chemical aqueous phase radical mechanism for tropospheric chemistry, Journal of Atmospheric Chemistry, 36, 231–284, 2000.

Hong, A. P., Bahnemann, D. W., and Hoffmann, M. R.: Cobalt(ii) Tetrasulfophthalocyanine On Titanium-dioxide .2. Kinetics and Mechanisms of the Photocatalytic Oxidation of Aqueous Sulfur-dioxide, Journal of Physical Chemistry, 91, 6245–6251, doi: 10.1021/j100308a035, 1987.

Hopfner, A.: Vapor Pressure Isotope Effects, Angewandte Chemie-international Edition, 8, 689–699, doi:10.1002/anie.196906891, 1969.

Hoppe, P.: NanoSIMS: A new tool in cosmochemistry, Applied Surface Science, 252, 7102–7106, 2006.

Hoppel, W., Frick, G., Fitzgerald, J., and Wattle, B.: A cloud chamber study of the effect that nonprecipitating clouds have on the aerosol size distribution, Aerosol Science and Technology, 20, 1–30, 1994.

Hoppel, W., Pasternack, L., Caffrey, P., Frick, G., Fitzgerald, J., Hegg, D., Gao, S., Ambrusko, J., and Albrechcinski, T.: Sulfur dioxide uptake and oxidation in sea-salt aerosol, Journal of Geophysical Research-atmospheres, 106, 27 575–27 585, doi: 10.1029/2000JD900843, 2001.

Hoppel, W. A. and Caffrey, P. F.: Oxidation of S(IV) in sea-salt aerosol at high pH: Ozone versus aerobic reaction, Journal of Geophysical Research-atmospheres, 110, D23 202, doi:10.1029/2005JD006239, 2005.

Hoppel, W. A., Frick, G. M., and Larson, R. E.: Effect of Nonprecipitating Clouds On the Aerosol Size Distribution In the Marine Boundary-layer, Geophysical Research Letters, 13, 125–128, doi:10.1029/GL013i002p00125, 1986.

Huygen, C.: The sampling of sulfur dioxide in air with impregnated filter paper, Analytica Chimica Acta, 28, 349–360, 1963.

Iida, K., Stolzenburg, M., McMurry, P., Dunn, M. J., Smith, J. N., Eisele, F., and Keady, P.: Contribution of ion-induced nucleation to new particle formation: Methodology and its application to atmospheric observations in Boulder, Colorado, J. Geophys. Res., 111, D23 201–, doi:10.1029/2006JD007167, 2006.

IUPAC: Data Sheet VI.A2.8, URL `http://www.iupac-kinetic.ch.cam.ac.uk`, 2009.

Janssen, A., Geisler, T., Putnis, C., and Putnis, A.: The mechanism of oxidation and "leaching" of ilmenite during natural and experimental alteration, Geochimica Et Cosmochimica Acta, 71, A440–A440, 2007.

Jayne, J. T., Davidovits, P., Worsnop, D. R., Zahniser, M. S., and Kolb, C. E.: Uptake of SO2(g) By Aqueous Surfaces As A Function of pH - the Effect of Chemical-reaction At the Interface, Journal of Physical Chemistry, 94, 6041–6048, doi:10.1021/j100378a076, 1990.

Jedrysek, M. O., Kaluzny, A., and Hoefs, J.: Sulphur and oxygen isotope ratios in spruce needles as a tracer of atmospheric pollution, Journal of Geophysical Research-atmospheres, 107, 4353, doi:10.1029/2001JD000527, 2002.

Jezierski, P., Szynkiewicz, A., and Jedrysek, M. O.: Natural and anthropogenic origin sulphate in an mountainous groundwater system: S and O isotope evidences, Water Air and Soil Pollution, 173, 81–101, doi:10.1007/s11270-005-9028-3, 2006.

Jickells, T. D., An, Z. S., Andersen, K. K., Baker, A. R., Bergametti, G., Brooks, N., Cao, J. J., Boyd, P. W., Duce, R. A., Hunter, K. A., Kawahata, H., Kubilay, N., laRoche, J., Liss, P. S., Mahowald, N., Prospero, J. M., Ridgwell, A. J., Tegen, I., and Torres, R.: Global iron connections between desert dust, ocean biogeochemistry, and climate, Science, 308, 67–71, doi:10.1126/science.1105959, 2005.

John, W., Hering, S., Reischl, G., Sasaki, G., and Goren, S.: Characteristics of Nuclepore Filters With Large Pore-size .2. Filtration Properties, Atmospheric Environment, 17, 373–382, doi:10.1016/0004-6981(83)90054-9, 1983.

Jones, A., Roberts, D., and Slingo, A.: A climate model study of indirect radiation forcing by anthropogenic sulphate aerosols., Nature, 370, 450–453, 1994.

Judeikis, H. S., Stewart, T. B., and Wren, A. G.: Laboratory studies of the heterogeneous reactions of SO2, Atmospheric Environment, 12, 1633–1641, 1978.

Kaaden, N., Massling, A., Schladitz, A., Mueller, T., Kandler, K., Schuetz, L., Weinzierl, B., Petzold, A., Tesche, M., Leinert, S., Deutscher, C., Ebert, M., Weinbruch, S., and Wiedensohler, A.: State of mixing, shape factor, number size distribution, and hygroscopic growth of the Saharan anthropogenic and mineral dust aerosol at Tinfou, Morocco, Tellus B, 61, 51–63, doi:10.1111/j.1600-0889.2008.00388.x, 2009.

Kasper-Giebl, A., Koch, A., Hitzenberger, R., and Puxbaum, H.: Scavenging efficiency of 'aerosol carbon' and sulfate in supercooled clouds at Mt. Sonnblick (3106 m a.s.l., Austria), Journal of Atmospheric Chemistry, 35, 33–46, 2000.

Katoshevski, D., Nenes, A., and Seinfeld, J. H.: A study of processes that govern the maintenance of aerosols in the marine boundary layer, Journal of Aerosol Science, 30, 503–532, doi:10.1016/S0021-8502(98)00740-X, 1999.

Keene, W. C. and Pszenny, A. A. P.: Comment on "Reactions at interfaces as a source of sulfate formation in sea-salt particles" (I), Science, 303, 628b, 2004.

Kester, D. R., Duedall, I. W., Connors, D. N., and Pytkowic, R.: Preparation of Artificial Seawater, Limnology and Oceanography, 12, 176–179, 1967.

Kim, B. G. and Park, S. U.: Transport and evolution of a winter-time Yellow sand observed in Korea, Atmospheric Environment, 35, 3191–3201, doi:10.1016/S1352-2310(00)00469-6, 2001.

Knipping, E. M., Lakin, M. J., Foster, K. L., Jungwirth, P., Tobias, D. J., Gerber, R. B., Dabdub, D., and Finlayson-Pitts, B. J.: Experiments and simulations of ion-enhanced interfacial chemistry on aqueous NaCl aerosols, Science, 288, 301–306, 2000.

Koch, D., Jacob, D., Tegen, I., Rind, D., and Chin, M.: Tropospheric sulfur simulation and sulfate direct radiative forcing in the Goddard Institute for Space Studies general circulation model, Journal of Geophysical Research, 104, 23 799–23 822, 1999.

Kreidenweis, S. M., Walcek, C. J., Feingold, G., Wanmin, G., Jacobson, M. Z., Cheol-Hee, K., Xiaohong, L., Penner, J. E., Nenes, A., and Seinfeld, J. H.: Modification of aerosol mass and size distribution due to aqueous-phase SO2 oxidation in clouds: Comparisons of several models, Journal of Geophysical Research, 108, D7–4213, doi: 10.1029/2002JD002697, 2003.

Krouse, H., Grinenko, L., Grinenko, V., Newman, L., Forrest, J., Nakai, N., Tsuji, Y., Yatsumimi, T., Takeuchi, V., Robinson, B., Stewart, M., Gunatilaka, A., Plumb, L., Smith, J., Buzek, F., Cerny, J., Sramek, J., Menon, A., Iyer, G., Venkatasubramanian, V., Egboka, B., Irogbenachi, M., and Eligwe, C.: Stable Isotopes: Natural and Anthropogenic Sulphur in the Environment, chap. 8. Case Studies and Potential Applications, pp. 307–416, Wiley, Chichester, 1991.

Krouse, H. R. and Grinenko, V. A.: Stable isotopes : natural and anthropogenic sulphur in the environment, vol. 43, Wiley, Chichester, 1991.

Kulmala, M.: How particles nucleate and grow, Science, 302, 1000–1001, 2003.

Kulmala, M., Vehkamaki, H., Petaja, T., Maso, M. D., Lauri, A., Kerminen, V. M., Birmili, W., and McMurry, P. H.: Formation and growth rates of ultrafine atmospheric particles: a review of observations, Journal of Aerosol Science, 35, 143–176, 2004.

Kulmala, M., Riipinen, I., Sipila, M., Manninen, H. E., Petaja, T., Junninen, H., Maso, M. D., Mordas, G., Mirme, A., Vana, M., Hirsikko, A., Laakso, L., Harrison, R. M.,

Hanson, I., Leung, C., Lehtinen, K. E. J., and Kerminen, V. M.: Toward direct measurement of atmospheric nucleation, Science, 318, 89–92, doi:10.1126/science.1144124, 2007.

Kumar, A. and Sarin, M. M.: Aerosol iron solubility in a semi-arid region: temporal trend and impact of anthropogenic sources, Tellus Series B-chemical and Physical Meteorology, 62, 125–132, doi:10.1111/j.1600-0889.2009.00448.x, 2010.

Kumar, A., Sarin, M. M., and Srinivas, B.: Aerosol iron solubility over Bay of Bengal: Role of anthropogenic sources and chemical processing, Marine Chemistry, 121, 167–175, doi:10.1016/j.marchem.2010.04.005, 2010.

Laaksonen, A., Kulmala, M., Berndt, T., Stratmann, F., Mikkonen, S., Ruuskanen, A., Lehtinen, K. E. J., Maso, M. D., Aalto, P., Petaja, T., Riipinen, I., Sihto, S. L., Janson, R., Arnold, F., Hanke, M., Ucker, J., Umann, B., Sellegri, K., O'Dowd, C. D., and Viisanen, Y.: SO2 oxidation products other than H2SO4 as a trigger of new particle formation. Part 2: Comparison of ambient and laboratory measurements, and atmospheric implications, Atmospheric Chemistry and Physics, 8, 7255–7264, 2008.

Lai, A. C.: Investigation of Electrostatic Forces on Particle Deposition in a Test Chamber, Indoor and Built Environment, 15, 179–186, 2006.

Laj, P., Fuzzi, S., Facchini, M. C., Lind, J. A., Orsi, G., Preiss, M., Maser, R., Jaeschke, W., Seyffer, E., Helas, G., Acker, K., Wieprecht, W., Moller, D., Arends, B. G., Mols, J. J., Colvile, R. N., Gallagher, M. W., Beswick, K. M., Hargreaves, K. J., StoretonWest, R. L., and Sutton, M. A.: Cloud processing of soluble gases, Atmospheric Environment, 31, 2589–2598, doi:10.1016/S1352-2310(97)00040-X, 1997a.

Laj, P., Fuzzi, S., Facchini, M. C., Orsi, G., Berner, A., Kruisz, C., Wobrock, W., Hallberg, A., Bower, K. N., Gallagher, M. W., Beswick, K. M., Colvile, R. N., Choularton, T. W., Nason, P., and Jones, B.: Experimental evidence for in-cloud production of aerosol sulphate, Atmospheric Environment, 31, 2503–2514, doi:10.1016/S1352-2310(96)00217-8, 1997b.

Laskin, A., Gaspar, D. J., Wang, W. H., Hunt, S. W., Cowin, J. P., Colson, S. D., and Finlayson-Pitts, B. J.: Reactions at interfaces as a source of sulfate formation in sea-salt particles, Science, 301, 340–344, 2003.

Lee, C. C. W. and Thiemens, M. H.: The delta O-17 and delta O-18 measurements of atmospheric sulfate from a coastal and high alpine region: A mass-independent isotopic anomaly, Journal of Geophysical Research-Atmospheres, 106, 17 359–17 373, 2001.

Lelieveld, J. and Heintzenberg, J.: Sulfate Cooling Effect On Climate Through In-cloud Oxidation of Anthropogenic SO2, Science, 258, 117–120, doi: 10.1126/science.258.5079.117, 1992.

Leung, F. Y., Colussi, A. J., and Hoffmann, M. R.: Sulfur isotopic fractionation in the gas-phase oxidation of sulfur dioxide initiated by hydroxyl radicals, Journal of Physical Chemistry A, 105, 8073–8076, 2001.

Leung, F.-Y., Colussi, A., Hoffmann, M., and Toon, G.: Isotopic fractionation of carbonyl sulfide in the atmosphere: Implications for the source of background stratospheric sulfate aerosol, Geophys. Res. Lett., 29, 1474, doi:doi:10.1029/2001g1013955, 2002.

Levin, Z., Ganor, E., and Gladstein, V.: The effects of desert particles coated with sulfate on rain formation in the eastern Mediterranean, Journal of Applied Meteorology, 35, 1511–1523, 1996.

Li, L., Chen, Z. M., Zhang, Y. H., Zhu, T., Li, J. L., and Ding, J.: Kinetics and mechanism of heterogeneous oxidation of sulfur dioxide by ozone on surface of calcium carbonate, Atmospheric Chemistry and Physics, 6, 2453–2464, 2006.

Li, L., Chen, Z. M., Zhang, Y. H., Zhu, T., Li, S., Li, H. J., Zhu, L. H., and Xu, B. Y.: Heterogeneous oxidation of sulfur dioxide by ozone on the surface of sodium chloride and its mixtures with other components, Journal of Geophysical Research-Atmospheres, 112, D18 301, doi:10.1029/2006JD008207, 2007.

Liao, H. and Seinfeld, J. H.: Global impacts of gas-phase chemistry-aerosol interactions on direct radiative forcing by anthropogenic aerosols and ozone, Journal of Geophysical Research-atmospheres, 110, D18 208, doi:10.1029/2005JD005907, 2005.

Liao, H., Adams, P., Chung, S., Seinfeld, J., Mickley, L., and Jacob, D.: Interactions between tropospheric chemistry and aerosols in a unified general circulation model, Journal of Geophysical Research, 108, D1 4001, doi:10.1029/2001JD001260, 2003.

Lin, Y., Sim, M. S., and Ono, S.: Multiple-sulfur isotope effects during photolysis of carbonyl sulfide, Atmos. Chem. Phys., 11, 10 283–10 292, doi:doi:10.5194/acp-11-10283-2011, 2011.

Liu, X. H. and Seidl, W.: Modeling study of cloud droplet nucleation and in-cloud sulfate production during the Sanitation of the Atmosphere (SANA) 2 campaign, Journal of Geophysical Research-atmospheres, 103, 16 145–16 158, doi:10.1029/98JD00972, 1998.

Low, M. J. D., Goodsel, A. J., and Takezawa, N.: Reactions of gaseous pollutants with solids. I. Infrared study of the sorption of sulfur dioxide on calcium oxide, Environmental Science & Technology, 5, 1191–1195, doi:10.1021/es60059a003, 1971.

Luz, B. and Barkan, E.: The isotopic ratios O-17/O-16 and O-18/O-16 in molecular oxygen and their significance in biogeochemistry, Geochimica et Cosmochimica Acta, 69, 1099–1110, 2005.

Lyons, J. R.: Atmospherically-derived mass-independent sulfur isotope signatures, and incorporation into sediments, Chemical Geology, 267, 164–174, 2009.

Maekelae, J. M., Aalto, P., Jokinen, V., Pohja, T., Nissinen, A., Palmroth, S., Markkanen, T., Seitsonen, K., Lihavainen, H., and Kulmala, M.: Observations of ultrafine aerosol particle formation and growth in boreal forest, Geophysical Research Letters, 24, 1219–1222, 1997.

Mamane, Y. and Gottlieb, J.: Heterogeneous reactions of minerals with sulfur and nitrogen oxides, Journal of Aerosol Science, 20, 303–311, 1989.

Mariotti, A., Germon, J. C., Hubert, P., Kaiser, P., Letolle, R., Tardieux, A., and Tardieux, P.: Experimental-determination of Nitrogen Kinetic Isotope Fractionation - Some Principles - Illustration For the Denitrification and Nitrification Processes, Plant and Soil, 62, 413–430, 1981.

Mayer, B., Feger, K. H., Giesemann, A., and Jaeger, H. J.: Interpretation of sulfur cycling in two catchments in the Black Forest (Germany) using stable sulfur and oxygen isotope data, Biogeochemistry, 30, 31–58, 1995.

McCabe, J. R., Savarino, J., Alexander, B., Gong, S. L., and Thiemens, M. H.: Isotopic constraints on non-photochemical sulfate production in the Arctic winter, Geophysical Research Letters, 33, L05 810, doi:10.1029/2005GL025164, 2006.

Mertes, S., Galgon, D., Schwirn, K., Nowak, A., Lehmann, K., Massling, A., Wiedensohler, A., and Wieprecht, W.: Evolution of particle concentration and size distribution observed upwind, inside and downwind hill cap clouds at connected flow conditions during FEBUKO, Atmospheric Environment, 39, 4233–4245, 2005a.

Mertes, S., Lehmann, K., Nowak, A., Massling, A., and Wiedensohler, A.: Link between aerosol hygroscopic growth and droplet activation observed for hill-capped clouds at connected flow conditions during FEBUKO, Atmospheric Environment, 39, 4247–4256, 2005b.

Millero, F. J.: Physical-chemistry of Seawater, Annual Review of Earth and Planetary Sciences, 2, 101–150, 1974.

Mitra, S., Brinkmann, J., and Pruppacher, H.: A wind tunnel study on the drop-to-particle conversion, Journal of Aerosol Science, 23, 245 – 256, doi:10.1016/0021-8502(92)90326-Q, 1992.

Moore, J., Stanitski, C., and Jurs, P.: Chemistry: The Molecular Science, Brooks/Cole - Thomson Learning, USA, 2005.

Moore, K. F., Sherman, D. E., Reilly, J. E., and Collett, J. L.: Drop size-dependent chemical composition in clouds and fogs. Part I. Observations, Atmospheric Environment, 38, 1389–1402, doi:10.1016/j.atmosenv.2003.12.013, 2004a.

Moore, K. F., Sherman, D. E., Reilly, J. E., Hannigan, M. P., Lee, T., and Collett, J. L.: Drop size-dependent chemical composition of clouds and fogs. Part II: Relevance to interpreting the aerosol/trace gas/fog system, Atmospheric Environment, 38, 1403–1415, doi:10.1016/j.atmosenv.2003.12.014, 2004b.

Morales, C.: The airborne transport of Saharan dust: A review, Climatic Change, 9, 219–241, doi:10.1007/BF00140538, 10.1007/BF00140538, 1986.

Mukai, H., Tanaka, A., Fujii, T., Zeng, Y. Q., Hong, Y. T., Tang, J., Guo, S., Xue, H. S., Sun, Z. L., Zhou, J. T., Xue, D. M., Zhao, J., Zhai, G. H., Gu, J. L., and Zhai, P. Y.: Regional characteristics of sulfur and lead isotope ratios in the atmosphere at several Chinese urban sites, Environmental Science & Technology, 35, 1064–1071, 2001.

Ndour, M., Nicolas, M., D'Anna, B., Ka, O., and George, C.: Photoreactivity of NO2 on mineral dusts originating from different locations of the Sahara desert, Physical Chemistry Chemical Physics, 11, 1312–1319, 2009.

Nicolas, M., Ndour, M., Ka, O., D'Anna, B., and George, C.: Photochemistry of Atmospheric Dust: Ozone Decomposition on Illuminated Titanium Dioxide, Environmental Science & Technology, 43, 7437–7442, 2009.

Nielsen, H., Pilot, J., Grinenko, L., Grinenko, V., Lein, A., Smith, J., and Pankina, R.: Stable Isotopes: Natural and Anthropogenic Sulphur in the Environment, chap. 4. Lithospheric Sources of Sulfur, pp. 65–132, John Wiley and Sons, 1991.

Norman, A. L., Barrie, L. A., Toom-Sauntry, D., Sirois, A., Krouse, H. R., Li, S. M., and Sharma, S.: Sources of aerosol sulphate at Alert: Apportionment using stable isotopes, Journal of Geophysical Research-atmospheres, 104, 11 619–11 631, 1999.

Norman, A. L., Anlauf, K., Hayden, K., Thompson, B., Brook, J. R., Li, S. M., and Bottenheim, J.: Aerosol sulphate and its oxidation on the Pacific NW coast: S and O isotopes in PM2.5, Atmospheric Environment, 40, 2676–2689, 2006.

Norris, G., Vedantham, R., Wade, K., Brown, S., Prouty, J., and Foley, C.: EPA Positive Matrix Factorization (PMF) 3.0 Fundamentals and User Guide, U.S. Environmental Protection Agency, Office of Research and Development, Washington, DC, 2008.

Novak, M., Jackova, I., and Prechova, E.: Temporal Trends in the Isotope Signature of Air-Borne Sulfur in Central Europe, Environmental Science & Technology, 35, 255–260, 2001.

Nriagu, J. O., Rees, C., Mekhtiyeva, V., Lein, A., Fritz, P., Drimmie, R., Pankina, R., Robinson, B., and Krouse, H. R.: Stable Isotopes: Natural and Anthropogenic Sulphur in the Environment, chap. 6., pp. 177–266, John Wiley and Sons, 1991.

Ohizumi, T., Fukuzaki, N., and Kusakabe, M.: Sulfur isotopic view on the sources of sulfur in atmospheric fallout along the coast of the Sea of Japan, Atmospheric Environment, 31, 1339–1348, 1997.

Ono, S., Wing, B., Johnston, D., Farquhar, J., and Rumble, D.: Mass-dependent fractionation of quadruple stable sulfur isotope system as a new tracer of sulfur biogeochemical cycles, Geochimica et Cosmochimica Acta, 70, 2238–2252, 2006.

Oum, K. W., Lakin, M. J., DeHaan, D. O., Brauers, T., and Finlayson-Pitts, B. J.: Formation of molecular chlorine from the photolysis of ozone and aqueous sea-salt particles, Science, 279, 74–77, 1998.

Pacchioni, G., Clotet, A., and Ricart, J. M.: A theoretical study of the absorption and reaction of SO2 at surface and step sites of the MgO(100) surface, Surface Science, 315, 337–350, 1994.

Park, S. H., Song, C. B., Kim, M. C., Kwon, S. B., and Lee, K. W.: Study on size distribution of total aerosol and water-soluble ions during an Asian dust storm event at Jeju Island, Korea, Environmental Monitoring and Assessment, 93, 157–183, doi: 10.1023/B:EMAS.0000016805.04194.56, 2004.

Patris, N., Mihalopoulos, N., Baboukas, E. D., and Jouzel, J.: Isotopic composition of sulfur in Size-resolved marine aerosols above the Atlantic Ocean., Journal of Geophysical Research-Atmospheres, 105, 14,449–14,457, 2000.

Patris, N., Cliff, S. S., Quinn, P. K., Kasem, M., and Thiemens, M. H.: Isotopic analysis of aerosol sulfate and nitrate during ITCT-2k2: Determination of different formation pathways as a function of particle size, Journal of Geophysical Research-Atmospheres, 112, D23 301, doi:10.1029/2005JD006 214, 2007.

Pincus, R. and Baker, M.: Effect of precipitation on the albedo susceptibility of clouds in the marine boundary layer, Nature, 370, 250–252, 1994.

Pruppacher, H. and Klett, J.: Microphysics of Clouds and Precipitation, Kluwer Academic Publishers, second edn., 1997.

Putnis, A.: Mineral replacement reactions: from macroscopic observations to microscopic mechanisms, Mineralogical Magazine, 66, 689–708, doi:10.1180/0026461026650056, 2002.

Rani, A., Prasad, D. S. N., Madnawat, P. V. S., and Gupta, K. S.: The Role of Free-fall Atmospheric Dust In Catalyzing Autoxidation of Aqueous Sulfur-dioxide, Atmospheric Environment Part A-general Topics, 26, 667–673, 1992.

Redington, A. L., Derwent, R. G., Witham, C. S., and Manning, A. J.: Sensitivity of modelled sulphate and nitrate aerosol to cloud, pH and ammonia emissions, Atmospheric Environment, 43, 3227–3234, 2009.

Rees, C. and Holt, B.: Stable Isotopes: Natural and Anthropogenic Sulphur in the Environment, chap. 3., pp. 43–64, John Wiley and Sons, 1991.

Rees, C. E., Jenkins, W. J., and Monster, J.: Sulfur Isotopic Composition of Ocean Water Sulfate, Geochimica et Cosmochimica Acta, 42, 377–381, 1978.

Roithner: Preliminary Information: Hexagonal High-Power UV LED H2A1 UV Series T, Roithner Lasertechnik GmbH, Vienna, Austria.

Rubasinghege, G., Elzey, S., Baltrusaitis, J., Jayaweera, P. M., and Grassian, V. H.: Reactions on Atmospheric Dust Particles: Surface Photochemistry and Size-Dependent Nanoscale Redox Chemistry, Journal of Physical Chemistry Letters, 1, 1729–1737, 2010.

Rudyak, V. Y., Dubtsov, S. N., and Baklanov, A. M.: Measurements of the temperature dependent diffusion coefficient of nanoparticles in the range of 295-600 K at atmospheric pressure, Journal of Aerosol Science, 40, 833–843, doi:10.1016/j.jaerosci.2009.06.006, 2009.

Rufus, J., Stark, G., Smith, P. L., Pickering, J. C., and Thorne, A. P.: High-resolution photoabsorption cross section measurements of SO2, 2: 220 to 325 nm at 295 K, J. Geophys. Res., 108, E2 5011, doi:10.1029/2002JE001931, 2003.

Saltzman, E. S., Brass, G., and Price, D.: The mechanism of sulfate aerosol formation: Chemical and sulfur isotopic evidence, Geophysical Research Letters, 10, 513–516, 1983.

Sander, R. and Crutzen, P. J.: Model study indicating halogen activation and ozone destruction in polluted air masses transported to the sea, J. Geophys. Res., 101, 9121–9138, doi:10.1029/95JD03793, 1996.

Sander, R., Lelieveld, J., and Crutzen, P. J.: Modelling of the nighttime nitrogen and sulfur chemistry in size resolved droplets of an orographic cloud, Journal of Atmospheric Chemistry, 20, 89–116, 1995.

Sander, R., Crutzen, P. J., and von Glasow, R.: Comment on "Reactions at interfaces as a source of sulfate formation in sea-salt particles" (II), Science, 303, 628c, 2004.

Sanusi, A. A., Norman, A.-L., Burridge, C., Wadleigh, M., and Tang, W.-W.: Determination of the S isotope composition of methanesulfonic acid, Analytical Chemistry, 78, 4964–4968, doi:10.1021/ac0600048, 2006.

Savarino, J., Lee, C. C. W., and Thiemens, M. H.: Laboratory oxygen isotopic study of sulfur (IV) oxidation: Origin of the mass-independent oxygen isotopic anomaly in atmospheric sulfates and sulfate mineral deposits on Earth, Journal of Geophysical Research-Atmospheres, 105, 29 079–29 088, 2000.

Savarino, J., Bekki, S., Cole-Dai, J. H., and Thiemens, M. H.: Evidence from sulfate mass independent oxygen isotopic compositions of dramatic changes in atmospheric oxidation following massive volcanic eruptions, Journal of Geophysical Research-Atmospheres, 108, D21–4671, doi:10.1029/2003JD003737, 2003a.

Savarino, J., Romero, A., Cole-Dai, J., Bekki, S., and Thiemens, M. H.: UV induced mass-independent sulfur isotope fractionation in stratospheric volcanic sulfate, Geophysical Research Letters, 30, 21 2131, 2003b.

Schwarzenboeck, A., Heintzenberg, J., and Mertes, S.: Incorporation of aerosol particles between 25 and 850 nm into cloud elements: measurements with a new complementary sampling system, Atmospheric Research, 52, 241–260, doi:10.1016/S0169-8095(99)00034-4, 2000.

Seinfeld, J. H. and Pandis, S. N.: Atmospheric Chemistry and Physics, Wiley & Sons, New York, 1998.

Shaka, H., Robertson, W. H., and Finlayson-Pitts, B. J.: A new approach to studying aqueous reactions using diffuse reflectance infrared Fourier transform spectrometry: application to the uptake and oxidation of SO2 on OH-processed model sea salt aerosol, Physical Chemistry Chemical Physics, 9, 1980–1990, 2007.

Shon, Z. H., Davis, D., Chen, G., Grodzinsky, G., Bandy, A., Thornton, D., Sandholm, S., Bradshaw, J., Stickel, R., Chameides, W., Kok, G., Russell, L., Mauldin, L., Tanner, D., and Eisele, F.: Evaluation of the DMS flux and its conversion to SO2 over the southern ocean, Atmospheric Environment, 35, 159–172, 2001.

Sievering, H., Boatman, J., Galloway, J., Keene, W., Kim, Y., Luria, M., and Ray, J.: Heterogeneous Sulfur Conversion In Sea-salt Aerosol Particles - the Role of Aerosol Water Content and Size Distribution, Atmospheric Environment Part A-general Topics, 25, 1479–1487, 1991.

Sievering, H., Gorman, E., Ley, T., Pszenny, A., Springer-Young, M., Boatman, J., Kim, Y., Nagamoto, C., and Wellman, D.: Ozone oxidation of sulfur in sea-salt aerosol particles during the Azores Marine Aerosol and Gas Exchange experiment, J. Geophys. Res., 100, 23 075–23 081, 1995.

Sievering, H., Lerner, B., Slavich, J., Anderson, J., Posfai, M., and Cainey, J.: O3 oxidation of SO2 in sea-salt aerosol water: Size distribution of non-sea-salt sulfate during the First Aerosol Characterization Experiment (ACE 1), J. Geophys. Res., 104, 21 707–21 717, 1999.

Sievering, H., Cainey, J., Harvey, M., McGregor, J., Nichol, S., and Quinn, P.: Aerosol non-sea-salt sulfate in the remote marine boundary layer under clear-sky

and normal cloudiness conditions: Ocean-derived biogenic alkalinity enhances sea-salt sulfate production by ozone oxidation, J. Geophys. Res., 109, D19 317, doi: doi:10.1029/2003JD004315, 2004.

Sinha, B., Harris, E., Hoppe, P., Mertes, S., Gnauk, T., van Pinxteren, D., and Herrmann, H.: Source category specific CCN activation curves based on SEM and AFM single particle analysis from the Hill Cap Cloud Thuringia (HCCT) field experiments and the effect of cloud processing on the mixing state of accumulation mode aerosol: A combined SEM, AFM study during HCCT 2010, in prep. for Atmospheric Chemistry and Physics, 12, 2012a.

Sinha, B., Poehlker, C., Wiedemann, K., Harris, E., Hoppe, P., Kilcoyne, A., Andreae, M. O., Gunthe, S. S., Poeschl, U., and Borrmann, S.: Investigating the chemical composition and mixing state of secondary aerosol particles using NanoSIMS, in prep. for Atmospheric Measurement Techniques, 2012b.

Sinha, B. W., Hoppe, P., Huth, J., Foley, S., and Andreae, M. O.: Sulfur isotope analyses of individual aerosol particles in the urban aerosol at a central European site (Mainz, Germany), Atmospheric Chemistry and Physics, 8, 7217–7238, 2008a.

Sinha, V., Williams, J., Crowley, J. N., and Lelieveld, J.: The comparative reactivity method - a new tool to measure total OH reactivity in ambient air, Atmospheric Chemistry and Physics, 8, 2213–2227, 2008b.

Sinha, V., Custer, T. G., Kluepfel, T., and Williams, J.: The effect of relative humidity on the detection of pyrrole by PTR-MS for OH reactivity measurements, International Journal of Mass Spectrometry, 282, 108–111, 2009.

Slodzian, G., Chaintreau, M., Dennebouy, R., and Rousse, A.: Precise in situ measurements of isotopic abundances with pulse counting of sputtered ions, European Physical Journal-applied Physics, 14, 199–231, 2001.

Slodzian, G., Hillion, F., Stadermann, F. J., and Zinner, E.: QSA influences on isotopic ratio measurements, Applied Surface Science, 231-2, 874–877, 2004.

Sofen, E., Alexander, B., and Kunasek, S. A.: The impact of anthropogenic emissions on atmospheric sulfate production pathways, oxidants and ice core Delta17O(sulfate), Atmospheric Chemistry and Physics, 11, 3565–3578, 2011.

Solomon, S.: Technical Summary in Climate Change 2007: The physical science basis. Contribution of the working group I to the Fourth Assessment Report of the Intergovernmental Panel on Climate Change., Cambridge University Press, New York, 2007.

Solomon, S., Qin, D., Manning, M., Chen, Z., Marquis, M., Averyt, K., Tignor, M., and H.L., M.: Climate Change 2007: The physical science basis. Contribution of the working group I to the Fourth Assessment Report of the Intergovernmental Panel on Climate Change., p. 996, Cambridge University Press, New York, 2007.

Stoyan, D.: Stochastik fuer Ingenieure und Naturwissenschaftler, Wiley-VCH, 1998.

Strauss, H.: The isotopic composition of sedimentary sulfur through time, Palaeogeography Palaeoclimatology Palaeoecology, 132, 97–118, doi:10.1016/S0031-0182(97)00067-9, 1997.

Suhre, K., V, C., Mari, C., Rosset, R., Johnson, D. W., Osborne, S., Wood, R., Andreae, M. O., Bandy, B., Bates, T. S., Businger, S., Gerbig, C., Raes, F., and Rudolph, J.: Chemistry and aerosols in the marine boundary layer: 1-D modelling of the three ACE-2 Lagrangian experiments RID B-1068-2008, Atmospheric Environment, 34, 5079–5094, doi:10.1016/S1352-2310(00)00221-1, 2000.

Sullivan, R. C., Guazzotti, S. A., Sodeman, D. A., and Prather, K. A.: Direct observations of the atmospheric processing of Asian mineral dust, Atmospheric Chemistry and Physics, 7, 1213–1236, 2007.

Tanaka, N., Rye, D. M., Xiao, Y., and Lasaga, A. C.: Use of Stable Sulfur Isotope Systematics for Evaluating Oxidation Reaction Pathways and in-Cloud Scavenging of Sulfur-Dioxide in the Atmosphere, Geophysical Research Letters, 21, 1519–1522, 1994.

Tanaka, T. Y. and Chiba, M.: A numerical study of the contributions of dust source regions to the global dust budget, Global and Planetary Change, 52, 88–104, doi: 10.1016/j.gloplacha.2006.02.002, 2006.

Thornton, D. and Bandy, A.: Sulfur dioxide and dimethyl sulfide in the central pacific troposphere, Journal of Atmospheric Chemistry, 17, 1–13, 1993.

Thornton, D., Bandy, A., Blomquist, B., Davis, D., and Talbot, R. W.: Sulfur dioxide as a source of condensation nuclei in the upper troposphere of the Pacific Ocean, Journal of Geophysical Research, 101, 1883–1890, 1996.

Tichomirowa, M., Haubrich, F., Klein, M., and Matschullat, J.: Regional and temporal (1992-2004) evolution of air-borne sulphur isotope composition in Saxony, southeastern Germany, central Europe, Isotopes in Environmental and Health Studies, 43, 295–305, 10256016, 2007.

Tilgner, A., Heinold, B., Nowak, A., and Herrmann, H.: Meteorological characterisation of the FEBUKO hill cap cloud experiments, Part I: Synoptic characterisation of measurement periods, Atmospheric Environment, 39, 4185–4194, 2005.

Tilly, J., Lewicki, M., Tomaszewski, Z., and Toczkowski, J.: Use of Ilmenite Decomposition Products In A Gas Desulfurization Process, Journal of Chemical Technology and Biotechnology, 52, 301–310, 1991.

Torfs, K. M., VanGrieken, R., and Buzek, F.: Use of Stable Isotope Measurements to Evaluate the Origin of Sulfur in Gypsum Layers on Limestone Buildings, Environmental Science & Technology, 31, 2650–2655, 1997.

Trebs, I., Meixner, F. X., Slanina, J., Otjes, R., Jongejan, P., and Andreae, M. O.: Real-time measurements of ammonia, acidic trace gases and water-soluble inorganic aerosol species at a rural site in the Amazon Basin, Atmos. Chem. Phys., 4, 967–987, 2004.

Troy, R. C. and Margerum, D. W.: Nonmetal Redox Kinetics - Hypobromite and Hypobromous Acid Reactions With Iodide and With Sulfite and the Hydrolysis of Bromosulfate, Inorganic Chemistry, 30, 3538–3543, doi:10.1021/ic00018a028, 1991.

Tsai, I.-C., Chen, J.-P., Lin, P.-Y., Wang, W.-C., and Isaksen, I.: Sulfur cycle and sulfate radiative forcing simulated from a coupled global climate-chemistry model, Atmos. Chem. Phys., 10, 3693–3709, 2010.

Tucker, W. A. and Nelken, L. H.: Handbook of Chemical Property Estimation Methods, chap. 17. Diffusion Coefficients in Air and Water, American Chemical Society, 1982.

Turekian, V. C., Macko, S. A., and Keene, W. C.: Application of stable sulfur isotopes to differentiate sources of size-resolved particulate sulfate in polluted marine air at Bermuda during spring, Geophysical Research Letters, 28, 1491–1494, 2001.

Twomey, S.: Pollution and the planetary albedo, Atmospheric Environment, 8, 1251–1256, doi:10.1016/0004-6981(74)90004-3, 1974.

Twomey, S.: Aerosol, Clouds and Radiation, Atmospheric Environment, 25A, 2435–2442, 1991.

Ullerstam, M., Vogt, R., Langer, S., and Ljungstrom, E.: The kinetics and mechanism of SO2 oxidation by O-3 on mineral dust, Physical Chemistry Chemical Physics, 4, 4694–4699, 2002.

Ullerstam, M., Johnson, M. S., Vogt, R., and Ljungstrom, E.: DRIFTS and Knudsen cell study of the heterogeneous reactivity of SO2 and NO2 on mineral dust, Atmospheric Chemistry and Physics, 3, 2043–2051, 2003.

Umann, B., Arnold, F., Schaal, C., Hanke, M., Uecker, J., Aufmhoff, H., Balkanski, Y., and Dingenen, R. V.: Interaction of mineral dust with gas phase nitric acid and sulfur dioxide during the MINATROC II field campaign: First estimate of the uptake coefficient gamma(HNO3) from atmospheric data, Journal of Geophysical Research-Atmospheres, 110, D22 306, doi:10.1029/2005JD005906, 2005.

US-EPA: Method 6 - Determination of Sulfur Dioxide Emissions from Stationary Sources, URL `http://www.epa.gov/ttn/emc/`, 2010.

Usher, C. R., Al-Hosney, H., Carlos-Cuellar, S., and Grassian, V. H.: A laboratory study of the heterogeneous uptake and oxidation of sulfur dioxide on mineral dust particles, Journal of Geophysical Research-Atmospheres, 107, D23 4713, doi: 10.1029/2002JD002051, 2002.

van Loon, G. and Duffy, S.: Environmental Chemistry: A Global Perspective, Oxford University Press, 2000.

van Pinxteren, D., Birmili, W., Fomba, W., Gnauk, T., Iinuma, Y., Mertes, S., Mildenberger, K., Merkel, M., Mueller, C., Mueller, K., Poulain, L., Spindler, G., Henning, S., Stratmann, F., Tilgner, A., Wex, H., Wolke, R., Wiedensohler, A., Zhijun, W., Boettger, T., Borrmann, S., Harris, E., Roth, A., Schneider, J., Sinha, B., George, I., Heard, D. E., Whalley, L., D'Anna, B., George, C., Mueller, M., Amedro, D., Fittschen, C., Scheomaker, C., Collett, J., Lee, T., and Herrmann, H.: Hill Cap Cloud Thuringia 2010 - Overview and First Results, European Aerosol Conference, 2011.

von Glasow, R.: Importance of the surface reaction OH+Cl- on sea salt aerosol for the chemistry of the marine boundary layer - a model study, Atmospheric Chemistry and Physics, 6, 3571–3581, 2006.

von Glasow, R. and Crutzen, P. J.: Model study of multiphase DMS oxidation with a focus on halogens, Atmospheric Chemistry and Physics, 4, 589–608, 2004.

von Glasow, R. and Sander, R.: Variation of sea salt aerosol pH with relative humidity, Geophysical Research Letters, 28, 247–250, 2001.

von Glasow, R., Sander, R., Bott, A., and Crutzen, P. J.: Modeling halogen chemistry in the marine boundary layer - 2. Interactions with sulfur and the cloud-covered MBL, Journal of Geophysical Research-atmospheres, 107, D17, doi:10.1029/2001JD000943, 2002.

Wadleigh, M. A.: Sulphur isotopic composition of aerosols over the western North Atlantic Ocean, Canadian Journal of Fisheries and Aquatic Sciences, 61, 817–825, doi: 10.1139/f04-073, 2004.

Wagner, F., Bortoli, D., Pereira, S., Costa, M., Silva, A., Weinzierl, B., Esselborn, M., Petzold, A., Rasp, K., Heinold, B., and Tegen, I.: Properties of dust aerosol particles transported to Portugal from the Sahara desert, Tellus B, 61, 297–306, doi:10.1111/j.1600-0889.2008.00393.x, URL `http://dx.doi.org/10.1111/j.1600-0889.2008.00393.x`, 2009.

Weber, R. J., Marti, J. J., McMurry, P. H., Eisele, F. L., Tanner, D. J., and Jefferson, A.: Measurements of new particle formation and ultrafine particle growth rates at a clean continental site, Journal of Geophysical Research-atmospheres, 102, 4375–4385, doi:10.1029/96JD03656, 1997.

Whalley, L., George, I., and Heard, D. E.: OH and HO2 measurements in and out of cloud during the HCCT-2010 campaign, in prep. for Atmospheric Chemistry and Physics, 12, 2012.

Winterholler, B.: Sulfur Isotope Analysis of Aerosol Particles by NanoSIMS, Ph.D. thesis, Johannes Gutenberg-Universitaet, Mainz, 2007.

Winterholler, B., Hoppe, P., Andreae, M. O., and Foley, S.: Measurement of sulfur isotope ratios in micrometer-sized samples by NanoSIMS, Applied Surface Science, 252, 7128–7131, 2006.

Winterholler, B., Hoppe, P., Foley, S., and Andreae, M. O.: Sulfur isotope ratio measurements of individual sulfate particles by NanoSIMS, International Journal of Mass Spectrometry, 272, 63–77, 2008.

Xiao, H., Carmichael, G. R., Durchenwald, J., Thornton, D., and Bandy, A.: Long-range transport of SOx and dust in East Asia during the PEM B Experiment, Journal of Geophysical Research-Atmospheres, 102, 28 589–28 612, 1997.

Yiin, B. S. and Margerum, D. W.: Kinetics of Hydrolysis of the Chlorosulfate Ion, Inorganic Chemistry, 27, 1670–1672, doi:10.1021/ic00283a002, 1988.

Young, L. H., Benson, D. R., Kameel, F. R., Pierce, J. R., Junninen, H., Kulmala, M., and Lee, S. H.: Laboratory studies of H2SO4/H2O binary homogeneous nucleation from the SO2+OH reaction: evaluation of the experimental setup and preliminary results, Atmospheric Chemistry and Physics, 8, 4997–5016, 2008.

Yuskiewicz, B. A., Stratmann, F., Birmili, W., Wiedensohler, A., Swietlicki, E., Berg, O., and Zhou, J.: The effects of in-cloud mass production on atmospheric light scatter, Atmospheric Research, 50, 265–288, 1999.

Zasypkin, A., Grigor'eva, V., Korchak, V., and Gerschenson, Y.: A formula for summing of kinetic resistances for mobile and stationary media: I. Cylindrical reactor, Kinetics and Catalysis, 38, 842–851, 1997.

Zender, C., Newman, D., and Tegen, I.: Quantifying mineral dust mass budgets: terminology, constraints, and current estimates, EOS, 85, 509–512, doi:10.1029/2004EO480002, 2004.

Zhang, J. Z. and Millero, F. J.: The Rate of Sulfite Oxidation In Seawater, Geochimica Et Cosmochimica Acta, 55, 677–685, doi:10.1016/0016-7037(91)90333-Z, 1991.

Zhang, X. Y., Zhuang, G. S., Chen, J. M., Wang, Y., Wang, X., An, Z. S., and Zhang, P.: Heterogeneous reactions of sulfur dioxide on typical mineral particles, Journal of Physical Chemistry B, 110, 12 588–12 596, 2006.

Zhu, S., Butler, T., Sander, R., Ma, J., and Lawrence, M. G.: Impact of dust on tropospheric chemistry over polluted regions: a case study of the Beijing megacity, Atmospheric Chemistry and Physics, 10, 3855–3873, 2010.

Zuo, Y. G. and Zhan, J.: Effects of oxalate on Fe-catalyzed photoxidation of dissolved sulfur dioxide in atmospheric water, Atmospheric Environment, 39, 27–37, doi: 10.1016/j.atmosenv.2004.09.058, 2005.

Curriculum Vitae

Personal information

Birthdate: 05/08/1987 (Melbourne, Australia)
Nationality: Australian and British

Education and Professional Experience

02/2009 - 05/2012 *Doctoral Degree*, Max Planck Institute for Chemistry, Mainz

- **Experience and skills**:
  - Participation in the campaign 'Hill Cap Cloud Thuringia 2010', in cooperation with the Leibniz Institute for Tropospheric Research
  - Scientific visit to the Stable Isotope Geobiology Laboratory at the Massachusetts Institute of Technology in November-December 2011 to carry out high precision measurements of sulfur isotope fractionation during oxidation reactions with a Finnigan MAT-253
  - NanoSIMS isotopic analysis, scanning electron microscope imaging and EDX analysis, ICP-OES, computer skills (Excel, Grapher, LaTeX, multivariate statistics, and other common programs), laboratory skills
- **Awards**:
  - Travel Grant for the Tenth Informal Conference on Atmospheric and Molecular Sciences (TICAMS), Copenhagen, 2011
  - Travel Grant for the Goldschmidt Conference, Prague, 2011

- **Conference Presentations**:
  - International Symposium on Isotopomers, Amsterdam, 2010 - Poster: *A laboratory study on the fractionation of sulfur isotopes during SO_2 oxidation*
  - American Geophysical Union Fall Meeting, San Francisco, 2010 - Talk: *Fractionation of sulfur isotopes during atmospheric processes*
  - HCCT Campaign First Data Meeting, Leipzig, 2011 - Talk: *Sulfur isotopes measured at HCCT*
  - Tenth Informal Conference on Atmospheric and Molecular Sciences, Copenhagen, 2011 - Talk: *Investigating cloud chemistry with sulfur isotopes*
  - Goldschmidt Conference, Prague, 2011 - Talk: *Cloud processing measured with sulfur isotopes during HCCT 2010*
  - American Geophysical Union Fall Meeting, San Francisco, 2011 - Poster: *Fractionation of sulfur isotopes during heterogeneous oxidation of SO_2*

02/2008 - 12/2008 *Honours Degree in Antarctic Science*, University of Tasmania, Australia and University Centre in Svalbard (UNIS), Norway
Note: This degree was certified as equivalent to a Master of Science by the Johannes Gutenberg University of Mainz, June, 2009

- **Thesis title**: *Weathering processes and remediation options for polychlorinated biphenyl and polycyclic aromatic hydrocarbon contamination at Kinnvika Station, Svalbard*, supervised by Dr. Roland Kallenborn (UNIS), Dr. Andrew McMinn (University of Tasmania) and Dr. Ian Snape (Australian Antarctic Division)
- **Skills gained**: Extraction of organics from soil, separation by silica gel chromatography, GC-MS analysis of PCBs and PAHs, PCA statistical analysis of results
- **Awards**:
  - First Class Honours
  - University Medal from the University of Tasmania for Outstanding Results
  - Tasmania Antarctic Scholarship
  - Entry on to the Dean's Roll of Excellence for 2008

02/2005 - 12/2007 *Bachelor Degree in Antarctic Science*, University of Tasmania, Australia

- **Major fields of study**: Chemistry, Antarctic Science
- **Minor fields of study**: Botany, Zoology, Antarctic and Oceans Law and Policy
- **Student Exchange**: August 2007 - May 2008 at the University Centre in Svalbard
- **Awards**:
  - Tasmania National Undergraduate Scholarship
  - J.N. Baxter Memorial Prize for Outstanding Proficiency in First Year Organic Chemistry
  - Royal Australian Chemical Institute Prize for Excellence in First Year Chemistry
  - Winifred Curtis Prize for Greatest Proficiency in First Year Plant Science
  - Percy Ash Scholarship for Outstanding Proficiency in Second Year Chemistry
  - Royal Australian Chemical Institute Prize for the Best Chemistry Graduate
  - Entry on to the Dean's Roll of Excellence, 2005 - 2007

2000 - 2004 Acceleration Program at the University High School, Melbourne

- **Final-year subjects**: French, English Language, Specialist Mathematics, Mathematical Methods, Biology, Chemistry
- **Result**: TER (percentile ranking) Score of 99.7